Particulate Emissions from Gasoline Direct Injection Engines

A thesis submitted in partial fulfilment of the requirements

for the degree of Doctor of Philosophy

Felix C P Leach

Oriel College

DPhil, Hilary 2014

Particulate Emissions from Gasoline Direct Injection Engines

Felix Leach DPhil
Oriel College, University of Oxford Department of Engineering Science

A thesis submitted in partial fulfilment of the requirements for the degree of Doctor of Philosophy, Hilary term 2014

ABSTRACT

Direct injection spark ignition (DISI) engines are the next generation of gasoline fuelled engines. Their greater fuel economy and reduced CO_2 emissions compared with port fuel injection (PFI) engines has led to their popularity. However, DISI engines produce a greater number of particulate matter (PM) emissions than PFI engines. Concern over the health effects of PM emissions, and forthcoming European legislation to regulate them from gasoline powered vehicles has led to an increased interest in the study of PM formation, measurement, and characterisation.

A model was developed by Aikawa *et al*, the PM index, correlating PM emissions with fuel composition. PM emissions are thought to be linked both to the vapour pressure (VP) and the double bond equivalent (DBE) of the components of the fuel. However, there was no independent control of these parameters and the study was undertaken on a PFI engine. In this thesis, experiments have been conducted to validate this model and extend it, as the PN index, to DISI engines.

Fuels have been designed using Raoult's law and UNIFAC (with careful consideration of octane number) such that the DBE and VP of the fuel mix could be varied independently. The design of the fuels was such that the component parts would co-evaporate upon injection into the cylinder, ensuring a homogeneous mixture of the components at the point of ignition.

The PN index has been tested on a single cylinder engine, at a matrix of test points, using these model fuels, and their PM emissions have been analysed using a Cambustion DMS500. The results show that the PN index is followed closely using model fuels, provided that these

model fuels contain a ‘light-end’ (in this case 5 % v/v n-pentane). Imaging of in-cylinder evaporation and in-cylinder measurement of hydrocarbons shows how the composition of model fuels affects their PM emissions.

The PN index has also been tested using commercial fuels on a single cylinder engine and a Jaguar V8 engine; the results again show that the PN index is also an excellent predictor of PN emissions for market fuels from both of these engines.

PN emissions have been evaluated from two fuels representing the EU5 reference fuel specification, developed using the PN index to give a difference in PM emissions. Testing these fuels on both a single cylinder engine and a Jaguar V8 engine has shown up to a factor of three variation in observed PN emissions. This has important implications for forthcoming European emissions legislation. The results of these tests were fed into the recommendations for the EU6 reference fuel specification.

The PN index has also been investigated in a Jaguar V6 engine with five different fuels with a spread of calculated PN indices over a simulated NEDC. Here the PN emissions have been measured using two PN, and one PM instrument and the results compared. The results show that the trends of the PN index are followed, but not as closely as predicted. Detailed analysis shows that this discrepancy is due to other effects, for example cold start, dominating the PN emissions in certain phases.

PN emissions have been measured from a highly boosted engine at a variety of operating points using 14 different fuels. It has been shown that for a large variety of engine operating parameters PN emissions from highly boosted engines behave as expected. When changing the fuels, the results show that a variation of over three orders of magnitude can be observed. The predictions of the PN index are inconclusive however, with further work suggested to fully evaluate the PN index on highly boosted engines.

Table of Contents

Nomenclature

#	Number of particles
A	Instrument transfer function
AFR	Air Fuel Ratio
AKI	Anti-Knock Index
a_{mn}	Measure of energy of interaction
APC	AVL Particle Counter
ASOG	Analytical Solution of Groups
ASVP	Air Saturated Vapour Pressure
BMEP	Brake Mean Effective Pressure
BON	Blending Octane Number
BP	Boiling point
C	Number of Carbon atoms
c	Concentration of the solute
CARB	California Air Resources Board
C_c	Cunningham slip correction factor
CI	Compression Ignition
CNG	Compressed Natural Gas
COPD	Chronic Obstructive Pulmonary Disease
CoV	Coefficient of Variance
CPC	Condensation Particle Counter
CPMA	Centrifugal Particle Mass Analyser
d	Particle diameter
DBE	Double Bond equivalent
D_f	Fractal Dimension
DHA	Detailed Hydrocarbon Analysis
DISI	Direct Injection Spark Ignition
d_m	Electrical Mobility Diameter
DMA	Differential Mobility Analyser
DMS	Differential Mobility Spectrometer
DPF	Diesel Particle Filter
d_{va}	Vacuum Aerodynamic Diameter
DVPE	Dry Vapour Pressure Equivalent
E	Electric Field Strength
e	conversion error
e	Elementary charge
EEPS	Engine Exhaust Particle Sizer
EGR	Exhaust Gas Recirculation
ELPI	Electrical Low Pressure Impactor
EPA	Environmental Protection Agency
ET	Evaporation Tube
EU	European Union
FBP	Final Boiling Point
F_d	Drag Force
F_e	Force due to an Electric Field
fFID	fast Flame Ionisation Detector
FID	Flame Ionisation Detector
FSN	Filter Smoke Number
FTP75	A US drive cycle
GDI	Gasoline Direct Injection
GEM	Gasoline, Ethanol, and Methanol
GPF	Gasoline Particulate Filter
HC	HydroCarbon
HEPA	High Efficiency Particulate Absorb
HVAC	Heating, Ventilation, and Air Conditioning
i	Ring current
IBP	Initial Boiling Point
ICE	Internal Combustion Engine
IMEP	Indicated Mean Effective Pressure
k_h	Henry's law coefficient
KLSA	Knock Limited Spark Advance
Kn	Knusden number
LEV	Low Emission Vehicles
m/m	by mass
MFC	Mass Flow Controller
MON	Motor Octane Number
MSS	Micro Soot Sensor
MTBE	Methyl Tert-butyl ether
n	Number of charges per particle
n	Particle number concentration in mode
N_a	Avogadro's number
NA	Naturally Aspirated
NEDC	New European Drive Cycle
OR	Odds ratio
P	Pressure
PAH	Polycyclic Aromatic Hydrocarbon
PASS	Photo Acoustic Soot Sensor
PFI	Port Fuel Injection
PI	Positive Ignition
PM	Particulate Matter
PM	Particle Mass
PMP	Particle Measurement Programme
PN	Particle Number
PNC	Particle Number Counter
PND	Particle Number Dilution
PTFE	PolyTetraFluoroEthylene
P_{vp}	Vapour Pressure
PWr	Power to Weight ratio
Q	Sample flow

q	Normalised molecular surface area
r	Normalised molecular Van der Waals volume
R	Molar gas constant
R_0	Universal gas constant
Re	Reynolds Number
RMS	Root Mean Square
RON	Research Octane Number
RR	Relative risk
RVP	Reid Vapour Pressure
s	Real particle size spectrum
SGDI	Spray Guided Direct Injection
SI	Spark Ignition
SMPS	Scanning Mobility Particle Sizer
SNR	Signal to Noise Ratio
T	Absolute temperature
T/C	Turbocharged
T90	Temperature at which 90% of a fuel has evaporated
THC	Total Hydrocarbons
TWC	Three-way-catalyst
UHC	Unburned Hydrocarbon
ULG	Unleaded Gasoline
UNECE	United Nations Economic Commission for Europe
UNIFAC	UNIversal Functional Activity Coefficient
UNIQUAC	UNIversal QUAsi Chemical
V	Velocity of particle in flow
v/v	by volume
WGDI	Wall Guided Direct Injection
WHO	World Health Organisation
WLTC	Worldwide harmonized Light vehicles Test Cycle
WLTP	Worldwide harmonized Light vehicles Test Procedures
x	Molar fraction of liquid phase
y	Molar fraction of vapour phase
z	Coordination number
Γ	Group residual activity coefficient
$\Delta_r H_\Theta$	Standard reaction enthalpy
η	Dynamic viscosity
θ	Area fraction
λ	Mean free path of gas
λ	actual AFR / Stoichiometric AFR
μ	Count mean diameter
ρ_g	Density of gas
σ_g	Geometric standard deviation
Υ	Activity coefficient
Φ	Segment fraction

Acknowledgements

First and foremost, my profound thanks goes to Prof Richard Stone, my supervisor, for his vast input into this project, his patient advice and guidance, and limitless knowledge and practical assistance. This could not have happened without him.

The co-located Combustion and Cryogenics groups have been a wonderful source of advice, support, and friendship over the past 3.5 years, for that I thank Huayong Zhao, Fan Xu, Mengchen Hu, Kun Liang, Nathan Hinton, Joe Camm, and Ian Berryman, as well as Ben Williams from the Combustion Physics and Non-Linear Optics group in the Department of Physics. In addition the MCR and SCR communities of Exeter and Oriel Colleges have been a wonderful source of friendship and support over my time as a graduate student, and I am grateful to them and all of my friends.

Within the Department of Engineering Science I would like to thank Paul Bailey, John Brumfitt, Sara Downs, Alex Harper, Derek Pobgee, Darren Soden, Sukarni Wheeler, and Bob Yapp and the many other fantastic support staff for their tireless support of me and this project.

I would like to thank EPSRC and Jaguar Land Rover for funding this research; in particular I am very grateful to Dave Richardson at JLR, my industrial supervisor, for all of his advice, help, and support throughout the project which was invaluable. At JLR I would also like to thank Mike Braisher, Derek Fennel, David Hayden, Rishin Patel, Jamie Turner, Adam Weall, and Nick Wicks who have helped a great deal, in particular with engine testing at Whitley and the ULTRABOOST project.

In the wider academic community Martin Davy (previously of Loughborough University and now Oxford) has been a huge help in my fuel modelling and development of the UNIFAC model, I thank him for the many useful conversations we have had. Sam Akehurst and Andrew Lewis at the University of Bath facilitated and ran the ULTRABOOST testing there, I am hugely grateful to them for this and for their patience with my particulate measurements.

The team at Cambustion have been brilliant both with technical support and advice in particular with the DMS and fFIDs, there I would like to thank Andy Barron, Chris Nickolaus, Mark Peckham, Kingsley Reavell, and Jonathan Symonds.

Roger Cracknell and Sarah Remmert (Shell Global Solutions), David Richardson (Coryton Advanced Fuels), and John Williams (BP), have all been a great source of advice and support with fuels, as well as supplying most of the fuel used in the project, for which I am very grateful. Discussions with Roger Cracknell on fuel volatility effects were very useful. I am bound to note that nothing present in this thesis suggests that Shell endorses my conclusions.

Last, but by no means least, I am so grateful to my family – my parents Beverly and Charles and my sister Alice for all of their support, and my grandparents Kenneth, the late Jean and Chief, I thank them all from the bottom of my heart.

1. Introduction to particulate matter emissions

Particulate matter (PM) emissions are a pollutant causing air quality problems, and ultimately a degradation in public health. Recently there has been an increase in concern about PM emissions, and their effect on human health. In 2012 the World Health Organisation (WHO) declared Diesel exhaust (a large source of PM emissions) to be a carcinogen, putting it in the same category as asbestos [1, 2]. Recent advances in gasoline (petrol) engine technology have pushed the field in the direction of Gasoline direct injection (GDI) engines, which have a better volumetric efficiency, and lower specific fuel consumption, however these engines produce more PM emissions. Throughout this thesis the focus is on particle number (PN) emissions, rather than the historically measured quantity of particle mass, despite the fact that number, unlike mass, is not a conserved quantity. However, the health impact of PM emissions is thought to be strongly linked to the number of particles emitted, rather than the mass emitted Indeed smaller particles, which make almost no contribution to the mass emission, penetrate further into the lungs before deposition [3], and are much more likely to pass into the bloodstream.

1.1. Direct injection gasoline engines

There are two types of internal combustion engine (ICE), compression ignition (CI) commonly referred to as Diesel and spark ignition (SI) engines. SI engines generally have a higher power output from better air use, but CI engines have higher thermal efficiencies from higher compression ratios and reduced throttling losses. Direct injection spark ignition (DISI) engines are seen as a way of possibly combining the advantages of both.

Until recently SI engines have mostly used port fuel injection (PFI) where the fuel is injected at low pressure into an inlet manifold before the fuel / air mixture is inducted into the engine. This produces a homogeneous mixture inside the cylinder.

Developments in injector technology, being able to produce a directional spray of small diameter droplets, allowed the introduction of GDI engines. With DISI, the fuel is injected directly into the cylinder at fuel pressures of up to 200 bar. This causes charge cooling within the cylinder as the fuel evaporates, which increases the density of the charge. This has a number of benefits, it gives a higher mass flow of air for a given volume flow, which leads to an increase in volumetric efficiency; it also allows for an increased compression ratio for a given fuel's anti-knock performance.

DISI engines can also reduce losses at part load operation by operating in stratified mode, where fuel is injected near the spark plug, creating a near-stoichiometric mixture at the point of ignition, with a lean background mixture in the cylinder. This has the advantage of reducing part load fuel consumption, although full load cannot be reached under stratified operation. DISI engines can be switched between stratified (for part load) and homogeneous operation (full load).

Two types of GDI engines exist; wall guided (WGDI) and spray guided (SGDI). With a wall guided engine using early injection the fuel is injected towards a bowl in the piston, which deflects it and causes in-cylinder mixing designed to achieve a stratified mixture around the spark plug. However, fuel films form on the piston crown and cylinder walls, which burn with a diffusion flame causing large quantities of unburned hydrocarbons (UHCs) and particulates to be emitted. SGDI uses the characteristics of the injector to guide the fuel spray in the cylinder; it allows fuel to be injected towards the spark plug, which gives potential for ultra-fast burn, which leads to an improvement in fuel economy.

As the fuel is not being directly injected at the cylinder surfaces, and has the potential to be fully evaporated at the point of ignition, it should lead to a reduction in UHCs and particulates. A schematic of the three types of gasoline fuel injection discussed is shown in Figure 1.1.

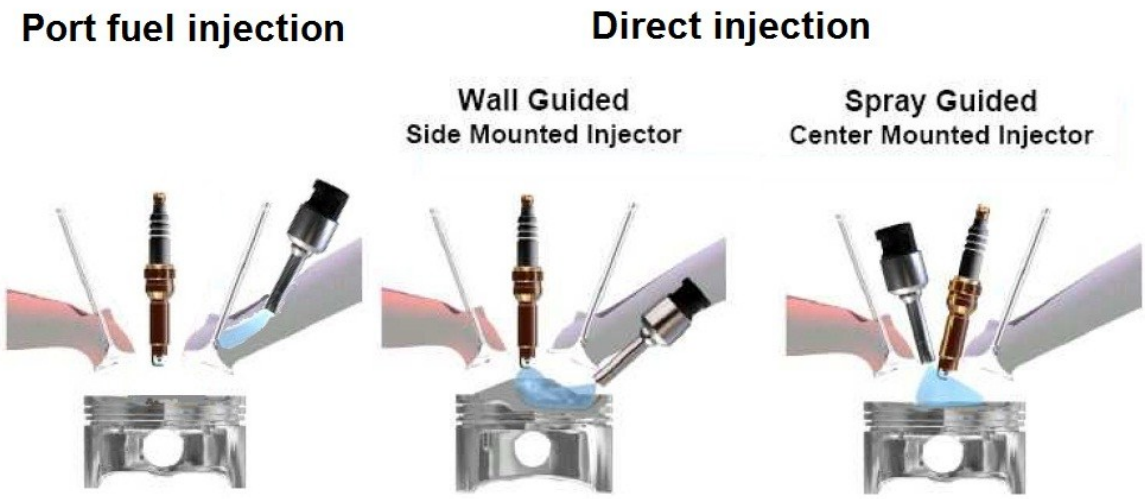

Figure 1.1: Schematic of port fuel injected (PFI), wall guided direct injection (WGDI), and spray guided direct injection (SGDI) engines (adapted from [4])

One of the main disadvantages of DISI engines is that the effect of direct injection (regardless of the spray guidance) is to produce a less homogeneous mixture. This tends to lead to an increase in Particulate Matter emissions. This can clearly be seen in Figure 1.2 [5] where the PN and PM emissions for a variety of engine technologies are shown, and it can be seen that DISI engines on average produce around an order of magnitude more particle number emissions, and significantly more particle mass than PFI engines.

There have been various attempts at reducing the increase in PM emissions caused by the transition to DISI engines, for example by combining PFI and GDI technology such as undertaken by Ikoma *et al* [6]; the additional complication and cost of such a strategy has generally outweighed any benefits.

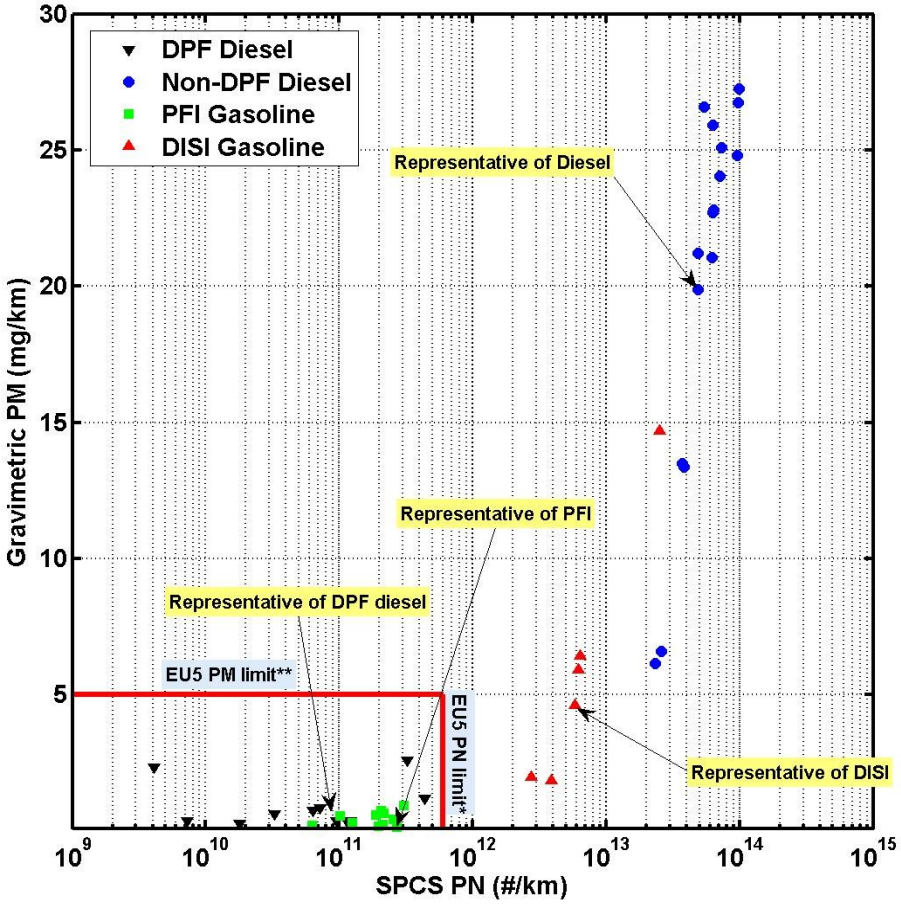

Figure 1.2: Example particulate matter emissions, mass vs number for a variety of engine technologies [5], Reprinted with permission from SAE Paper No. 2010-01-0786 © 2010 SAE International. Further use or distribution of this material is not permitted without prior permission from SAE.

1.2. Composition, formation and health effects

Particulate Matter in engine exhaust originates from the combustion process in-cylinder. During the combustion of any hydrocarbon, formation of particulate carbon (soot) is almost always observed. Soot itself is not chemically defined, it consists of up to 10 percent by mol. hydrogen, alongside the carbon, with an atomic C:H ratio of around 8 : 1 [7].

Most of the soot formed during combustion is subsequently oxidised, either in-cylinder or in the exhaust port and piping, especially if there is a lean mixture present giving an excess of O_2, alongside the O and OH naturally present, which oxidises the soot. It should be noted that a lean mixture does not guarantee that all of the soot will be oxidised because, particularly in direct injection engines, the mixture is not completely homogeneous, and there will be areas of mixture that are locally rich.

Coalescence of polycyclic aromatic hydrocarbons (PAHs) has been shown to be responsible for the initiation of soot formation. In particular this is due to the polymerisation of acetylene, which is known to form in large concentrations during fuel-rich combustion [7]. A proposed chemical mechanism for the initial formation of aromatic species during combustion is shown in Figure 1.3.

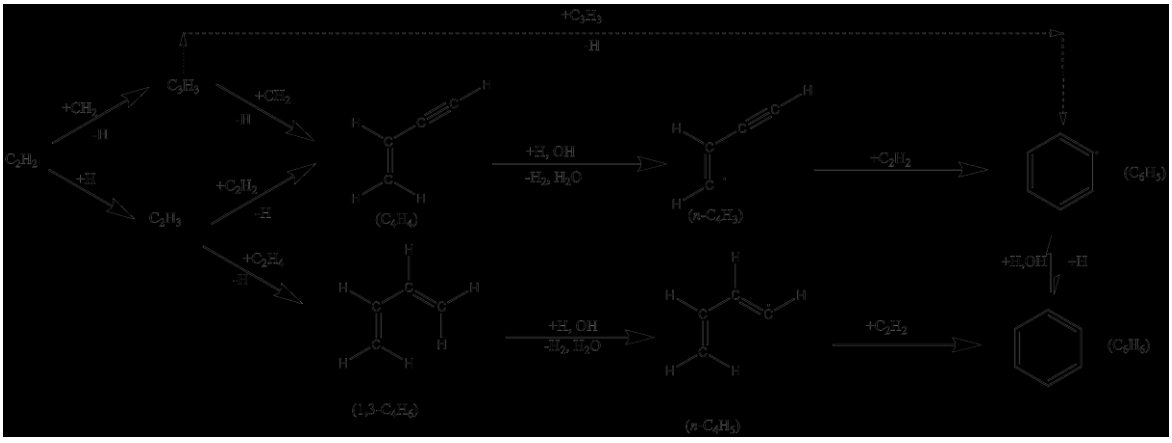

Figure 1.3: Suggested pathways for initial aromatic formation during combustion (adapted from [7])

Once these initial aromatics have been formed (either due to the process described above, or due to their presence in the combustion fuel) there are a number of pathways hypothesised for their subsequent development into soot particles, an example of one of these pathways is shown in Figure 1.4.

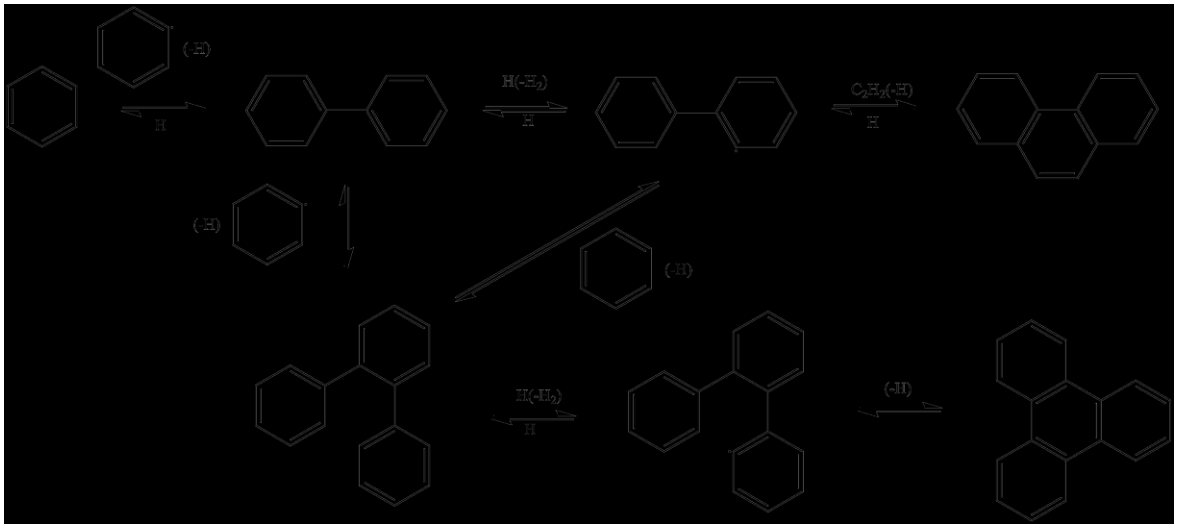

Figure 1.4: Example reaction pathway for PAH growth mechanism (adapted from [7])

The reaction pathways described here are fully reversible, generally at temperatures greater than 1800 K, so at these higher temperatures these same processes also lead to the decomposition of PAHs.

Once PAHs have become four-ringed or larger, they can collide and form clusters, these clusters can then continue to react with acetylene to eventually form soot particles.

In parallel with these soot formation processes, soot oxidation will also be occurring, so as to reduce the soot concentration. The final balance between these two processes gives the initial exhaust particulate emission. This, of course, leaves open the possibility of particulate free combustion in an engine, were all of the soot formed to oxidise.

1.2.1. Modes of particulate emissions

Most gasoline exhaust aerosols today show a bilognormal distribution of particulate size with two distinct modes, so common is this trend that they have been given names: nucleation and accumulation, reflecting their formation provenance. A typical particle size distribution shown in gasoline exhaust aerosol is shown in Figure 1.5. In this spectrum it can clearly be seen that a bilognormal distribution is followed (note that the abscissa is

plotted logarithmically), with one mode centred on approximately 15 nm diameter (the nucleation mode), and a second centred on approximately 55 nm (the accumulation mode).

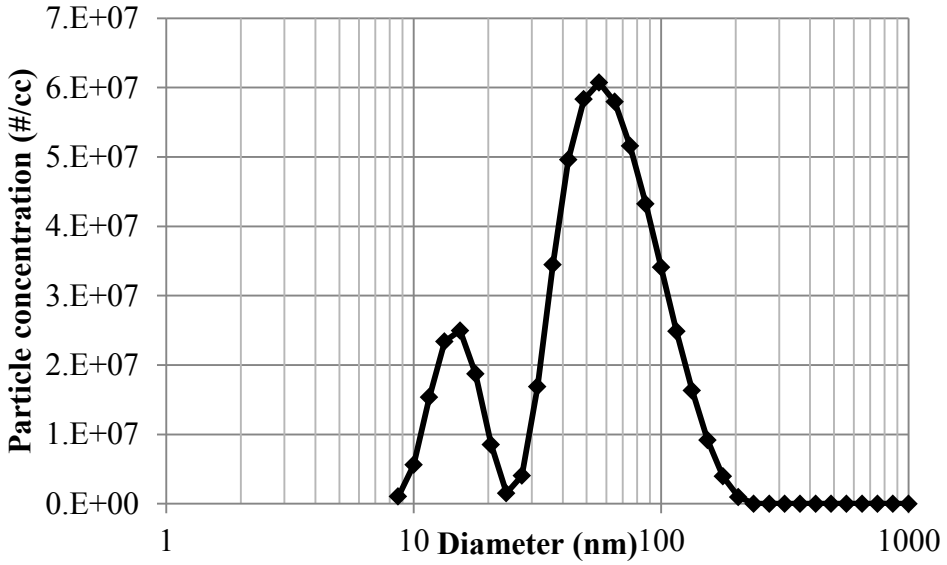

Figure 1.5: Typical particulate emission spectrum from a gasoline engine, in this case a Jaguar AJ126 V6 SGDI engine

Nucleation mode

Nucleation mode particles are characterised by having a diametric size less than approximately 20 nm, and are roughly spherical. Their formation is thought to occur as the exhaust cools and volatile particles pass from gas phase to a condensed phase in the cool, dilute conditions of engine exhaust. Initially, immediately after exhaustion from the cylinder, the aerosol temperatures are very high, and hence almost all of the volatile species present (mainly hydrocarbons such as unburned fuel and partial combustion products) will be in the gas phase. As the exhaust gas cools (on passage through the tail pipe) and dilutes (generally with a very high dilution ratio upon exit from the tail pipe) the species tend to exhibit one of two behaviours. Species either condense and adsorb onto existing solid matter (these particles then tend to form an accumulation mode particle) or the gas phase species nucleate into new particles; this process forms the nucleation mode,

and gives it its name. Often, the nucleation mode can contain up to 90 % of the particle number emission whilst, due to their small size, only containing 1-20 % of the mass [8]. Formation, and measurement of this mode depends strongly on the dilution ratio and cooling conditions of the exhaust and the sampling conditions. For these reasons it can be very difficult to measure, particularly as there tend to be very large numbers of very small particles, and repeatability of results in this region is often poor.

Accumulation mode

Accumulation mode particles generally lie in the size range 40-200 nm. Their formation is thought to occur when fuel molecules undergo pyrolysis at high temperatures, using the processes described on page 5 to form carbon spherules, which are found to be approximately 15-40 nm in diameter [9]. Two processes can then cause these particles to grow; firstly gaseous phase species in the exhaust condense and adsorb onto these spherules, causing them to grow – the composition of some of these condensed species leads to some of the health effects of particles described in Section 1.2.4 . The larger the surface area of these spherules gives a greater area to adsorb onto. The second process is that these spherules can agglomerate by colliding and sticking together using a sintering process [10], which produces particles with a fractal like shape[1] [11]. This can clearly be seen in Figure 1.6, showing a large fractal like shaped accumulation mode particle. Of note in this image is that transmission electron microscopy requires a very low pressure, such that it is likely that any volatile species adsorbed onto this particle have evaporated.

[1] Technically, accumulation mode particles are aggregates rather than agglomerates, as the forces that hold them together are chemical or sinter-like forces, whereas an agglomerate is held together by physical forces (e.g. Van der Waal's) and the primary particles retain their original shape – clearly not the case here. Accepted terminology however, seems to be to refer to them as agglomerates.

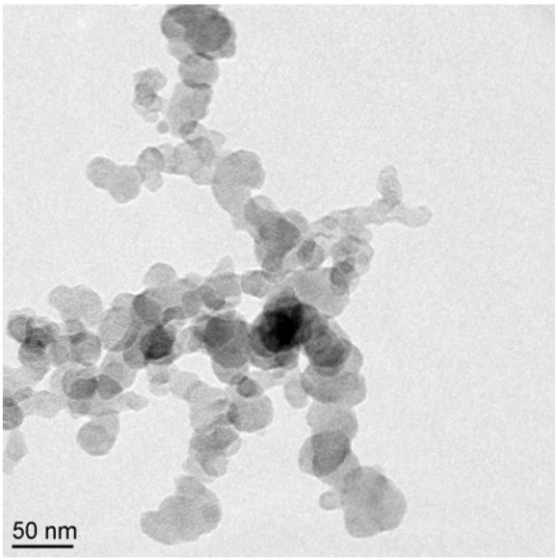

Figure 1.6: Transmission Electron Microscope image of an accumulation mode particle [12]

It should be noted that some exhaust aerosols contain a third mode – the coarse mode – generally of a diameter higher than 1 μm. These particles are thought to be from re-entrained deposits on the combustion chamber and exhaust system [8] and other deposits (e.g. rust) [3]. This mode has not been considered in this thesis.

1.2.2. Particle diameter

For a particle such as that shown in Figure 1.6, defining a diameter is not trivial – it is not spherical. Non-spherical particles tend to be defined by an equivalent diameter, defined depending on the criteria of interest, or measurement capability, such a diameter is defined as the diameter of a spherical particle which would exhibit the same behaviour as this particle.

Common equivalent diameters include mass equivalent and volume equivalent diameters. Whilst such diameters may appear to be useful, measurement restrictions on large quantities of nano-sized particles mean that their measurement is impossible under most circumstances.

A key parameter in describing fractal like shapes is the fractal dimension D_f which is a ratio describing how the measured shape of a fractal changes with the scale of the instrument measuring it. Eggersdorfer *et al* [10] describe how this can be used to characterise nanoparticle shapes, although some other size parameter is also needed to describe the overall scale of the particle. Considering the fractal geometry of particles, Meakin (1987) [13] proposed an agglomerate mobility diameter relating their shape to how the agglomerate behaved in a net-stationary suspension of particles undergoing Brownian motion, and how often they would collide.

Different methods of measuring particles tend to report different diameters, for example differential mobility analysers (DMA) and DMSs report electrical mobility diameter (d_{m}), whilst other instruments such as an aerosol mass spectrometer (AMS) measure vacuum aerodynamic diameter (d_{va}).

Vacuum aerodynamic diameter is an equivalent diameter defined as the diameter an equivalent spherical particle would have with the same terminal velocity in a free-molecular region (defined as where the Knusden number $\mathrm{Kn} >> 1$) as the particle of interest. [14]

Electrical mobility diameter is a practical equivalent diameter for measuring engine exhaust particles. This diameter is a result of a force balance between the electrical force experienced by charged particles passing through an electric field, and the drag force that they experience.

The force experienced on a particle in an electric field is $F_e = neE$ where n is the number of charges on a particle, e is the elementary charge, and E is the electric field strength. It can be assumed that a particle reaches its terminal velocity very quickly, so throughout classification the electrical force and the drag force are equal and opposite.

The drag force experienced by a particle depends on the Reynolds number (Re) of the flow that it is in. For Re > 1000, the drag force can be expressed as Newton's drag - $F_d = 0.44\frac{\pi}{8}\rho_g d^2 V^2$, where ρ_g is the density of the gas the particle is suspended in, d is the diameter of the particle (assumed spherical), and V is the velocity of the particle through the flow [15]. However for nano-sized particles flowing through air, Re << 1, and this Newtonian drag does not apply, in this region Stokes law holds. Stokes law states that the drag force on a particle is $F_d = 3\pi\eta V d$ where η is the dynamic viscosity of the air. A key assumption here is that the velocity of the gas at the particle surface is zero. For particles smaller than 15 μm, this is not the case, as their size is close to the mean free path of the gas (λ) (the mean free path is the average distance between molecular collisions). In this case Stokes law over predicts the drag; however this 'slip' can be corrected for using the Cunningham correction factor (C_c), leaving the drag force as:

$$F_d = \frac{3\pi\eta V d}{C_c}$$

where C_c is evaluated as: $C_c = 1 + \frac{2.52\lambda}{d}$ for particles as small as 100 nm.

For particles smaller than 100 nm Brownian motion of particles becomes important and a number of empirical correlations exist for the Cunningham correction factor, for example Allen and Raabe (1982 and 1985) [16, 17] and Buckley and Loyalka (1989) [18].

Equating the electrical and drag forces:

$$\frac{3\pi\eta V d}{C_c} = neE$$

so the electrical mobility diameter can be expressed as:

$$d_m = \frac{C_c neE}{3\pi\eta V}$$

Electrical mobility diameter may be significantly larger than the volume equivalent diameter of the particle for fractal like agglomerate particles, as the electrical mobility diameter is dependent of the conditions of the air that the sample is conditioned in, and there is the possibility of a particle aligning in the electric field, giving a minimum drag force.

For engine exhaust, different methods of measurement giving a different equivalent diameter will report different diametric values at most operating conditions [14], therefore care must be taken when comparing data from the literature as to which diameter has been measured and reported.

As the only instrument used in this thesis capable of reporting a particle diameter is a DMS, particle diameters referred to throughout this thesis will always be electrical mobility diameters.

1.2.3. Effect of GDI engine parameters on PM emissions

Although the main focus of this thesis is on the effect of fuel composition on particulate emissions, it should be noted that a wide variety of engine operating parameters have an effect on particulate emissions. The parameters covered here are not intended to be an exhaustive list, rather, some of the more commonly encountered operating parameters and their effects.

Generally the largest effect observed is the air fuel ratio (AFR), where a rich mixture is often observed to give approximately an order of magnitude larger number of particles, compared to the stoichiometric case [5]. This is what would be expected given the

reduction in soot oxidation that is possible with less air present than would be sufficient to burn all of the fuel.

The effect of increasing the engine load (torque) on particulate emissions is well documented for Diesel engines, as load increases, so too do the PN emissions [19], this mainly arises from the change in AFR as the load is increased on a Diesel engine. The same effect of load on PN emissions is observed in GDI engines. However, for nearly all operating conditions the AFR in a GDI engine is constant, so this cannot be the reason in this case. However, as load increases, so too do in-cylinder pressures, the increase in-cylinder pressure may result in the fuel penetrating less far into the cylinder before evaporation, resulting in a less homogeneous mixture, and hence higher PN emissions. The increase in load will result in the amount of fuel present in the cylinder also increasing (though to retain the AFR, the amount of air present also increases, this is achieved by throttling), with more fuel present, the chance of fuel impinging the wall and piston also increases, such fuel will burn as a liquid in a pool fire and hence increase the PM emissions.

The effect of spark timing on PN emissions will depend on where the initial ignition timing was. Assuming that the timing is such that the engine is at maximum brake torque (MBT) (the maximum load for a given condition), then deviations from either side of MBT will result in a decrease in particulate emissions, mirroring the effect of engine load on particulates. Early ignition will lead to there being a longer time for combustion, at lower temperatures and pressures, leading to a decrease in PM emissions. Retarding the ignition from MBT increases the exhaust temperature, leading to more post-flame oxidation of particulates, hence a decrease in PM emissions.

Injection timing is a key calibration parameter, affecting many factors. An early injection is desirable to get the full benefit of GDI – charge cooling, with its associated fuel consumption and CO_2 emissions benefits. On the other hand very late injection can be used for stratified engine operation, as described on page 2. The effect of injection timing on particulate emissions is a similar compromise, early injection can reduce PN emissions as there is more time for mixture preparation, however too early an injection can result in the fuel impinging on the piston, causing piston wetting, and the fuel will burn in a pool fire, causing a sharp increase in particulate emissions. Later injection obviously trades these two effects off in the opposite direction.

The inlet air temperature is a trade-off between emissions and efficiency, a low intake temperature increases the mass of air inducted into the cylinder of a given volume, and hence improves volumetric efficiency, low intake temperatures can also reduce combustion knock. However a higher intake air temperature is likely to reduce particulate emissions as there will be better direct injection mixture preparation, as the higher temperatures will promote spray evaporation.

Exhaust gas recirculation (EGR) is often used in combustion engines to reduce NO_x emissions by reducing combustion temperatures. In addition EGR reduces throttling losses in SI engines because, for a given load, the throttle plate must be opened further due to the presence of already burnt gas. However by introducing burnt gas with particulates already present, the effect is to increase overall particulate emissions. On the other hand, hot EGR can improve mixture preparation, and hence reduce particulate emissions. Therefore the effect of EGR is mixed, and depends on the engine operating point, and the levels of EGR.

Increases in exhaust back pressure are avoided if possible by engine designers, as they increase the work required to exhaust the cylinder, increasing the pumping work, resulting

in a decrease in engine efficiency. Common sources of an increase in exhaust back pressure include the addition of a turbocharger or a particle filter. An increase in exhaust back pressure will increase the residuals present in the cylinder, and increase the charge temperature, as was the case for the inlet air temperature, the effect of this is to improve mixture homogeneity, and this will lead to a decrease in particulate emissions.

1.2.4. Health effects

Given the concern about the effect of particulates on human health, and the classification of Diesel exhaust as a carcinogen, there is a great deal of research into the health effects of particulate emissions. However, as with all medical research, there are many variables to consider, and particulates are not solely responsible for all of the conditions they are known to affect, rather they can be an exacerbating factor for existing conditions, as well as being primarily responsible for other conditions [20]. It will never be possible to deconvolve the exact impact of particulates on any specific illness and there will always be other factors, however given large sample sizes, good generalisations can and are being made as to the effect of particulate emissions on human health.

Particulate emissions can come from many sources, cigarettes, frying, and cleaning (in particular vacuuming), indeed Boies *et al* [21] conducted a study at Paddington train station, and found the largest PM emissions in the region of the smokers ramp and the fast food restaurant, rather than in areas close to the Diesel trains. There are also multiple sources of particulate emissions from vehicles, not only engine exhaust, but also brake dust, and tyre wear. Air pollution is made up of this complicated mix, which can undergo ageing processes too; it is not possible to deconvolve only the effects of particulate emissions from engine exhaust.

Studies tend to use one of two approaches, either they will compare, generally for a large group of people, exposure to particulates and occurrences of various illnesses, this is an epidemiological approach, although for these studies, it is often not possible to break down the contribution of particulates relative to other pollutants. Alternatively studies expose tissue (often just cells) to a particulate, or a particular chemical, and look for the effect, this is a toxicological approach.

Initial studies into the effect of PM emissions on health focussed on large particles (around 10 μm in diameter) known as PM_{10} because such particles dominate emissions from coal and wood burning. Total UK emissions of PM_{10} in 2001 were 180 kilotonnes [22], and such particles are thought to cause around 37,000 deaths in Europe every year [23]. Levels of PM_{10} and $PM_{2.5}$ (similarly particles around 2.5 μm in diameter) are now regulated both in the USA and Europe ($PM_{2.5}$ in Europe from 2015) [24, 25].

As regulation, and technological development, has reduced the levels of PM_{10}, and all particles greater than 1 μm in diameter in the atmosphere, research has begun to focus on ultrafine particles – those in the sub-micron size range.

Whilst most of the initial interest and regulation into PM emissions, and atmospheric air quality has focussed on the mass of particles (PM_{10} and $PM_{2.5}$ legislation specifies an annual mass dosage limit) recent studies have shown that the health effects of particles seem to be dependent on the number of particles and their Lung Deposited Surface Area (LDSA). Donaldson *et al* [26] in a toxicological study showed that the number of particles (both PM_{10} and ultrafine particles) and their surface area deposited on the lungs had a powerful inflammatory effect on the lungs, and ultimately led to an encouragement of the development of tumours and fibrosis. Donaldson *et al* [27] showed that particles deposited in the lungs led to a release of free radicals from the particle that disrupted the redox

reactions on the surface of the lungs and ultimately led to DNA damage. The harmful effects of particulates are thought to be due to two mechanisms; particulates and the components that are adsorbed onto them increase the levels of free radicals and reactive oxidation species, this leads to an increase in oxidant species relative to antioxidants – this is oxidative stress, and this is thought to be the pathology of many diseases [3].

The effect of particulate matter on lung cancer has been long understood, mainly as a result of cigarette smoking. PAHs adsorbed onto particles are able to bond covalently with DNA, RNA, and proteins, and when the resultant products are processed by one of the body's organs this can promote cancerous growth in that organ.

The effect of particulates on certain cardiovascular diseases is thought to be due to the particles promoting the inception of blood clots, which lead to thromboses, strokes, and myocardial infarctions (commonly known as heart attacks). Gehring *et al* (2006) [28] found an adjusted relative risk (RR) for women living within 50 m of a main road of 1.7 for cardiopulmonary mortality based on a sample size of 4,800. In other words those women were 1.7 times more likely to die from diseases of the heart and lungs compared with women who lived more than 50 m from a main road.

McConnell *et al* (2006) [29] report that children living within 75 m of a main road experience a 30 % increase in the likelihood that they will develop asthma. Similarly, Perez *et al* (2009) [30] reported that 9 % of all childhood asthma cases of a sample taken in Long Beach, California, were directly attributable to proximity to traffic. Living in close proximity to a road is not just dangerous for children, Ranft *et al* [31] show a link between mild cognitive impairment (a precursor of dementia and Alzheimer's disease) in the elderly (the average age of their sample was 75) for those who lived within 50 m of a main road.

Nemmar *et al* [32] show that ultrafine particles (in their work defined as smaller than 100 nm) passed into the human bloodstream within a minute of inhalation, and Peters *et al* [33] showed that the risk of heart attacks increased after an exposure to air pollution of only two hours. In an epidemiological study, Franck *et al* [34] found that by comparing calls to the emergency services, and particle distributions in the PM_{10}, $PM_{2.5}$, and < 100 nm regions, that the odds ratio (OR) for a hypertensive crisis (acute high blood pressure, which can lead to organ and cardiovascular damage) for the particle size < 100 nm for 2-7 days after exposure was significant, with an OR = 1.06, this was by far the highest OR compared with PM_{10} and $PM_{2.5}$, showing that the smallest particles have the greatest effect on this type of health effect.

It is clear therefore that PM emissions are harmful to human health; there is strong evidence to suggest that PM emissions increase the risk of heart attack, stroke, lung and other types of cancer, asthma, chronic obstructive pulmonary disease (COPD), bronchitis, dementia, and Alzheimer's disease. Whilst the precise effects and mechanisms are not clear, great efforts to reduce particulate emissions will reap significant health rewards for the population.

1.3. Effect of fuel composition on PM emissions

It is not surprising that different fuels have different levels of particulate matter emissions, and it is almost inevitable that even a single engine will not always be tested with the same fuel. Accounting for the influence of different fuel properties on PM emissions is very important in order to be able to compare tests, as well as to work towards an overall reduction in particulate emissions.

Double bond equivalent

It has been recognised that the coalescence during combustion of PAHs is responsible for the initiation of soot as discussed in the mechanisms shown on page 5 and supported by Frenklach *et al* [35]. Therefore it is expected that a high level of aromatic compounds in the combustion fuel would lead to a higher level of PM emissions, and indeed the literature supports this both for gasoline and Diesel engines [36, 37].

Hydrocarbons present in fuel that are close to benzene rings are therefore expected to have an increased effect on PM emissions, such that a likely dependence on PM emissions from common components might be[2] [38]:

paraffins (alkanes) < olefins (alkenes) & napthenes (cycloalkanes) < aromatics (arenes)

A convenient numerical way of accounting for this property is using the double bond equivalent (DBE). DBE is a measure of how unsaturated a hydrocarbon is, and can be easily calculated from:

$$DBE = \frac{2C - H + 2}{2} \qquad (1.1)$$

where C and H are the number of carbon and hydrogen atoms respectively present in an organic compound. As an example, toluene (methyl benzene, $C_6H_5.CH_3$) has a DBE of 4 as the corresponding saturated compound would be heptane (C_7H_{16}), which has a DBE of 0.

Evaporative performance

Given the importance of mixture preparation on particulate emissions already seen, it is to be expected that some measure of the evaporative performance of the fuel will play an important role in PM emissions. There are several measures of a fuel's evaporative

[2] Standard petrochemical industry terminology is to use descriptions such as paraffin, olefin, naphthene etc. to describe hydrocarbon structure, despite these contravening IUPAC conventions, and the terms being obsolete in all other industries. For this reason they are referred to as such throughout this thesis.

performance, vapour pressure is the pressure at a given temperature exerted by the vapour phase of a particular component on its liquid (and, under certain circumstances, solid) phase when at thermodynamic equilibrium [39]. It is a measure of the evaporative tendency of a liquid, and a measure of the net rate at which molecules leave the liquid boundary. At pressures below the vapour pressure only the vapour phase exists. A high vapour pressure means that a fuel is more likely to evaporate at a given temperature, and hence should be a better prepared mixture and give lower particulate emissions. Vapour pressure of gasoline is often presented as Reid vapour pressure (RVP) or dry vapour pressure equivalent (DVPE), these are discussed further in Section 3.3.1.

Vapour pressure is not the only measure of evaporative performance of a fuel, and can be skewed by the presence of components at the extremes, e.g. a large amount of 'light-end' components such as butane. Such presence may give a fuel with a high vapour pressure, but some components with a very high boiling point may also be present that are being masked by the presence of large numbers of low boiling point components. This can be taken into account by looking at the distillation curve of the fuel, and values such as the final boiling point (FBP) or the T90 (the temperature at which 90 % by volume of the fuel has evaporated) can be used as an alternative measure of the fuels evaporative performance. T90 may be preferable so that the presence of a small amount of very high boiling point components does not skew results. A high T90 means that a fuel is less likely to have evaporated at a given temperature, and hence should be a less well prepared mixture and give higher particulate emissions.

Oxygenates

Most of the interest in oxygenate compounds in fuels has focussed on ethanol. Ethanol (a 'biofuel') is seen as a way of reducing net CO_2 emissions from vehicles, and in low quantities can be a 'drop-in' for straight gasoline, however there are concerns about its

increased use, in particular due to increased ethanol production causing food shortages in developing countries [40, 41], such discussion, however, is outside the scope of this thesis.

In Europe, E5 (meaning a 5 % by volume blend of ethanol in gasoline) is now mandated [42]; in the USA, blends of E10 are ubiquitous, and E15 is legal for sale as gasoline in 2001 model year vehicles and later.

Ethanol has a high enthalpy of vaporisation, and so it is expected that the evaporative performance of ethanol compared to gasoline will be poor. Ethanol also has a much lower volumetric energy density compared with gasoline. This means that on an equivalent cycle using a high ethanol content fuel, a higher volume of fuel will need to be injected, and its evaporation will be poorer. Therefore there will be more spray to break up, and it will not break up as quickly as a result of ethanol's high enthalpy of vaporisation and low energy density. It is therefore expected that ethanol will increase particulate emissions, as the mixture preparation will be poor, and so similar to the effect of vapour pressure, an increase in PM emissions will be seen. This predicted increase is noted in the literature, for example by Chen *et al* [43].

Table 1.1 shows the enthalpy of vaporisation and volumetric energy density of gasoline, ethanol, and some other common oxygenate fuels.

Table 1.1: Enthalpies of vaporisation and lower heating values of common oxygenates

	$\Delta \boldsymbol{H_{vap}}$ (kJ/mol)	$\Delta \boldsymbol{H_{vap}}$ (kJ/kg stoichiometric mixture)	**LHV** (MJ/L)
Gasoline (representative)	35.4	20	31.3
Methanol	38.3	159	17.9
Ethanol	47.9	92	21.2
n-Butanol	51.0	57	26.8
Methyl tert-butyl ether (MTBE)	30.0	27	26.0

Sources: [44-47]

It has previously been noted (see Section 1.2.3) that AFRs rich of stoichiometric increase particulate emissions. This is true of ethanol, but the increase PM emissions rich of stoichiometric for ethanol is very small and, compared to gasoline, is in reality a dramatic reduction in particulate emissions (E10 showing a greater than order of magnitude reduction in PM emissions compared with straight gasoline) [48]. This reduction is thought to be due to the fact that the presence of oxygen in the fuel molecule reduces the concentration of important intermediate species to the formation of precursors to soot [49].

The effect of ethanol on particulate emissions therefore is mixed, depending on the stoichiometry, with a smaller increase in PM emissions due to evaporative performance seen at stoichiometric and lean conditions, but a large decrease (relative to gasoline) at rich conditions.

Whilst most of the research into the effect of oxygenate components in fuel on particulate emissions has focussed on ethanol, other oxygenates added to fuel include methanol, MTBE (Methyl tert-butyl ether), and butanol as well as combination blends such as gasoline, ethanol, and methanol (GEM) blends. The effect of such oxygenates on PM emissions is expected to be similar to that of ethanol, making an allowance for their different vapour pressures, and calorific values.

1.3.1. PM index

Recently, attempts have been made to draw together some of these parameters to try and quantify the effect of fuel composition on PM emissions. Aikawa *et al* [50] conducted tests with a PFI engine and developed a model linking fuel composition with PM emissions. Their model – the PM index - links PM emissions with the vapour pressure

(VP) and DBE of the components in the fuel weighted by mass fraction (W_t). Their PM index is shown in Equation 1.2.

$$I(VP, DBE) = \sum_{i=1}^{n} \left[\frac{DBE_i + 1}{VP_i}\right] W_{ti} \qquad (1.2)$$

In their work, Aikawa *et al* [50] evaluate the vapour pressure at 443 K by means of an empirical correlation with boiling point, shown in Equation 1.3.

$$\begin{aligned} VP(443K) = \exp(&8.34075219000144e^{-16} \times BP^6 \\ &- 2.53682333132270e^{-12} \times BP^5 \\ &+ 3.10013311128865e^{-9} \times BP^4 \\ &- 2.02889046987065e^{-6} \times BP^3 \\ &+ 7.47155341895910e^{-4} \times BP^2 \\ &- 1.67354730090773e^{-1} \times BP \\ &+ 26.0923223622962) \end{aligned} \qquad (1.3)$$

where BP is in Kelvin and VP in kPa.

It should also be noted that Aikawa *et al* evaluated the vapour pressure at a range of temperatures, and found that a temperature of 443 K gave the best correlation between particulate emissions and their PM index. The correlation between vapour pressure evaluation temperature and PM emissions that they found at a variety of evaluation temperatures can be seen in Figure 1.7.

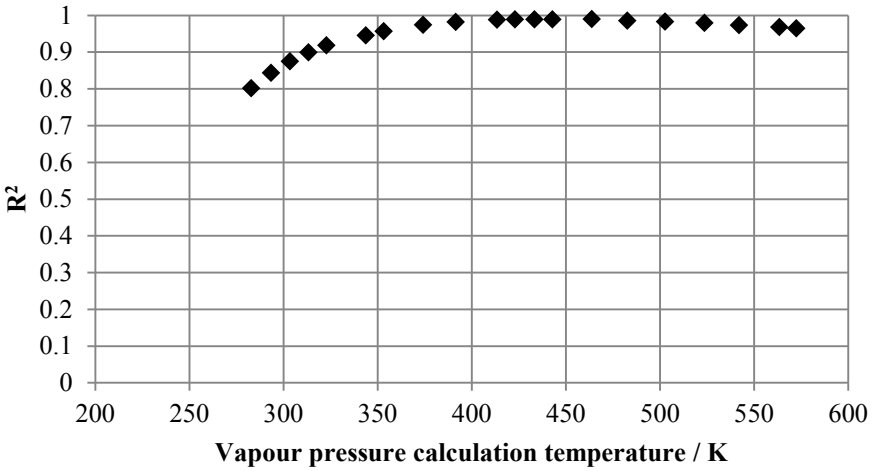

Figure 1.7: Determination coefficient between vapour pressure calculation temperature and PN emission (data from [50])

Aikawa *et al* found a very strong correlation ($R^2 = 0.95$) between their PM index and measured particulate emissions, this can be seen in Figure 1.8. PM emissions were measured over the NEDC, counting solid particles using a PMP compliant system [51].

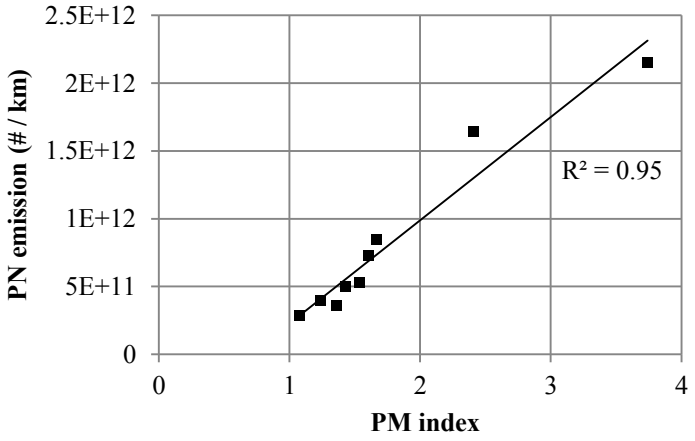

Figure 1.8: Relationship between PN (# / km) and PM index over NEDC (data from [50])

The work undertaken by Aikawa *et al* [50] used a PFI engine, and had no independent control of the fuel vapour pressure or DBE (their index parameters). Testing was done using four commercial fuels and a base fuel, to which eight different components were

added. Indolene (a US emissions testing reference fuel) was used as a base fuel, to which were added 10 % by mass of components such as 2,2,4-trimethylpentane, dodecane, ethylbenzene, and 1,2,4-trimethylbenzene. Their calculated PM index range of the fuels tested was 1.01 – 3.86. Splash blending these components in this way is unlikely to reflect real world gasoline performance.

In addition Aikawa *et al* [50] calculated the index range of over 1,400 worldwide fuels, based on a detailed hydrocarbon analysis of these fuels, and Figure 1.9 summarises the PM index distribution. Figure 1.9 shows a very broad range of the PM index of these worldwide fuels, with a mean of 2.12 and a standard deviation of 0.81. Based on these indices, a variation of approximately an order of magnitude on PM emissions from the same vehicle could be expected when tested using fuels at the observed extremes of the PM index.

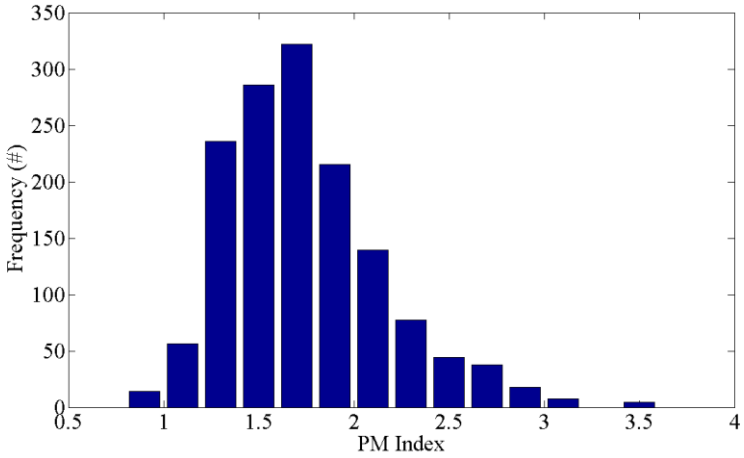

Figure 1.9: Range of PM indices of a selection of commercially available fuels worldwide (data from [50])

In a companion paper to Aikawa *et al*, Khalek *et al* [52] tested a 2009 model year WGDI vehicle over the FTP75 drive cycle with three different fuels representative of the spectrum of fuels available in the USA. Solid particle emissions were measured using an

engine exhaust particle sizer (EEPS) in compliance with CFR Part 1065 [53] (the US legally compliant counting method), for one fuel, there is a comparison between the EEPS and an AVL particle counter (APC) – a counter that would comply with a legally compliant counting system in Europe, which shows good agreement between the two counters.

Unfortunately Khalek *et al* do not calculate the PM index for their fuels tested, nor is it possible to calculate it from the information given, however they do list some of the fuel parameters relevant to PM emissions; these are shown in Table 1.2. To be able to calculate the PM index, a detailed hydrocarbon analysis would be needed, as would the vapour pressure at 443 K for each component. However, from the parameters given, one might expect the relative emissions from these fuels to be in the order A > B > C (using Aikawa *et al* methodology) or alternatively A > C > B (using the parameters listed earlier in this section).

Table 1.2: Test fuel composition in Khalek *et al* [52]

	Fuel A	**Fuel B**	**Fuel C**
RVP (psi)	8.97	14.7	8.96
Paraffins (% m/m)	54.8	46.2	41.6
Aromatics (% m/m)	40.9	43.9	31.6
Olefins (% m/m)	0.05	0.142	6.88
Oxygenates (% m/m)	0.00	0.00	10.1
T90 (°C)	158.9	131.5	175.3

The observed particulate emissions are shown in Figure 1.10, it can be seen that (using the FTP-75 composite data presented) they fall in the order C > A > B (this trend is also reflected in the particle mass data collected). It is of interest that Fuel C gives such a high result, perhaps in a WGDI engine a high T90 is a limiting factor, particularly as this fuel exhibited large peaks in PN during acceleration events.

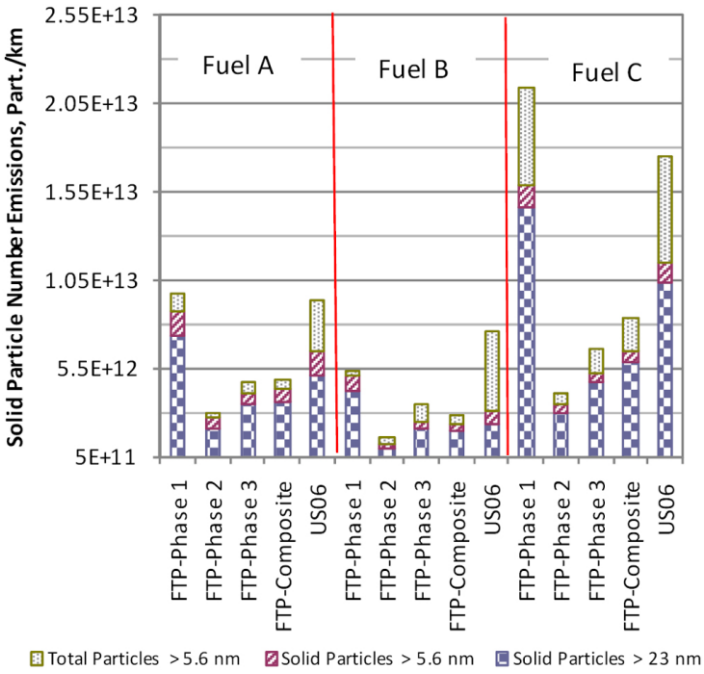

Figure 1.10: Observed PM emissions from three different fuels from Khalek et al [52], Reprinted with permission from SAE Paper No. 2010-01-2117 © 2010 SAE International. Further use or distribution of this material is not permitted without prior permission from SAE.

A paper developing the PM index concept by two of the same authors of the original paper - Aikawa and Jetter [54] – analyses the PM emissions (both mass and number) using 10 different commercial fuels from a 2.4 L WGDI engine vehicle over the FTP75 cycle and PN was measured according to PMP [51] and with an EEPS in parallel for particle size data. The compositions of the fuels tested can be seen in Table 1.3. Again calculation of the PM index required a full (and expensive) detailed hydrocarbon analysis.

Table 1.3: Test fuel composition in Aikawa and Jetter [54, 55]

Fuel	**A**	**B**	**C**	**D**	**E**	**F**	**G**	**H**	**I**[1]	**J**[1]
Aromatics (% m/m)	44.2	44.9	31.6	27.3	21.4	29.0	31.9	33.2	23.5	38.3
FBP[2] (°C)	197	151	210	206	196	205	284	212	211	187
PM index (1/kPa)	1.59	0.90	2.54	1.70	1.08	1.99	1.35	2.05	3.00	1.44

1. Fuels I and J are not commercial fuels, rather specially blended for low / high PN
2. RVP is not stated for these fuels, FBP is the measure of volatility given, it is not clear why, as FBP is not used in the PM index.

Similar to the previous work, Aikawa and Jetter report a close agreement between their PM index and the overall PM emissions over a weighted FTP75 cycle; this can be seen in Figure 1.11. However they also report that the correlation between the PM index and the PM emission decreases significantly for Phase 2 (more highway style driving) and Phase 3 (warm start) compared with Phase 1 (cold start). This suggests that perhaps their PM index is only valid for cold start, and that the relative weighting of the VP in their index accounts for this, although, as Aikawa and Jetter say, the lower overall PN expected from Phase 2 and 3 and hence worse signal to noise ratio (SNR) from the instrumentation may also account for this.

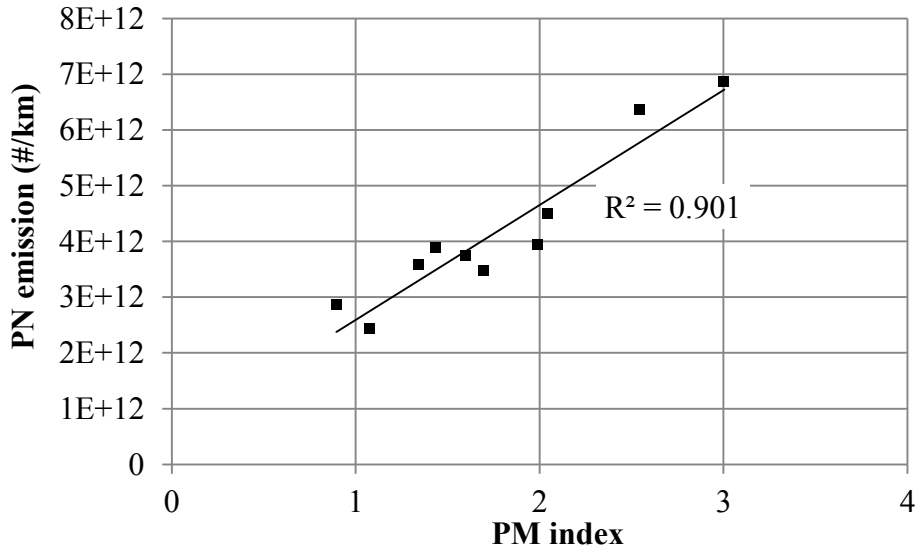

Figure 1.11: Relationship between PN (# / km) and PM index over FTP75 (weighted) (data from [54])

Aikawa and Jetter also analysed the particle size distributions from the 10 fuels, these are shown in Figure 1.12. It can be seen that the fuel composition has little effect on the size distributions observed by Aikawa and Jetter. It can also be seen that the distributions are unimodal, with the nucleation mode particles being removed both by the catalyst and the PMP sampling procedure.

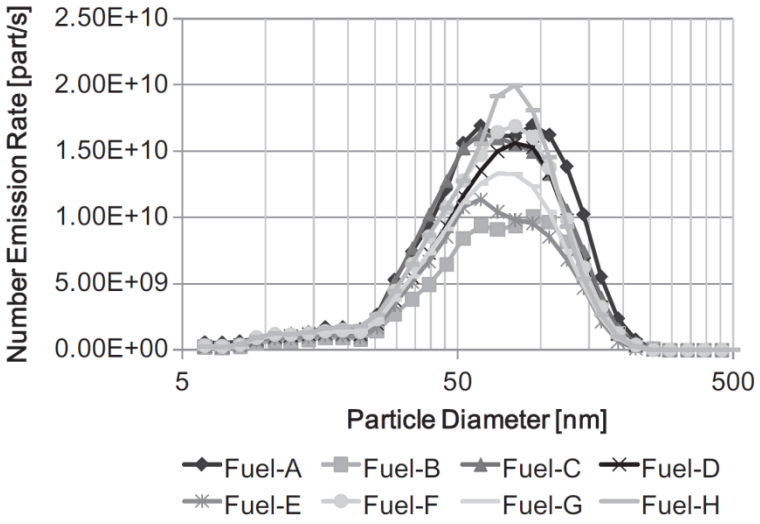

Figure 1.12: Fuel effects on particle size distributions found by Aikawa and Jetter [54], Figure courtesy of SAGE Publications

The California Air Resources Board (CARB) evaluated the PM index when they were drafting the LEV III emissions standards [56], and on the basis of two data points for fuels with very similar PM indexes (1.44 and 1.58), concluded that *"a correlation between PM Index and PM emissions could not be ascertained for the fuels tested"*. Their results are shown in Figure 1.13.

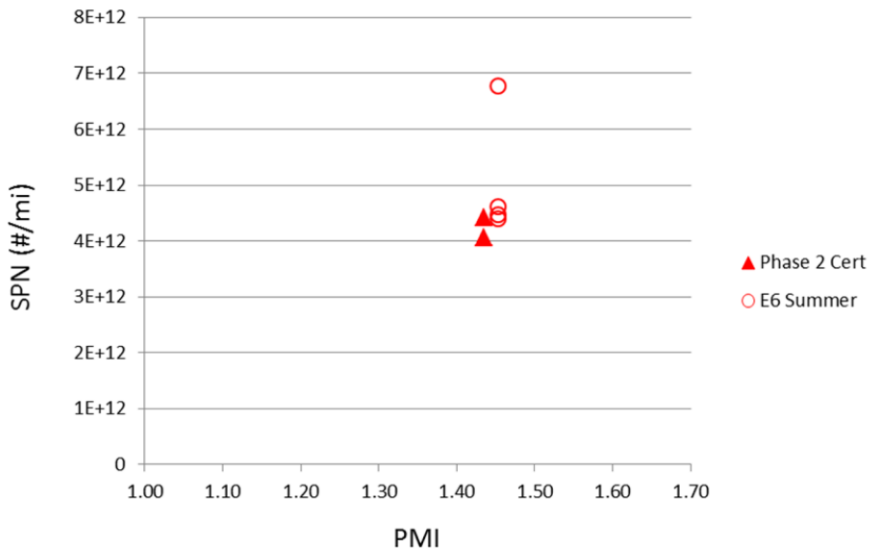

Figure 1.13: PM emission vs PM index from CARB report [56], figure courtesy of CARB

Elsewhere in the report, with five fuels tested, CARB conclude that *"Solid Particle Number emission rate remains unchanged, regardless of the fuel composition."* CARB also found little correlation between the PM index and PM mass emission for these five fuels, and on this basis have not pursued the PM index further. The CARB fuel selection was limited in scope however, and does not represent the spectrum of fuels available in the market that would be required for an effect on PN emissions to be seen.

1.3.2. Effect of fuel composition on other automotive emissions

The US EPA issued a report [57] comparing the effects of 5 gasoline parameters (T50, T90, Ethanol content, Aromatic content, and DVPE) on several emissions from vehicles including Total Hydrocarbons (THC), NO_x, CH_4, CO, and PM (mass only). A rigorous matrix of fuels was used, ensuring independent control over the parameters. The composition of the fuels is shown in Table 1.4. These fuels were tested on 15 different cars from the 2008 model year, selected on the basis of high sales, over the LA92 cycle (a Californian certification cycle, using a similar procedure to FTP75, but with a more aggressive drive cycle).

There is a large data set presented in the EPA report, which it is not possible to show all of here, the data is presented using a normalisation such that it is possible to compare the relative effects of the parameters on various emissions despite the fact that they have different magnitudes and units. It is interesting to note that this report found little correlation between PM mass and RVP, but a strong correlation between PM mass and T90, suggesting that while fuel volatility is important, how it is accounted for in any potential index is important.

Table 1.4: Fuel composition for EPA report on fuel effects on emissions [57]

Fuel	T90 (°C)	EtOH (% v/v)	DVPE (kPa)	Aromatics (% v/v)
1	149	10	69	15
2	171	0	69	15
3	149	10	48	15
4	171	10	69	15
5	149	0	48	35
6	171	10	48	15
7	149	0	48	15
8	149	0	69	15
9	171	0	69	35
10	171	10	48	35
11	149	10	69	35
12	171	10	69	35
13	171	0	48	35
14	171	0	48	15
15	149	0	69	35
16	149	10	48	35
20	149	20	48	15
21	149	20	48	35
22	149	20	69	15
23	171	20	48	15
24	171	20	69	15
25	171	20	69	35
26	171	15	69	35
27	171	15	48	15
28	149	15	48	35
30	163	10	69	35
31	163	20	48	35

Figure 1.14 shows the effect observed in the EPA report for the fuel parameters on various emissions, a positive coefficient implies that as this property is increased, the relevant emission increases, and the size of the arrow implies the strength of that change. The EPA also reports a number of data for the effects of these fuel properties on toxic compound emissions. The trend for PM, that increasing quantities of ethanol, aromatics, and increasing, T50, and T90 increases PM emissions, is as expected on the basis of other evidence in the literature; it is also of interest to note that acting to reduce PM through tweaking fuel composition should also have a positive effect on all other emissions with

the exception of CO. However improvements in catalyst technology should enable this expected increase in CO to be moderated.

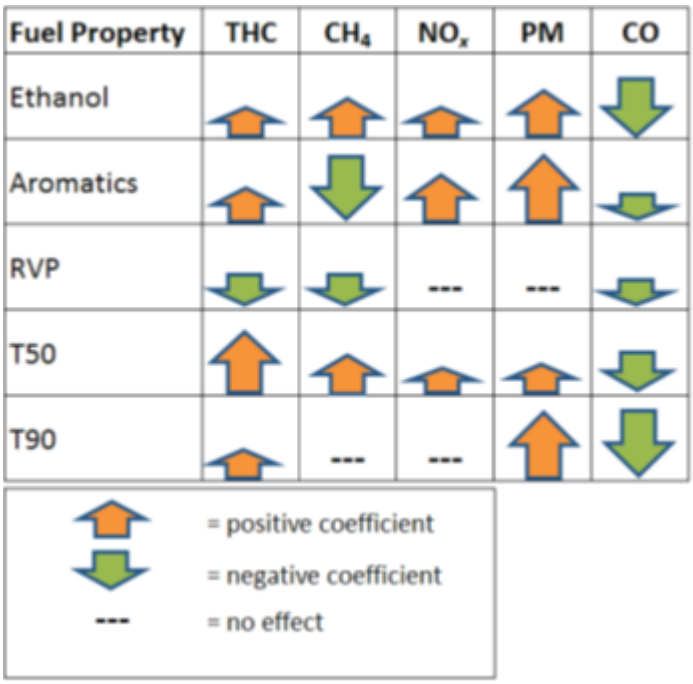

Figure 1.14: Effect of various fuel parameters on various emissions for cold start (adapted from [57])

1.4. Measuring particulate emissions

The earliest efforts to measure particulate emissions focussed on the heaviest emitting devices – at the time heavy duty Diesel engines and gas turbine engines fitted to aircraft (aircraft regulation was introduced in 1981 [58]). Measurement of these initially high emissions focussed on visible emissions, and the first measurement devices were smoke meters. A smoke meter [59] collects soot on a filter, shines light at this collected sample, measures the absorption of the light on the sample, and presents the results as filter smoke number (FSN) based on how black the filter has become and the volume of exhaust gas – this is an expression of particle mass. As emissions levels have decreased, the smoke levels in exhaust have decreased drastically, and this method has now reached its detection limit; other measurement techniques are required.

Given the increased concern over the health effects of particulate emissions, and the impact of particle number rather than mass on the health impact from particles, measuring particle number and size is very important. Condensation particle counters (CPC) [60] are the instrument used to measure particle number emissions according to the legislatively required PMP protocol [51]. They are fully described later in this thesis in Section 2.6, and provide a very accurate way of counting particles; however they can provide no particle size information

A differential mobility analyser (DMA) is a particle classifier, it uses electrical mobility techniques to effectively act as a band pass filter for particles. A DMA can be coupled to a CPC to give a scanning mobility particle sizer (SMPS), which is useful to obtain accurate size spectra of particulates from engines at steady state, however because of its scanning nature, its time response for a full spectrum is too long to obtain any transient information.

The differential mobility spectrometer (DMS) [61] uses the same properties of particles as a DMA to measure both their size and number. It operates over a size range of 5 nm-1 μm, which covers the spectrum of particles likely to be emitted from a vehicle, and it is fully described later in Section 2.5. The DMS is the particle size measurement instrument used throughout this thesis.

The engine exhaust particle sizer (EEPS) [62] developed by TSI operates on a very similar principle to the DMS. It can provide a size spectrum of 5-560 nm, and operates at atmospheric pressure (unlike the DMS), this means that because of the mobility inversion problem discussed in Section 2.5 it can only measure a more limited size spectrum, but the chances of volatile material evaporating off particles is reduced.

Another particle sizer is the electrical low pressure impactor (ELPI) [63]. An ELPI is a cascade impactor; it can measure size spectra from 30 nm-3 μm. Charged particles are classified on several electrometers in a cascade formation by inertial impaction; so this instrument measures aerodynamic diameter. As the lower cut off of its size spectrum is 30 nm the ELPI is unable to measure the nucleation mode; given that there is much interest in these small particles due to their health effects, this is a major drawback.

For the last 35 years, PM legislation has been based on a gravimetric method of quantifying PM mass emissions [64]. PM is collected from a filter in a manner prescribed by legislation, the filter is weighed before and after testing, and the difference is the PM mass emitted. Filters are generally made of glass fibre or glass fibre with a polyretrafluoroethylene (PTFE) coating, and a typical filter weighs 150 mg. As the PM mass emitted from modern engines can be as low as 10 μg over a drive cycle (for a vehicle equipped with a DPF) - this represents < 0.1 % of filter mass, great care must be taken in filter handling, filter conditioning, and the humidity and temperature of the weighing room must be carefully controlled. Nevertheless, at the lowest emissions levels, it is reported that these factors and measurement uncertainties can contribute up to 90 % of the mass increase observed [64, 65].

As particle mass is still a legislated quantity, and given the difficulties with smoke meters reaching their detection limits, and errors in gravimetric (filter mass) methods making up to 90 % of the observed particle mass at modern emission levels, other methods of measuring particle mass are available and being investigated with a view to forthcoming legislation.

A photo acoustic soot sensor (PASS) [66] measures mass by exposing a sample to infra-red light and detecting the resonance amplified acoustic standing wave with a

microphone, the amplitude of the standing wave is proportional to the carbon mass of the sample (it is unable to measure any adsorbed HC or sulphur fraction of particles).

A centrifugal particle mass analyser (CPMA) [67] uses opposing electrical and centrifugal forces to measure particle mass, it can be used to generate a particle mass spectrum, or to measure particle density. The CPMA is an important instrument as it can accurately measure particles with very small mass, and measures total mass of particles rather than just carbon mass.

A good overview of a wide variety of particulate emission measurement techniques and instruments both for particle number and particle mass is found in Giechaskiel *et al* [64, 68].

1.5. Emissions legislation in Europe

The European Union (EU) legislates for a variety of tailpipe emissions from vehicles, which must be complied with before a vehicle can be sold. Emissions (HC, CO_2, NO_x, CO, and particulates) are tested by 'driving' the vehicle (often with a robot driver) on a chassis dynamometer over a predetermined drive cycle. The emissions are measured, and normalised by the distance driven.

The current EU legislation is set down in Regulation (EC) No 715/2007 of the European Parliament and of the Council of 20 June 2007 [69] and Commission Regulation (EC) 692/2008 of 18 July 2008 [70], this is known as Euro 5, and its successor Euro 6. While the legislation legislates for a variety of different vehicle types, here the focus will be on category M1 - *"Vehicles designed and constructed for the carriage of passengers*

and comprising no more than eight seats in addition to the driver's seat" [70], and on positive ignition (PI) engines.

The dates for the promulgation of the Euro 5 and Euro 6 legislation for this category of vehicles are shown in Table 1.5.

Table 1.5: Dates of promulgation of European emissions legislation

Euro 5		Euro 6	
New type approval	**New registrations**	**New type approval**	**New registrations**
1 September 2009	1 January 2011	1 September 2014	1 September 2015

Euro 5 introduced a particle number limit for Compression Ignition (CI) engines of 6×10^{11} particles per km. This has had the result of effectively forcing the use of Diesel particulate filters (DPFs) on all new Diesel vehicles. Euro 5 does not limit particle number from PI engines.

Euro 6 will regulate particle number emissions from PI engines for the first time, the legislation mandates a particle limit of 6×10^{11} particles per km (the same as for CI engines), with a derogation to 6×10^{12} particles per km for three years (i.e. until 1 September 2017) [71]. It is of note that the introduction of a particle number limit effectively removes the need for a particle mass standard, as for most vehicles in this category; the number limit is around 100 times more stringent that the mass limit.

The legislation is tested over a defined drive cycle. The current drive cycle used in Europe is the New European Drive Cycle (NEDC). It consists of four repeats of a cycle representative of urban driving (the ECE-15 urban driving cycle), which covers a distance of roughly four kilometres in total, followed by one extra urban driving cycle. In total the cycle covers 11 km and takes 1180 s. The speed time trace of the NEDC is shown in

Figure 1.15. The NEDC is also used to provide the urban, extra-urban, and overall fuel economy figures for vehicles sold in the EU.

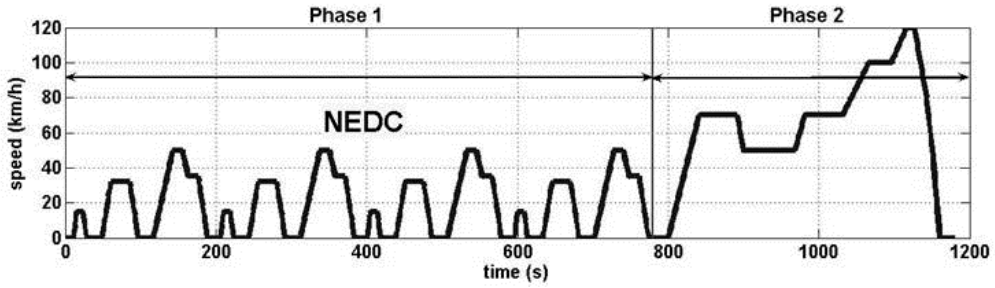

Figure 1.15: New European Drive Cycle speed – time trace, it can be seen that this is a relatively 'smooth' drive cycle with slow accelerations [47]

There are criticisms of the NEDC; it is a very light load cycle, and does not have any provision for taking into account the extras that are fitted to modern cars, such as electrical load and HVAC systems. The very slow accelerations and decelerations of the NEDC are not viewed as being very representative of real world driving, and this is reflected in the variation between advertised fuel consumption figures and those experienced by consumers.

In the USA a similar function is fulfilled by the FTP75 cycle, defined by the US Environmental Protection Agency (EPA). It can be seen that the cycle is much less smooth than the NEDC, the sharper accelerations in the FTP75 cycle are probably more representative of real world driving, and are likely to lead to higher fuel consumption, and higher emissions relative to the NEDC. Like the NEDC, the effect of electrical load and HVAC systems is not taken into account on the FTP75 cycle. The speed time trace of the FTP75 cycle is shown in Figure 1.16. Results are often presented as 'weighted' results, where the weighting factors of 0.43 for the cold start part of the cycle, 1.0 for the middle

part of the cycle, and 0.57 for the repeat of the first phase with a fully warm engine are used.

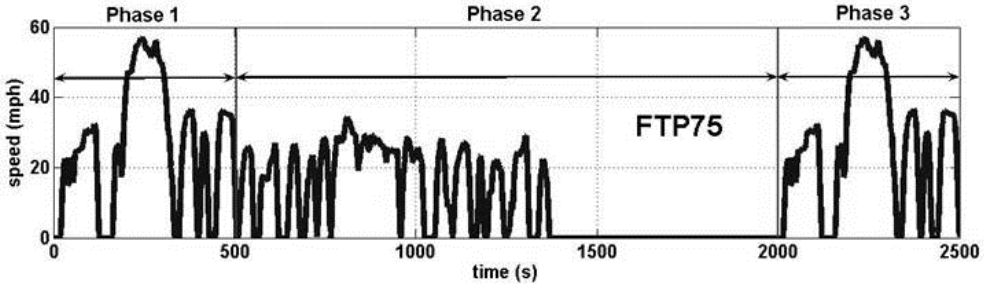

Figure 1.16: US FTP75 drive cycle speed – time trace, it can be seen that this is more 'spiky' drive cycle compared to the NEDC with fast accelerations [47]

At the time of writing there is an effort to overcome some of the limitations of the NEDC, and its poor reflection of real world driving. The Worldwide harmonized light vehicles test procedures (WLTP) is being developed by the European Union, Japan, and India under the auspices of the United Nations Economic Commission for Europe (UNECE) World Forum for Harmonization of Vehicle Regulations [72]. It was originally intended to be adopted as the test cycle worldwide, however it now seems that the USA will not participate. The Worldwide harmonized light vehicles test cycle (WLTC) divides vehicles into three classes based on their power to weight ratio (PWr), and there is a different cycle for each class. Most European mid-market vehicles have a PWr of around 50-100 kW/ton, and at the extremes, a Tata Nano has a PWr of 41 kW/ton and a Lotus Elise has a PWr of 179 kW/ton; so the 34 kW/ton lower limit for Class 3 effectively mandates its use for all European passenger vehicles.

The WLTP test procedure also imposes stricter limits than the NEDC or FTP75 on various parameters which influence the test, including road load, gear changes, and total car mass (including for example cargo and passengers). The speed time trace can be seen

in Figure 1.17, it can be seen from this that the cycle is much less smooth than the NEDC, and so should give a comparatively higher fuel consumption than the NEDC. With these new limits and a new cycle, it is hoped that the adoption of the WLTP will mean that testing procedure will more accurately reflect real-world driving (although such a reflection can never be too good, given the variety of driving conditions experienced) and that fuel consumption and emissions data will be more accurate.

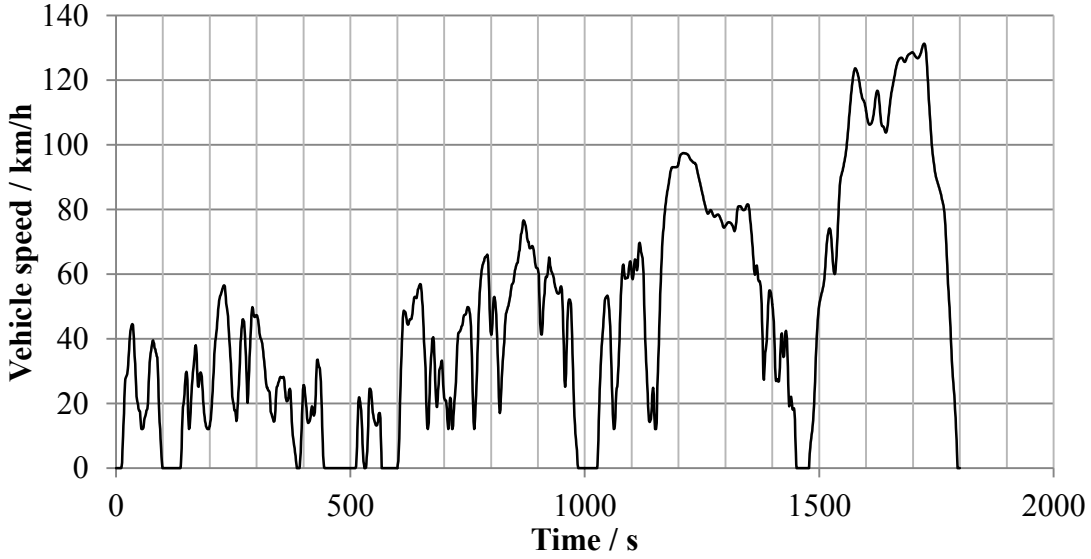

Figure 1.17: WLTC class 3 drive cycle speed-time trace (data from [72])

1.6. Legally compliant testing

The drive cycles mentioned in Section 1.5 form a part of a legally compliant emissions test. The legislation also specifies a sampling system and other aspects. In order to comply with Euro 5 and Euro 6, particulate emissions must be sampled in accordance with the technical requirements laid down in UN ECE Regulation 83 [73] which is based on the PMP protocol [51]. The sample from the exhaust is inducted into a stainless steel dilution tunnel, containing high efficiency particulate absorb (HEPA) filtered air, a sample is taken 10-20 tunnel diameters downstream of the induction point by a probe facing upstream and

parallel to the wall of the tunnel. Subsequently the sample is conditioned as described in Section 2.6 in accordance with the PMP protocol.

Such legally compliant testing is designed to ensure a fair test across many different vehicle types; however it is very expensive, and requires a lot of test equipment. Results representative of a legally compliant test can be obtained without vehicles from engines only. With good load mapping and a transient dynamometer, a drive cycle can be 'driven' on an engine and the results be representative of a legally compliant test. This is an invaluable research tool, and is obviously cheaper than a full legally compliant test; however for homologation purposes a vehicle will still need to be tested according to the protocol described earlier in this section.

Most engine testing is done on engines fitted with dynamometers not capable of such transient operation; the engines are only capable of steady state operation. In this case, useful data can still be obtained by using so called 'minimap' points. To achieve this, an engine fitted to a vehicle is mapped on a cycle residency plot through a drive cycle test, where at every moment, the load and speed of the engine is recorded. From this plot certain key test points can be identified based on points either with known high emissions, or based on frequency of residency over the drive cycle. An example cycle residency plot, and chosen minimap points for the NEDC, FTP75 and Highway (another US drive cycle) cycles is shown in Figure 1.18.

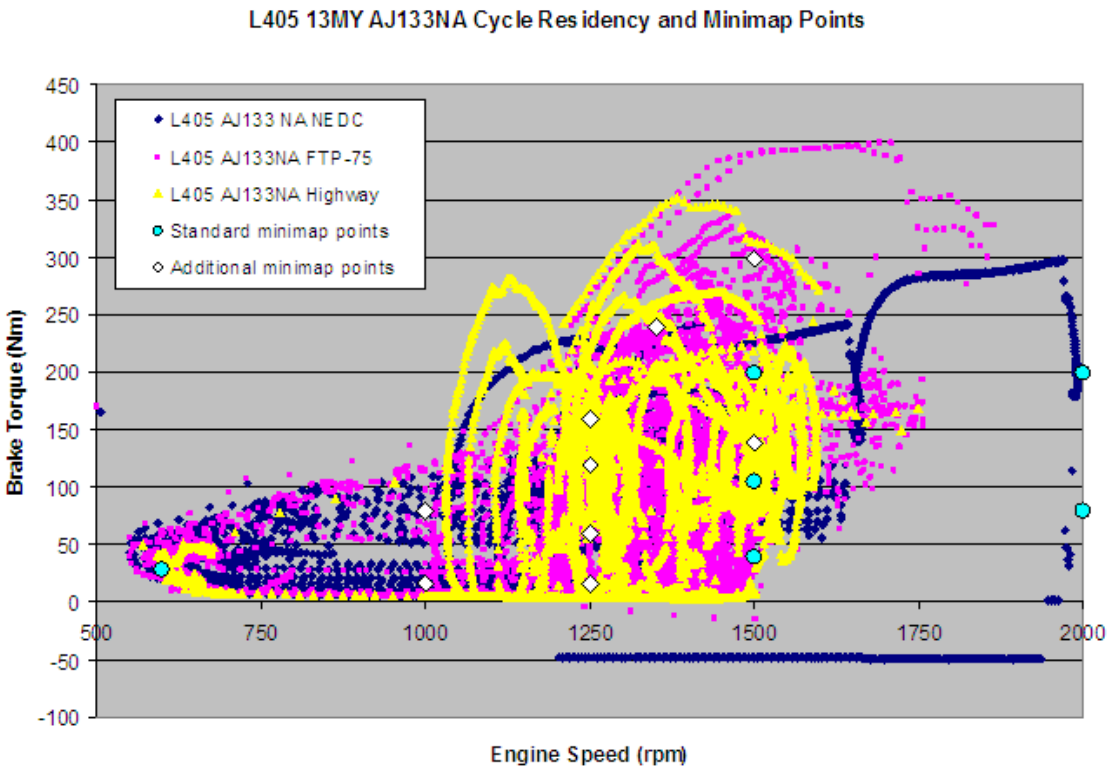

Figure 1.18: AJ133 drive cycle engine map residency diagram [74]

Using this method, it is possible to map a legally compliant test for a vehicle, onto a steady state, engine only, operation. Engines tested in this way will almost certainly not have the required sampling systems for a legally compliant test either, however for comparative research work, this minimap method ensures a cost effective, and quicker, approach to reducing emissions from vehicles.

1.7. Chapter 1 summary

In this Chapter, GDI engines have been noted as an emerging engine technology set to dominate the spark ignition market for the foreseeable future. GDI engines have superior fuel consumption and CO_2 emissions relative to PFI engines but higher particulate emissions. Particulate emissions have been shown to follow bilognormal distributions with differing formation mechanisms for the two modes, and GDI engine operating

conditions have been shown to have an effect on both the number of the particles emitted, and their size distribution.

Particulates are detrimental to human health, in particular increasing the likelihood of cardiopulmonary diseases, cancers, and dementia, indeed Diesel exhaust has been classified as a carcinogen by the WHO [1]. In addition the number of particles emitted has been shown to be more important from a health perspective, than their mass. Fuel effects on particulate emissions have been discussed, and DBE, oxygenate content, T90, and vapour pressure have been shown to be important fuel parameters for particulate emissions, and a PM index has been introduced. A large number of instruments for measuring particulate emissions have been discussed, and the information that can be obtained from each evaluated. Emissions legislation in Europe and the USA has been discussed, alongside legally compliant test methods, which give repeatable results.

2. Experimental equipment and data processing

2.1. Single cylinder engine with optical access

The primary engine used in this work has been a single cylinder engine with optical access. The spray guided direct injection combustion system in this engine is essentially the same as on the Jaguar AJ133 V8 engine, which has also been used, and is described in Section 2.2. A schematic of the AJ133 combustion system is shown in Figure 2.1.

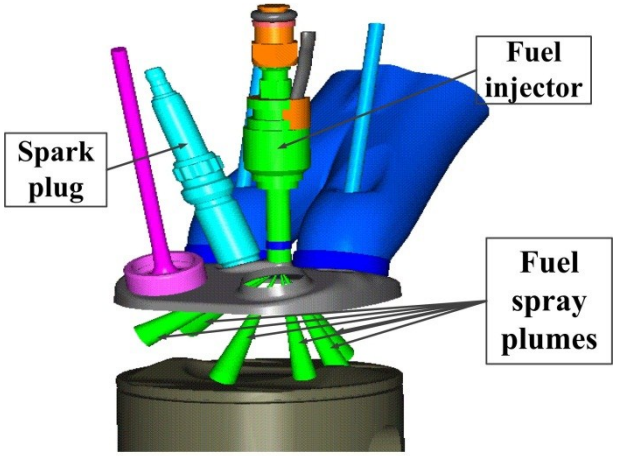

Figure 2.1: Layout of AJ133 combustion system showing a centrally mounted fuel injector and spark plug (adapted from [75])

The combustion system consists of a centrally mounted spark plug and fuel injector, which operates at fuel pressures of up to 150 bar and is capable of multiple injections per cycle. The six jet spray is guided such that four jets spray downwards into the combustion chamber, and two straddle the spark plug, this gives the potential for stratified operation.

Although using a single cylinder engine is not a totally accurate representation of 'real world' performance, the advantages of using a single cylinder optical access engine

include no cylinder – cylinder variations in compression or mixture preparation. These are primarily caused by limited manufacturing tolerances and differing cycle by cycle injector performance. Compared with a 'real' engine with similar cylinder size fuel consumption will be reduced as will the torque output, such that a smaller capacity dynamometer can be used. The reduced fuel consumption is particularly useful in this case, as pure fuel components, which can be very expensive, are being used.

Another advantage of using this single cylinder engine is the optical access capability. There are two main optical accesses used; the first through a fused silica window in the piston crown, using a mirror arrangement allowing images of the fuel spray and combustion to be reflected out through the 'Bowditch' piston. The arrangement is shown in Figure 2.2.

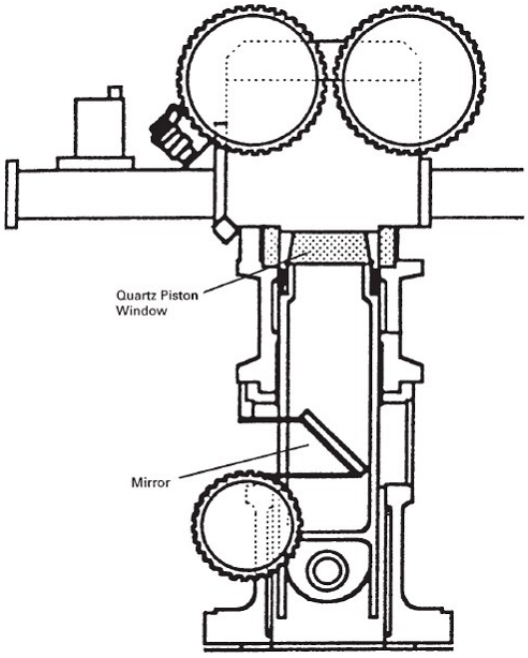

Figure 2.2: Optical engine schematic showing the Bowditch piston with a quartz window and mirror arrangement [76]

The second optical access is through a fused silica window in the pent roof of the combustion chamber. This is not large enough to allow camera access, but gives access for illumination, either using laser techniques (not used here) or LEDs which can be used to illuminate the fuel sprays.

The engine can operate both PFI and SGDI modes, up to 2000 rpm (limited by the mass of the Bowditch assembly). The salient features of the engine are shown in Table 2.1.

Table 2.1: Single cylinder engine parameters

Bore (mm)	89
Stroke (mm)	90.3
Cylinder capacity (cc)	562
Compression ratio	11.1 : 1
Fuel injection pressure (bar)	150
IVO (CAD aTDC)	33.5
IVC (CAD aTDC)	241.5
EVO (CAD bTDC)	245
EVC (CAD aTDC)	5

2.1.1. Optical engine builds

As the engine has optical components it does not possess the same heat transfer characteristics as 'real' engines; aluminium has a thermal conductivity of 205 $Wm^{-1}K^{-1}$, and fused silica 1.3 $Wm^{-1}K^{-1}$ [77]. In addition the need for line of sight optical access means that the design of the combustion chamber and piston is necessarily different to that of the AJ133 V8. It is clear that the engine will not have the same thermodynamic properties as the AJ133 on which it is based. As the thermodynamic properties will change with different engine configurations, results obtained with different configurations cannot be compared directly.

The engine can be operated in a number of different configurations ranging from a full optical liner with a full bore optical piston – allowing a large amount of optical access, to an aluminium piston, with an aluminium annulus between the cylinder barrel and cylinder head, only allowing optical access through the pent roof. There are an increasing number of restrictions on engine operation as more optical components are added, as they are more fragile than their metal counterparts. In this work the particulates data is obtained using a titanium piston, with a steel blank, with a mid-height steel cylinder barrel with an aluminium alloy annulus above, this is the closest configuration to that of a thermodynamic engine (although in no way mimics a thermodynamic engine), and allows the widest range of engine operation. The engine configuration for taking spray images is using a titanium piston, with a fused silica window, with a mid-height metal liner with an aluminium alloy annulus modified to accept a fast FID probe.

2.2. AJ133 V8 engine

The AJ133 5.0 L naturally aspirated V8 engine was used for steady state testing of the PN index. The engine has been fully described by Sandford *et al* [75]. The configuration is the same as the single cylinder engine described in Section 2.1 (which is based on the design of this engine), with a centrally mounted spark plug and fuel injector. The engine has four camshafts, two inlet and exhaust, with each inlet camshaft fitted with a low lift, and a high lift cam, which enables good full load performance, whilst maximising low load fuel economy. The engine is fitted with two three-way-catalysts (TWCs), one to each bank of four cylinders. The specifications of the engine are show in Table 2.2, and a cross-sectional view of the engine is shown in Figure 2.3.

Table 2.2: Specifications of the AJ133 V8 engine

Type	V8
Bore × Stroke	92.5× 93.0 mm
Displacement	4999 cm^3
Valves per cylinder	2 intake, 2 exhaust
Compression ratio	11.5 : 1
Maximum fuel pressure	150 bar

Although the engine is capable of 283 kW (385 hp) at 6500 rpm and a maximum torque of 515 Nm, the dynamometer that it is fitted to restricts its operation to 56 kW, 2800 rpm, and 280 Nm - relatively light load, low speed conditions. The data acquisition system for the engine has been comprehensively described by Twiney [78].

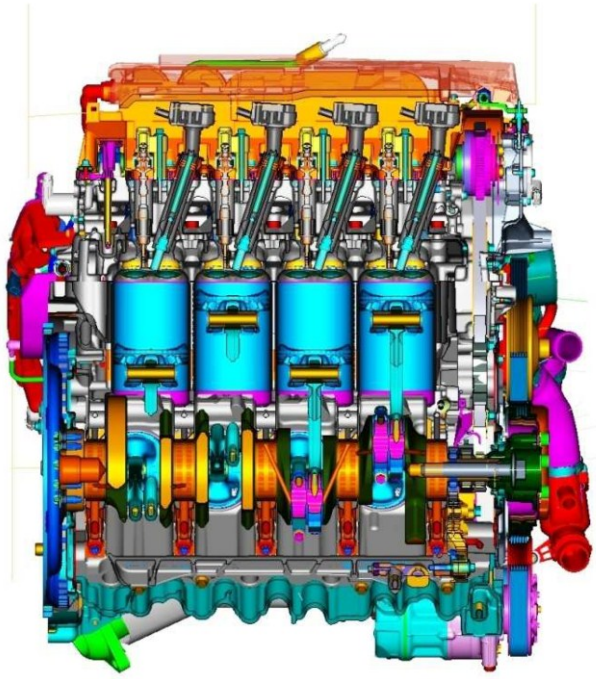

Figure 2.3: Cross section through the AJ133 engine [75], Reprinted with permission from SAE Paper No. 2009-01-1060 © 2009 SAE International. Further use or distribution of this material is not permitted without prior permission from SAE.

2.3. AJ126 V6 supercharged engine

The drive cycle work was performed on an AJ126 3.0 L V6 supercharged engine. The AJ126 is based on AJ133 V8 technology (see Section 2.2); the V6 shares its all-aluminium

construction with the AJ133, and again is fitted with four camshafts in the same way as the AJ133. The supercharger is mounted in the 'V' of the engine and is a Roots-type twin vortex supercharger. The engine is fitted with a water-cooled intercooler, and Bosch engine management software. The engine is fitted with two close coupled standard three-way-catalysts. Table 2.3 shows the engine specification, and an image of the engine is shown in Figure 2.4.

Table 2.3: Specifications of the AJ126 V6 engine

Type	V6
Bore × Stroke	84.5× 89.0 mm
Displacement	2995 cm^3
Valves per cylinder	2 intake, 2 exhaust
Compression ratio	10.5 : 1
Maximum fuel pressure	150 bar

The engine was fitted to a transient dynamometer and was controlled by a ‘turn-key’ CP Engineering system, the engine test cell was also fitted with a full emissions analysis suite including a Horiba MEXA.

Figure 2.4: CAD image of the AJ126 V6 supercharged engine [79]

2.4. UB100 ULTRABOOST engine

Downsizing engines is one of the techniques being considered to increase fuel economy and reduce CO_2 emissions from internal combustion engines. The engine produced by the ULTRABOOST project is designed to be a 60 % downsized engine to achieve a 35 % reduction in fuel consumption and CO_2 emissions. The engine is described in Turner *et al* [80], and a comprehensive outline of the design process has been given by Turner *et al* [74, 81]. The key specifications of the UB100 engine are given in Table 2.4, and an image of the engine is shown in Figure 2.5.

Table 2.4: Specifications of the UB100 engine

Type	Inline 4 cylinder
Bore × Stroke	83 × 92 mm
Displacement	1991 cm^3
Valves per cylinder	2 intake, 2 exhaust
Compression ratio	9:1
Maximum fuel pressure	200 bar
Peak BMEP	35 bar
Peak cylinder pressure	150 bar

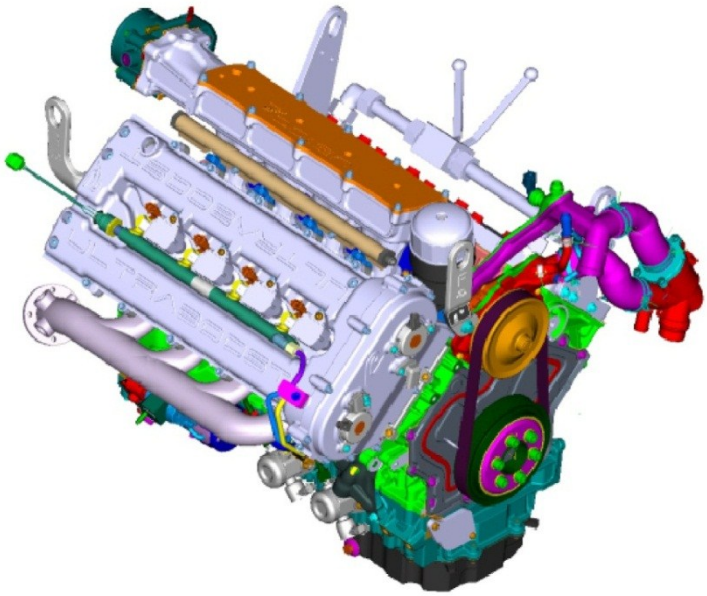

Figure 2.5: CAD view of the UB100 engine showing AJ133 base engine, new cylinder head, and coolant bypass (adapted from [74])

The aim of the ULTRABOOST project has been to produce a 2.0 L I4 engine with the same torque curve and power output as the naturally aspirated AJ133 5.0 L V8 engine. Such aggressive downsizing means that the UB100 operates at a BMEP of up to 35 bar (AJ133 maximum BMEP is 12.6 bar), and peak cylinder pressures reach 150 bar (AJ133 peak cylinder pressure is 85 bar). The downsizing has been achieved by blanking off and bypassing the coolant of one bank of cylinders on an AJ133 engine, fitting liners to the remaining four cylinders to reduce their capacity to approximately 500 cc each, and fitting an all new cylinder head. The water, oil, and high pressure fuel pumps are all AJ133 standard components, as are the cams, main bearings, and fuel injectors (although the injection pressure has been raised slightly).

The UB100 engine is a 'proof of concept' design, and not all of the features of the ultimate engine are included. In particular, the turbocharger (which will be a Honeywell GT30) and supercharger (which will be a clutched Eaton R410TVS) are not fitted; rather their effects are mimicked using an external charging system.

2.5. DMS500

One of the more successful techniques for measuring particulates in exhaust has been exploiting the electronic mobility of particles. Both the differential mobility spectrometer (DMS) and differential mobility analyser (DMA) use this technique.

The DMS used throughout this work has been the Cambustion DMS500. It uses the electronic mobility of particles to classify them in to 22 'bins', and post processing to fit two spectra to these, a raw spectrum and a bilognormal fit. The latter can be used not only to obtain a number spectrum, but also to obtain a mass spectrum. The DMS500 used can measure particles of size $5 < d_p < 1000$ nm.

The following describes the set up for the DMS500 when sampling engine exhaust; the set up would be slightly different when sampling other aerosols. Initially the sampled aerosol is passed through a cyclone, then through a 10 : 1 diluter. The sample pressure is then dropped to 250 mbar by a restrictor and the sample flows into the DMS via a heated sample line. Once inside the DMS the sample passes through a charger before entering the classifier column (Figure 2.6); there, particles with a larger electrical mobility diameter move further down the column before impacting a ring. How far each particle travels before impacting a ring is a function of aerodynamic drag and particle charge, both related to size.

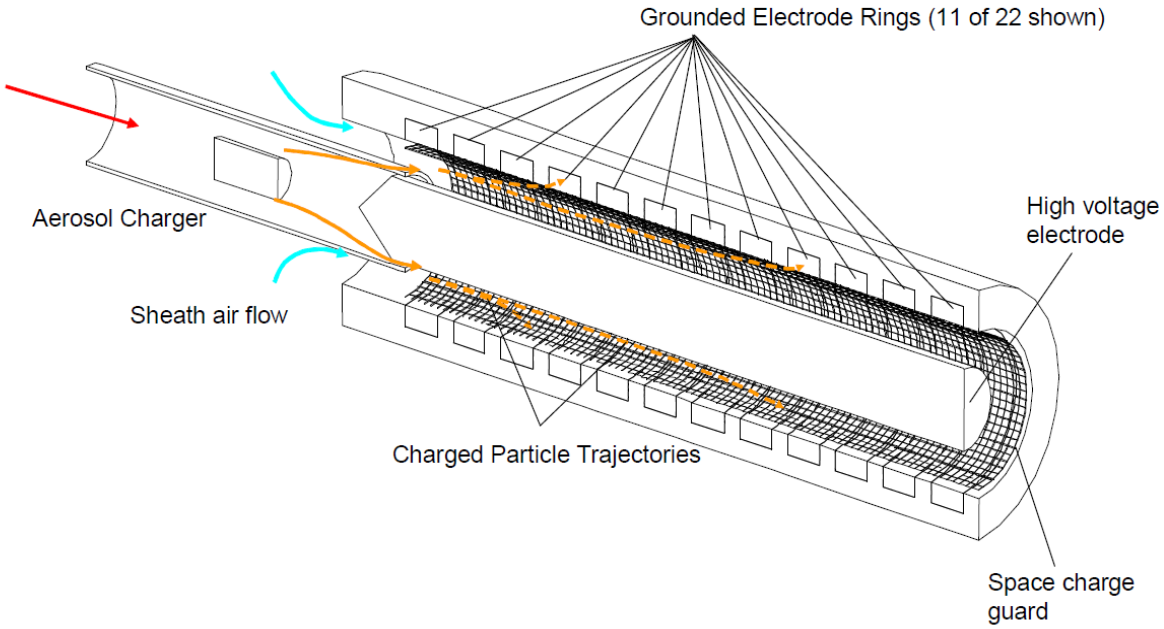

Figure 2.6: DMS500 classifier column schematic, engine exhaust enters in the top left of the image, and particulates impact one of the grounded electrode rings shown in the centre to bottom right [61], figure courtesy of Cambustion

The cyclone removes particles larger than 1000 nm, which cannot be measured by this instrument, and would otherwise foul the DMS. The reduced sample pressure decreases the transit time of the aerosol down the heated sample line and discourages particle formation / growth. It also enables the response time of the device to be

approximately 0.25 s. Additional discussion of the advantage of this low sample pressure due to the mobility inversion point is on page 53. The sample line is approximately 5 m in length and its temperature can be user selected; in this work it has been heated to 150 °C, to minimise any vapour phase condensation.

The classifier column consists of a central HT voltage electrode, surrounded by 22 grounded electrode rings, each connected to a high sensitivity electrometer. Particles are guided down the classifier column by the sheath air flow, and are deflected by the electric field from the high voltage electrode onto one of the electrode rings. This produces a very small (of order 1 fA) current, which is recorded by an electrometer, and hence the logging software.

2.5.1. Particle charging

A corona discharge charger has a single fine wire as an ion source, which bombards the sample with a steady stream of charged ions that charge the particles in the sample. Particles of the same size may acquire different charge levels; this would result in them experiencing different electrostatic forces and hence impacting on different classifier rings, in effect causing an incorrect size to be measured. The charge distribution experienced by particles is normally distributed, and dependent on their size. A particle of 10 nm diameter has a distribution centred around +1 charge, with approximately an 80 % chance of carrying that charge, whereas a particle of 80 nm diameter distribution centred around + 4 charge and has around a 40 % chance of carrying that charge. A more detailed study of particle charging in a corona discharge charger can be found in Biskos *et al* [82]. Given this well understood behaviour, this effect is compensated for in the calibration of the DMS.

2.5.2. Electrical mobility

As particle size increases, the electrical mobility of a particle becomes a weaker function of its size. This occurs because the particle size increases beyond the mean free path of the gas in which it is carried. Above this point, charge and drag become roughly equal functions of diameter, and classifying the particles becomes more challenging. The point at which this occurs is called the mobility inversion point. The DMS avoids the problem by operating at a reduced pressure of 250 mbar; this increases the mean free path of air, and shifts the mobility inversion point to a size greater than 1000 nm. This can be seen in Figure 2.7; the mobility inversion point occurs at the minimum of this graph.

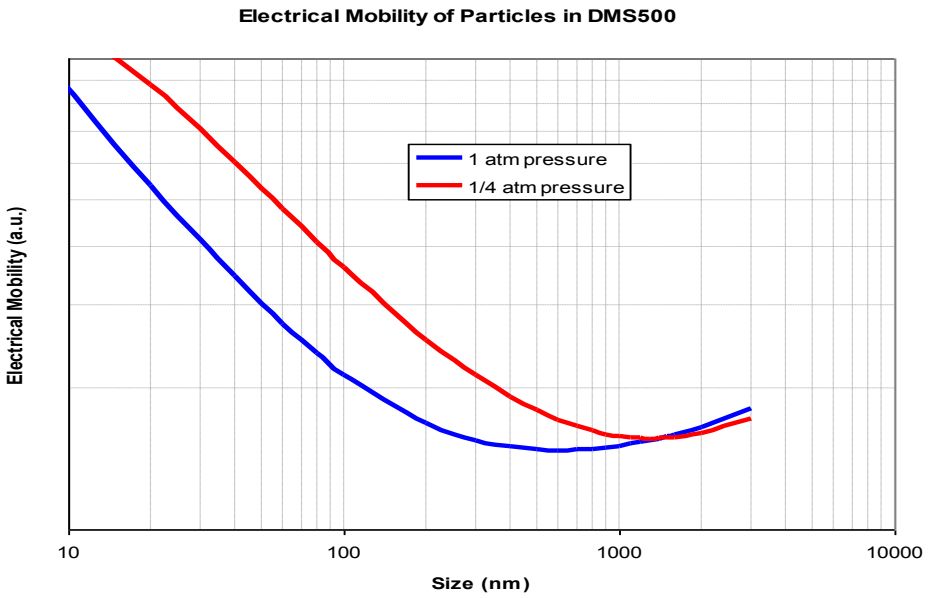

Figure 2.7: Effect of pressure on mobility inversion point showing that decreasing the classifier operating pressure to 250 mbar moves the inversion point > 1000 nm [83], figure courtesy of Cambustion

For this reason the cyclone has a more important role than just keeping the device clean; it must remove particles greater than 1000 nm to avoid them being mistaken for a particle with similar electrical mobility but a smaller diameter.

2.5.3. Obtaining a particle spectrum

It is desired to obtain the particle size distribution from the ring currents. The most basic conversion is:

$$\boldsymbol{i} = \boldsymbol{A}\boldsymbol{s} + \boldsymbol{e} \qquad (2.1)$$

where $\boldsymbol{i}$ is the ring current, $\boldsymbol{A}$ the instrument transfer function, $\boldsymbol{s}$ the real particulate size spectrum, and $\boldsymbol{e}$ the error in the conversion.

The DMS500 generates a raw spectrum of the particle distribution using an empirically determined inversion matrix using least squares minimisation with smoothing. These inversion matrices are supplied by the manufacturer and are specific for each instrument and the type of sampling being undertaken. These are effectively the transfer function, converting the raw ring currents into a size distribution spectrum.

2.5.4. Lognormal fitting

If it is now assumed that the transfer function in Equation 2.1 is lognormal the following can now be stated:

$$\boldsymbol{i} = n\boldsymbol{A}\boldsymbol{L}\left(\mu, \sigma_{\mathrm{g}}\right) + \boldsymbol{e} \qquad (2.2)$$

Where n is the particle number concentration in each mode, μ the count mean diameter (CMD) of the lognormal fit and σ_{g} the geometric standard deviation (GSD) of the fit. If it is assumed that aerosols follow multi-lognormal fit, for $\boldsymbol{m}$ log-normal fits to a spectrum:

$$\boldsymbol{i} = n_1\boldsymbol{A_1}\boldsymbol{l}\left(\mu_1, \sigma_{\mathrm{g1}}\right) + n_2\boldsymbol{A_2}\boldsymbol{l}\left(\mu_2, \sigma_{\mathrm{g2}}\right) + \cdots + n_{\mathrm{m}}\boldsymbol{A_{\mathrm{m}}}\boldsymbol{l}\left(\mu_{\mathrm{m}}, \sigma_{\mathrm{gm}}\right) + \boldsymbol{e} \qquad (2.3)$$

For a gasoline aerosol, a bilognormal fit is normally appropriate ($m = 2$). For a Diesel aerosol, trilognormal can be assumed ($m = 3$) (this takes into account the coarse mode described in Chapter 1) [3]. Such an approach also allows different transfer functions and calibrations for each differing aerosol component (e.g. accumulation and nucleation modes). The solution to n, μ, and σ_g in these equations is determined by minimising $\boldsymbol{e}$.

This minimisation is accomplished using a Bayesian algorithm, the details of which are discussed in Symonds [84].

Using lognormal fits brings several benefits. Less data are stored; only the CMD, GSD, and concentration of each mode need to be stored – rather than many datum points for a raw spectrum. Analysis of logarithmic fits is much easier than for a raw spectrum, and it provides a much clearer indication of the composition of the sample. It splits the modes allowing analysis to be conducted on accumulation and nucleation modes separately. Finally use of lognormal fits can suppress noise drastically - by a factor of up to 10^7 [84], particularly suppressing the noise at higher particle diameters. This is particularly important as noise in such parts of the spectrum can skew the particle mass distributions greatly.

It should be noted that the lognormal fits (blue and green lines in Figure 2.8) would not, when summed, result in the raw spectrum exactly. They are both fits, and calculated independently. The process of generating these differing interpretations of the data is shown in Figure 2.8.

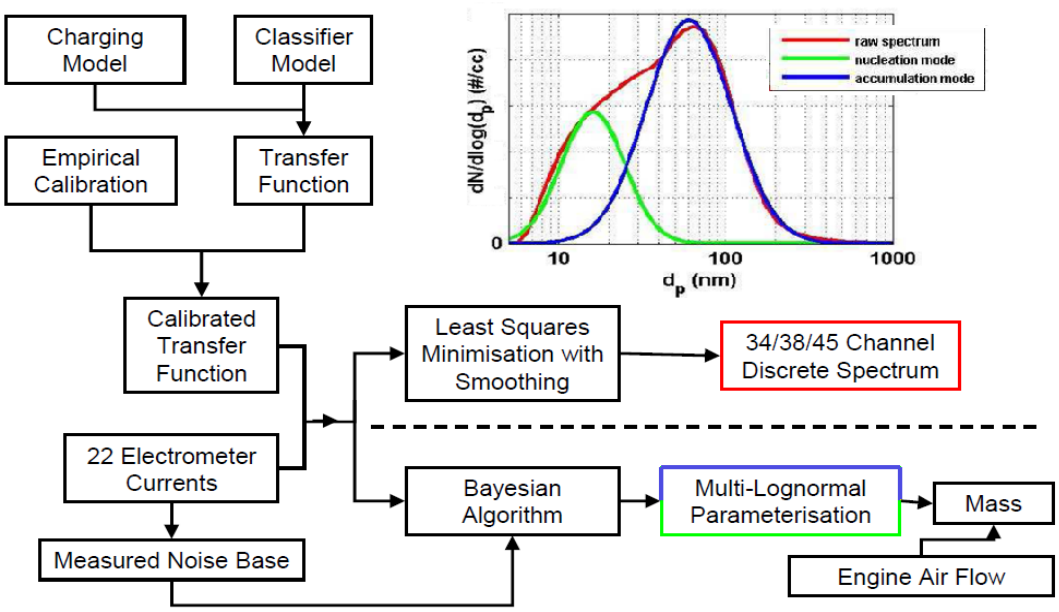

Figure 2.8: DMS500 data processing synopsis (adapted from [85])

The DMS500 measures and displays its RMS noise base, which is calculated when the auto-zero function is used. This noise base is valid only for the settings of gain and sample averaging used at that time. If the measured spectrum is within the RMS noise, lognormal fits will not be applied. A typical noise spectrum is shown as the blue area on Figure 2.9 and the noise is also recorded in the output file. The noise tends to increase as the DMS becomes dirtier, and for this reason, as a rule of thumb, the detection limit across the size range is around 10^5 particles per cc.

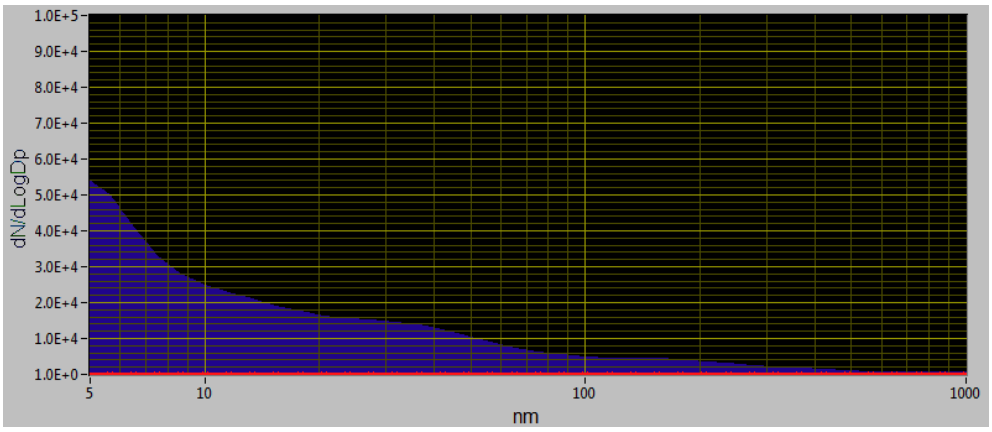

Figure 2.9: Example DMS500 noise spectrum showing an expected spectrum from a clean DMS

2.5.5. Mass calculation

A powerful result from use of the lognormal fits is the ability to use the Hatch-Choate conversion equations [15]. These allow any type of average diameter to be calculated from the log-normal parameters using an equation of the form:

$$d_{\mathrm{A}} = CMD\exp\left[b\ln^2\sigma_{\mathrm{g}}\right] \qquad (2.4)$$

b takes different values for different average diameters. Figure 2.10 shows the distribution of various average diameters that can be calculated using Hatch-Choate.

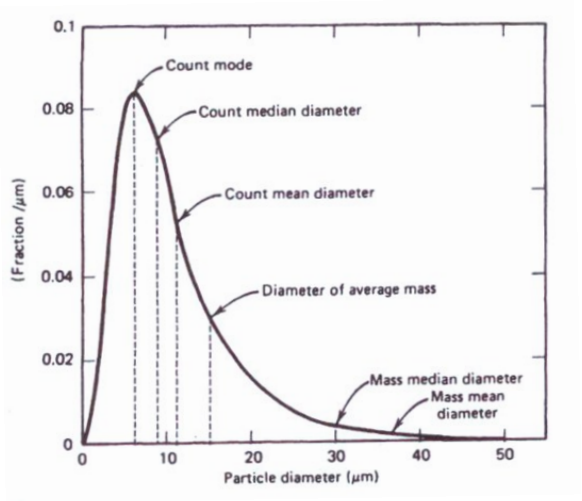

Figure 2.10: Hatch-Choate equation useful diameters [15], figure courtesy of John Wiley and Sons

For this application the most useful is the diameter of average mass ($d_{\bar{m}}$) where $b = 1.5$. This can be multiplied by the total number of particles to get the total mass.

This can then be extended to the d_p as calculated with the lognormal fits to:

$$\mathrm{m}(\mu g) = 1.72 \times 10^{-15} {d_{\mathrm{p}}}^{2.65}(\mathrm{nm}) \qquad (2.5)\ [84]$$

This equation has been used to calculate the mass spectrum from the particle size spectrum, and can be used to do so in real time.

2.5.6. Issues associated with fitting

Certain particle spectra can present problems for bilognormal fitting, particularly if the spectrum is from an engine that has not been measured before, operating outside a

'normal' region, or operating on an unusual fuel. To get an acceptable two mode distribution, correctly identifying the nucleation and accumulation modes, it is necessary to put size limits on the peaks of a spectrum (e.g. it should not be possible to have an accumulation mode peak at 10 nm). If the distribution of the spectrum is such that one or both of the peaks is very close to that limit, natural variations will cause the measured peak to shift either side of a limit and a phenomenon where the modes can split is observed. Figure 2.11, showing the magnitude of the lognormal fits and the raw spectrum, shows this clearly. A roughly constant magnitude of raw spectrum (the red line) should be being tracked by the yellow and green nucleation mode and accumulation mode lognormal fits. One of the checks - that the magnitudes of each of the two modes sum to approximately the magnitude of the raw spectrum - holds. However it can be seen that the modes have approximately the same value some of the time (it turns out this is the poor fitting case), and some of the time their magnitudes differ by a factor of two or three, with a step change between these two cases. This corresponds to virtually no change in the magnitude of the raw spectrum, or (on observation) to the particle size distribution.

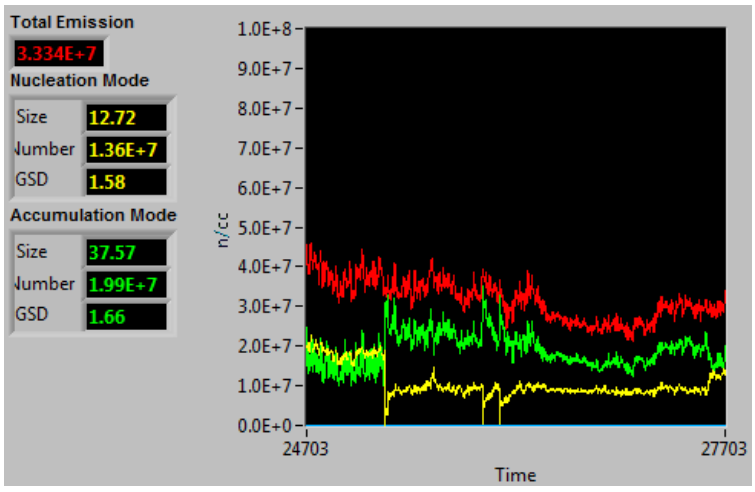

Figure 2.11: An example of mode splitting, it can be seen that the nucleation mode and accumulation modes have a step change in magnitude (in equal but opposite directions) at t ≈ 25200 and back at t ≈ 27500, throughout out the magnitude of the total emission remains roughly constant

The size distribution for the case where the each of the bilognormal fits have almost the same magnitudes is shown in Figure 2.12. It can be seen from the figure that the bilognormal fitting is poor, in this case because the limit on the accumulation mode fit is a minimum diameter of 30 nm, and in this case, the raw spectrum peak is at approximately 28 or 29 nm.

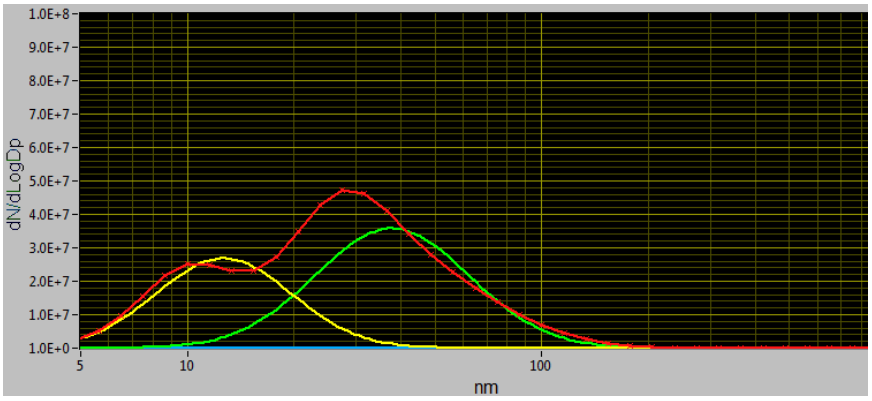

Figure 2.12: An example of a size spectrum where the bilognormal fitting is poor due to a limit on the logfitting algorithm of accumulation mode diameter > 30 nm, and the raw spectrum shows an accumulation mode diameter ≈ 28 nm

As the magnitude of the accumulation mode fit is often used alone (as it has been shown to replicate the results from the legislatively compliant PMP tests [5]) this mode splitting can be a big problem, and lead to misleading results. The method adopted to avoid this problem involves applying a digital filter to the raw spectrum.

2.5.7. Digital filtering

Regulation compliant particle counters [51] are required to have a 50 % count efficiency at $d_p = 23$ nm, and > 90 % count efficiency at $d_p = 41$ nm. This can be modelled using a Wiebe function, with appropriate parameters, as shown in Equation 2.6, and plotted in Figure 2.13.

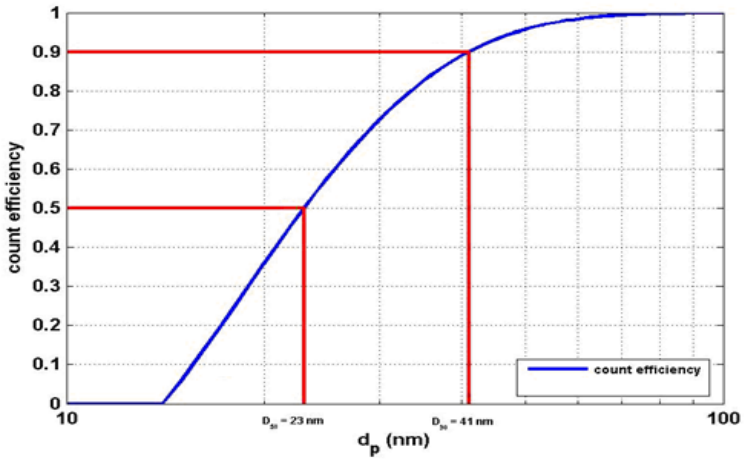

Figure 2.13: Wiebe function showing a 50 % count efficiency at 23 nm and a 90 % count efficiency at 41 nm (adapted from [86])

$$f = 1 - \exp\left[-3.54\left(\frac{d_\mathrm{p} - 14}{40}\right)^{1.09}\right] \ (\mathrm{d}_p \geq 14)$$
$$f = 0 \ (d_p < 14) \tag{2.6}$$

This digital filter can be multiplied by the raw particle spectrum (note not the raw current values) which is output from the DMS500. This can, to an extent, fulfil the same function as lognormal fitting, as the application of this filter will not only provide a good comparison with other particle counters, but also suppress the high levels of noise below 23 nm, which are associated with the nucleation mode, and are removed both in a PMP compliant particle measurement process and in a three way catalyst, with which all modern PI vehicles are fitted. This will avoid the lognormal fitting problem described above, whilst still meaning that comparisons with legally compliant tests and other particle counting systems are possible. This method, however, does not suppress the noise at higher particle diameters, so care must be exercised when converting such a number spectrum to a mass spectrum.

A comparison between sample data sets either showing the magnitude of the accumulation mode fit, or the magnitude of the Wiebe filtered data is show in Figure 2.14. It can be seen for many data sets (where this problem does not occur) the overall magnitudes of PM emissions are very similar, but for some data sets, where the fit is poor, it can make a large difference.

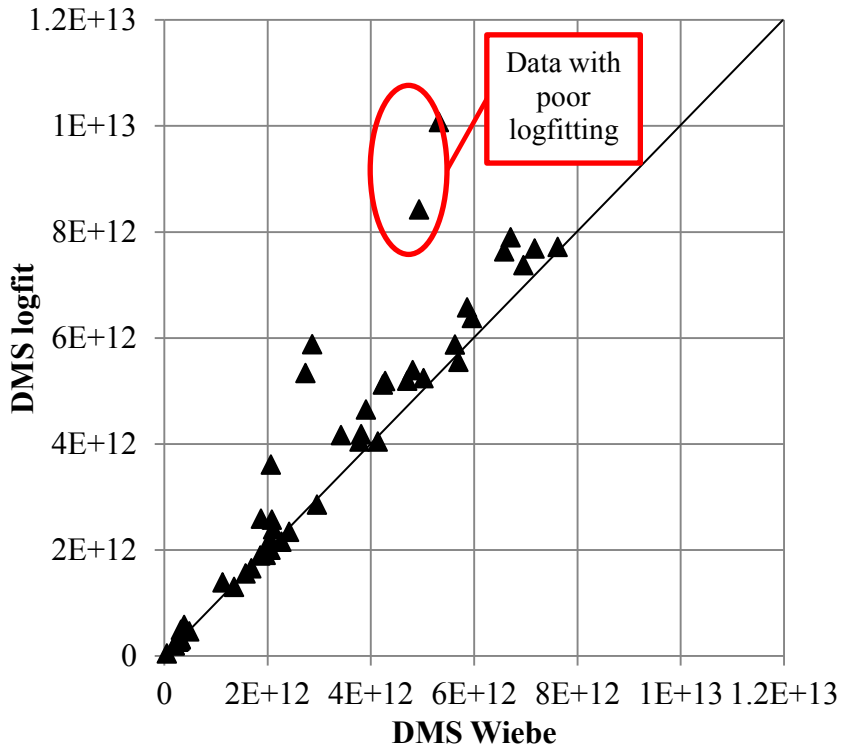

Figure 2.14: Comparison between lognormal fitted and Wiebe filtered data showing data acquired from an AJ126 engine

A sample particle number spectrum where the fitting is poor is shown in Figure 2.15, where it can be seen that the raw spectrum (green) is not matched by the Cambustion accumulation mode logfit data (blue) at all well, it will give far too large a particle number value. However applying the digital Wiebe filter to the spectrum recovers a much better approximation of the accumulation mode fit, complying with the requirements set out in the PMP protocol [51] and resulting in a much more realistic accumulation mode particle count.

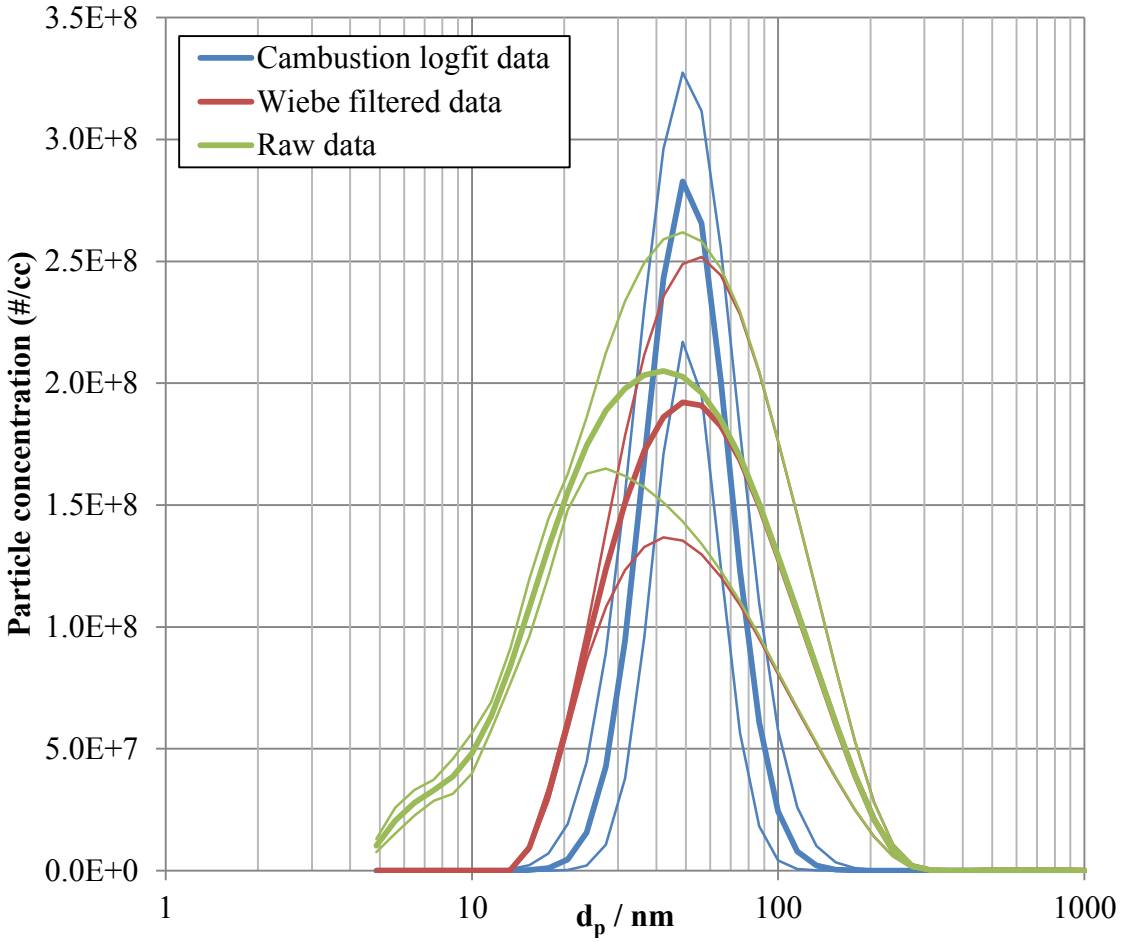

Figure 2.15: Raw (least squares minimised), Cambustion logfitted, and Wiebe filtered particle number spectra for data which has poor logfitting. The thick lines represent the mean (μ) and the thin lines the standard deviation (σ)

2.6. AVL particle counter

The AVL particle counter (APC) is a legally compliant particle counter, when used as part of a legally compliant system. The general layout and sampling procedure is shown in Figure 2.16 and is fully described in Giechaskiel *et al* [68].

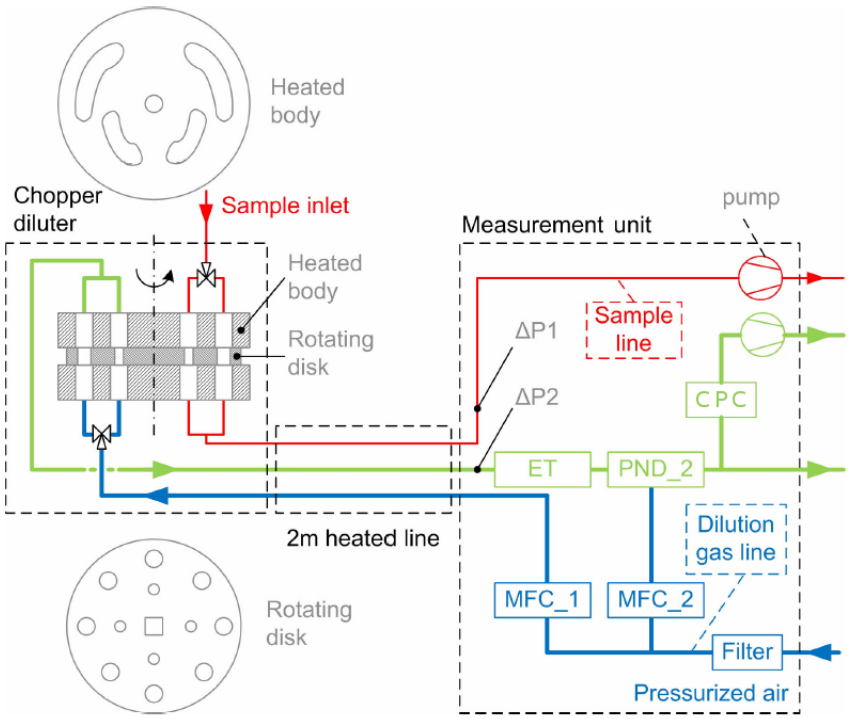

Figure 2.16: Schematic of the AVL particle counter, CPC represents a condensation particle counter, ET is an evaporation tube, MFC_1&2 are mass flow controllers, and PND is particle number dilution (adapted from [68])

The APC only counts solid particles, in line with the PMP measurement protocol [51]. To achieve this, and ensure that all of the volatile particles are removed, the APC passes the exhaust sample first through a hot diluter (at 150 °C); this evaporates volatile particles, and ensures that vapour phase species do not recondense at the exit from the diluter. Then the sample is passed through an evaporation tube (at 300 °C); which ensures that the semi-volatile particles (defined as those with a boiling point higher than that of water) are evaporated. Finally the sample is passed through a secondary diluter, which cools the sample, and reduces the partial pressure of the vapour phase species to prevent

recondensation; this dilution also ensures that the particle concentration is below 10^4 particles per cc, the detection limit of the counter.

At the core of the APC is a condensation particle counter (CPC) (a TSI model CPC-100), which is shown on Figure 2.16. A schematic of a CPC is shown in Figure 2.17, in a CPC, the sample passes through a saturator (held at 38.3 °C in a CPC-100), where the sample is saturated with butanol vapour.

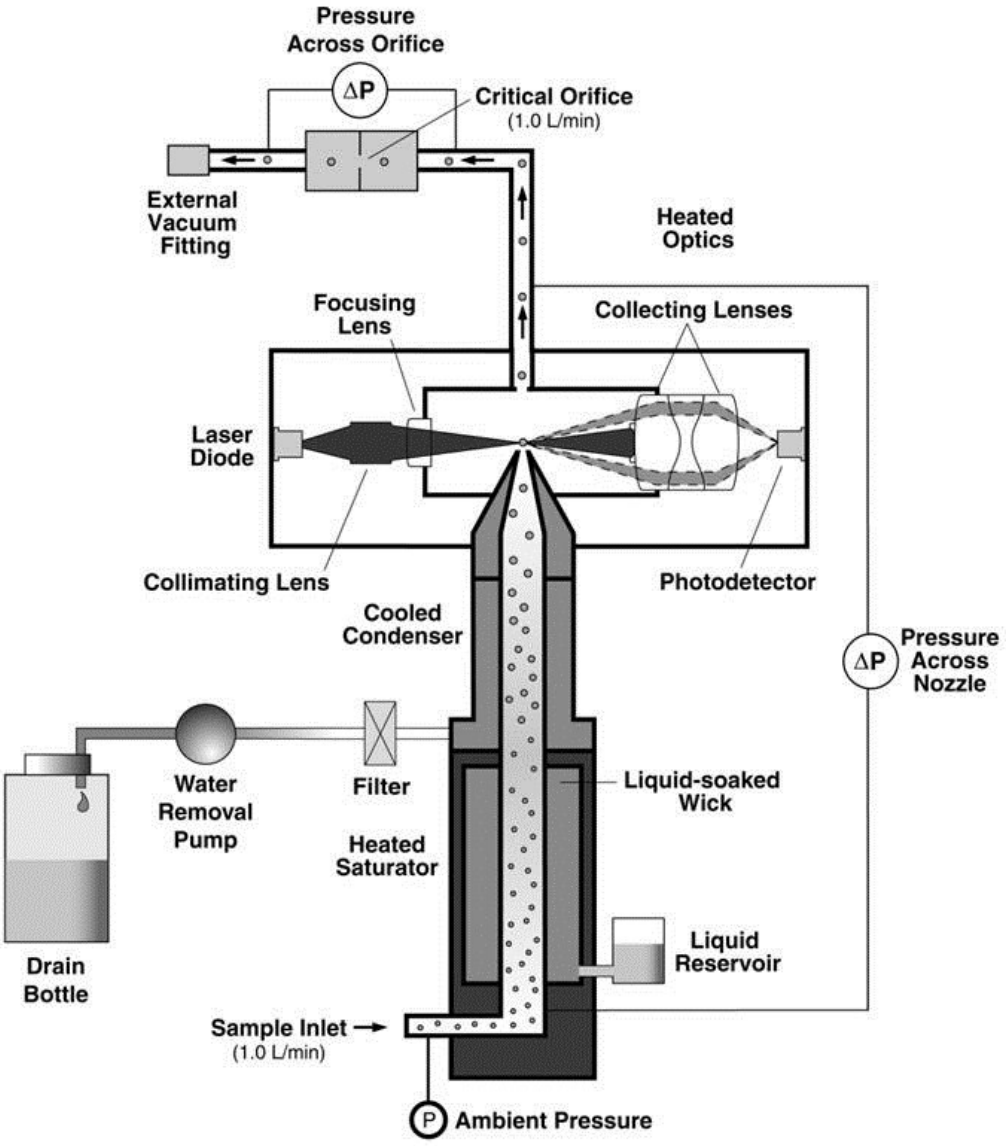

Figure 2.17: Schematic of a Condensation Particle Counter, with acknowledgement to TSI inc. [47]

The sample passes through a condenser (31 °C on a CPC-100), where the butanol vapour becomes supersaturated and the particles present in the sample act as nuclei for condensation of the butanol vapour, and the particles grow to approximately 10 µm in diameter. The sample is then passed through a laser, where a diode photodetector detects the scattered light from the (now relatively large) particles. The APC cannot provide any size information about the particles detected, and requires a much more dilute sample (10^4 particles per cc) compared with a DMS.

2.7. High speed camera

Spray and combustion images have been taken with a Photron FASTCAM 1024PCI high speed digital camera. The camera has variable speed-resolution combinations, for example: 1024 × 1024 pixels (maximum resolution) at 1000 fps, 512 × 256 pixels at 6,000 fps (the combination used in this work), and 128 × 16 pixels at 109,500 fps (maximum speed). The frame capture time is always 1.5 µs, independent of the frame rate. The possible field of view through the optical piston is shown in Figure 2.18.

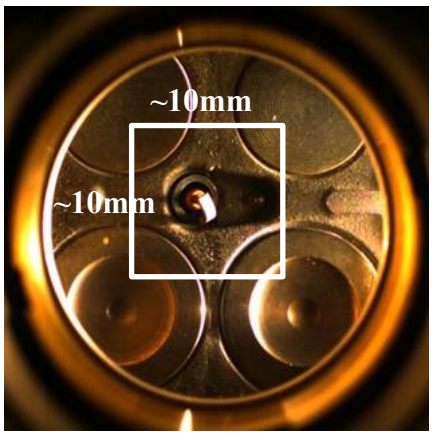

Figure 2.18: Field of view possible through the optical piston, the white square shows the area imaged in this work

For reasons of limited buffer space the camera is triggered such that only frames around the injection and combustion events are recorded. More discussion on recording injection and combustion images on this engine can be found in Chen [85]. The injection sprays were illuminated using an overdriven pulsed green LED array to give the maximum possible spray illumination. Discussion of the implementation of these LEDs can be found in Chapters 3 and 4 of Driver [87]. The field of view images throughout this work is shown as the white square on Figure 2.18. An example spray image is shown in Figure 2.19, showing a spray plume about 3 CAD after the start of injection, and an example combustion image shown in Figure 2.20, about half way through the visible combustion.

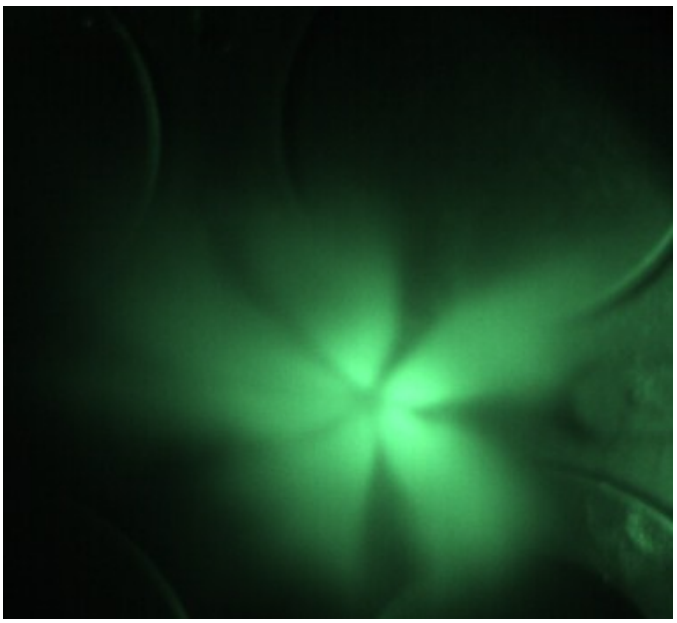

Figure 2.19: Example spray image showing clearly 6 separate spray plumes and inlet and exhaust valves visible in the background

It can be seen in both of these images that in addition to the spray and combustion, there is background illumination too, with the valves being clear on the spray image, and the spark plug prominent in the combustion image.

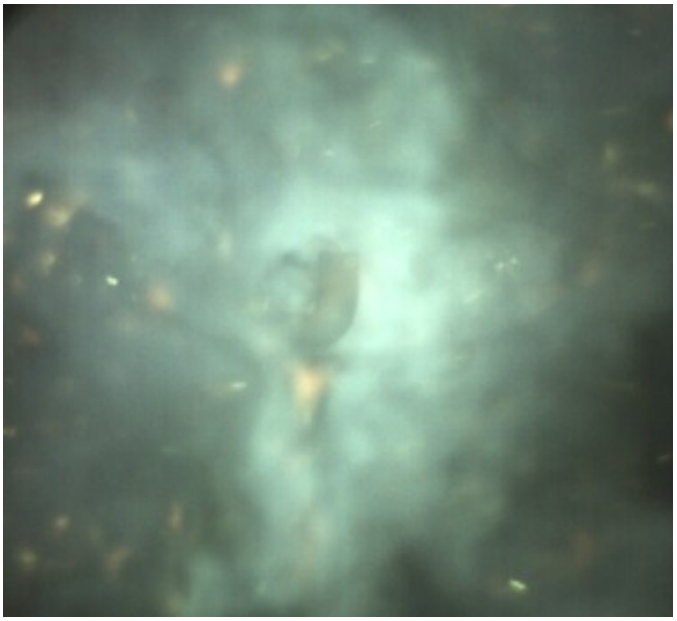

Figure 2.20: Example combustion image

2.7.1. Image analysis

There are a large number of optical analysis techniques used in engines to determine a number of parameters in-cylinder such as spray shape, temperature, pressure, AFR, and flow parameters. Many of these are detailed in Williams [88] and Zhao [89]. Mie scattering is an established technique used to provide a qualitative measure of the amount of liquid fuel droplets present in the fuel spray of GDI engines, for example Davy *et al* [90] use Mie scattering to analyse the effect of fuel composition on mixture evaporation. Mie scattering uses the Mie theory – a solution to Maxwell's equations - to describe the scattering of electromagnetic radiation from a sphere, it holds while the wavelength of the light is much larger than the diameter of the sphere ($>\sim 0.5\,\mu m$ - true for most fuel droplets). The intensity of the scattered light depends on the size (surface area) of a droplet, and the droplet number density (droplets on the outside of a spray are more likely to scatter than a droplet in the centre, which is effectively in the shade of other droplets).

Mie scattering can also be affected by background light scattering (for example off the cylinder head).

Two approaches have been taken to analyse the images acquired from the camera. The first uses the Mie scattering method to analyse the spray images to show the intensity of a spray, and show the amount of liquid fuel present. The pixel values of the images of the fuel spray are summed (integrated) in MATLAB using an approach developed in Taylor [91], these can then be averaged over a number of cycles and plotted through the images of injection. However, the pixel values of the images are not integrated directly. This would lead to varying levels of background illumination and reflections affecting the results. Rather, the code divides the images into regions and uses grey thresholding to try and eliminate the effect of pixels other than those in the spray plume. Further discussion of this technique can be found in Chen and Taylor [85, 91]. An example result is shown in Figure 2.21, comparing the sprays of two different fuels averaged over 50 cycles. Here it can be seen that upon injection (280 CAD bTDC), initially both fuels perform the same, but after injection, one fuel (the red line) evaporates slower, giving a larger plume, and a spray plume that lingers for longer before complete evaporation.

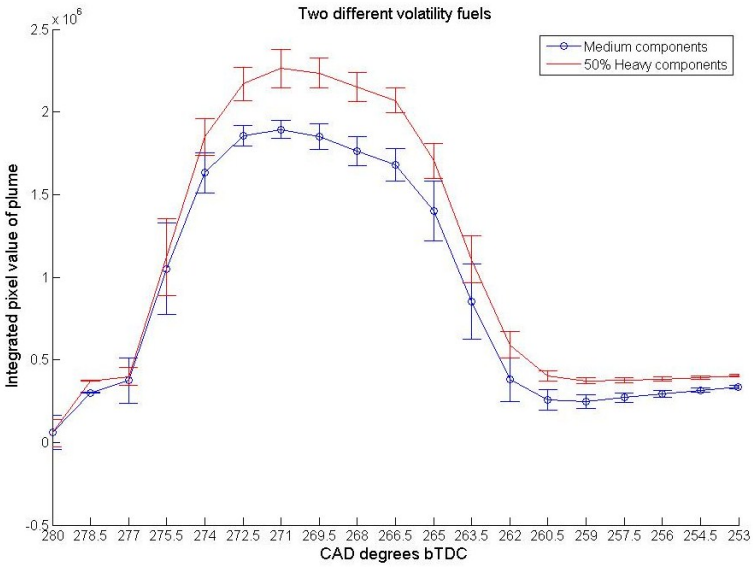

Figure 2.21: Example result from spray integration method

Another method of image analysis is to generate false colour images of the spray. This gives a different way of looking at these images. The false colour images give a spatial display of the penetration of the fuel spray, but in doing so the ability to average this over a number of cycles, and compare directly between the two fuels is lost, due to large cycle by cycle variations in the performance of the injector. The images for comparison need to be selected visually for those with a very similar initial injector spray. Using a similar method to that used in integrating the pixel values of the images and techniques described in Taylor [91], the backgrounds of the images are set to a grey scale, and the spray is false coloured depending on the grey scale value of an individual pixel. Then using the 'Jet' map the brightest pixels are coloured red and pixels of decreasing intensity are coloured through yellow and green to blue. Both grey thresholding and morphological opening are used to reduce the impact of the background lighting and reflections.

The selection of the grey threshold value has a large effect on the final image. A number of different values were tried, the compromise being capturing and applying false colour to the whole spray visible in the image and reducing any background caught in the false colouring process that the morphological opening method is also not able to eliminate. A comparison between several selected values of the grey threshold is shown in Figure 2.22. Here it can be seen particularly when the grey threshold is set to 17 and 25 evidence of the spray that has not been false coloured. Likewise it is clear when the grey threshold is set to 1 a great deal of the background including the engine valves has been false coloured. A grey threshold of 9 was chosen as offering the best compromise, particularly as the area of the valves that is illuminated is easy to exclude.

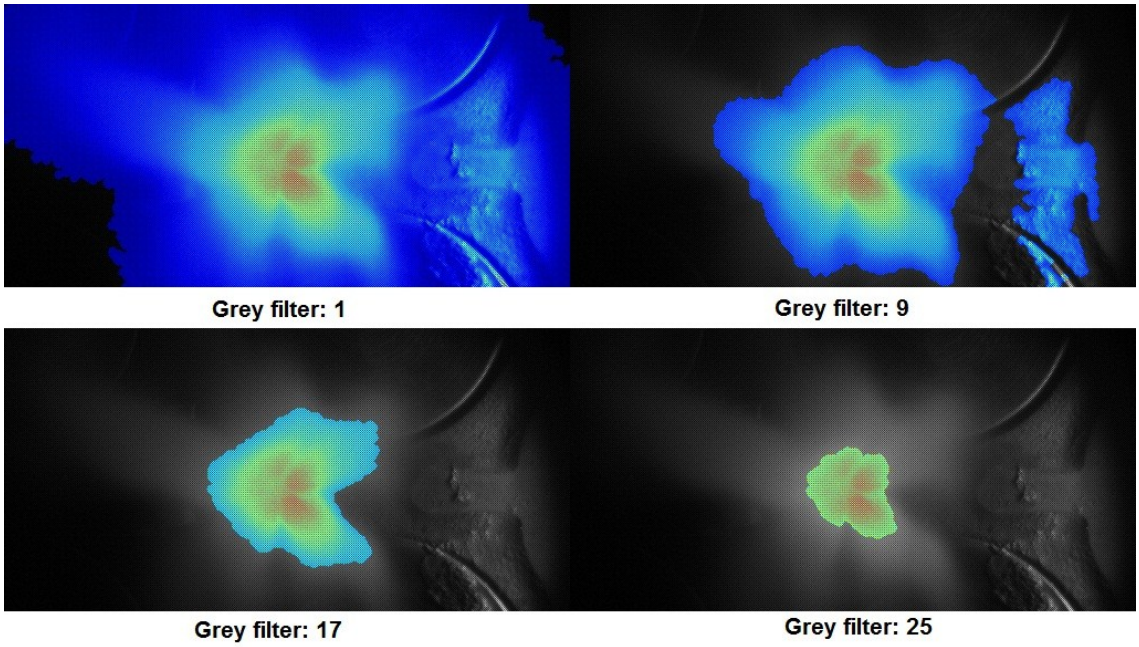

Figure 2.22: False colour images using 4 different grey threshold values

2.8. fFID

It is often useful to be able to measure levels of unburned hydrocarbons (UHCs), both in the cylinder and in the exhaust. The accepted method of measuring these is using a flame ionization detector (FID). When hydrocarbons are burned the combustion process produces ions roughly proportional to the number of carbon atoms present in the hydrocarbon across a wide range of concentrations [92]. The process by which this occurs is not fully understood, but is known as chemi-ionisation.

2.8.1. Chemi-ionisation

When an hydrocarbon is burned in a high temperature flame, positive ions appear in the reaction zone (CHO^+ and $C_3H_3^+$) mainly by the reactions $CH^* + O \rightarrow CHO^+ + e^-$ and $CH + C_2H_2 \rightarrow C_3H_3^+ + e^-$ [92]. The concentration of positive ions is thought to be around 10 × that of negative ions [93]. Around 1 ion per 10^6 C atoms present is formed [92].

FIDs measure these ions as they are given off by combustion. This ionisation process happens very quickly. For this measurement to be accurate, controlled combustion of the hydrocarbons needs to occur, with a fuel that does not contain carbon atoms. In this case hydrogen was chosen as the FID fuel.

2.8.2. Difference between a FID and a fast FID

Although the ionization process in combustion occurs very rapidly, conventional FIDs have a frequency response time of order 1-2 s. This is too slow to be able to detect the variation in hydrocarbons over one cycle of an engine. Conventional FIDs (Figure 2.23) pre-mix the sample and fuel gas prior to combustion, and rely on a pump to deliver a constant sample flow. The whole system is enclosed in an oven in order to prevent hydrocarbons condensing. It is this sample handling that gives them the slow response time but accurate results.

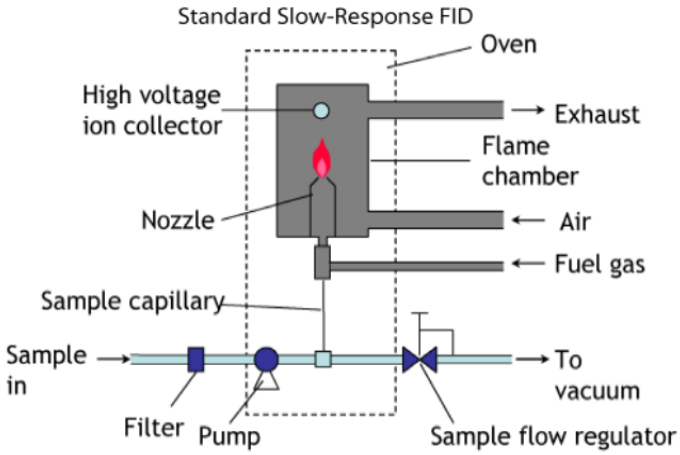

Figure 2.23: Schematic of conventional FID, with response time of order 1-2 s [94], figure courtesy of Cambustion

In contrast a fast FID (fFID) (Figure 2.24) is designed to achieve the fastest possible frequency response time. fFIDs use remote sampling heads, close to the sampling point, where the hydrocarbons are burned. fFIDs also mix the air, fuel gas, and the sample all at

the nozzle. The flame chamber is also operated at a pressure below atmospheric, which has the effect of drawing the sample through the (short) sample capillary very quickly. These features give the fFID a frequency response of a few milliseconds, short enough to be able to detect hydrocarbons within an engine cycle with good resolution. Care must be exercised in measuring hydrocarbons with a fFID however, as the output is proportional to the sample flow, which is not controlled directly (unlike a conventional FID), so careful setup and calibration is required.

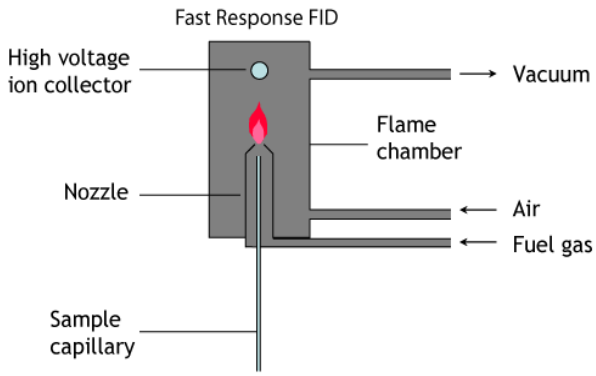

Figure 2.24: Schematic of fast response FID showing how the sample is drawn through by the vacuum, giving a response time of a few milliseconds [95], figure courtesy of Cambustion

For this work a Cambustion HFR400 fFID was used. It has 2 independent channels, a response time of ~ 4 ms, the electrode (high voltage ion collector) operates at 180 V DC [96]. A heated sampling probe is used to avoid hydrocarbons condensing. An in-situ calibration system has been developed in-house, allowing samples of air (0 % hydrocarbons) and a 'span' gas of known hydrocarbon concentration (e.g. 1760 ppm propane in Nitrogen) to be passed over the sample probe head, without it being removed from the engine. This can even be done while the engine is running. The development of the in-situ sampling system is discussed in Price [12].

The ions impacting on the electrode generate a current, which is output into a National Instruments PCI-MIO-16E-1 Data Acquisition (DAQ) card. This records the data at a rate

of once per crank angle, this is known as the high speed DAQ (HDAQ) system. Further discussion of the design and installation of HDAQ can be seen in Wang [97]. This current (in μA) can then be referred back to a hydrocarbon concentration thus:

$$i = \frac{Q[HC]N_a Ce}{60 \times 10^9} . \frac{P}{R_0 T} \qquad (2.7)\ [96]$$

Here Q is the sample flow in cc/min, $[HC]$ is the hydrocarbon concentration in ppm, N_a is Avogadro's number, C is the number of carbon atoms in the HC molecule, e is the electronic charge, P is the pressure, R_0 is the universal gas constant, and T is the absolute temperature.

2.8.3. In-cylinder sampling of Hydrocarbons

A great advantage of the HFR400 is that it can be adapted for in-cylinder sampling of hydrocarbons. This normally poses problems, as the hydrocarbon concentrations are significantly higher than in the exhaust, and the pressure variations are very large. The design of the HFR400 has two pressure chambers, a constant pressure (CP) chamber and a FID chamber. The CP chamber ensures that the flow entering the burner is at a constant pressure, the difference in pressure between the FID and the CP chamber draws a constant sample flow into the burner. The two chambers can be seen in Figure 2.25, the CP chamber is labelled 1 and the FID chamber 2.

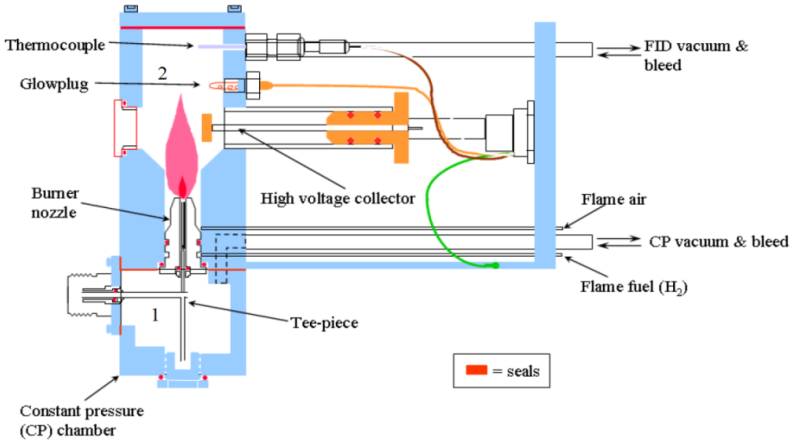

Figure 2.25: Layout of HFR400 fFID head (adapted from [98]), the sample enters through the Tee-piece (bottom left) and is burned and counted in the flame (centre-left), figure courtesy of Cambustion

For in-cylinder sampling the CP chamber needs to be enlarged greatly to allow for the greater variation in flows that are due to the pressure changes that occur inside the cylinder, this can be achieved by attaching a blanked-off length of hose to the CP chamber, this adds around 2 L of volume to the CP chamber. The pressure in the CP chamber must remain lower than the lowest pressure present in the exhaust or else back flow will occur and the signal is invalid. Another consideration for in-cylinder sampling is that hydrocarbon levels will be much higher than for sampling in the exhaust, so appropriate calibration gases should be chosen to ensure the linearity of the FID signal over the range (ideally around 50 % concentration of the maximum value expected).

2.9. Chapter 2 summary

In this Chapter the engines and experimental equipment used for the experimental work have been detailed. Engines used are the single cylinder engine with optical access, the AJ133 5 L naturally aspirated V8 engine, the AJ126 3.0 L supercharged V6 engine, and the UB100 2.0 L turbo-supercharged I4 engine. The particle measuring instrumentation, the DMS500 and the AVL particle counter, have been introduced, alongside the data analysis techniques for their outputs. The high-speed camera, for optical analysis of spray and combustion has been detailed, alongside data analysis techniques for the images taken. The fFID to measure hydrocarbon levels in-cylinder and in the exhaust has been described.

3. Fuels and fuel modelling

3.1. Gasoline

Gasolines contain a blend of hydrocarbons distilled from crude oil feedstock. Generally gasolines contain the fractions in the boiling point range 30-200 °C, this roughly corresponds to components with carbon numbers mostly in the range C_5-C_{12} [99]. As no two batches of gasoline are likely to be the same, and complete compositional breakdown of gasoline is very expensive to obtain, it is common to define gasoline in terms of certain key bulk parameters. Among the most important of these parameters are volatility, energy content, and octane rating.

3.1.1. Volatility

The volatility of gasoline is normally expressed as vapour pressure (VP) and is a tightly controlled parameter. Gasoline is normally at the more volatile end of the distillates of crude oil. If the gasoline volatility is too high, then fuel may vaporise in the lines prior to injection, causing so-called vapour lock and fuel pumps and fuel injectors may not work properly. If the volatility is too low, the fuel will not vaporise, and the vehicle may not start, and due to poor mixture preparation, there will be high levels of particulate emissions. A closer look at volatility and vapour pressure is included on page 95.

3.1.2. Energy content

The energy content (calorific value) of a typical gasoline is 31 MJ/litre or around 44 MJ/kg, although this can vary by approximately ± 10 % depending on the gasoline composition. Oxygenates have a lower energy content compared with other gasoline

components (as the - OH part of the molecule does not contribute to combustion), for example the calorific value of E85 is typically 22.6 MJ/litre or 31.85 MJ/kg. This leads to nominal adverse fuel consumption figures for flex-fuel vehicles as fuel is sold on a volumetric basis, rather than an energy basis.

3.1.3. Octane rating

The intended process of combustion in an internal combustion engine is deflagration – combustion at subsonic speeds driven by heat transfer. Under certain conditions auto-ignition of a local area ahead of the flame front (which has been initiated due to the normal operation of the spark plug) – can occur. In a positive ignition engine auto-ignition is commonly known as knock, this can cause a sharp rise in cylinder pressure and damage to engine components[3].

The mechanisms that cause knock are not completely understood but are related to cylinder pressure, temperature, and the autoignition chemistry of the local mixture. Knock can be mitigated by retarding the spark timing, reducing the compression ratio, or reducing the load. Long straight chain molecules are known to be more susceptible to autoignition compared with branched chain molecules, while molecules containing aromatic rings are the most resistant of all. Components can be added to the fuel to supress knock; tetraethyl lead was a common additive, until it was phased out for automotive use on environmental grounds as it is extremely toxic and acts to poison catalytic converters.

[3] A second unwanted burning mechanism distinct from auto-ignition can occur – preignition. This occurs when deflagration type combustion occurs before the spark plug fires, often caused by hot spots in the engine. This phenomenon can be equally damaging, especially if it leads to auto-ignition.

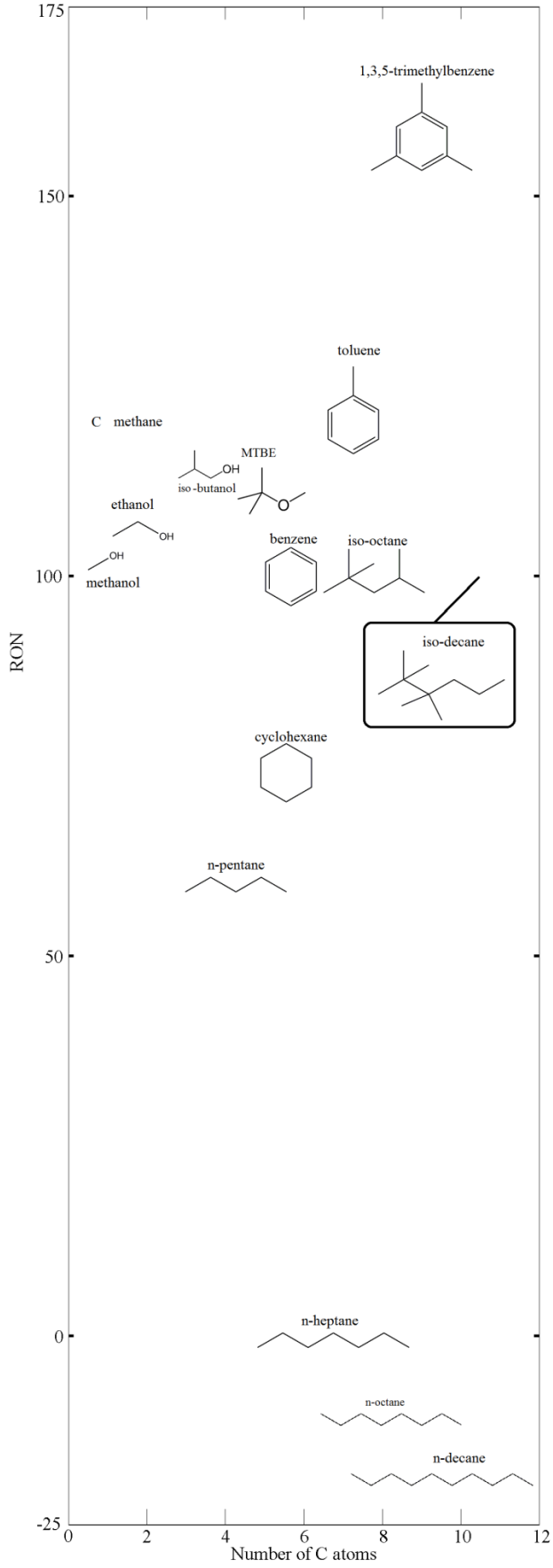

Figure 3.1: A graphical representation of RON of various gasoline components shown as their chemical structure

Octane rating is a measure of the anti-knock characteristics of fuels. An empirical scale, it is defined by two points; the knocking characteristics of n-heptane which has a RON = 0 and iso-octane (2,2,4-trimethylpentane) which has a RON = 100. The RON of various chemical components is shown in Figure 3.1.

There are three commonly used definitions of octane rating research octane number (RON), motor octane number (MON), and anti-knock index (AKI). RON is measured in a variable compression ratio single cylinder engine at 600 rpm, 125 °F (52 °C) inlet temperature at standard pressure with fixed spark timing. MON is measured at 900 rpm, 300 °F (149 °C) inlet temperature with spark timing that varies with compression ratio. AKI is simply the linear average of RON and MON [100]. MON generally provides a guide to how a fuel will perform under full load conditions, and RON under part load conditions. In the UK RON is the most commonly used definition, and has been used in this thesis.

The knock characteristics of a fuel component when it is blended with other components are of obvious interest to this thesis. Blending octane number (BON) is an attempt to measure these blending characteristics as the mixture behaviours can be non-linear. BON is calculated by the same method as RON, except the components are mixed 20 % by volume with a 60 % iso-octane, 40 % n-heptane mix [101].

Anderson *et al* [102] present a convincing case for formulating octane numbers, particularly for oxygenate blends, on a molar basis using RON, rather than by volume using BON; this method makes much more chemical sense. Where possible in this thesis, this method has been used (for example with the model fuels), however for fuels where the complete compositional breakdown is not known, it is not possible to calculate RON on this basis, as commercial fuels are blended by volume, so the BON method has been used.

3.2. Evaporation modelling

It is desired to be able to model the evaporation characteristics of fuels, as knowing the importance of mixture preparation on particulate emissions, knowledge of how the mixture might evaporate in a GDI engine is of great importance. In addition, if speciality model fuels are designed so as to be able to precisely vary fuel parameters independently knowing that they have the similar evaporation characteristics to market fuels ensures that these fuels are representative of real world behaviour.

3.2.1. Raoult's law

The simplest model for evaporation uses the Raoult-Dalton law [103], commonly known as Raoult's law. Raoult's law relates the vapour pressure of an ideal solution to the vapour pressure of each of its chemical components as a pure liquid by the molar fraction of each component present. Raoult's law is shown in Equation 3.1:

$$y_i P = x_i P_{\mathrm{vp}i} \qquad (3.1)$$

here y_i is the molar fraction of component i in vapour, x_i is the molar fraction of component i in liquid, $P_{\mathrm{vp}i}$ is the vapour pressure of component i, P is the pressure of the mixture.

Raoult's law requires there to be ideal mixing in the mixture, which gives Raoult's law its linear relationship.

Ideal mixing for liquid mixtures is equivalent to ideal behaviour in gases (indeed Raoult's law assumes ideal behaviour in both the liquid and the gas). Ideal mixing assumes that the average strength of the interactions between all of the molecules is equal regardless of the composition of the molecules in the liquid mixture. As intermolecular interactions in liquids are strong (unlike in gases) they cannot usually be neglected (as they are in the ideal gas assumption).

Molecules that are similar will have similar interactions for example, in a mixture of n-heptane and n-octane, the molecules are similar, and so the strength of the molecular interactions are very similar; such a mixture could be considered ideal. The more the molecules differ from each other, the less ideal the mixture behaviour will be.

Mixtures of oxygenate compounds with hydrocarbons will never be ideal, as the –OH part of an oxygenate makes it much more polar, and capable of hydrogen bonding, which has a different strength to other molecular interactions, and hence such a mixture is not ideal. The extreme of non-ideal mixing is phase separation.

An ideal mixture is one where the enthalpy of mixing is zero. This means that the change in Gibbs free energy on mixing can be entirely attributed to the entropy of mixing, which arises from the fact that when two different molecules mix, there is inevitably an increase in disorder (entropy). This means that there is no heat gain/loss upon isothermal mixing in an ideal mixture. A common method of calculating the enthalpy of mixing is the Flory-Huggins solution [104].

Ideal mixing cannot be assumed for mixtures of aromatics and paraffins [105] so Raoult's law in isolation is not appropriate for modelling the evaporation behaviour of ULG and its blends, even for blends containing no oxygenates.

3.2.2. UNIFAC

The UNIversal Functional Activity Coefficient method (UNIFAC) was proposed by Fredenslund *et al* [106], so as to extend Raoult's Law to account for non-ideal mixing. It combines the analytical solution of groups (ASOG) method, relating activity coefficients to molecular structural group interactions, with the UNIQUAC (UNIversal QUAsiChemical) model [107]. It is a semi-empirical model to predict non-ideal mixture behaviour based on molecular size and known interactions. It breaks molecules into

functional groups to model interactions using empirical data from experimentally determined interactions.

The model essentially breaks down into two parts: the combinatorial part, due to the differences in size and shape of the molecules; and the residual part, due to energy interactions.

The UNIFAC method uses existing experimental data characterising the interaction between pairs of structural groups to map those known interactions to predictions of interactions that may not have been obtained experimentally. UNIFAC's success stems from its reduction of a very large experimental data set of interactions into a simple structural group model, with which any molecule of interest can be built up, for example iso-octane is made up of five CH_3 groups, and one each of a CH_2 group, a CH group and a C group. The activity coefficient of each molecule is divided into two parts, one part (the combinatorial - γ_i^C) is the contribution due to size and shape differences, and the other (the residual - γ_i^R) due to known molecular interactions - which changes the enthalpy of mixing. The combinatorial portion of the activity coefficient is used directly from the UNIQUAC method [107].

The key equations are shown below [108]:

$$\ln \gamma_i = \ln \gamma_i^C + \ln \gamma_i^R$$

$$\ln \gamma_i^C = \ln \frac{\Phi_i}{x_i} + \frac{z}{2} q_i \ln \frac{\theta_i}{\Phi_i} + l_i - \frac{\Phi_i}{x_i} \sum x_j l_j$$

$$\ln \gamma_i^R = \sum_k v_k^{(i)} \left(\ln \Gamma_k - \ln \Gamma_k^{(i)} \right)$$

$$\ln \Gamma_k = Q_k \left[1 - \ln \left(\sum_m \theta_m \psi_{mk} \right) - \sum_m \frac{\theta_m \psi_{km}}{\sum_n \theta_n \psi_{nm}} \right]$$

$$l_i = \frac{z}{2} (r_i - q_i) - (r_i - 1)$$

$$\theta_i = \frac{q_i x_i}{\sum_j q_j x_j}$$

$$\psi_{mn} = \exp \left(-\frac{a_{mn}}{T} \right)$$

$$\Phi_i = \frac{r_i x_i}{\sum_j r_j x_j}$$

$$r_i = \sum_k v_k^{(i)} R_k$$

$$q_i = \sum_k v_k^{(i)} Q_k$$

x_i is the molar fraction of component i
θ_i is the area fraction
Φ_i is the segment fraction
r_i is the normalised molecular Van der Waals volume
q_i is the normalised molecular surface area
Γ_k is the group residual activity coefficient and $\Gamma_k^{(i)}$ is the same in a solution only of molecules of type i
$v_k^{(i)}$ is the number of groups of type k in the molecule i

In calculating the combinatorial part with UNIQUAC (and hence UNIFAC), as this part is dependent on the size and shape of the molecules, r_i, the normalised molecular Van der Waals volume, and q_i, the normalised molecular surface area are the important parameters, and these can be looked up, for example in Poling *et al* [108]. Both r_i and q_i by convention are normalised with respect to a CH_2 unit in polyethylene. The $\frac{z}{2} q_i \ln \frac{\theta_i}{\Phi_i}$ term is a direct result of the Flory-Huggins solution, with a small modification from the coordination number (z). A value of $z = 6$ would represent cubic packing of assumed spherical molecules, and a value of $z = 12$ represents hexagonal packing. Throughout the literature it is reported that calculations are insensitive to z, and a value of $z = 10$ is commonly assumed [108], and this value has been used here.

The other terms in the combinatorial part of the activity coefficient represent Guggenheim's corrections to Flory-Huggins estimates of entropy of mixing, which tend to slightly overestimate. The correction comes to around 5 % under most circumstances.

The residual contribution to the activity coefficient is calculated according to the ASOG method. Parameter a_{mn} is a measure of the energy of interaction between groups m and n and is evaluated experimentally, it is tabulated in Poling *et al* [108], and it should be noted that despite being a measure of energy, it has units of temperature (Kelvin). Care needs to be exercised as $a_{mn} \neq a_{nm}$. $\ln \Gamma_k^{(i)}$ is a factor such that as $x_i \rightarrow 1$, $\gamma_i \rightarrow 1$ – i.e. that a solution of only one molecule has an activity coefficient of unity, the limit case.

UNIFAC provides temperature-dependent activity coefficients (γ_i), which modify the Raoult-Dalton law to account for deviations from ideal mixing, as shown in Equation 3.2:

$$y_i P = \gamma_i x_i P_{vpi} \qquad (3.2)$$

An activity coefficient $\gamma_i > 1$ means that the molecules within the mixture are repelling each other more than the ideal case, and a mixture is more likely to evaporate at a given temperature compared with the ideal case. An activity coefficient $\gamma_i < 1$ means that the molecules within a mixture are more strongly attracted to each other compared with the ideal case, and such a mixture is less likely to evaporate at a given temperature.

3.2.3. Evaporation model

Using Raoult's law, with the UNIFAC modifications written above, it is possible to model many evaporative parameters. A model has been written in MATLAB which can model vapour pressure (VP), ratios of species evaporation, and distillation. To model vapour pressure, the code reads the initial molar composition of the liquid fuel, and requires the user to input the VP calculation temperature. The code then performs the UNIFAC calculation, at the user input temperature to provide γ for each component. The code then uses the modified Raoult's law to calculate the vapour phase composition, and pressure. This is the vapour pressure.

To model distillation, a starting temperature is selected – normally 293 K and the molar composition of the fuel is read in the same way, a UNIFAC / Raoult's law calculation is performed to calculate the composition of the liquid and the vapour at this temperature. The temperature is then incremented in user defined increments (a smaller step size gives a 'smoother' distillation curve), if, following a recalculation of the UNIFAC / Raoult's law parameters, the pressure of the vapour phase remains at 1 bar (the distillation is assumed to take place at a pressure of 1 bar), then a 'molar step' is removed from the liquid composition, and the new vapour phase composition calculated (modelling evaporation),

the process then repeats. If, following a recalculation of the UNIFAC / Raoult's law parameters, the pressure of the vapour phase is less than 1 bar, then the temperature is incremented and the process repeats. If, following a recalculation of the UNIFAC / Raoult's law parameters, the pressure of the vapour phase is greater than 1 bar, the distillation has progressed too far, and the temperature, for the current molar fuel composition, is decremented by 100 × the temperature step size; and the process is repeated. This will continue until the temperature reaches a point where there is no liquid fuel left – this is the final boiling point (FBP).

It is of interest to model the ratios of species evaporation, so that when designing a model fuel there is good coevaporation of its components. If this was not the case, when a fuel evaporated upon injection into the cylinder, areas of the mixture would be locally rich in a particular component. If this were the case, the combustion would not be representative of normal operation, and the emissions could also be misleading.

Given this target for model fuel design, the UNIFAC model was capable of modelling ratios of species evaporation. In particular, for the model fuels shown in Section 3.4.1 the paraffin to aromatic evaporation ratio was of interest, it being expected that because of their near-linear mixing, paraffins of similar boiling points would evaporate together, and likewise aromatics. Therefore a paraffin to aromatic evaporation ratio close to unity will result in paraffins and aromatics of similar boiling points evaporating together. For other fuels it might be of interest to model the oxygenate to paraffin ratio or the oxygenate to aromatic ratio, but as oxygenates were not added to the model fuels in Section 3.4.1 this was not investigated.

In order to model this, a calculation temperature is selected by the user (for the results presented below, a temperature of 170 °C was selected as being representative of the in-

cylinder conditions during evaporation). Then, as before, a UNIFAC / Raoult's law calculation is performed to calculate the composition of the liquid and the vapour at this temperature, and then user defined molar steps are removed from the liquid into the vapour state, and a new liquid and vapour composition is calculated at each step. This is all conducted at constant pressure[4]. The results are then presented as a ratio of aromatic to paraffin components present in the vapour.

Evaporation model validation

To validate this model, a distillation curve of a fuel, of known composition, with an experimentally determined distillation curve, was modelled using the model described above and the results compared with the distillation curve obtained experimentally by BP (with thanks to John Williams of BP) [109].

The composition of the model fuel is shown in Table 3.1, and, while it is a simplified fuel (commercial gasolines tend to have many more components present) it is representative of commercial gasoline.

Table 3.1: Model validation fuel composition [109]

Component	% v/v
iso-pentane	15.0
n-heptane	5.00
2,2,4-trimethylpentane (iso-octane)	15.0
2-methylpentane (iso-hexane)	10.0
1-hexene	15.0
toluene	20.0
cyclopentane	20.0

[4] Clearly, in reality, in the cylinder, this process does not occur at constant pressure, but, assuming early direct injection, the assumption of constant pressure is reasonable, as the cylinder pressure is roughly constant during induction, and by selecting a high calculation temperature some of the effects of compression can be taken into account.

The results in Figure 3.2 show that the UNIFAC model follows the experimentally obtained distillation curve closely, with the exception of the beginning and end of the distillation. This can be attributed to distillation equipment artefacts. For example, the model shows mols evaporated (as they change phase from liquid to vapour), and converts to volume, whereas any experimental distillation apparatus measures volume of distillate recovered.

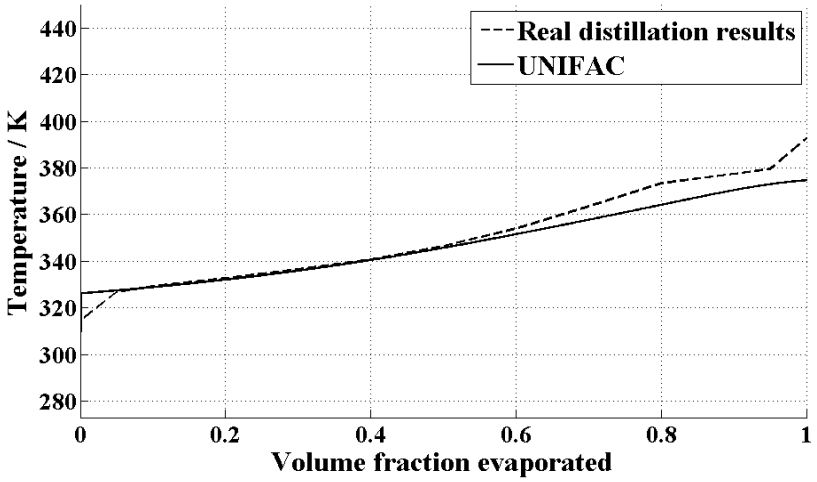

Figure 3.2: Comparison between UNIFAC model and experimental results for the distillation of ULG, real distillation results courtesy of BP [109]

The model also holds for fuels with high oxygenate content. Here a model gasoline representing the Indolene test fuel has been used, as used by Greenfield *et al* [110], with the exception that the Naphthalene component has not been included, as it was clear from the final boiling point of the distillation curve, that it was not present in the fuel. The composition of this model gasoline can be seen in Table 3.2.

Table 3.2: E85 model gasoline composition, adapted from [110]

Component	%v/v
n-butane	6.24
iso-pentane	16.5
cyclohexane	18.7
toluene	16.1
ethylbenzene	13.0
2,2,4-trimethylpentane (iso-octane)	16.6
n-decane	12.8

Shown in Figure 3.3 is a comparison of the UNIFAC model with the experimentally obtained distillation results for E85 (a blend of 85 % v/v ethanol with gasoline) alongside data obtained from an alternative model using the modified separation of cohesive energy density (MOSCED) method [111]. It can be seen that the experimental results and the UNIFAC model track very closely, with UNIFAC slightly better predicting than MOSCED. Shown in Figure 3.4 is a comparison of the UNIFAC model with the experimentally obtained distillation results for M56 (a blend of 56 % v/v methanol with gasoline) alongside another result from the alternative MOSCED model. It can be seen that, again, the experimental results and the UNIFAC model track very closely with the exception of the last 10 % of the distillation, here the MOSCED model is superior to UNIFAC.

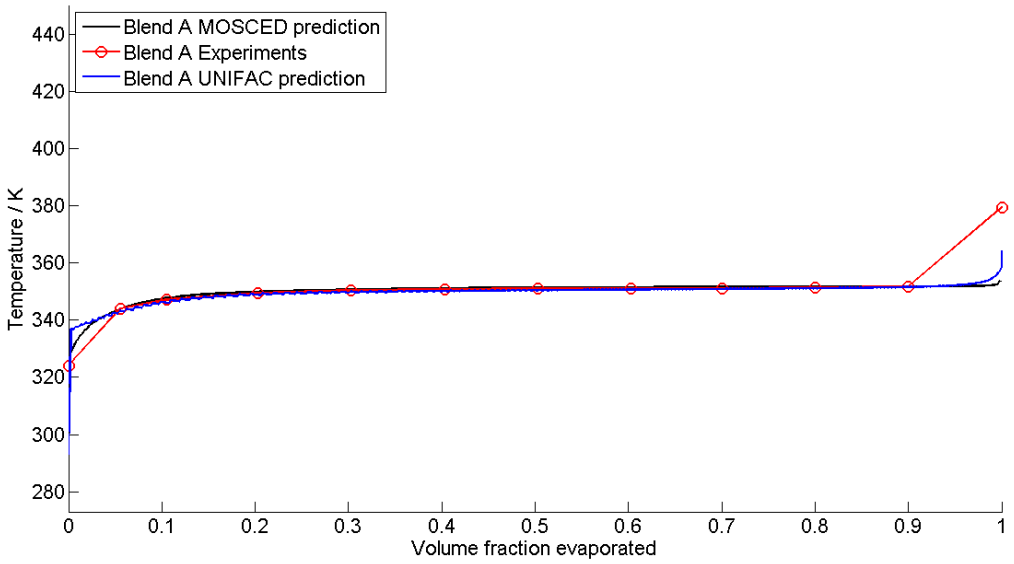

Figure 3.3: Comparison between UNIFAC model, MOSCED model [111], and experimental results for the distillation of E85 [111]; the three results can be seen to follow each other closely

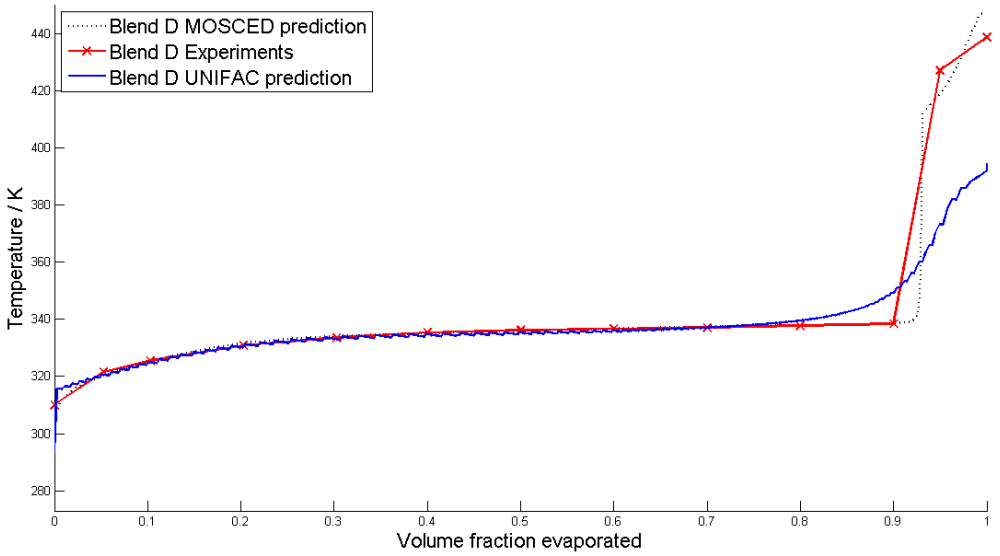

Figure 3.4: Comparison between UNIFAC model, MOSCED model [111], and experimental results for the distillation of M56 [111]; the three results can be seen to follow each other closely

Evaporation modelling results

A sample of the results of the model is shown in Figure 3.5 and Figure 3.6. These are plotted such that perfect coevaporation of aromatic and paraffin components is indicated by a straight line at unity on the ordinate. These results were used to set iso-octane : n-octane and iso-decane : n-decane ratios alongside the octane number which is discussed in the octane number considerations Section 3.4.1. The results are shown in Figure 3.5 for the 'T' blends of model fuels (representing fuels where only the aromatic composition was varied) and Figure 3.6 for the 'D' blends (representing fuels with varying volatility and fixed aromatic composition). Understanding what the model is predicting is easy to see in the results of the T100 fuel, a mixture (by volume) of 95 % toluene and 5 % n-pentane[5], where the more volatile n-pentane evaporates more quickly initially, in preference to the toluene, before the toluene 'catches up' for the rest of the evaporation.

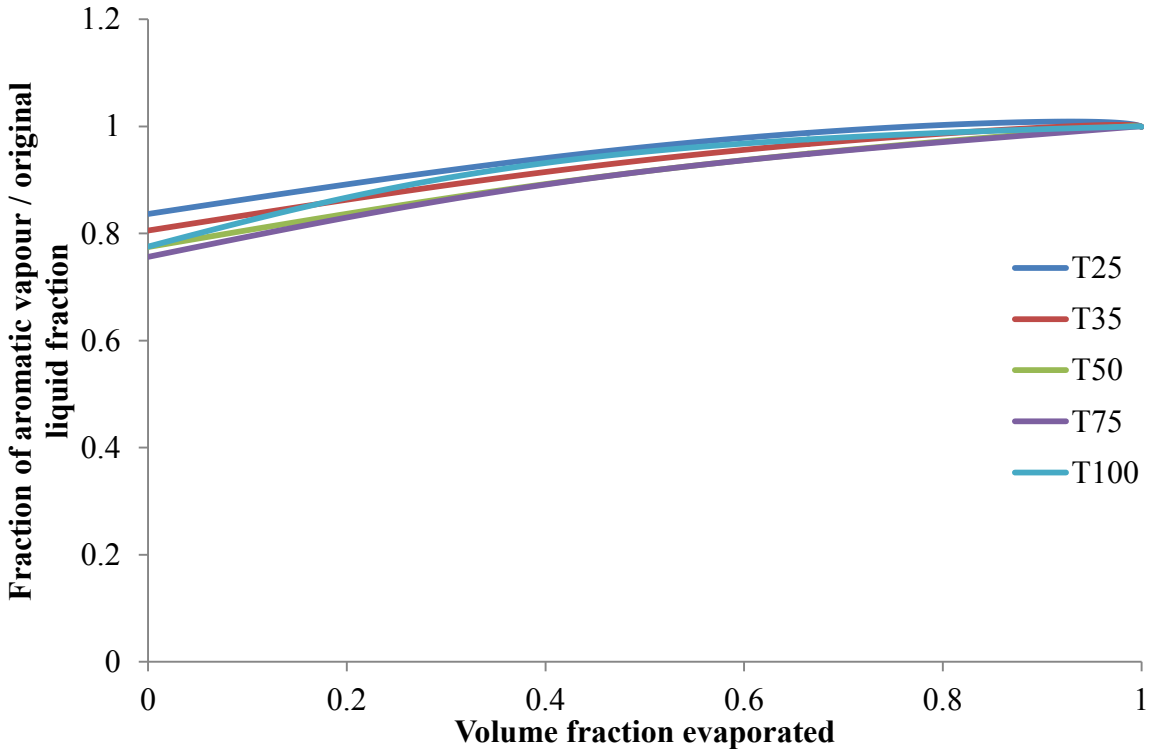

Figure 3.5: UNIFAC model results on 'T' blends, there is little difference between the fuel blends, and only small differences in paraffin to aromatic ratio can be seen

[5] The initial nomenclature for the model fuels was developed before it was decided to add 5 % (v / v) n-pentane to all of the fuels; hence T100 is not 100 % toluene, rather a 95 % toluene, 5 % n-pentane mixture.

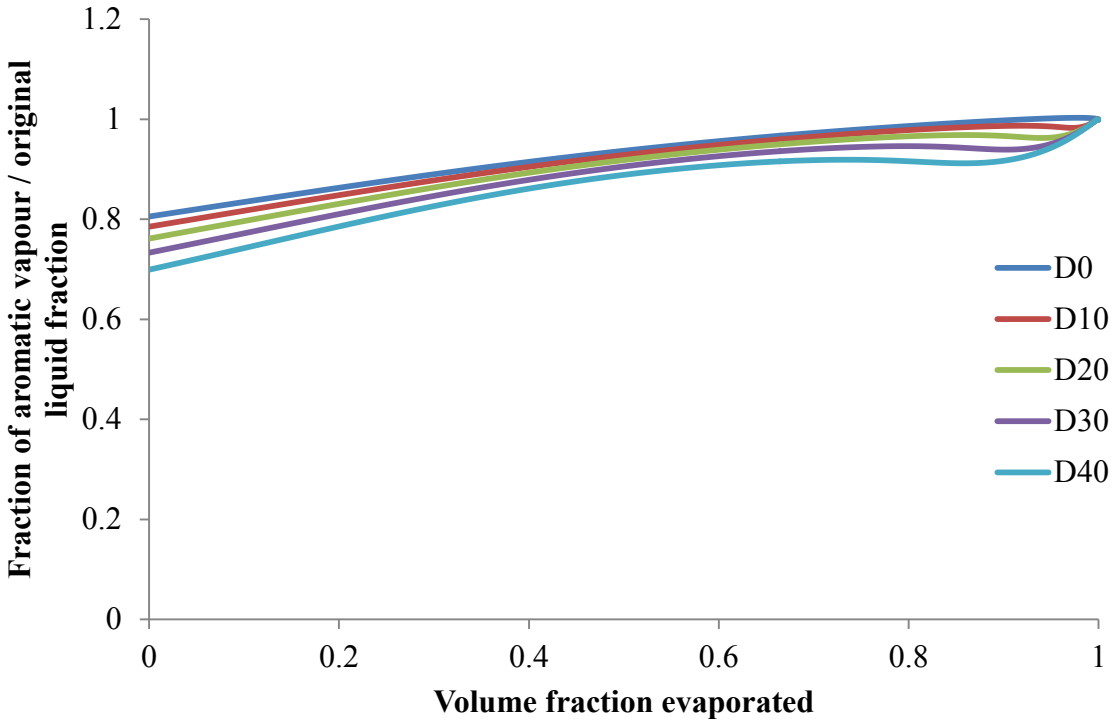

Figure 3.6: UNIFAC model results on 'D' blends, again there are few differences between the fuel blends, and only small variations in paraffin to aromatic ratio can be seen

It should be noted that this model of evaporation assumes distillation type evaporation of a fuel spray, rather than flash boiling type evaporation. Flash-boiling occurs when the fuel evaporates so quickly on injection that it essentially evaporates as it leaves the injector; in an 'onion skin' type of evaporation, with the outer layers evaporating first, regardless of their composition. This is known to occur in DISI engines [112], and perhaps a combination of the two methods of evaporation would occur, however modelling it, and potential interactions between the two models, would require detailed knowledge of spray patterns and is outside the scope of this thesis, particularly given the aim of this modelling to ensure mixture co-evaporation (as if flash boiling occurs, the mixture must be co-evaporating).

3.3. PN index

As discussed in Section 1.3.1 Aikawa *et al* [50] use a PM index that is of the same form as Equation 3.3 (repeated from 1.3.1), but there is insufficient compositional information of their fuels available in their paper for the PM index to be calculated independently.

$$PM\ index = \sum_{i=1}^{n} \left[\frac{DBE_i + 1}{VP_{(443K)i}} \right] W_{ti} \qquad (3.3)$$

The vapour pressure used in the PM index is not a direct measurement, but comes from an empirical relation between the normal boiling point of each component and its vapour pressure at 443 K.

To avoid confusion in this thesis the term PN index is used for other indexes relating particulate emissions to fuel composition.

Commercial fuels are often supplied with a data sheet that includes standard data, and the methods by which it has been calculated or tested. An example data sheet showing the data usually available is shown in Figure 3.7. This is a typical data sheet for a European fuel, a US data sheet would probably use RVP instead of DVPE as the vapour pressure evaluation method, and would include initial boiling point (IBP), T50 (the temperature at which 50 % of the fuel has evaporated), T90 (the temperature at which 90 % of the fuel has evaporated), and final boiling point (FBP) as the parameters governing distillation characteristics rather than % evaporated at 70 °C, 100 °C, and 150 °C.

Petrochem Carless Ltd
Head Office - Cedar Court
Guildford Road, Fetcham
Leatherhead
Surrey, KT22 9RX
Telephone 44 (0) 1372 360000
Fax 44 (0) 1372 380400

PETROCHEM CARLESS

Petrochem Carless BVBA
Orteliuskaai 2-4/Bus 26
2000 Antwerp
Belgium
Telephone + 323 2059370
Fax + 323 2263126

Certificate of Analysis

Lot : [redacted]
Batch :

Customer Name [redacted]
Customer No
Consignee
Delivery Address

PCL Order Reference [redacted]
Customer Reference
Customer Item Code
Customer Description

Product Name [redacted]
Product Number
Certificate No
Certificate Date
Approval Date
Approved By:
Checked by
Approval Status
Spec No

Method	Description	Min	Max	Results	Unit
ASTM D4052	Density at 15°C	0.7480	0.7540	0.7516	g/mL
ASTM D4052	Specific Gravity at 15°C			0.7523	Ratio
Distillation					
ASTM D86	I.B.Pt.			35.1	°C
ASTM D86	Evaporated at 70°C	24.0	40.0	36.4	%
ASTM D86	Evaporated at 100°C	50.0	60.0	57.9	%
ASTM D86	Evaporated at 150°C	83.0	90.0	86.4	%
ASTM D86	F.B.Pt.	190	210	196.6	°C
ASTM D86	Residue		2.0	1.0	% vol
Engine Tests					
ASTM D2699	R.O.N.	95.0		99.4	Units
ASTM D2700	M.O.N.	85.0		88.4	Units
FIA					
ASTM D1319	Aromatics	29.0	35.0	32.8	% vol
ASTM D1319	Olefins	3.0	13.0	5.7	% vol
ASTM D1319	Saturates			56.7	% vol
General Properties					
EN 13016-1	Vapour pressure (DVPE) 37.8°C	56.0	60.0	58.2	kPa
ASTM D525	Oxidation Stability	480		>480	minutes
ASTM D381	Gum, - washed		4	<0.5	mg/100mL
ASTM D130	Copper Corrosion, 3hrs at 50°C			1A	
EN 237	Lead		5.0	<2.5	mg/L
ASTM D3231	Phosphorous Content		1.3	<0.2	mg/L
IP 490	Sulphur Content		10	<3.0	mg/kg
IP 466	Ethanol	4.7	5.3	4.8	% vol
IP 466	Oxygen Content	1.7	2.0	1.76	% mass
IP 466	Other Oxygenates			NONE	% v/v
IP 438 ANNEX B	Water Content		0.015	0.0130	% v/v
EN 238	Benzene		1.0	<0.1	% v/v
To Be Recorded					
ASTM D5291	Carbon Content			85.61	% m/m
ASTM D5291	Hydrogen Content			12.63	% m/m
CALCULATION	H/C Mass Ratio			0.1475	Ratio
CALCULATION	O/C Mass Ratio			0.0206	Ratio
CALCULATION	Atomic H/C Ratio			1.7573	Ratio
CALCULATION	Atomic O/C Ratio			0.0154	Ratio
IP 12	Gross Calorific Value			45.04	MJ/kg
IP 12	Net Calorific Value			42.36	MJ/kg
CALCULATION	Net Calorific Value			18212	Btu/lb

Printed : 10/07/2012 Page 1

This certificate is generated electronically and is therefore valid without a signature

Figure 3.7: Example fuel specification sheet showing the parameters typically available regarding gasoline composition

Detailed hydrocarbon analysis (DHA) of fuels uses a chromatographic method to provide a complete compositional breakdown of the 200-300 hydrocarbons present in a typical gasoline. It is an expensive test, and not typically performed for gasoline. Calculation of the PM index requires a DHA as each of the components is evaluated individually then incorporated into the index as a linear sum. As discussed in Section 3.2, mixtures of hydrocarbons do not behave as a linear combination of their parameters, and the method used by Aikawa *et al* [50] does not take this non-linear behaviour into account at all.

Given the information on fuel composition that is typically available, it is possible to adapt the PM index by making small changes such that a PN index for fuels can be calculated without doing expensive, and time consuming extra analysis. This has obvious advantages. The industry standard is that fuels are blended by volume fraction; this is a small adaptation from the mass fraction used in the PM index. Fortunately, as can be seen from Figure 3.7, parameters that can be used to calculate the DBE are included on a typical specification sheet; these are the aromatic content, olefin content, oxygenate content, and paraffin content, and a measure of vapour pressure – DVPE or RVP. Other important parameters which are known to have an effect on PN emissions – T90 and oxygenate content – are also included.

Unfortunately the definition of these terms is not quite what would be expected. The standard for measuring these parameters, ASTM D1319 [113], defines them as follows: *"**aromatics**: the volume % of monocyclic and polycyclic aromatics, plus aromatic olefins, some dienes, compounds containing sulfur and nitrogen, or higher boiling oxygenated compounds, **olefins**: the volume % of alkenes, plus cycloalkenes, and some dienes, and **paraffins**: the volume % of alkanes, plus cycloalkanes."*

This could be a problem for calculating DBE, as all of those components have differing DBEs; monocyclic aromatics (4), polycyclic aromatics (>7), aromatic olefins (>5), dienes (2 or 3), oxygenates (0), alkenes (1), cycloalkenes (2), alkanes (0), and cycloalkanes (1). However, knowledge of typical gasoline composition, and these compounds can quickly narrow the range – for example, the simplest polycyclic aromatic compound, Napthalene ($C_{10}H_8$), has a boiling point of 218 °C, which means it is very unlikely to be present in any significant quantities in gasoline.

The concept of developing a PN index is to use these bulk properties, so provided that the average DBE of these components is correct small deviations will not matter. For this reason, and the boiling point considerations noted above, it is unlikely that the *aromatics* listed will contain significant quantities of anything else, so aromatics are assigned a DBE of 4; *olefins* may include some cycloalkenes, but may also include some paraffins, these will have opposing effects on the net DBE, so olefins are assigned a DBE of 1; the *paraffin* part of the specification sheet is obtained as volume remaining after the aromatics, olefins, and oxygenates have been accounted for, it seems safe to assign paraffins a DBE of 0.

With this in mind a PN index is introduced, with the vapour pressure being evaluated as dry vapour pressure equivalent (DVPE) with units of kPa and the use of volume fraction (V_i). The PN index is shown in Equation 3.4.

$$\text{PN index} = \frac{\sum_{i=1}^{n}[DBE_i + 1]V_i}{DVPE\ (\text{kPa})} \qquad (3.4)$$

DVPE was used as the measure of vapour pressure since this is a European standard measurement, which is evaluated at 310.95 K and the index has always been calculated here by volume fractions; an industry standard for fuel mixing.

Comparisons using some model fuels indicate that these changes have an effect of up to a 50 % on the relative difference between the PM index and the PN index. This difference is explored in Section 3.3.2.

3.3.1. Vapour pressure

The vapour pressure of gasoline is measured in accordance with EN 13016-1 [114] and an equivalent US standard and is expressed as dry vapour pressure equivalent (DVPE) or Reid vapour pressure (RVP). This standard uses a temperature of 37.8 °C (310.95 K), whereas the PM index in [50] uses absolute vapour pressure at a temperature of 443 K. DVPE is intended to be equivalent to RVP [114], and is calculated from a statistical correlation equation to give a dry Reid vapour pressure. The differences between Reid vapour pressure, DVPE and air saturated vapour pressure (ASVP), are all small (and comparable to uncertainties when they are measured or modelled); they are all essentially absolute vapour pressures.

DVPE can easily be converted to ASVP from Equation 3.5 [114].

$$DVPE(kPa) = (0.965 ASVP(kPa)) - 3.78 \qquad (3.5)$$

The difference between ASVP and VP comes from the dissolved air in the liquid in the ASVP test. This can be approximated from Henry's law, which is shown in Equation 3.6 [39].

$$p = k_h c \qquad (3.6)$$

Here p is the partial pressure of the solute gas in solution, k_h is a temperature dependent coefficient, and c is the concentration of the solute.

k_h can be calculated from the van't Hoff equation, shown in Equation 3.7, which is temperature dependent.

$$\frac{d \ln k_h}{dT} = \frac{\Delta_r H^{\ominus}}{RT^2} \tag{3.7}$$

$\Delta_r H^{\ominus}$ is the standard reaction enthalpy evaluated at a temperature T and R is the molar gas constant. The van't Hoff equation shows that for an endothermic reaction ($\Delta_r H^{\ominus} > 0$), k_h increases as T rises, the opposite is true for an exothermic reaction. A fuller explanation and derivation of the van't Hoff equation is shown in Atkins [39].

Henry's law can then be used to calculate the air dissolved in the liquid at 273.15 K that will come out of solution at 310.95 K. This will provide an approximate conversion from VP to ASVP.

The effect of the vapour pressure used on the PM index has been investigated. Using the method used by Aikawa *et al* [50] and discussed in Section 1.3.1, which estimates the vapour pressure from the boiling points of components, the vapour pressure at 443 K has been calculated, weighted by mass, as in the PM index. This vapour pressure can then be compared to the vapour pressure, evaluated at 443 K, as shown in Reid *et al* [103]. The two vapour pressures have been calculated for the model fuels shown in Section 3.4.1, and plotted, the comparison can be seen in Figure 3.8. It can be seen that there is an extremely good correlation (R^2 = 0.998) between the two vapour pressures, so the estimate used by Aikawa *et al* is a good one.

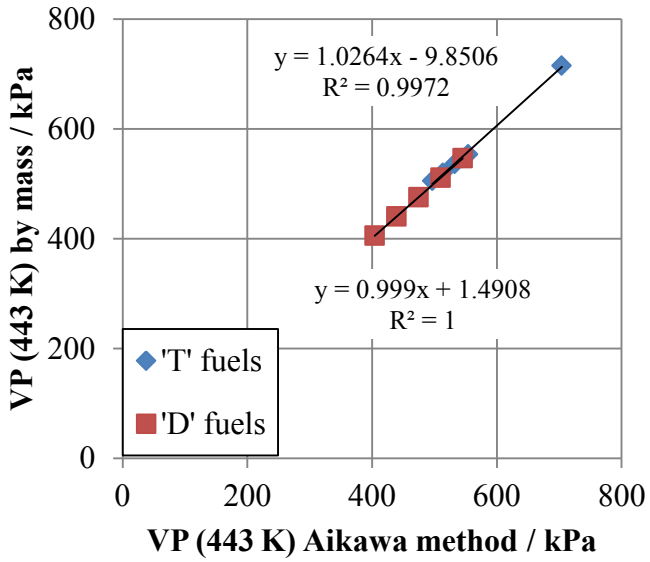

Figure 3.8: Comparison between VP (443 K) as estimated in Aikawa *et al* [50] and VP (443 K) as calculated from Reid *et al* [103]. 'T' fuels are those listed in Table 3.10 beginning with a 'T', similarly for 'D'fuels

However the PN index, in contrast to the PM index, evaluates the vapour pressure at 310.95 K (using the RVP or DVPE method). Given that the vapour pressure is the pressure at a given temperature exerted by the vapour phase of a particular component on its liquid phase when at thermodynamic equilibrium, reducing the calculation temperature will drastically reduce the value of the vapour pressure. This reduction is not linear though; heavier components (say C10) will reduce faster than the lighter components. The UNIFAC model described in Section 3.2, as it is an evaporative model, can also be used to give the vapour pressure of a fuel mixture (given that the vapour pressure needs to be calculated by the model to model distillation), this should more accurately reflect the real vapour pressure of the fuel. The vapour pressure for the same model fuels has been calculated in this way, with the results still weighted by mass, as in Aikawa *et al*, at a temperature of 310.95 K, and the results compared with the method used by Aikawa *et al*, this is shown in Figure 3.9.

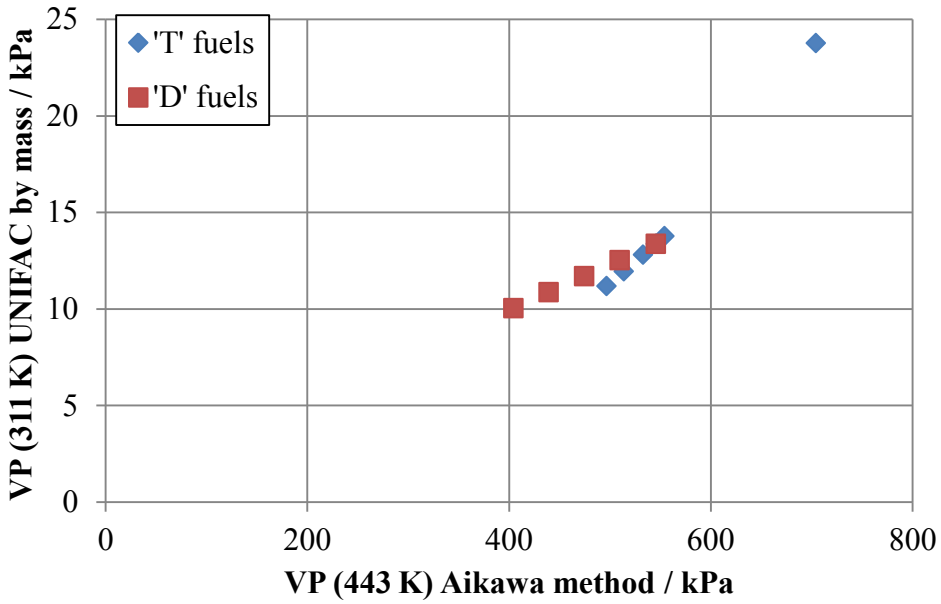

Figure 3.9: Comparison between VP (443 K) as estimated in Aikawa *et al* [50] and VP (311 K) as calculated from Reid *et al* [103] by mass. 'T' fuels are those listed in Table 3.10 beginning with a 'T', similarly for 'D'fuels

It can be seen that the effect of reducing the vapour pressure calculation temperature to 310.95 K has had a non-linear effect, with the fuels containing more heavy components having a comparatively lower vapour pressure.

The final step is to compare the DVPE as calculated by the UNIFAC model, weighted by volume, as in the PN index calculation, with vapour pressure calculated according to the method used by Aikawa *et al* for the same model fuels. The results are shown in Figure 3.10, and it can be clearly seen that the effect of switching from a mass weighting to a volume weighting is to even further magnify the effect of the heavier components (as they have a larger density), meaning that the fuel with the fourth lowest vapour pressure according to the Aikawa method, now has the lowest vapour pressure overall.

Comparing vapour pressures in this way gives an idea of how the PM index and the PN index might compare.

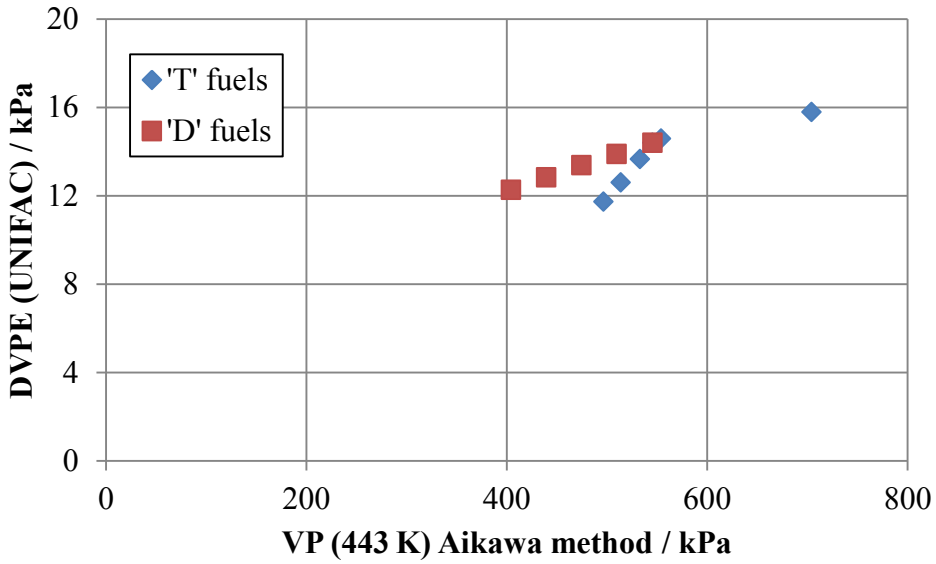

Figure 3.10: Comparison between VP (443 K) as estimated in Aikawa *et al* [50] and DVPE as calculated using the UNIFAC model. 'T' fuels are those listed in Table 3.10 beginning with a 'T', similarly for 'D'fuels

When calculating the PN index for the model fuels mixed from pure components, for which the complete compositional breakdown was known, but DVPE was not known, the PN index was calculated using VP calculated at 310.95 K (using the UNIFAC method discussed in Section 3.2.2) then converted to DVPE using the method discussed in this section. For commercial gasolines, the stated DVPE or RVP was used.

3.3.2. Comparison of PN index with PM index

The differences between the PN index and the PM index are a change from weighting of components by mass (PM index) to the weighting of components by volume (PN index), which is the industry standard. This is expected to give a lower weighting to the DBE of heavier components in the fuel. Reducing the vapour pressure calculation temperature reduces the magnitude of the vapour pressure by factors of between 20-40, with the heavier hydrocarbons experiencing a greater reduction. This will increase the magnitude of the PN index by a similar amount. Overall the change is expected to

increase the impact of the double bond equivalent of the fuel on the index relative to the vapour pressure significantly.

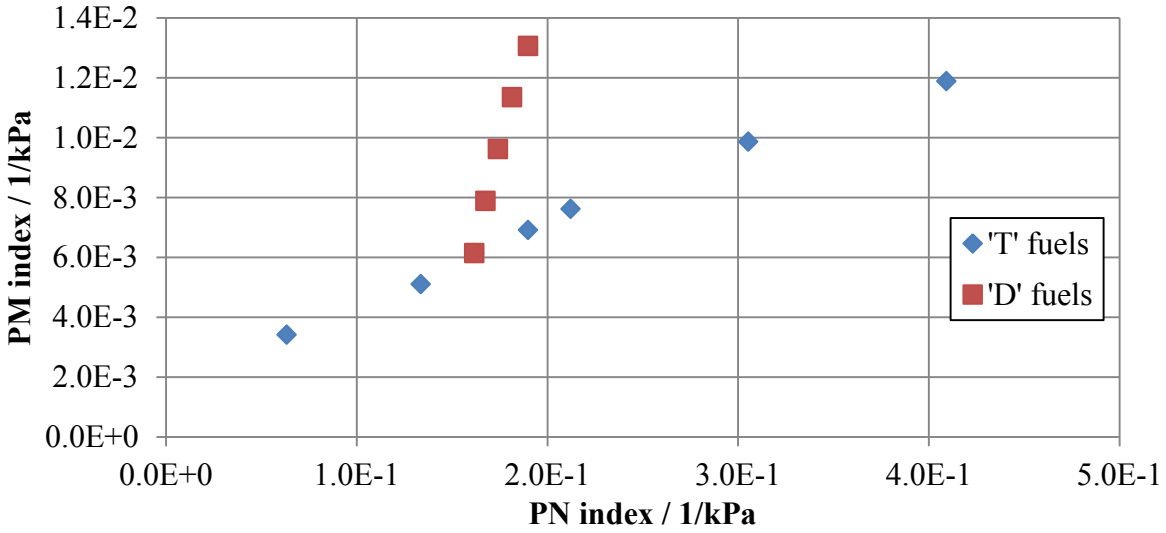

Figure 3.11: Comparison of PM index and PN index for model fuels. 'T' fuels are those listed in Table 3.10 beginning with a 'T', similarly for 'D'fuels

Figure 3.11 shows the comparison between the PM index and the PN index for the model fuels. It can be seen that the expected trends are present – the PN index has a magnitude 30-40 times greater than the PM index, and a greater range. The effect of the heavier components present in the fuel has been supressed, and the fuels with the highest DBE now have the highest PN index.

3.3.3. Error in the PN index

The PN index is of course not an exact quantity, as the quantities used to calculate it have an error associated with them, so a potential error on the PN index can be calculated by cascading down the reproducibility from the appropriate test methods (specified in the relevant legislation [70]), and assuming a 'worst case' effect of each of the errors. Reproducibility is defined as *"The difference between two single and independent results,*

obtained by different operators working in different laboratories on identical test material" [70].

For the DVPE test [114], the reproducibility (*R*) is a fixed value of 2.75 kPa. The DBE is calculated from the stated olefin and aromatic content, the reproducibility of the parameters is shown in Table 3.3. The T90 is determined according to EN-ISO 3405 [115]. The reproducibility is defined as $R = 0.019(T90 + 59.77)$. Oxygenate content is determined according to EN 14517 [116]. The reproducibility is defined as $R = 0{,}0251\,X + 0{,}3510$ where *X* is (% v/v) present in sample.

Table 3.3: Reproducibility of DBE parameters for oxygenate containing samples [113]

	Valid range (%v/v)	Reproducibility (% v/v)
Aromatics	13-40	3.7
Olefins	4-33	$0.82X^{0.6}$ (X is (% v/v) present in sample)
Saturates	45-68	4.2

3.3.4. Application of the PN index to reference fuel specifications

As the trends of PN index had been shown to hold for commercially available gasolines, the Euro 5 emissions standards (CEC RF-02-08) [69] were investigated. The standard specifies a parameter range for the test fuel [70], and the parameters of the specification relevant to the PN index can be seen in Table 3.4.

Table 3.4: Euro 5 reference fuel specification [70]

	Min	Max
DVPE (kPa)	56.0	60.0
Olefins (% v/v)	3.0	13.0
Aromatics (% v/v)	29.0	35.0
Oxygenates (% v/v)[1]	4.7	5.3
T90[2] (°C)	150	210

1. The specification states that ethanol is the only oxygenate to be purposefully added to the fuel, so this value is stated here.
2. The specification actually gives a Final Boiling Point (FBP) value, and a maximum evaporated by 150 °C – these have been used to interpolate a T90 value.

These parameters can be arranged to give a maximum and minimum PN index possible with a reference fuel meeting the specification, as seen in Table 3.5. It can be seen that a variation in the index of approximately 24 % is theoretically possible.

Table 3.5: Euro 5 reference fuel parameters arranged for greatest PN index variation

	Min PN index	Max PN index
DVPE (kPa)	60.0	56.0
DBE+1 (% v/v)	2.19	2.53
T90 (°C)	210	150
Oxygenates (% v/v)	5.3	4.7
PN index (1/(kPa))	3.65	4.51

The same calculation can be undertaken for the draft of the US EPA Tier 3 reference fuel specification [117]. The US EPA Tier 3 specification is the first reference fuel specification to take into account the effect on fuel composition on PN emissions, and specifically cites the paper by Aikawa *et al* [50] when considering the formulation of reference fuels for particulate emissions. The specification also limits the levels of heavier aromatics in the test fuel, stating that they have a higher impact on particulate emissions. These will be tested using ASTM D5769 [118], a chromatographic method very similar to the European equivalent EN 14517 [116], which is already undertaken for a European

standard reference fuel specification sheet. The aromatic limits for Tier 3 gasoline are shown in Table 3.6.

Table 3.6: Aromatic levels permitted in USA EPA Tier 3 reference fuel specification [117]

Aromatic (% v/v)	Min	Max
C6 (benzene)	0.6	0.8
C7 (toluene)	4.4	5.5
C8	5.5	6.9
C9	5.0	6.2
C10+	4.0	5.0

The relevant parameters for the PN index in the Tier 3 reference fuel specification are shown in Table 3.7, and rearranged in Table 3.8 for the maximum variation. It can be seen that compared to the Euro 5 specification, a lower PN index overall is found, and there is only a 7 % possible variation in the index, showing the impact of the reference fuel design with the PM index in mind.

Table 3.7: US EPA Tier 3 reference fuel specification [117]

	Min	Max
DVPE (kPa)	60.0	63.4
Olefins (% v/v)	4.5	11.5
Aromatics (% v/v)	19.5	24.5
Oxygenates (% v/v)	14.6	15.1
T90 (°C)	154	166

Table 3.8: US EPA Tier 3 reference fuel parameters for greatest PN index variation

	Min PN index	Max PN index
DVPE (kPa)	63.4	60.0
DBE+1 (% v/v)	1.83	1.85
T90 (°C)	166	154
Oxygenates (% v/v)	15.1	14.6
PN index (1/(°C.kPa))	2.89	3.08

3.4. Experimental fuels

3.4.1. Model fuels

The target was to vary the DBE and VP independently with the model fuels; this would give the opportunity to investigate the parameters of the PN index independently. To this end, the model fuels were blended from pure components. Toluene and 1,3,5-trrimethylbenzene were chosen as aromatic components having medium and high boiling points (both with a DBE of 4), and then their paraffin counterparts were selected on the basis of having adjacent boiling points (see Table 3.9), with blends of paraffins selected to give co-evaporation, (checked using the UNIFAC model – see Section 3.2.2) with the corresponding aromatic component. The final paraffin blends, selected on the basis a trade-off between octane number and coevaporation were iso-octane : n-octane – 75 : 25, and iso-decane : n-decane – 24 : 76. Pentane was used to provide a volatile 'front end', so that the model fuel closer mimics market fuels, more discussions as to why n-pentane was added can be found in Section 4.2. When the volatility was varied, the aromatic content was kept at 35 %, because this is the upper limit for the aromatic content specified in EN228 [42] for European gasoline and it maintains the octane number above 70 (the minimum octane rating for the single cylinder optical access engine at part load using retarded inlet valve closure).

The octane number constraints are a limiting factor; Table 3.9 shows the RON and BON for all of the components included in the model fuels. As can be seen, for molecules with higher carbon numbers, when they are straight chain hydrocarbons, they tend to have very low RONs and BONs, but experience from the UNIFAC model showed that they promoted good co-evaporation. A compromise therefore had to be achieved when setting

the ratio of paraffin components between these two parameters, given that the components with the highest octane ratings (both aromatics) were limited to 35 %.

Table 3.9: Octane numbers and boiling points of model fuel components

Component	Boiling point (K)	RON	BON
n-pentane	309.22	62	60
iso-octane	372.39	100	100
n-octane	398.82	-18	-19
75/25 io/no mix	n/k	n/k	70
Toluene	383.79	120	109
2,2,3,3-tetramethylhexane	410.61	100	126
n-decane	447.30	-17	-41
24/76 id/nd mix	n/k	n/k	-1
1,3,5Trimethylbenzene	437.90	170	161

References: [47, 101, 108, 119, 120]

The final composition for the model fuels is shown in Figure 3.12, Figure 3.13 and Table 3.10, and a model of their distillation curves is shown in Figure 3.14. It can be seen that there is good control over the double bond equivalent and vapour pressure of the fuel, whilst still meeting the octane number limits. It can be seen that the vapour pressure variation achieved with the 'D' fuels is not as great as had been hoped; however because of the addition of 5 % by volume n-pentane, and the octane number considerations, it was not possible to get any greater variation.

Comparing the predicted distillation curves of the model fuels (Figure 3.14) and the market fuels tested in this thesis (Figure 3.2, Figure 3.3, Figure 3.4, Figure 3.15, Figure 3.16, Figure 3.17, and Figure 3.18), it can be seen that the volatility characteristics of the model fuels do not match the market fuels, the market fuels not having as great a volume of high or low volatility components, and hence giving a much flatter distillation curve.

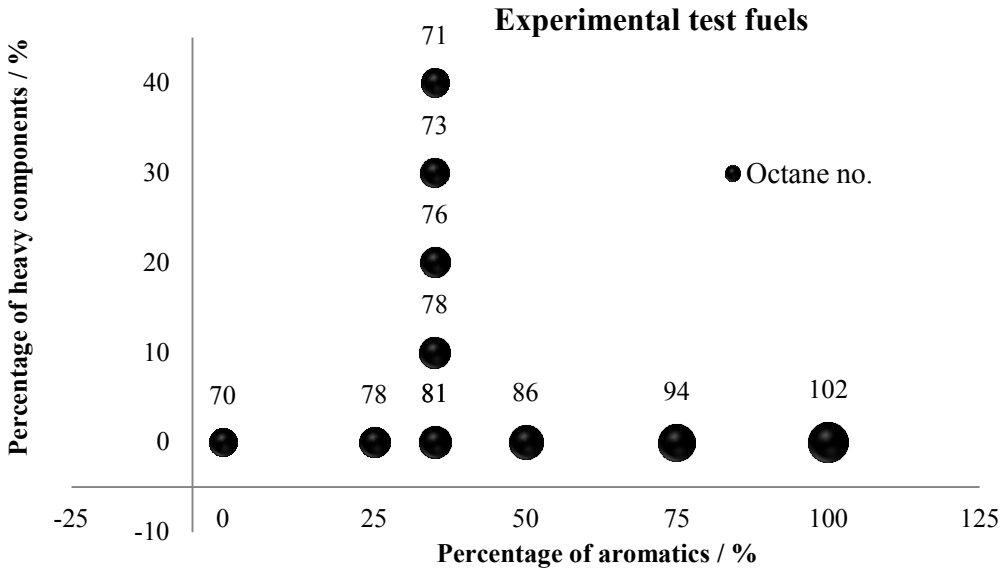

Figure 3.12: Research octane number (RON) and composition of the model fuels

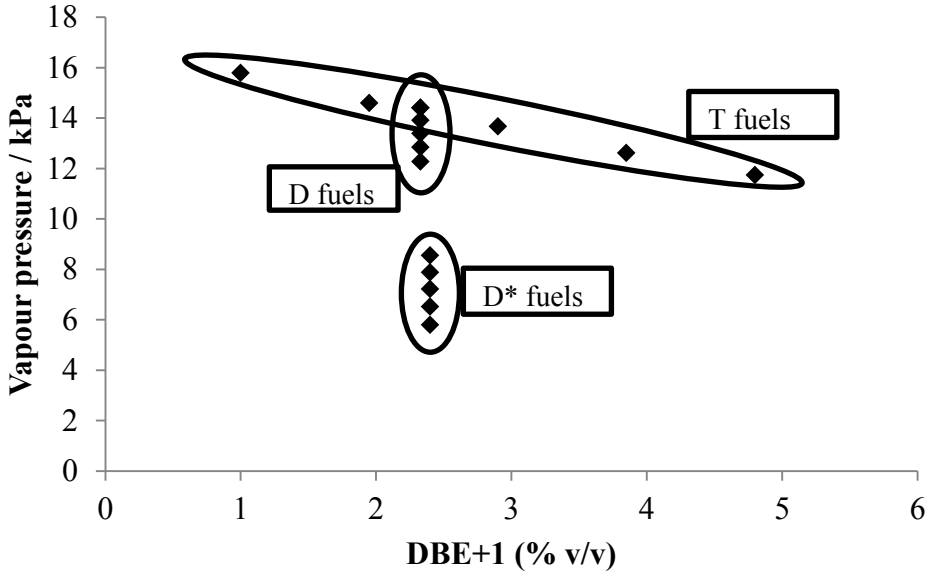

Figure 3.13: DBE and vapour pressure for the model fuels, a star (*) indicates a fuel with the same composition as an unstarred fuel, but without 5% v/v n-pentane

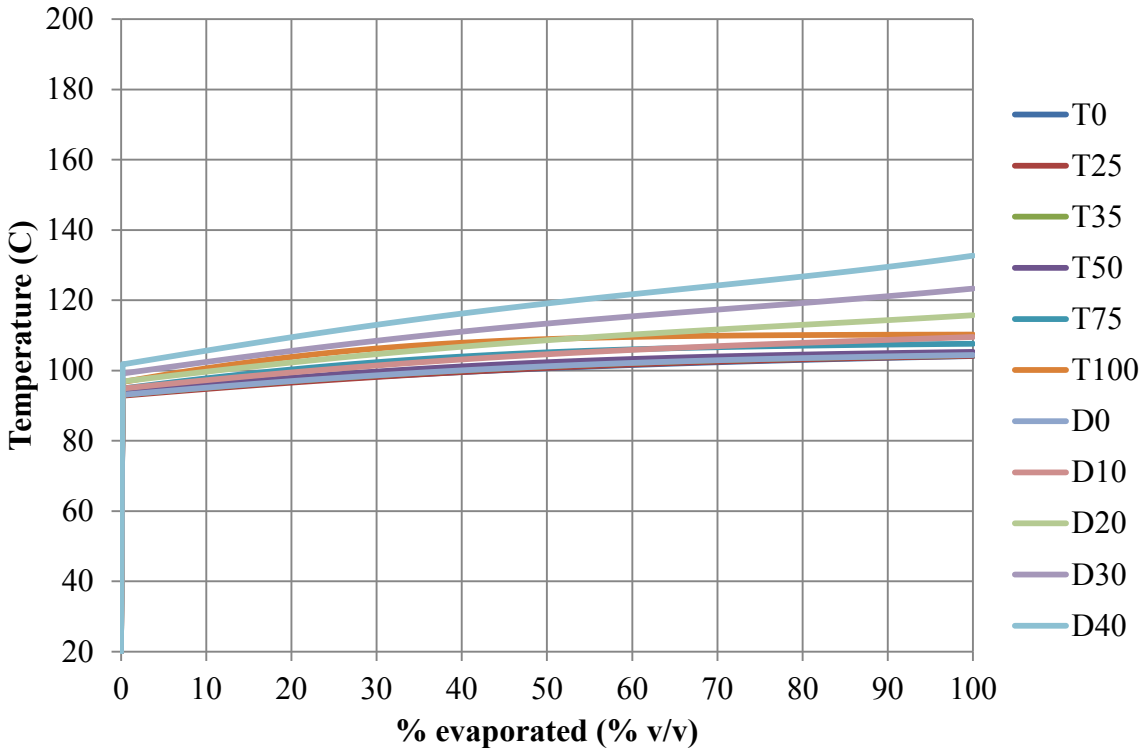

Figure 3.14: UNIFAC prediction of the distillation curves of the model fuels

Table 3.10: Model test fuel composition

Fuel	Light components	Medium components			Heavy components			DBE+1	VP[1] (kPa)	PM index[2]	PN index (×100)
% v/v	n-pentane	iso-octane	n-octane	Toluene	iso-decane[3]	n-decane	TMB[4]				
T0	5.00	71.25	23.75	0.00	0.00	0.00	0.00	1.00	15.37	0.341	6.51
T25	5.00	53.44	17.81	23.75	0.00	0.00	0.00	1.95	15.73	0.511	12.40
T35[5]	5.00	46.31	15.44	33.25	0.00	0.00	0.00	2.33	15.55	0.615	14.99
T42	5.00	41.32	13.78	39.90	0.00	0.00	0.00	2.60	15.41	0.684	18.50
T50	5.00	35.63	11.88	47.5	0.00	0.00	0.00	2.90	15.27	0.762	19.00
T75	5.00	17.81	5.94	71.25	0.00	0.00	0.00	3.85	14.75	0.987	26.09
T100	5.00	0.00	0.00	95.00	0.00	0.00	0.00	4.80	14.08	1.19	34.08
D0[5]	5.00	46.31	15.44	33.25	0.00	0.00	0.00	2.33	15.55	0.615	14.99
D10	5.00	41.68	13.89	29.93	1.48	4.69	3.33	2.33	14.92	0.789	15.62
D20	5.00	37.05	12.35	26.60	2.96	9.37	6.65	2.33	14.26	0.962	16.34
D30	5.00	32.42	10.81	23.28	4.45	14.08	9.98	2.33	13.56	1.13	17.18
D40	5.00	27.79	9.26	19.95	5.93	18.77	13.30	2.33	12.84	1.31	18.15
D0*	0.00	48.75	16.25	35.00	0.00	0.00	0.00	2.40	9.51	0.408	25.25
D10*	0.00	43.88	14.63	31.50	1.56	4.94	3.50	2.40	8.76	0.541	27.40
D20*	0.00	39.00	13.00	28.00	3.12	9.88	7.00	2.40	7.98	0.674	30.09
D30*	0.00	34.13	11.38	24.50	4.68	14.82	10.50	2.40	7.16	0.806	33.53
D40*	0.00	29.25	9.75	21.00	6.24	19.76	14.00	2.40	6.31	0.937	38.06

1. VP is estimated according to the UNIFAC model, not measured
2. PM index calculated by % mass as in [50]
3. 2,2,3,3-tetramethylhexane
4. 1,3,5-trimethylbenzene
5. N.B. T35 ≡ D0

A star (*) indicates a fuel with the same composition as an unstarred fuel, but without 5% v/v n-pentane

3.4.2. Commercial fuels

The PN index was tested with several market fuels often selected either because they were available on the site where the engine was tested, or selected by a project partner who had their own fuel investigation work to do.

Given the potential index variation found within the EU5 reference fuel specification, it was decided to have blended two fuels, which would meet the EU5 (CEC RF-02-08) reference fuel specification, but with the maximum possible PN index variation (see Section 3.3.4). The relevant parameters of their composition can be seen in Table 3.11, and their distillation curves shown in Figure 3.15. Unfortunately, the blending process was unable to meet the volatility specification exactly, but the error is small, and these two fuels are certainly representative of the CEC RF-02-08 specification. These fuels were tested in the AJ133 V8 engine, and the single cylinder, optical access engine.

Table 3.11: CEC RF-02-08 representative test fuel composition

	DBE+1 (% v/v)	DVPE (kPa)	T90 (°C)	Oxygenates (% v/v)	PN index (1/kPa)
W12/185	2.20	61.7	154.7	5.0	3.56
W12/186	2.49	59.9	176.5	5.0	4.16

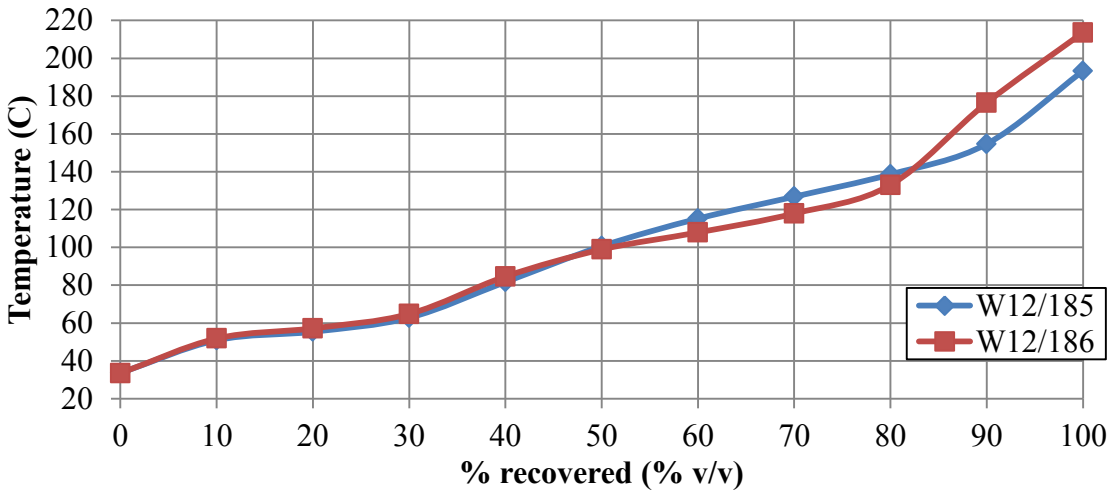

Figure 3.15: Distillation curves of the two CEC RF-02-08 representative test fuels using data from the fuel's data sheet

Five fuels giving a spread of the PN index were selected for the drive cycle experiments from a selection of fuels used for emissions tests at Jaguar Land Rover's Whitley Engineering Centre. At both ends of the PN index, fuels were selected that had a low (or high) index due to either a high (or low) vapour pressure or DBE, giving some form of independent control over these parameters. The properties of these fuels are shown in Table 3.12, and limited distillation curves shown in Figure 3.16 (due to the limited information available on the fuel specification sheets, only five distillation curve points are available). Of note from these fuels, 368b is compliant with the EU5 (CEC RF-02-08) reference fuel specification and TRIAS is a Japanese certification fuel. These fuels were tested on an AJ126 V6 engine, over a simulated NEDC.

Table 3.12: Drive cycle test fuel composition

	DBE+1 (% v/v)	VP (kPa)	T90 (°C)	Oxygenates (% v/v)	PN index (1/kPa)
421c	2.11	106.1	153.6	10.0	1.99
418c	1.98	92.9	143.9	10.2	2.15
368b	2.32	56.2	160	4.8	4.07
403c	2.28	47.8	175.3	0.0	4.77
TRIAS	2.95	57.3	147.7	0.0	5.14

* either DVPE or RVP depending on fuel analysis method

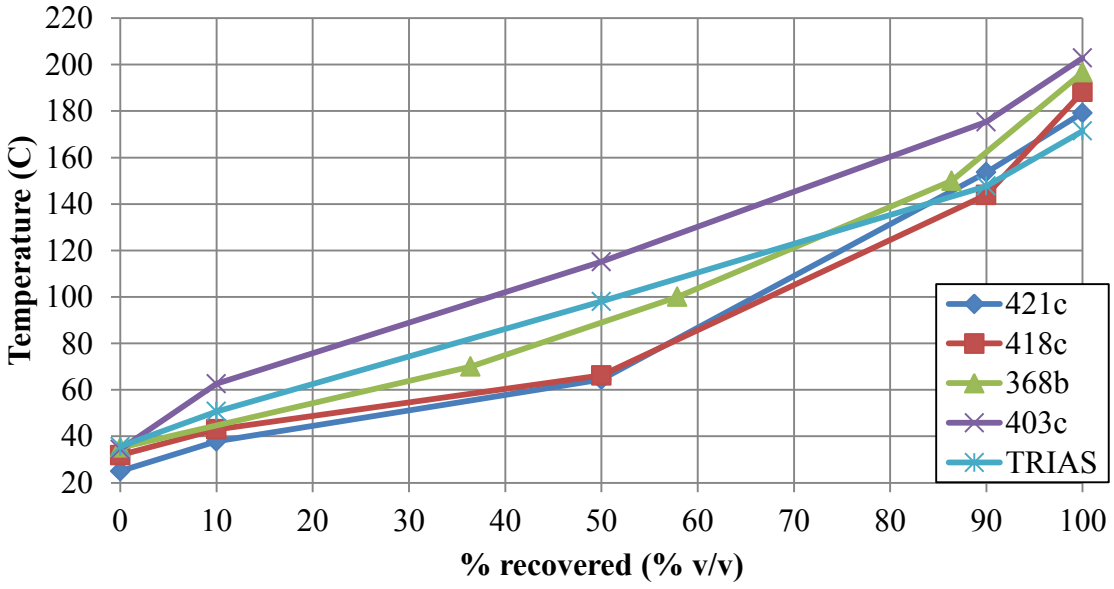

Figure 3.16: Distillation curves of the five drive cycle test fuels

Two EN228 compliant fuels were tested on the single cylinder, optical access engine. Their specifications and PN indices are shown in Table 3.13, and their distillation curves in Figure 3.17.

Table 3.13: EN228 compliant test fuel composition

	DBE+1 (% v/v)	DVPE (kPa)	T90 (°C)	Oxygenates (% v/v)	PN index (1/kPa)
S070907	2.58	70.6	148.9	0.00	3.66
S103275	2.25	88.6	132.5	4.87	2.54

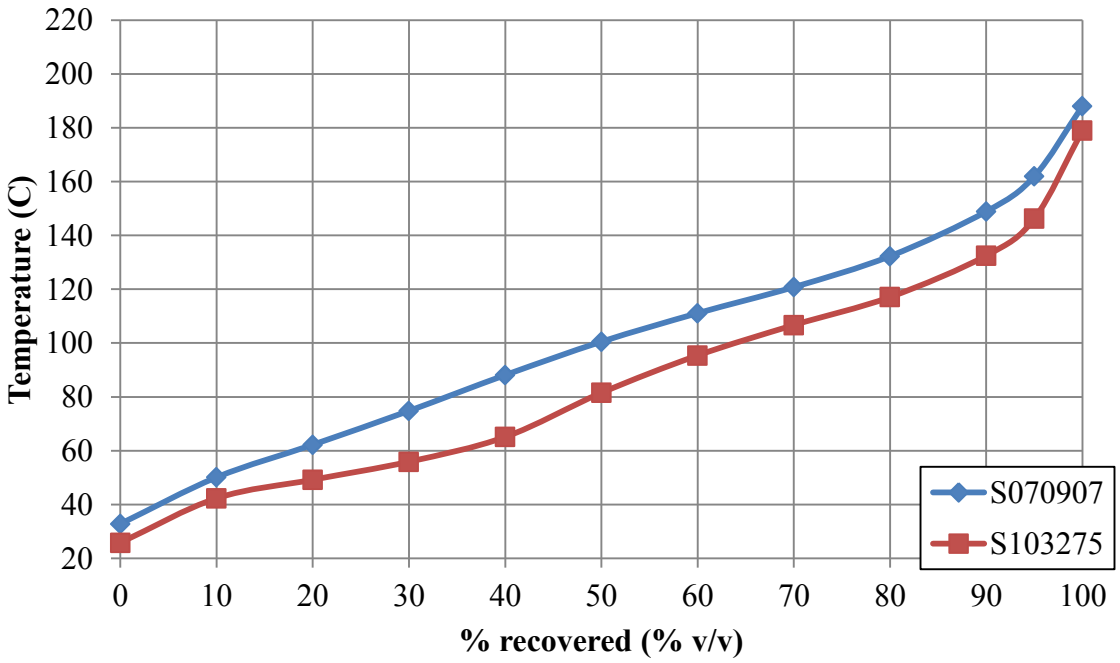

Figure 3.17: Distillation curves of the two EN228 compliant cycle test fuels using data from the fuel's data sheet

The fuels tested on the ULTRABOOST engine were chosen by the ULTRABOOST consortium and supplied by Shell, and the experiments measuring the particulate emissions were piggy-backed onto existing experiments. For this reason the fuel selection is not what would be chosen if one were focussing on solely measuring particulate emissions. A total of 15 fuels were tested, four were commercial gasolines (BASE, G, H, and I), of note

is that fuel G has an exceptionally high RON and MON with special components, and is a race fuel, the emissions from which may not be representative of fuels in the wider market. There were four specially blended with the aim of a RON vs. MON design of experiments exercise, to study the sensitivity of knock to RON and MON and to discover the engine's 'octane appetite'. Two fuels were specially blended to see if there was any impact of the fuel's laminar burning velocity (LBV)[6] [76], one with a high and one with a low LBV. Also tested was a matrix of alcohol based fuels, ethanol, methanol and tertiary (gasoline, ethanol, and methanol – GEM) blends. The relevant parameters and some notes on the fuels tested are shown in Table 3.14 and the distillation curves of four of the fuels are shown in Figure 3.18. From the distillation curves shown in Figure 3.18, it can be seen that fuel G (a very high octane fuel, which might be suitable for racing applications) has very different volatility characteristics to both the other fuels tested on the ULTRABOOST engine, and to the other market fuels whose distillation curves are shown in this thesis (Figure 3.2, Figure 3.3, Figure 3.4, Figure 3.15, Figure 3.16, and Figure 3.17).

[6] LBV is the speed at which a flame advances into a stationary unburnt mixture.

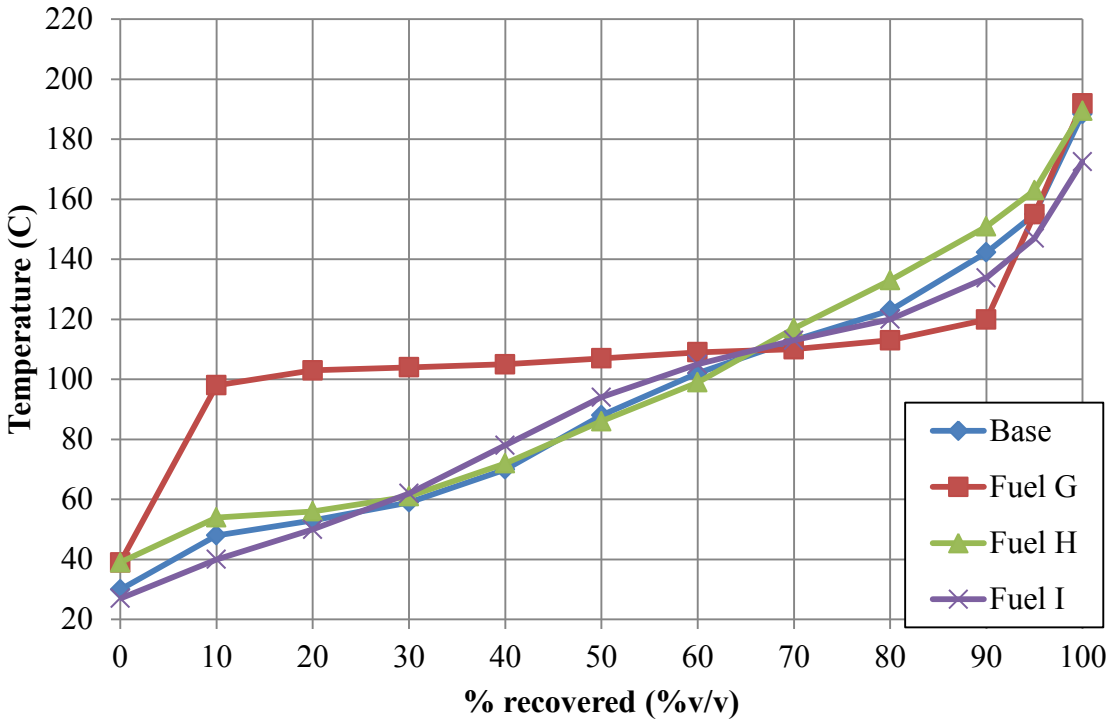

Figure 3.18: Distillation curves of the four of the fuels tested on the ULTRABOOST engine (data from [121]), it can clearly be seen that fuel G has a very different distillation profile to the other three fuels

The alcohol-based fuels (oxygenate fuels) do not share a common gasoline base (this is reflected in the non-oxygenate components displayed in Table 3.14). This means that the results between E20, GEM, M15, and E85 cannot be used independently to verify the impact of each oxygenate.

Table 3.14: ULTRABOOST test fuel composition

Fuel	Description	Purpose	RON	MON	DBE (×100)	RVP (kPa)	T90 (°C)	FBP (°C)	Oxy's (%v/v)	PN index
BASE	E5 base fuel used throughout test development	Included with repeats to monitor test repeatability and drift	97	85.3	247.5	75.0	142.3	188.4	E5	3.30
H	Minimum EN228 octane	To determine effect of RON	95.1	85	246.4	53.1	150.9	189.4	E5	2.64
I	Premium level octane fuel		98.7	86.5	257.1	97.4	133.8	172.5	E0	5.69
G	Very high octane fuel		111.6	101.2	326.7	57.4	119.9	191.9	E0	4.64
A	Decoupled RON / MON	Evaluate significance of RON vs MON	103.3	95	171.6	26.1	114.3	176.9	14% MTBE	6.57
B			101.4	88.8	269.8	68.0	132.5	175.6	10.5% MTBE	3.97
C			92.8	90.7	129.0	30.5	132.8	192.5	E0	4.23
D			88.6	87.3	132.5	32.9	141.0	190.3	E0	4.02
E	Fast burning fuel	Evaluate the impact of flame speed	95.1	82.2	298.7	28.7	132.5	137.5	E0	10.4
F	Slow burning fuel		104.2	92.6	259.5	23.3	135.6	139.2	E0	11.1
E20		Oxygenate performance, and effect of charge cooling	99.6	85.7	232.7	57.8	145.8	183.6	E20	4.03
E85			107.4	89.5	122.9	44.4	77.4	78.4	E85	2.77
M15			99.8	86.1	228.9	110.2	155.5	198.4	M15	2.08
GEM			106	88.1	152.6	84.4	73.9	187.1	M42, E23	1.81

3.5. Chapter 3 summary

In this Chapter gasoline as a complex mix of hydrocarbons has been described. Important parameters for describing the combustion performance of gasoline such as energy content, volatility, and octane rating have been introduced. Given the importance of mixture preparation on particulate emissions from GDI engines an evaporation model using the Raoult-Dalton law and UNIFAC has been written and validated against a variety of gasolines, including those containing large levels of oxygenates.

These models have shown that a linear mixing assumption is not correct for gasoline, and methods using such assumptions should not be used to estimate gasoline parameters. It has also been shown that rather than assuming mixing by volume, looking at molar composition of fuels gives better information about bulk parameters of mixtures.

Given the deviations observed here of model fuels from the properties of gasoline, care must be taken with use of model fuels such that the results are representative of market fuels. Given the use in the literature of model fuels to model the performance of gasoline, validation of the model fuels against market fuels for the parameters of interest must be done.

The PN index linking fuel composition with PM number emissions is introduced, differing from the PM index in being able to use standard properties of gasoline rather than requiring expensive additional testing to be done. The PM index and the PN index have been compared and their differences discussed. The PN index has then been applied to a variety of fuels, including both US EPA and European emissions testing reference fuels. Model fuels have been designed such that they mimic the behaviour of commercial fuels for the parameters of interest, and their composition described. The commercial gasolines used in experimental test work have also been described.

4. Single cylinder engine results

The first evaluation of the PN index has been undertaken with a single cylinder engine. While no single cylinder engine is fitted to production vehicles, in this case, as was described in Section 2.1, the single cylinder engine used has essentially the same combustion system, so results can be seen as representative. In addition, the single cylinder engine uses much less fuel than the V8 on which its combustion system is based, and with pure fuel components costing up to 150× as much per litre as commercially available fuels, this engine permits their testing, which would otherwise be prohibitively expensive. Finally, unlike production engines, this engine is oil-free, at least in the combustion chamber (as oil would interfere with optical access); so the effect of engine oil (a mix of heavy hydrocarbons) can be discounted, meaning that any results obtained are purely as a result of the fuels tested.

4.1. Evaluation of the PN index using model fuels

In total 11 model fuels were tested, and their composition, alongside the test matrix is shown as the first 11 fuels in Table 3.10 and Section 3.4.1. For these experiments the engine was run at a fixed operating point shown in Table 4.1. The engine was run with open loop lambda control with $\lambda = 0.9$. This is to reflect the rich mixture excursions which are known to have a large effect on the particulate matter emissions [122], and tend to dominate drive cycle particulate matter results. Using $\lambda = 0.9$ also improves the SNR of the DMS500.

Table 4.1: Engine operating point for model fuels

IMEP (bar)	1.8
Inlet air temperature (°C)	40
Coolant temperature (°C)	60
Lambda	0.9
RPM	1500
Start of ignition (°CA bTDC)	35
Start of Injection (°CA bTDC)	280

Figure 4.1 shows the PN emissions (in #/cm^3) for the set of fuels with only light and medium components present, but varying aromatic content (and hence DBE), these are referred to as the 'T' fuels. It can be seen in Figure 4.1 that the PN emissions increase with the PN index, but not linearly. Overlaid on Figure 4.1 (the black line) is the PN index calculated for these fuels. It can be seen that the effect of DBE on PM number emissions is greater than that predicted by the PN index for these experiments.

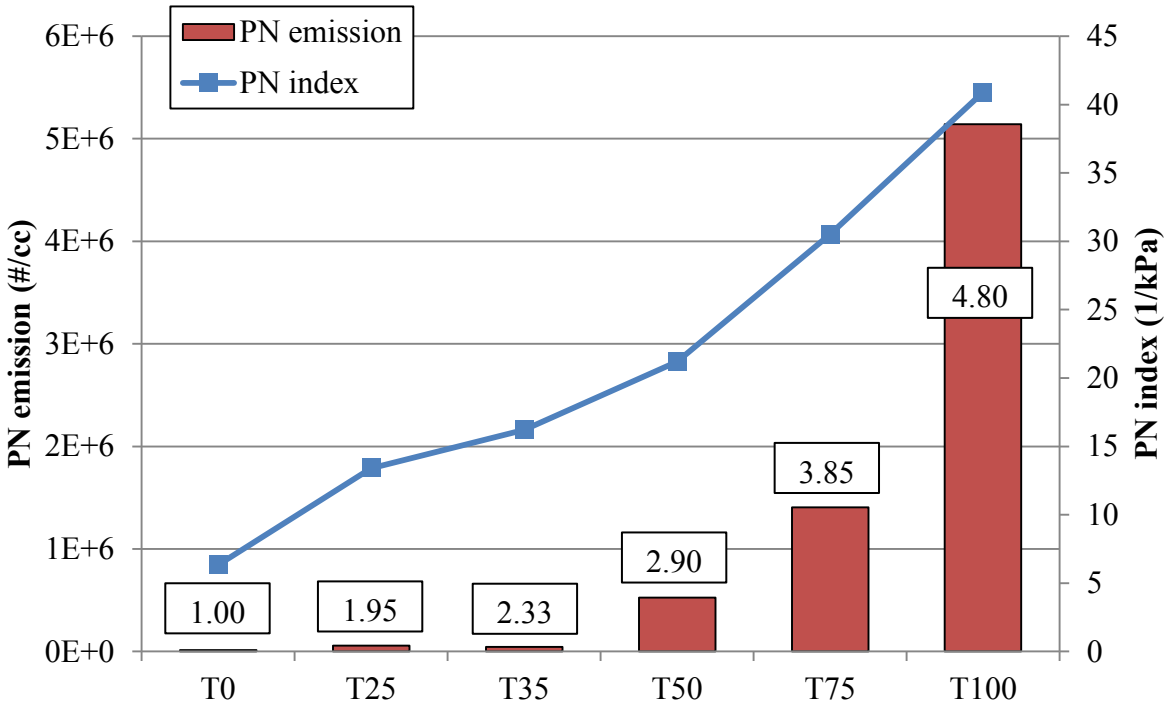

Figure 4.1: Accumulation mode logfit particulate number emissions and PN index dependence on the fuel aromatic content. The numbers above the bars represent the DBE+1 value

Similarly Figure 4.2 shows the PN emissions (in #/cm^3) for the set of fuels with constant DBE (in this case fixed by the 35 % aromatic content, the upper level for EN228 gasoline), but varying levels of decanes present (and hence vapour pressure), these are referred to as the 'D' fuels. Here it can be seen that again, as the vapour pressure of the fuel decreases, the PN emission increases, as predicted by the PN index. In this case however the effect, while definitely present, is less clear compared with that shown by the variation of DBE.

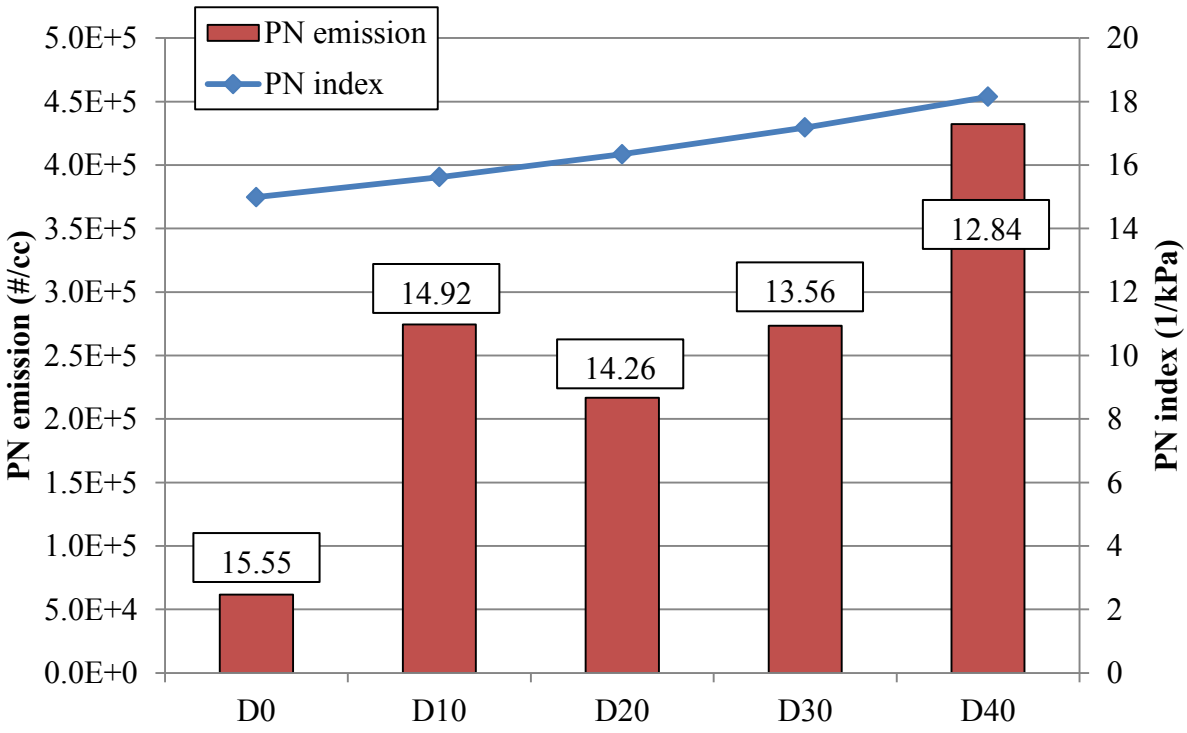

Figure 4.2: Accumulation mode logfit particulate number emissions and PN index value variation as the fuel vapour pressure is varied (fixed DBE) . The numbers above the bars represent the VP value

These model fuels have full independent control over volatility and DBE and validate the trends shown in the PM index [50]. Unfortunately, comparing the PN indices displayed in Figure 4.1 and Figure 4.2, it can be seen that the variation in PN index for fuels with fixed DBE and varying volatility is small.

Given the small variation in the PN index for the 'D' fuels relative to the 'T' fuels, these experiments were run again, with one extra fuel (T42 – a fuel with the same PM index as D40, but differing PN indices) and a longer sample taken, allowing the variation in steady state particulate emissions to be measured. These results are shown in Figure 4.3 and Figure 4.4, and unfortunately show that the particulates emitted from the 'D' fuels are at very similar levels. Whilst this is frustrating when attempting to validate the effect of vapour pressure on PN emissions, it is reassuring to note that these combined results do still closely follow the trends predicted by the PN index.

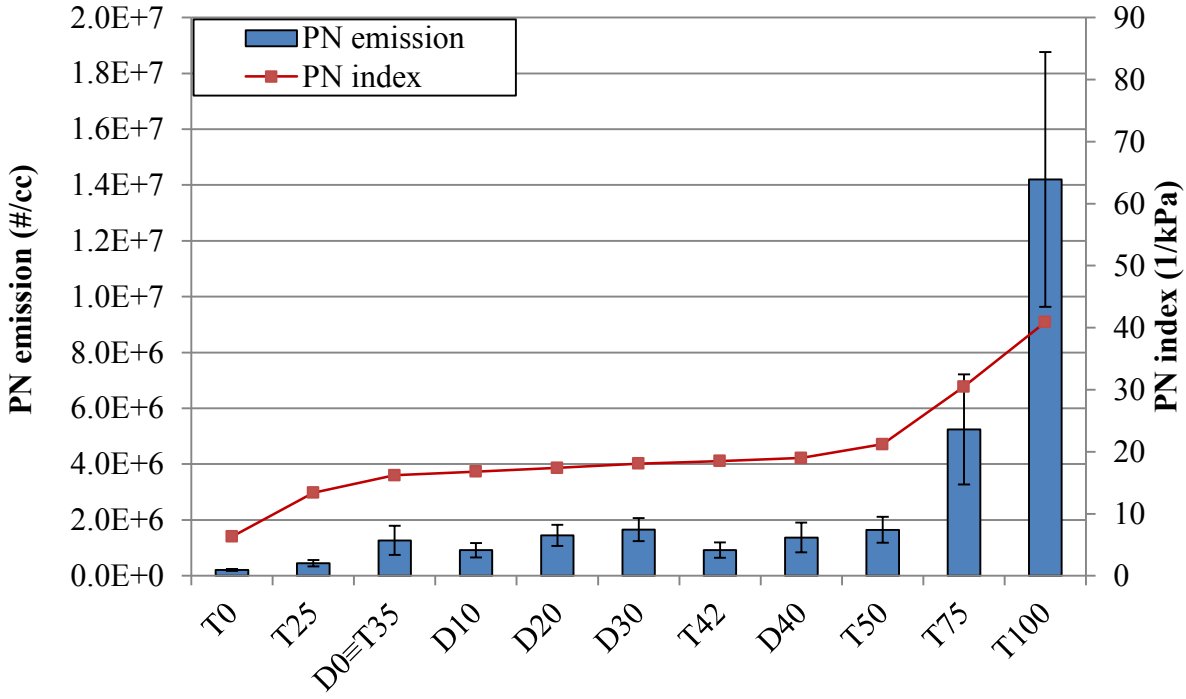

Figure 4.3: Wiebe filtered Particulate Number emissions and PN index value variation for model fuels, the error bars correspond to ± σ

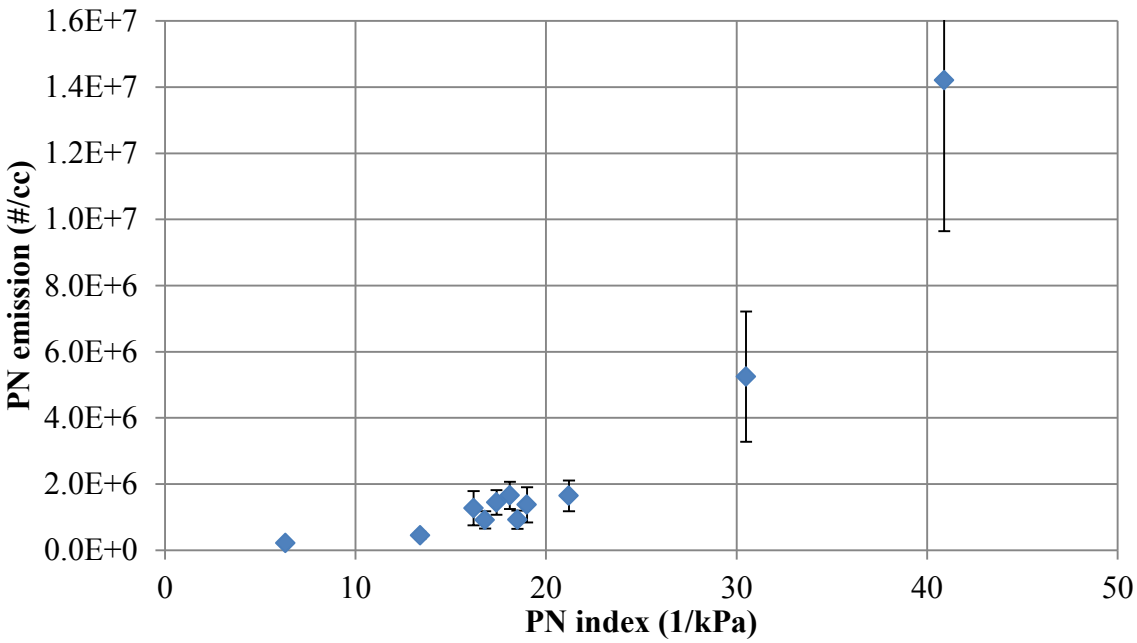

Figure 4.4: Wiebe filtered Particulate Number emissions vs PN index for model fuels, the error bars correspond to ± σ

The possible PN index variation while varying volatility, whilst keeping within the parameters noted in Section 3.4.1, is unfortunately small, and because of this the effects of the PN index on PN emissions are difficult to discern amid the normal variations in particles emitted (the error bars on Figure 4.3 and Figure 4.4 represent one standard deviation).

The results shown in Figure 4.3 have been plotted again in Figure 4.5, this time comparing the PM index and PN index value of each of these fuels, the PN emission is shown as proportional to the area of the 'bubbles' displayed (no error is plotted here for clarity, but the error can be seen in Figure 4.3). It can be clearly seen that the PN index appears to provide a better indication of the PN emission compared to the PM index, indeed two fuels with the same PN index, but very different PM indices (T42 and D40), give almost the same PN emission (within the error, as can be seen from Figure 4.3), and not the factor of two difference predicted by the PM index.

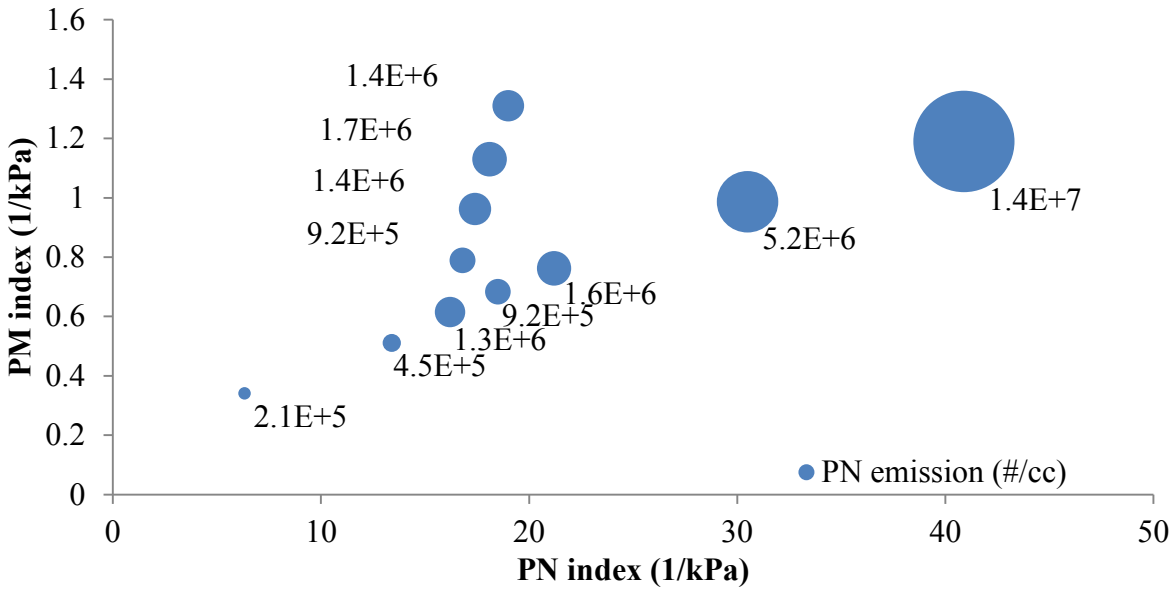

Figure 4.5: Comparison of PN index and PM index with the measured PN emission (represented by the 'bubble' size)

As discussed in Section 2.5.6, there can be issues associated with poor lognormal fitting from the DMS, which can be compensated for by applying a Wiebe function to the results digitally. The model fuel results have been analysed using both the logfitting and the Wiebe filter methods. The comparison between the two methods is shown in Figure 4.6. The results show that on the whole there is a good correlation between the two methods; however the logfit results tend to be higher than the Wiebe filtered results. In addition the standard deviation on the logfit results is much larger than the standard deviation on the Wiebe filtered results. For that reason the data analysis method used for the single cylinder engine results is the Wiebe filtering approach.

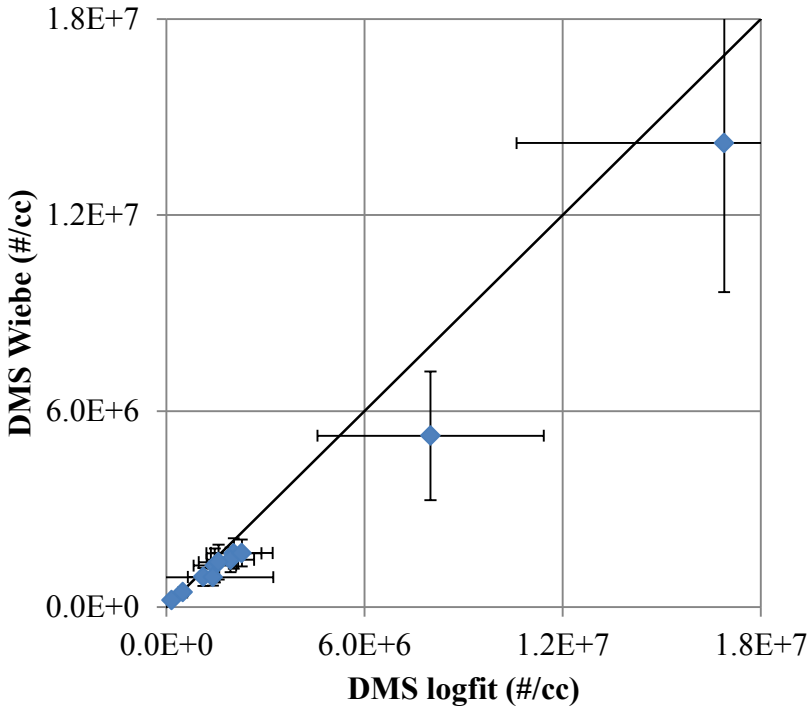

Figure 4.6: Comparison between lognormal fitting and Wiebe filtering for DMS data from the model fuels, the error bars correspond to ± σ

The variability of the particulates results can be analysed by looking at the Coefficient of Variance (CoV) of the particulates $\left(\frac{\sigma}{\mu}\right)$. Particulate data is naturally variable, particularly in the nucleation mode, and especially so from this single cylinder engine with optical access. Efforts were made to obtain reliable data by taking long samples (at least 90 s), however the CoVs of particulate data from this engine are still large. Whilst a CoV of less than 5 % (0.05) might be expected for combustion data, for particulates data from this engine, a CoV of less than 30 % might be seen as good, while anything greater than 50 % would give cause for concern. The CoVs of particulates for the model fuels are shown in Table 4.2. It can be seen that the Wiebe filtered data almost always has a lower CoV than the Logfit data, perhaps as more of the nucleation mode particulates are being removed. This is most notable for fuel 'D10', and this indicates very poor logfitting for

this fuel. Overall from these CoVs it can be seen that the particulates data is reliable, and not too variable.

Table 4.2: Coefficient of Variation for Particulates for model fuels

Fuel	Logfit	Wiebe
T0	0.28	0.16
T25	0.26	0.25
T42	0.42	0.30
T50	0.41	0.28
T75	0.43	0.38
T100	0.37	0.32
D0≡T35	0.44	0.41
D10	1.30	0.29
D20	0.37	0.26
D30	0.41	0.25
D40	0.38	0.39

4.1.1. Size distributions

The DMS data has been analysed to show the size distributions for the model fuels. As the single cylinder engine is not fitted with a catalyst it is expected that the particle spectrum will have large numbers of nucleation mode particles, in particular in the region < 10 nm. Particles in this region are highly variable, with good repeatability extremely difficult to achieve, their formation is very dependent on the dilution temperature and conditions in the exhaust; in addition most of these particles would be removed by a catalyst. This large variation of particles in the < 10 nm region can be seen in Figure 4.7 showing the variation for the 'D' fuels, displaying the least square minimisation spectrum (see Section 2.5.3). A variation of around an order of magnitude seen in the < 10 nm region for fuels where there is little variation across the rest of the spectrum.

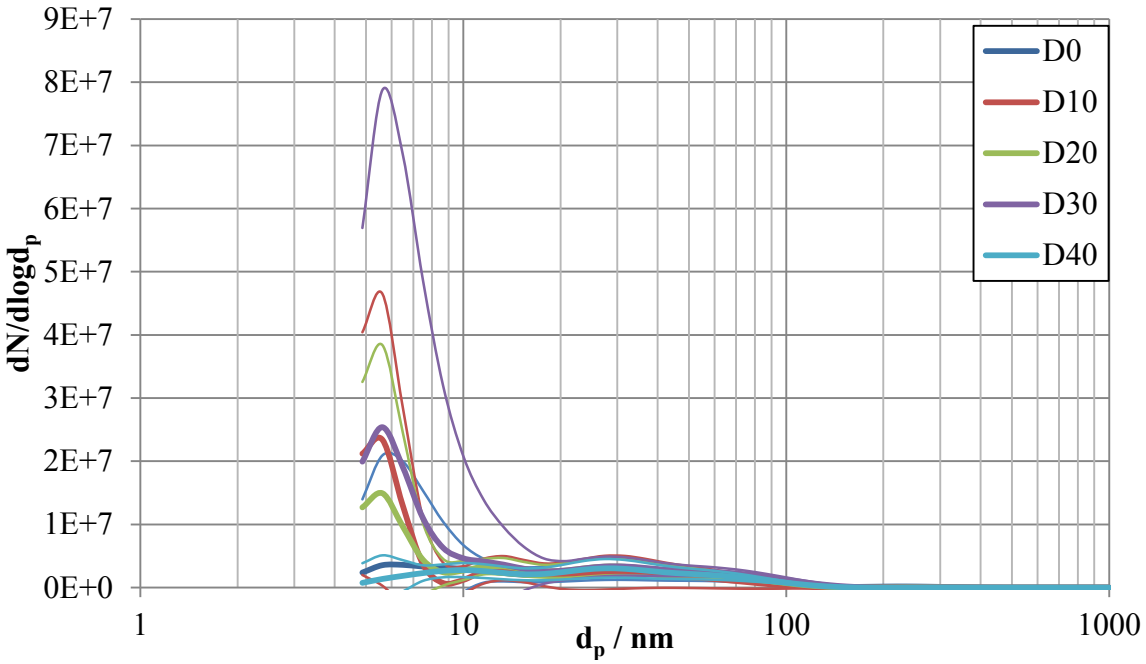

Figure 4.7: 'D' fuels size distributions, unfiltered showing large concentrations of particles < 10 nm, the error bands (defined by the narrow lines) correspond to ± σ

Figure 4.7 has been rescaled and shown as Figure 4.8 in order to be able to see the area of the spectrum > 10 nm. The results shown in the total particle count detected are also reflected here, with the difference between the 'D' fuels masked by the natural variation in particles emitted. However, it can clearly be seen that there is no difference in the size spectrums of the fuels, as the vapour pressure of the fuel is decreased. The size spectrum filtered by the Wiebe function for the 'D' fuels is shown in Figure 4.9. Filtering the results by the Wiebe function removes the highly variable parts of the size spectrum, and replicates a legally compliant test (see Section 2.5.7), in this case it also mimics the effect of the catalyst removing the nucleation mode particles. Figure 4.9 has the error bars omitted for clarity, and again shows the same results as the least square minimization spectrum, with no difference in size spectrum (other than magnitude) for an of the 'D' fuels.

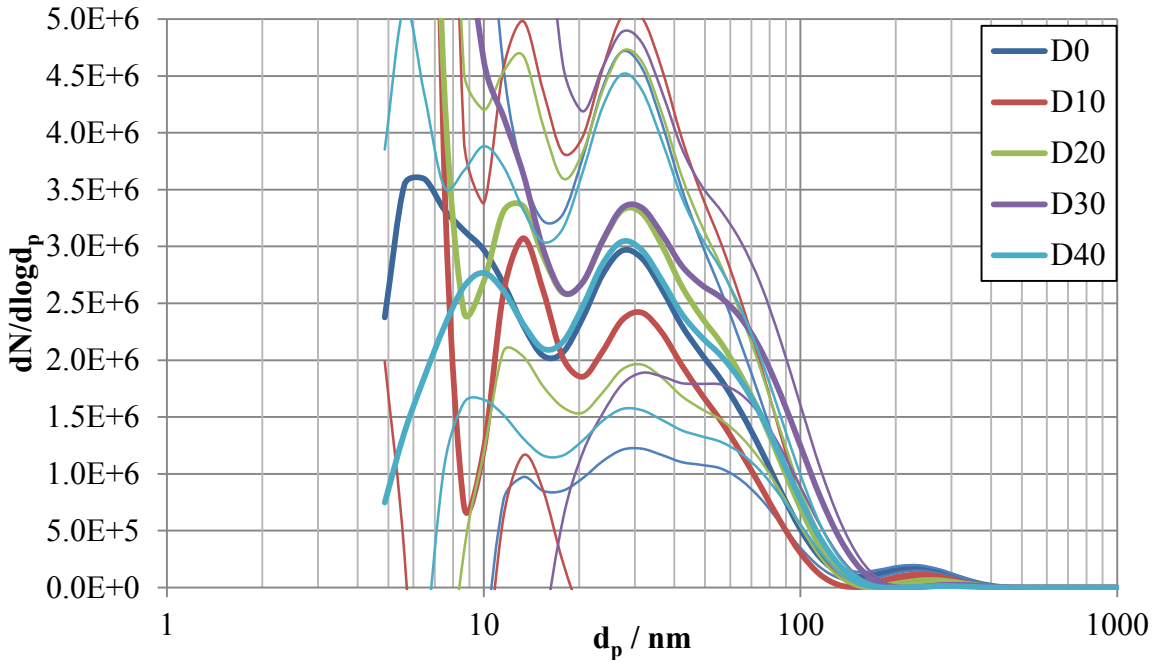

Figure 4.8: Figure 4.7 rescaled to show size distributions for 'D' fuels > 10 nm, the error bands (defined by the narrow lines) correspond to ± σ

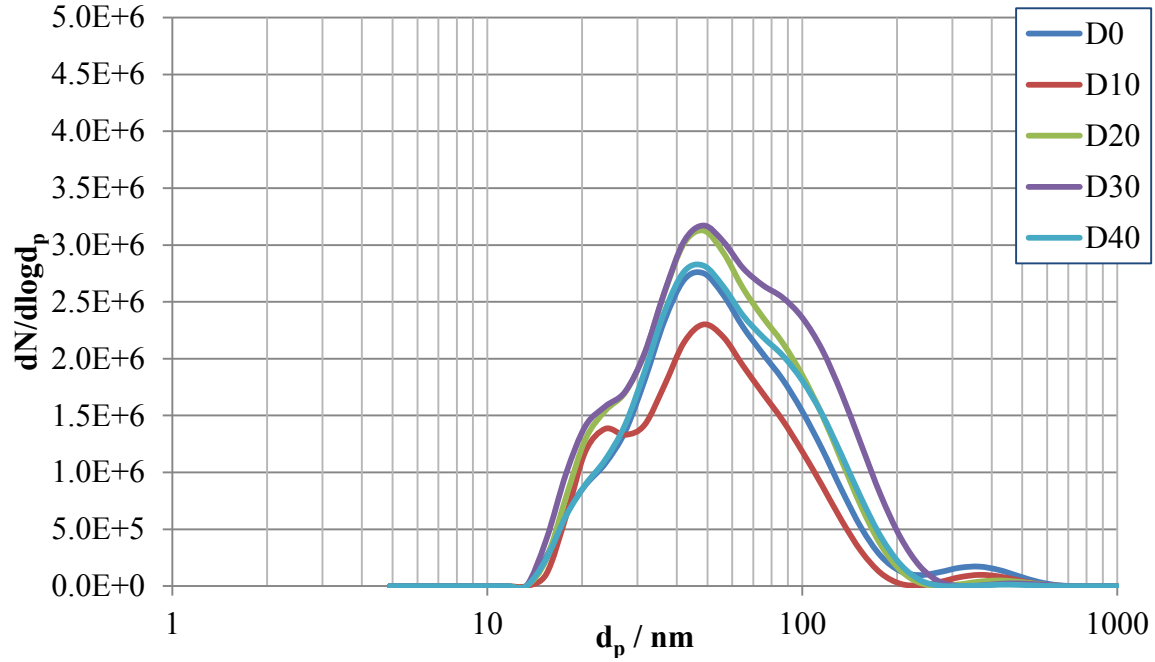

Figure 4.9: 'D' fuels size distributions, Wiebe filtered, it can be seen that the effect of the Wiebe filtering is to remove the nucleation mode

Figure 4.10 shows the least squares minimisation size spectrum (the 'raw' DMS, as discussed in Section 2.5) for the 'T' fuels, and Figure 4.11, the 'T' fuels size spectrum filtered by the Wiebe function. Again, as with the 'D' fuels, it can be seen that there is little variation in the size spectrums, other than magnitude. The results gained from the particle count analysis, are also reflected with a clear distinction in magnitude between each of the 'T' fuels on the size distributions.

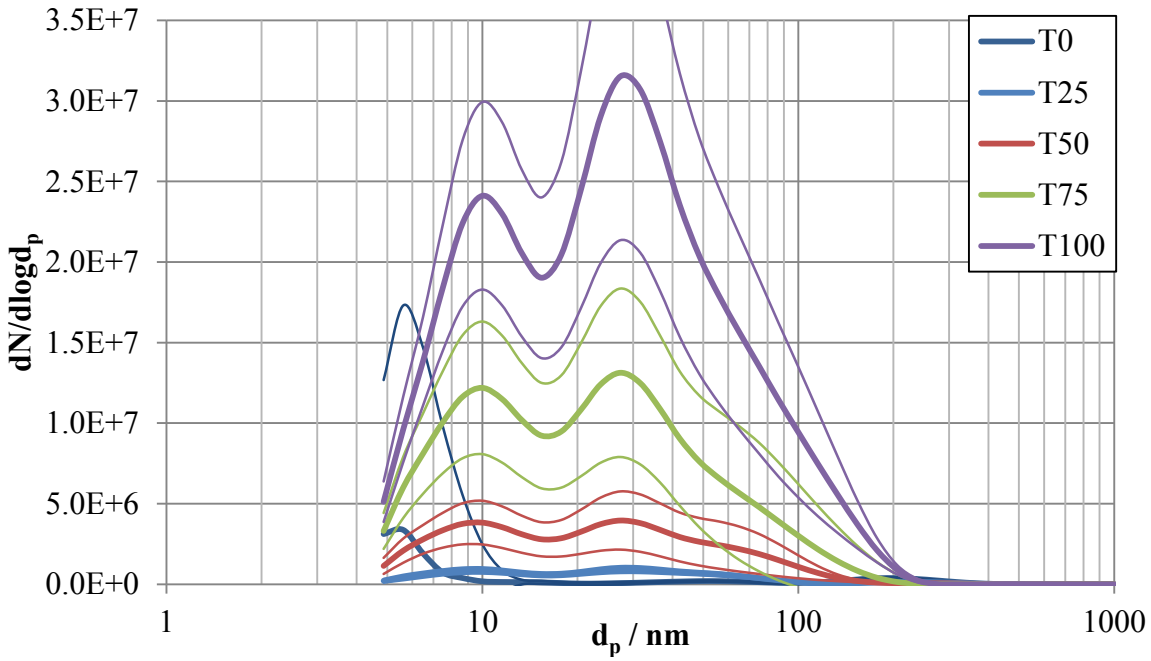

Figure 4.10: Least squares minimised 'T' fuels size distributions, the error bands (defined by the narrow lines) correspond to ± σ

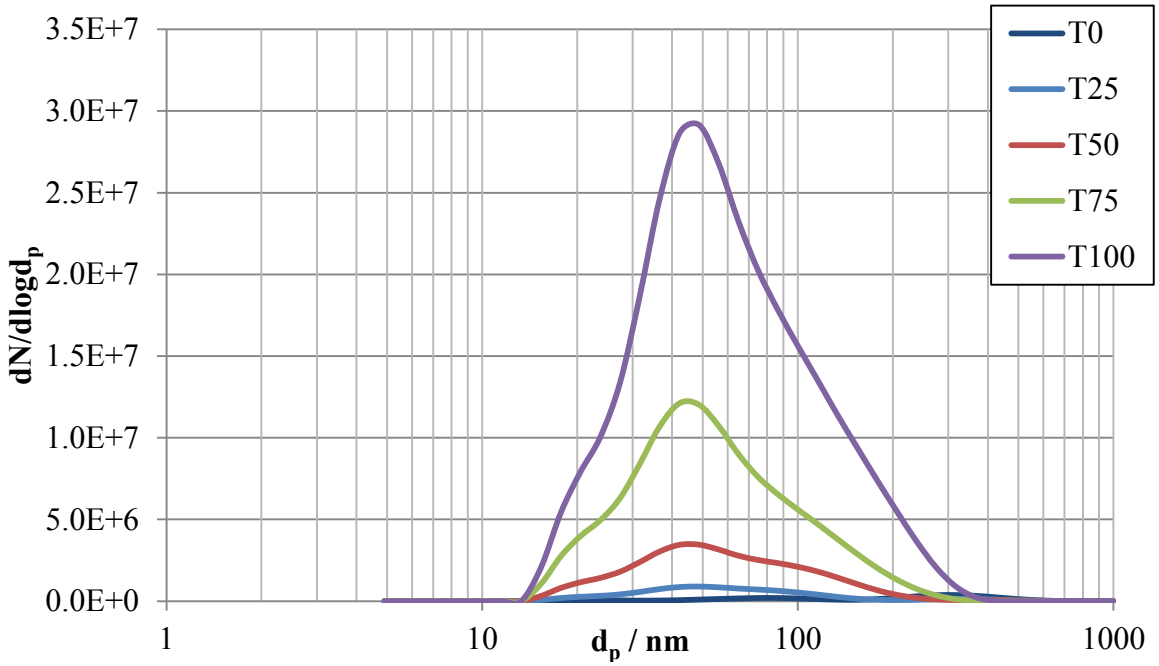

Figure 4.11: Wiebe filtered 'T' fuels size distributions, again showing that the Wiebe filter has removed the nucleation mode

The size spectrums between the 'T' and 'D' fuels have been compared in Figure 4.12 showing D40 and T42. Again there is no difference between the two fuels in their size spectrums, other than in their magnitude, with the magnitudes of each fuel lying within the standard deviation of each fuel, reflecting what was shown in Figure 4.3 and Figure 4.5.

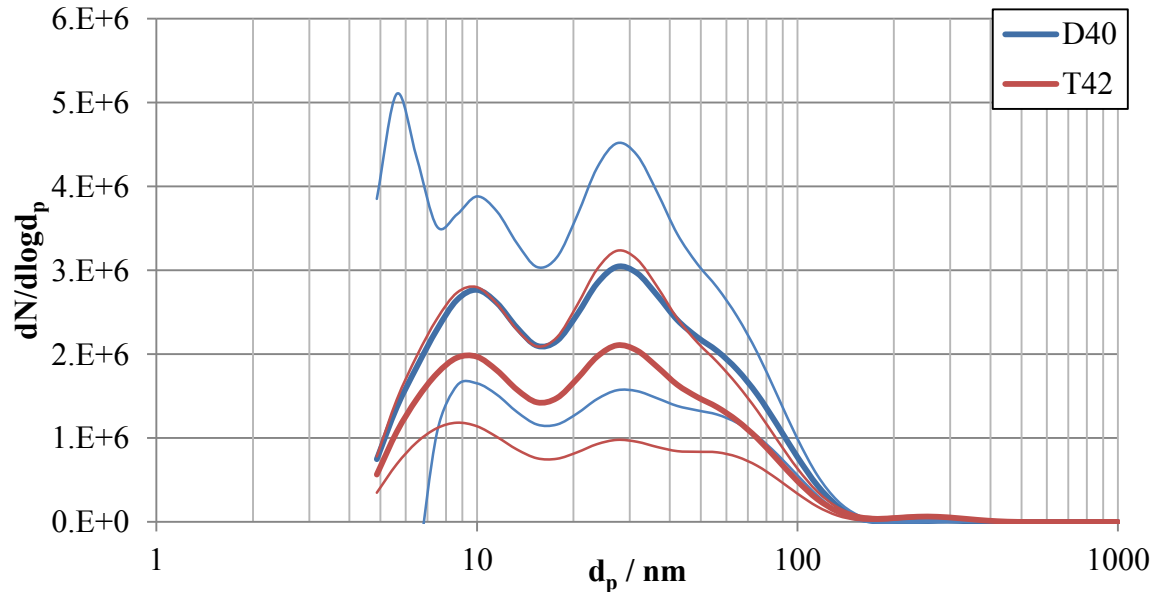

Figure 4.12: Size distribution comparison between T42 and D40, unfiltered, the error bands (defined by the narrow lines) correspond to ± σ

The results from the model fuels are very promising when evaluating the PN index. It is observed that the trends of the PN index are followed very closely by the PN emissions from these fuels. The parameters of the PN index have also been evaluated independently, showing that both DBE and VP have an impact on the PN emissions, as predicted by the PN index. No change in particle size distribution has been observed with the model fuels, the only significant difference is the concentration.

4.2. Importance of a light-end in model fuels

All of the model fuels, whose results are shown in Section 4.1 contain 5 % n-pentane by volume, which is used to mimic the 'light-end' found in commercially available fuels. It can be shown that the presence of this 'light-end' is vital with fuels mixed from pure components in order that their evaporative performance, and hence PN emissions, are comparable with commercially available fuels.

4.2.1. fFID results

Comparisons were run using identical fuels, with and without 5 % n-pentane present. Figure 4.13 shows the evolution of the in-cylinder hydrocarbon levels, measured using a fFID, 10 mm below the cylinder head gasket on the cylinder liner. Measurements were taken over 69 runs, and at each crank angle the average and standard deviation were calculated. The standard deviation was used to give an indication of the cycle-to-cycle variations. The fFID results give a measure of the gaseous hydrocarbons present.

Figure 4.13 shows that the rise time of the D40* (no pentane) fuel is slower, and it has much lower cycle-to-cycle variation than the D40 (with pentane), suggesting that the D40* fuel is forming a more homogeneous mixture than D40.

It can be seen that the hydrocarbon levels are significantly higher, and rise faster, when there is pentane in the fuel, indicating more rapid dispersion of the fuel in the cylinder (more gaseous phase fuel is present, sooner), and that the cycle-to-cycle variations are higher, which indicates lower mixture homogeneity. This (perhaps surprisingly) suggests that the mixture is less homogeneous when pentane is present, indicating that the presence of pentane leads to a breaking up of the spray sooner in the cylinder.

Figure 4.14 shows that the effect of pentane on the peak fFID signal is the same, regardless of where around the cylinder liner that the hydrocarbon levels are sampled. However, the circumferential variations in the fFID signal are smaller when there is no pentane, and this too suggests that the pentane reduces the homogeneity of the mixture.

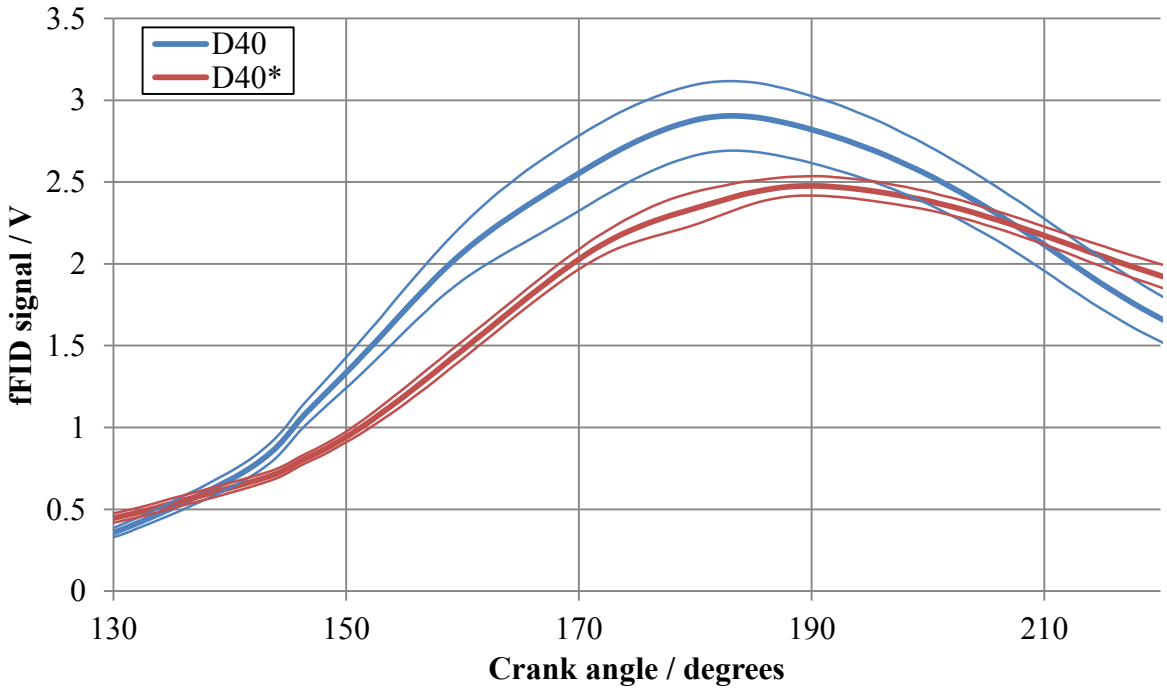

Figure 4.13: In-cylinder hydrocarbon levels for D40 (with n-pentane) and D40* (without n-pentane) sampled 10 mm below the cylinder head gasket and 45 °around from the front of the engine; the error bands (defined by the narrow lines) correspond to ± σ

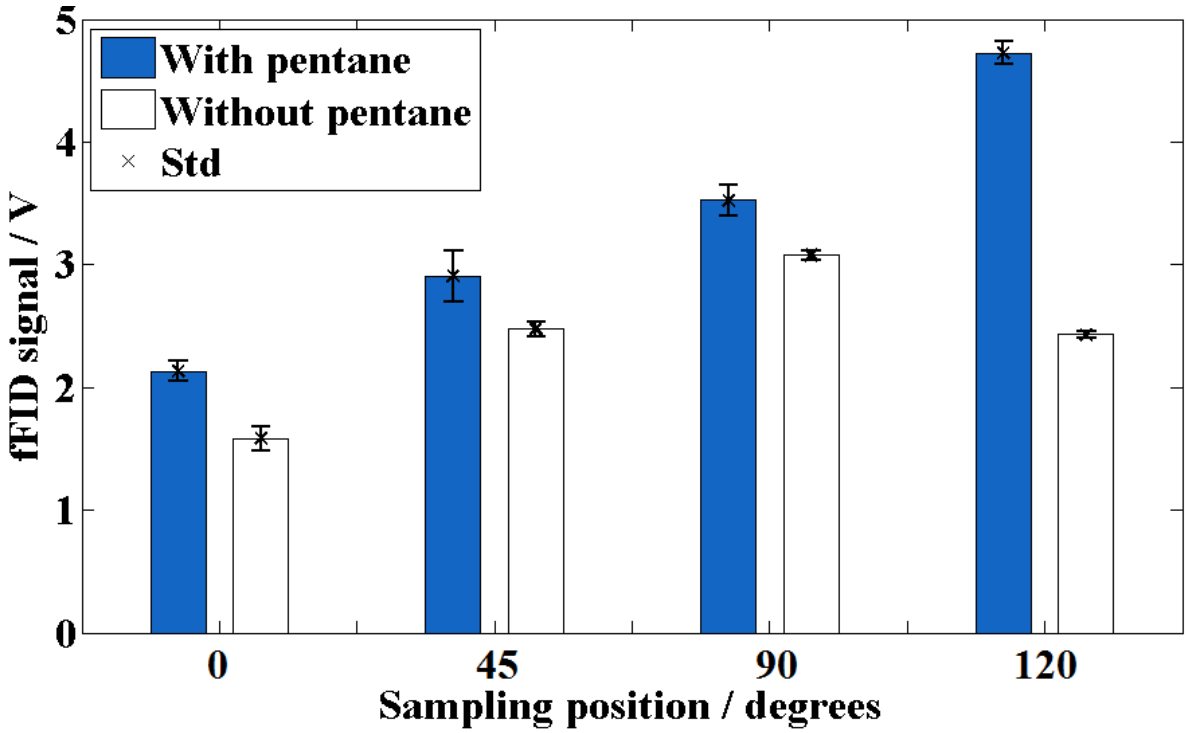

Figure 4.14: Effect of annular sampling position on the peak fFID signal for fuels with and without pentane; the standard deviation bars indicate the cycle-to-cycle variations in the mixture (0 ° is the front of the engine), the error bars correspond to ± σ

4.2.2. Spray imaging

The previous observations about fuel dispersion in Section 4.2.1 are supported by looking at images of the fuel spray during injection. Figure 4.15 shows parallel sets of false coloured images of the fuel spray, on the left, D40 (which includes 5 % v/v n-pentane) and, on the right, D40* (D40 without n-pentane). The images show liquid fuel only; areas with more liquid fuel present are coloured progressively blue – green – yellow – red, with red showing the most liquid fuel present. Fuel vapour will not scatter any light, and will not show up on these images. It can be seen that the presence of n-pentane causes the fuel spray to break-up more quickly, whereas the fuel without n-pentane disperses further into the cylinder before evaporation.

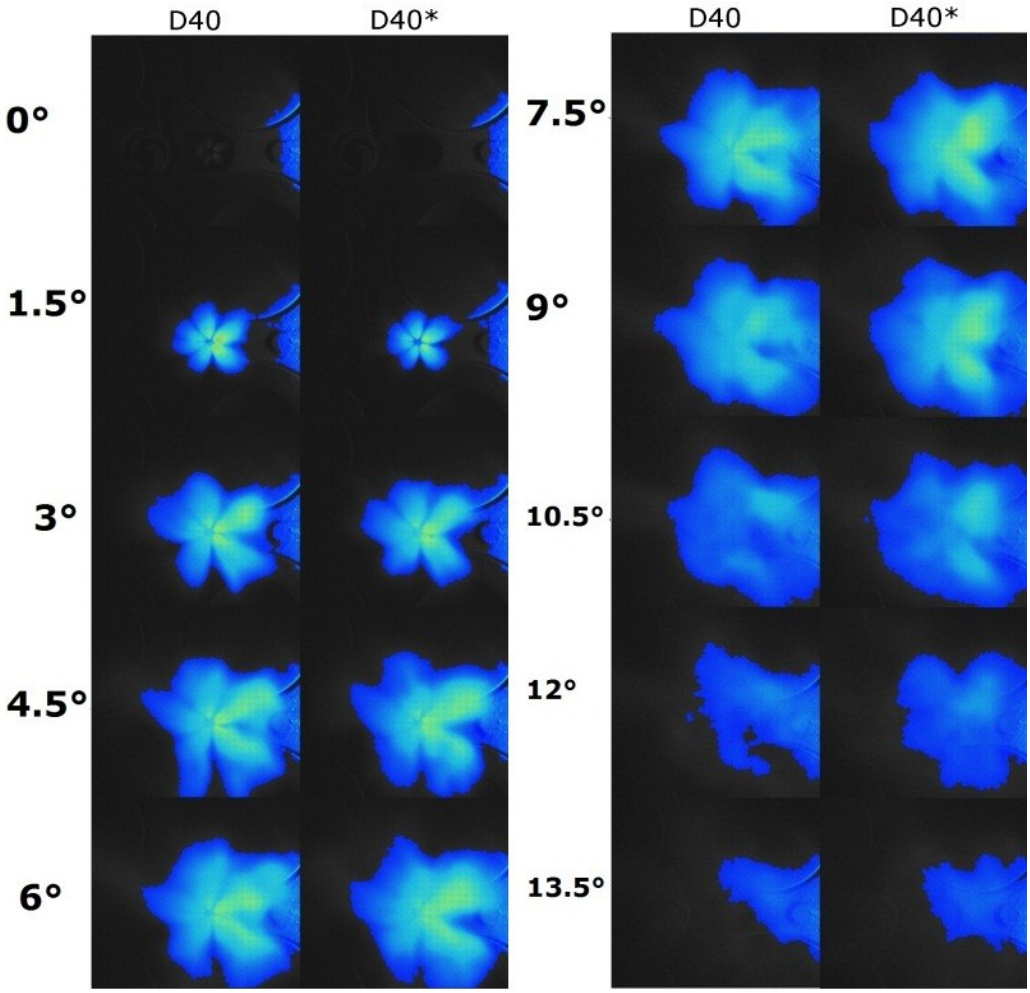

Figure 4.15: False colour images of the D40 fuel spray a) with pentane (D40) and b) without pentane (D40*), units of CAD after the start of injection

4.2.3. Particulate results

The effect of not adding pentane on the mixture homogeneity is also seen in the particulate emission results. Figure 4.16 shows the PN emissions (in #/cm^3) for the set of fuels with a constant DBE (again fixed at a 35 % aromatic content) but without 5 % pentane added, these are referred to as the 'D*' fuels. Figure 4.16 shows that as the vapour pressure of the fuel is decreased (with fixed DBE), the level of the PN emissions also decreases, due to the increased mixture homogeneity. This trend is the opposite to that predicted by the PN index, and observed in Figure 4.2 when n-pentane is used to provide a 'light-end'. This shows the importance of adding high vapour pressure

components, in small quantities, to make model fuels mixed from pure components more representative of commercial gasoline.

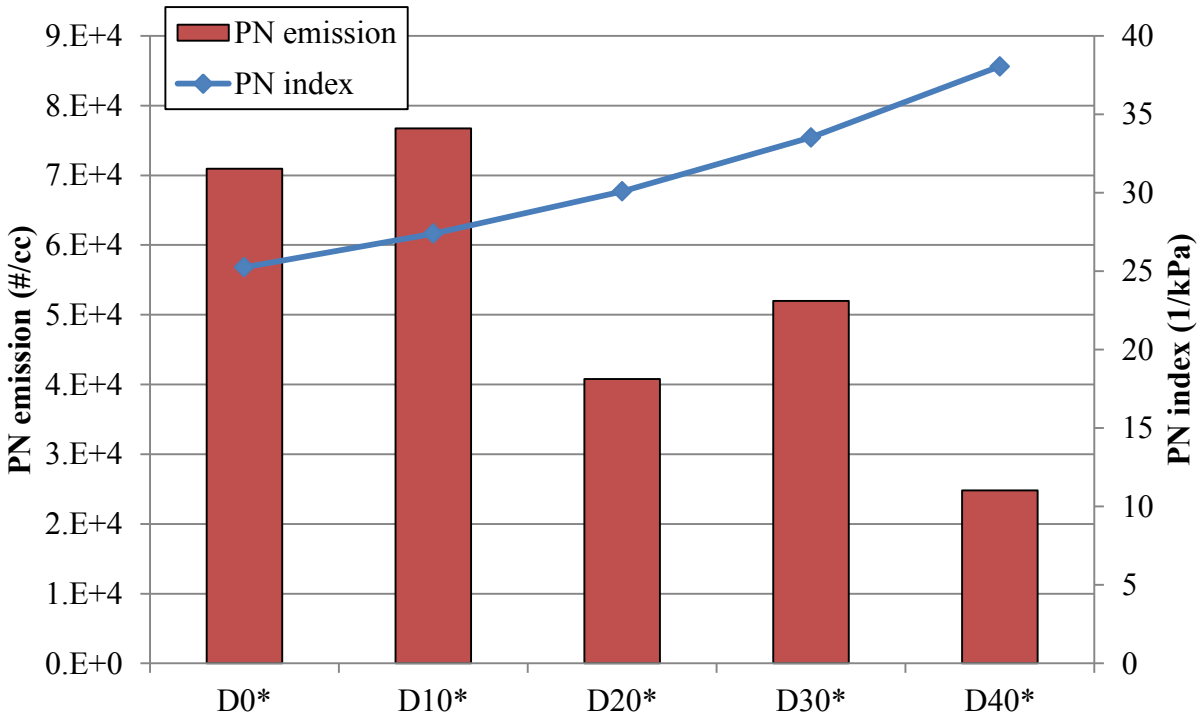

Figure 4.16: PN emissions as fuel Vapour pressure is varied for fuels without pentane

4.3. Evaluation of the PN index using commercially available fuels

The PN index has also been evaluated using some fuels representative of commercial gasolines available in the market. The fuels were tested at the same engine test point as the model fuels, but in addition a stoichiometric test point was included. Given the importance of even slight rich mixture excursions on PN emissions, a $\lambda = 1.01$ was chosen as the stoichiometric condition to avoid any slight rich mixture excursions due either to cycle-cycle variations as lambda was under open loop control. The engine test point is shown in Table 4.3.

Table 4.3: Engine operating point for market fuels

IMEP (bar)	1.8
Inlet air temperature (°C)	40
Coolant temperature (°C)	60
Lambda	0.9 & 1.01
RPM	1500
Start of ignition (°CA bTDC)	35
Start of Injection (°CA bTDC)	280

4.3.1. EN228 compliant fuels

Figure 4.17 shows the PN emissions (in #/cm^3) for two fuels that meet EN228 as specified in Section 3.4.2. Figure 4.17 shows that, for both stoichiometric and rich operation, the trends of the PN index are reflected in the PN emissions of two fuels representative of commercially available gasoline. Unfortunately the particulate emissions at the stoichiometric operating condition are very low, and on the edge of the measurement capability of the DMS – the signal to noise ratio is very low.

Given these low particulate levels, at the stoichiometric condition, the Cambustion logfitting algorithm will not fit a lognormal spectrum to the results, so the only analysis method available for these points is digital filtering using the Wiebe function. For the rich operating condition, a comparison between the Wiebe filtering method and the logfitting

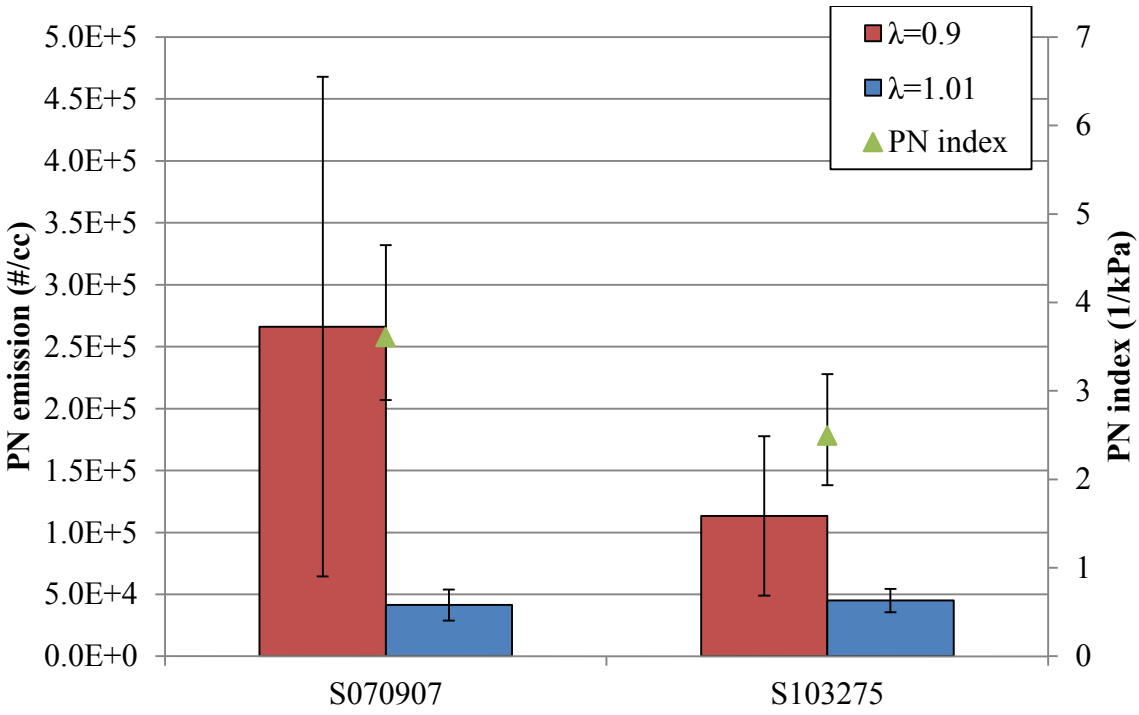

Figure 4.17: Wiebe filtered PN emissions from two EN228 compliant fuels, the error bars correspond to ± σ for the PN results and maximum error on the PN index

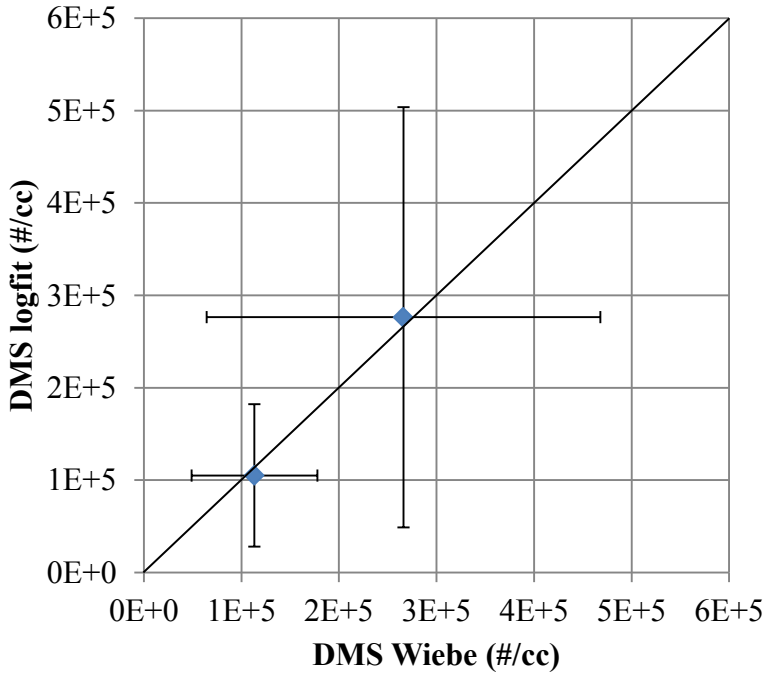

Figure 4.18: Comparison between lognormal fitting and Wiebe filtering for DMS data from the EN228 compliant fuels at λ = 0.9, the error bars correspond to ± σ

can be seen in Figure 4.18. It can be seen that the errors between the two methods, and the overall levels of particulates are very similar, suggesting that good lognormal fitting occurs, and that relying only on Wiebe filtering for the stoichiometric operating point will probably give reliable results.

The CoVs of the particulates data for the reference fuels are shown in Table 4.4 for the Wiebe filtered data and the Cambustion logfit data. Due to the low levels of particulates, CoV data is not available for the logfit data at the λ=1.01 operating point. With this data it can again be seen that the Wiebe filtered data is less variable than the Cambustion logfit data. These CoVs show that in general the results are not too variable, although the λ=0.9 does have higher variability than would be expected for a CoV of particulates from this engine.

Table 4.4: Coefficient of Variation of Particulates from EN228 fuels

	Wiebe filtered data		Cambustion logfit data	
Lambda	**S070907**	**S103275**	**S070907**	**S103275**
λ=1.01	0.30	0.21	n/a	n/a
λ=0.9	0.76	0.57	0.82	0.73

This verification of the index using commercial fuels is an important result as it shows that the index is applicable to commercially used fuels, when using a SGDI combustion system. This verification has not been shown before here, or in the literature.

The particle size distributions from each fuel are shown in Figure 4.19 and Figure 4.20. Unfortunately as the particle levels are so low, it is difficult to see the differences between each fuel. However it can be seen that the size distributions for the two fuels vary very little, with the only differences being in the magnitude of the distributions, the average mode diameters can be seen to be the same.

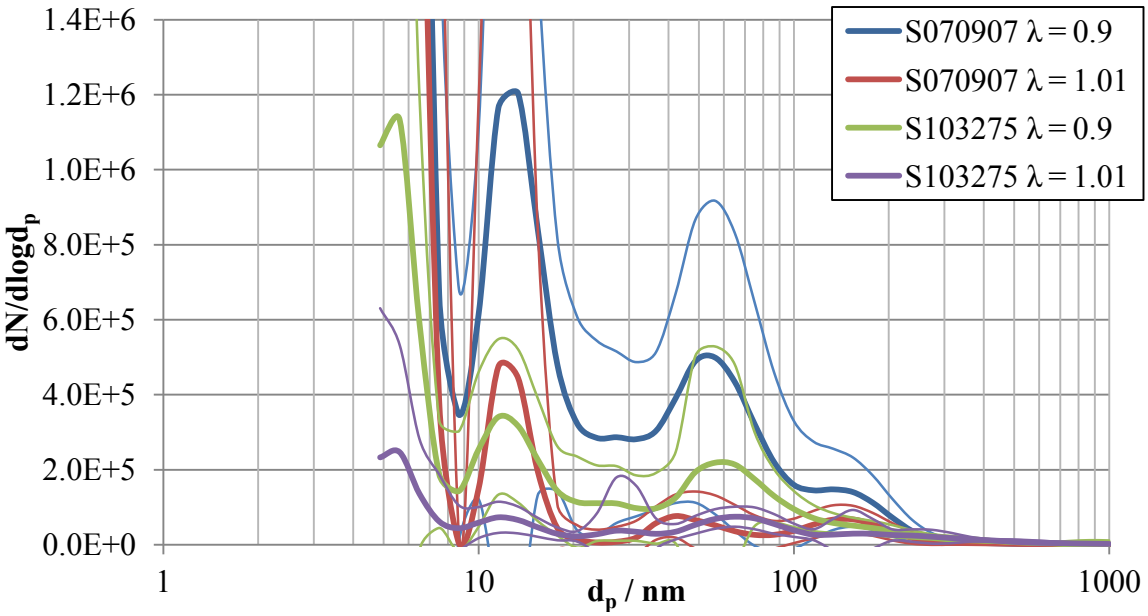

Figure 4.19: Least squares minimised size distributions for two EN228 compliant fuels at $\lambda = 1.01$ and $\lambda = 0.9$, the error bands (defined by the narrow lines) correspond to $\pm \sigma$

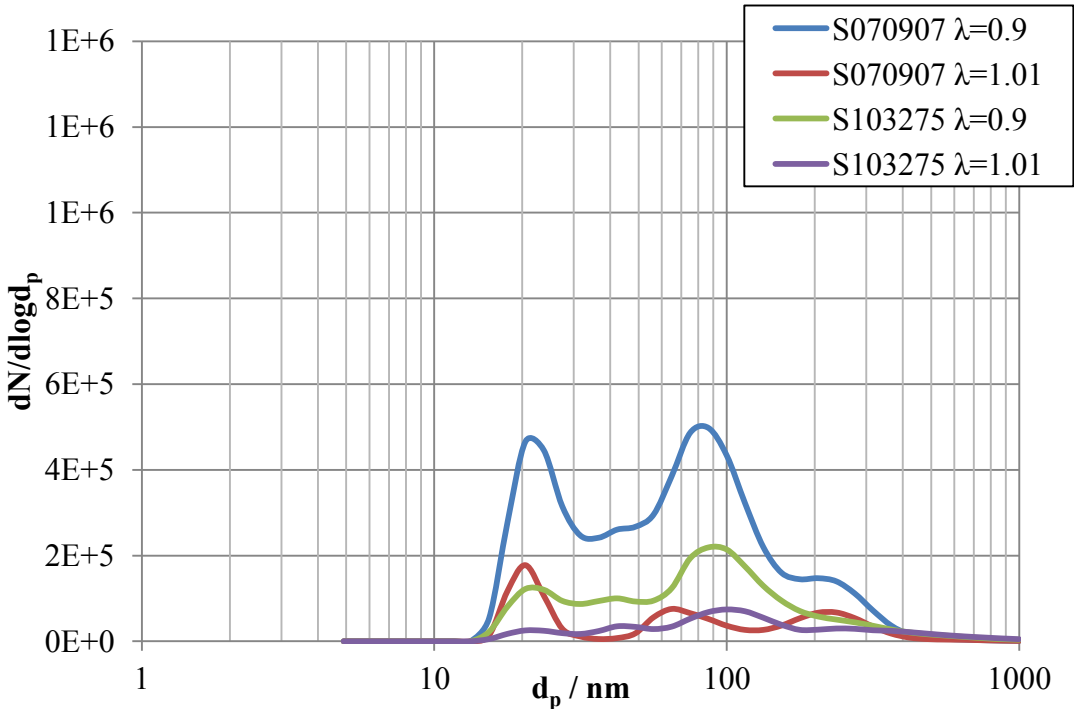

Figure 4.20: Wiebe filtered size distributions for two EN228 compliant fuels at $\lambda = 1.01$ and $\lambda = 0.9$

4.3.2. CEC RF-02-08 compliant fuels

Figure 4.21 shows the PN emissions (in #/cm^3) for two fuels which meet the CEC RF-02-08 reference fuel specification for testing against EU5 emissions legislation. The composition of these fuels is shown in Section 3.4.2. Fortunately, with these fuels, and with the engine in this configuration, the particle levels are much higher than with the engine fitted with more optical components, so the DMS signal is clear.

From these results it can be seen that the trends of the index are followed both at a stoichiometric and a rich condition, with a difference in PN emissions of around a factor of three (in fact greater than that predicted by the index). Indeed it can be seen that the effect of the fuel composition in this case is more important than the stoichiometry of the mixture, with the results from W12/186 at $\lambda = 1.01$ giving more than twice the number of particles than W12/185 at $\lambda = 0.9$.

Figure 4.22 shows the comparison between the Wiebe filtering and Cambustion logfitting methods of data analysis. It can be seen that there is little difference in the standard deviations between the methods, but the Cambustion logfitted results give much higher particulate emissions compared with the Wiebe filtered results. This is mainly due to the very large nucleation mode results from the W12/186 fuel, some of which have been assigned to the accumulation mode; this can be seen from the size spectrums in Figure 4.23, Figure 4.24, and Figure 4.25.

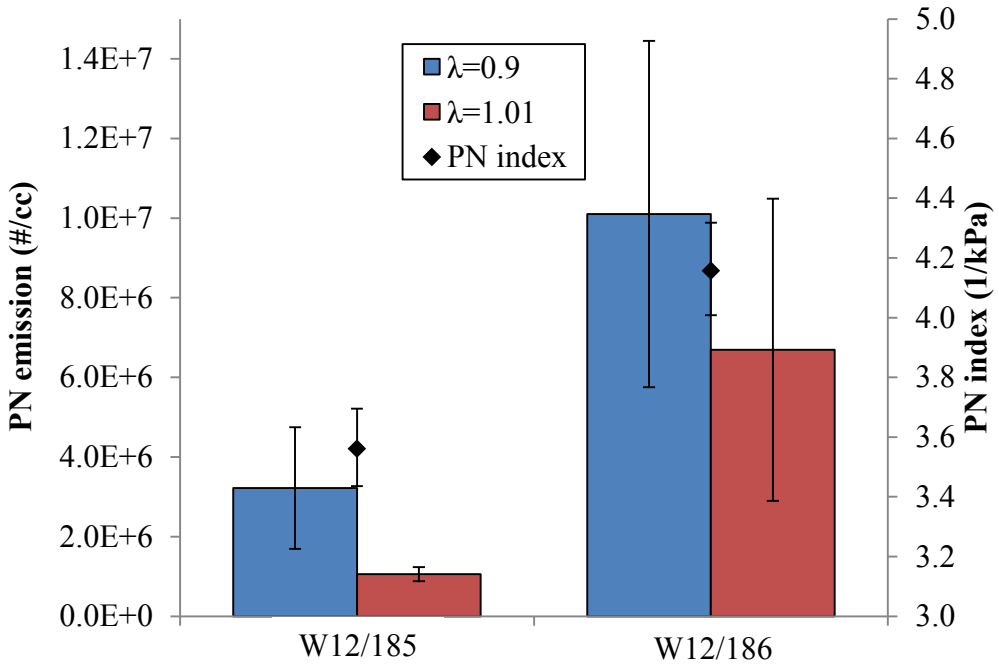

Figure 4.21: PN emissions from two fuels representing the EU5 Reference fuel specification, the error bars correspond to ± σ on the PN emissions and maximum error on the PN index

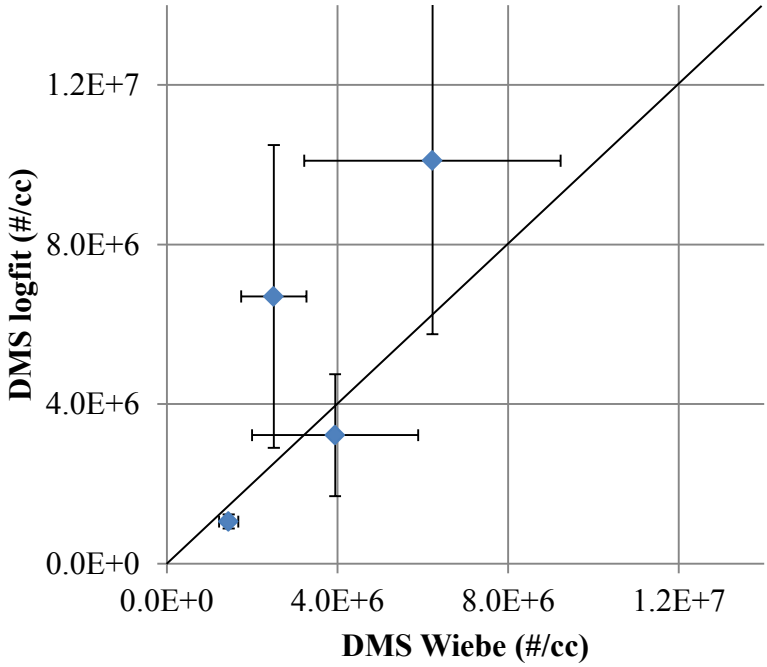

Figure 4.22: Comparison between lognormal fitting and Wiebe filtering for DMS data from the CEC RF-02-08 compliant fuels, the error bars correspond to ± σ

The CoVs of particulates data for the reference fuels for the Wiebe filtered data and the Cambustion logfit data are shown in Table 4.5. With this data it can be seen that there is no clear trend whether the logfit or the Wiebe filtered data is more reliable, however for most operating conditions / fuels, the difference is small. These CoVs show that in general the results are not too variable, with these CoVs falling in the range expected from this engine.

Table 4.5: Coefficient of Variation for particulates from reference fuels (Wiebe filtered data)

	Wiebe filtered data		Cambustion logfit data	
Fuel	**λ=0.9**	**λ=1.01**	**λ=0.9**	**λ=1.01**
W12/185	0.47	0.17	0.49	0.16
W12/186	0.43	0.57	0.48	0.30

Figure 4.23 shows the least squares minimised size distributions for W12/185 and W12/186. From Figure 4.23 it can be seen that W12/186 has an extremely large nucleation mode, with a very large variation in particulates in this mode, as is typical of the nucleation mode, unfortunately the large level of particles in this mode makes it difficult to see the rest of the particulate spectrum. Figure 4.23 has been rescaled in Figure 4.24; from Figure 4.24 and Figure 4.25 (the Wiebe filtered particle size spectrum) it can be seen that W12/186 has a larger average accumulation mode diameter (approximately 80 nm) than W12/185, with W12/185 not exhibiting much evidence of log-bi-modality, probably due to the large masking effect of the nucleation mode. This larger accumulation mode may be due to the higher levels of heavier aromatic components present in W12/186.

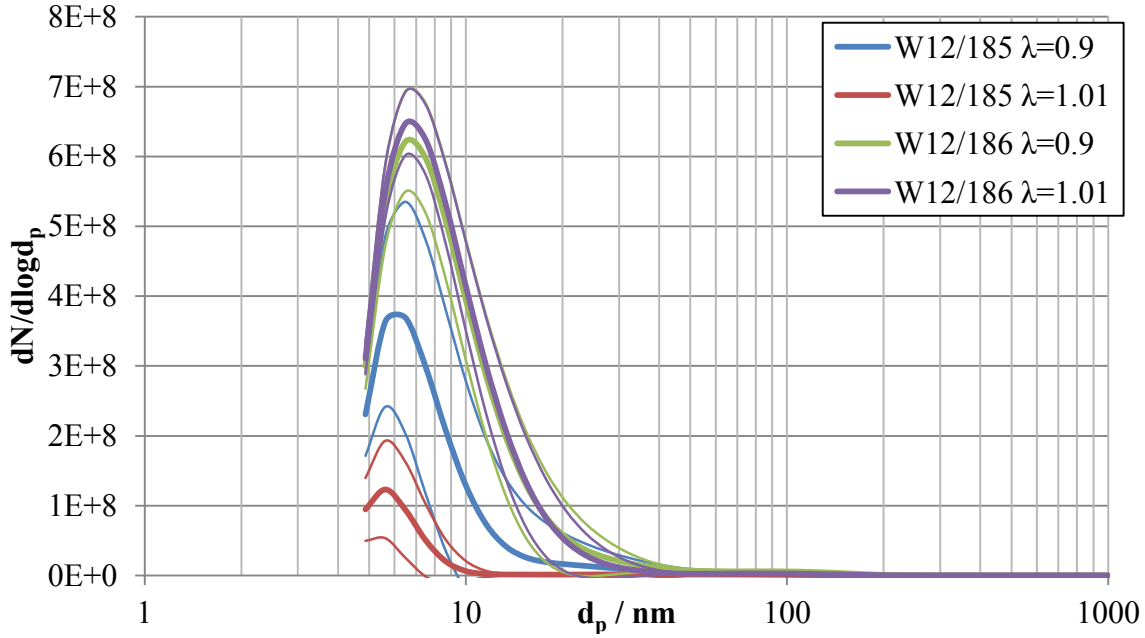

Figure 4.23: Least squares minimised size distributions for two CEC RF-02-08 fuels at $\lambda = 1.01$ and $\lambda = 0.9$, the error bands (defined by the narrow lines) correspond to ± σ

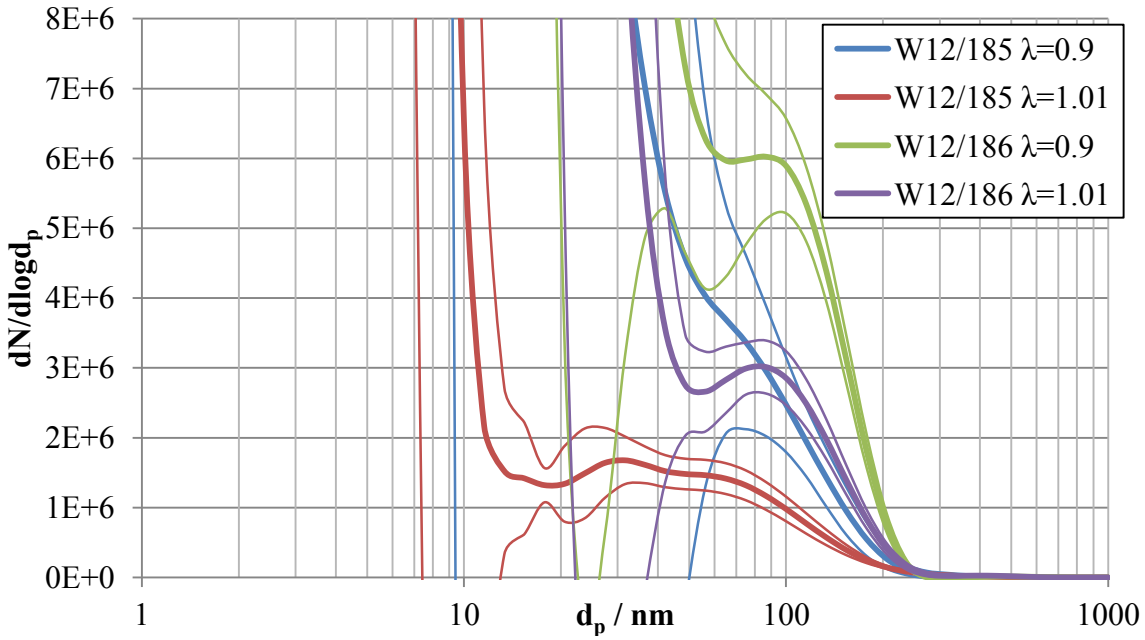

Figure 4.24: Figure 4.23 rescaled to show detail in > 30 nm region, the error bands (defined by the narrow lines) correspond to ± σ

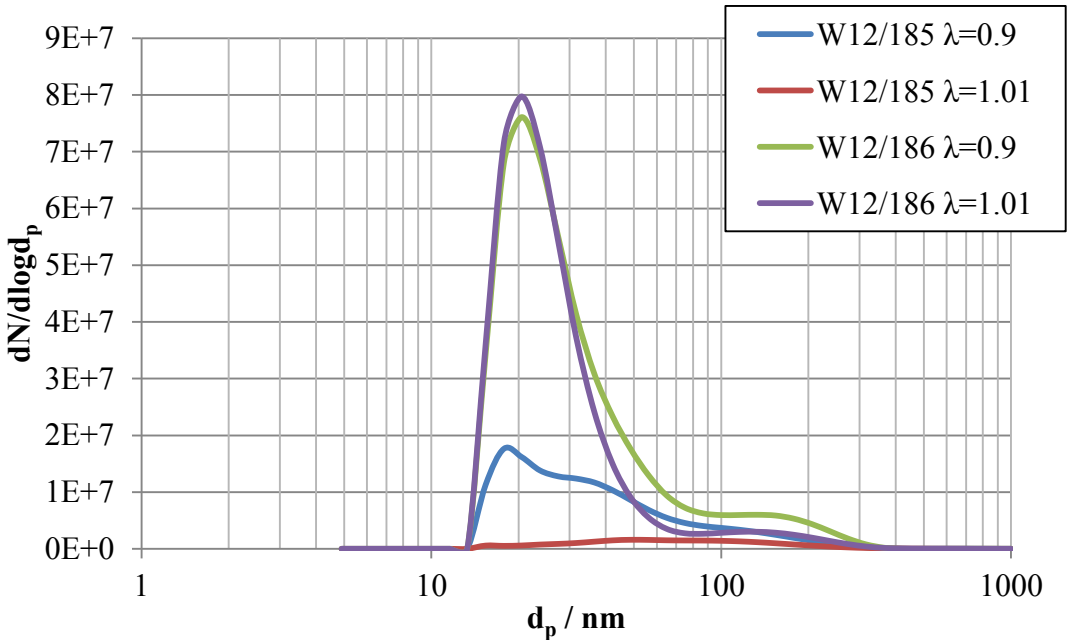

Figure 4.25: Wiebe filtered size distributions for two CEC RF-02-08 compliant fuels at $\lambda = 1.01$ and $\lambda = 0.9$

These results have important implications for the forthcoming EU6 emissions legislation, where PN emissions from gasoline vehicles will be regulated for the first time, as unless the reference fuel specification is changed or an allowance is made for a PN index, then batch to batch variations in PN emissions may be experienced with different fuels meeting the same specification. The results of these tests were taken forward by JLR to the European Automobile Manufacturers' Association (ACEA), and fed into the recommendations for the EU6 reference fuel specification at the European Commission.

4.4. Chapter 4 summary

The PN index has been evaluated on a single cylinder engine using a variety of fuels; model fuels mixed from pure components, two gasolines meeting EN228, and two gasolines meeting the stricter CEC RF-02-08 EU5 reference fuel specification.

These model fuels, which have independent control of DBE and VP (the component parts of the PN index), show that both DBE and VP independently affect the measured PN

emissions as is predicted by the PN index. The realistic range of VPs available with the model fuels due to octane number considerations restricts this evaluation a little. The PN index has been compared with the PM index developed in previous work by Aikawa [50], and the PN index is found to be a much better predictor of PN emissions from the model fuels than the PM index. The size particle distributions emitted from the model fuels have been observed, and very little variation in distribution seen, with all of the model fuels showing the same average diameters in both the nucleation and the accumulation modes.

The importance of including a 'light-end' (in this case 5 % v/v n-pentane) in the model fuels has been observed, with PN emissions from fuels containing increasing levels of decanes not following the PN index when these fuels do not contain a 'light-end'. Market gasolines do contain this 'light-end'. This trend has been investigated using high speed camera images of fuel spray, and fFID analysis in-cylinder, which shows that without the 'light-end', the fuel spray does not break-up as quickly on injection, and penetrates further into the cylinder before evaporating, hence forming a more homogeneous mixture, and lowering PN emissions, contrary to the expected trend. Whilst this might be welcomed, 'light-ends' are present in market fuels to ensure, amongst other things, good cold start performance. Therefore model fuels must be representative of market fuels in order for investigations of their PN emissions to be relevant, and a 'light-end' helps ensure this.

The PN emissions from four market fuels have also been measured on the single cylinder engine, and again found to follow the PN index, in fact exceeding the emissions predicted by the index. Indeed two fuels, which meet the CEC RF-02-08 EU5 reference fuel specification have been shown to have a factor of three difference in PN emissions; a result which has important implications for legislators formulating Particle Number emissions standards.

5. Multi cylinder engine results

5.1. Evaluation of the PN index at steady state

The PN index has been evaluated by running three fuels (BASE, W12/185, and W12/186) on the AJ133 V8 engine at steady state. A description of the engine can be found in Section 2.2. The composition of these fuels is shown in Section 3.4.2. For these experiments the engine was run at the fixed operating point shown in Table 5.1. The IMEP of 2.0 bar is a low value which was chosen to be close to the optical engine test point, and had fuel consumption benefits. The engine was run with standard ECU closed loop lambda control with $\lambda = 1.0$, and the standard engine calibrations for valve timing/lift, injection timing, and spark timing.

Table 5.1: AJ133 engine operating point

IMEP (bar)	2.0
Inlet air temperature (°C)	20
Coolant temperature (°C)	80
Lambda	1.0
RPM	1500

Particulate emissions were measured using a Cambustion DMS500, and the same data analysis techniques as the other engines' results used, these have been outlined in Section 2.5. In this case, the PN emissions could be sampled from both upstream and downstream of the catalyst through a pneumatically switched sampling valve, this valve was heated by a hot air gun to ensure that the line temperatures for the sample remained high enough to avoid any condensation nucleation. The sampling arrangement is shown in Figure 5.1.

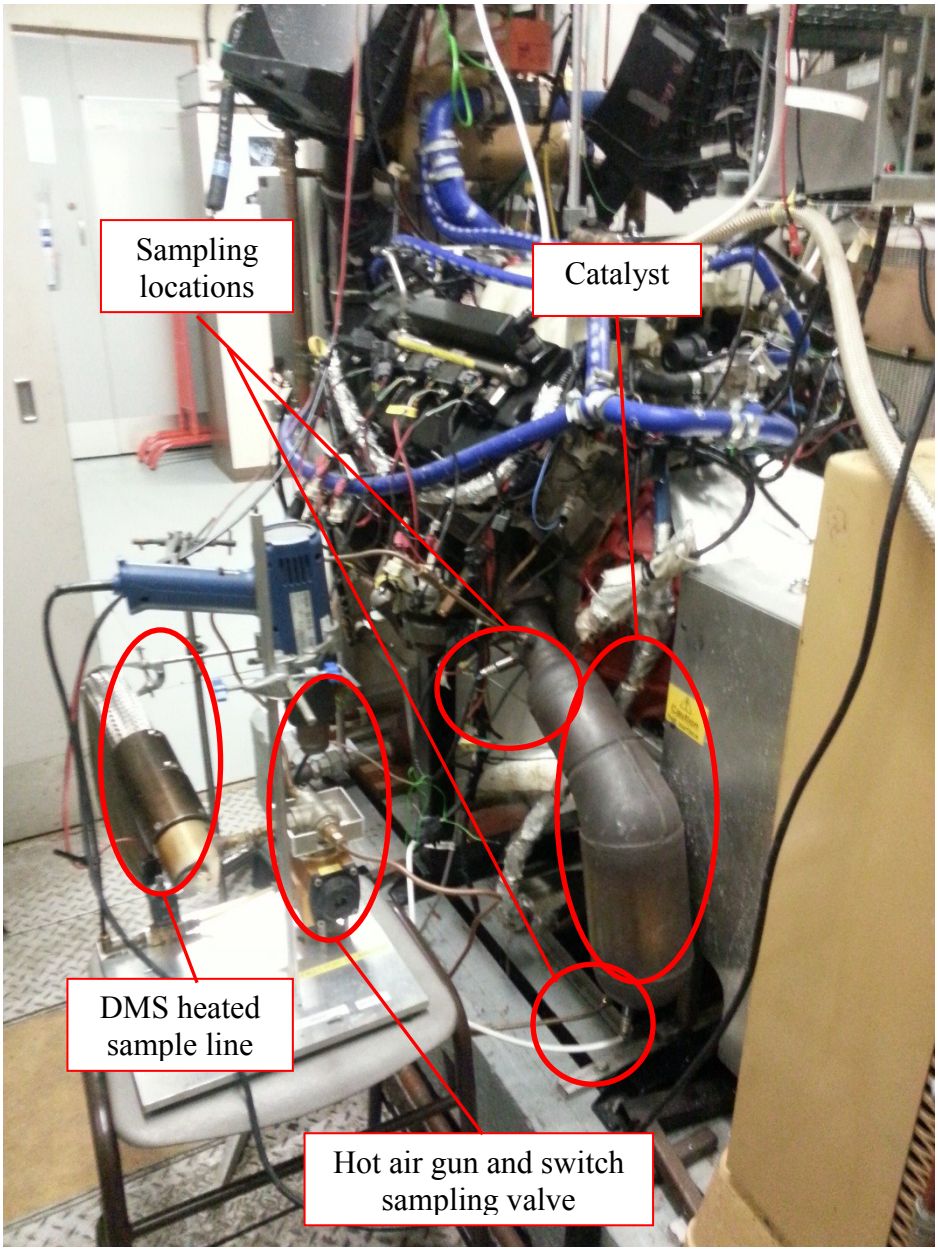

Figure 5.1: Picture showing pre- and post-catalyst DMS sampling position through a switch sampling valve on the AJ133 V8 engine

The fuel change procedure for the AJ133 engine involved switching to a new fuel tank and then running the engine until approximately 5 L of fuel had been used (as measured by the ECU) before any data was taken. This ensured that the fuel being burned was all new fuel, as the fuel system on this AJ133 is fitted with recirculation loops for overpressure protection, so initially the engine will be running on a mixture of the old and new fuels;

allowing for 5 L of fuel to pass through ensures that all of the fuel lines are filled with the new fuel.

5.1.1. DMS500 results

The PN emissions for the fuels tested on the AJ133 engine as measured by the DMS500 are shown in Figure 5.2. It can be clearly seen that the PN emissions of the fuels follow the PN index, with BASE fuel (also used on the Ultraboost testing) and W12/185 having very similar PN indexes, and also having very similar PN emissions, and W12/186 has a higher PN index, and a higher measured PN emission.

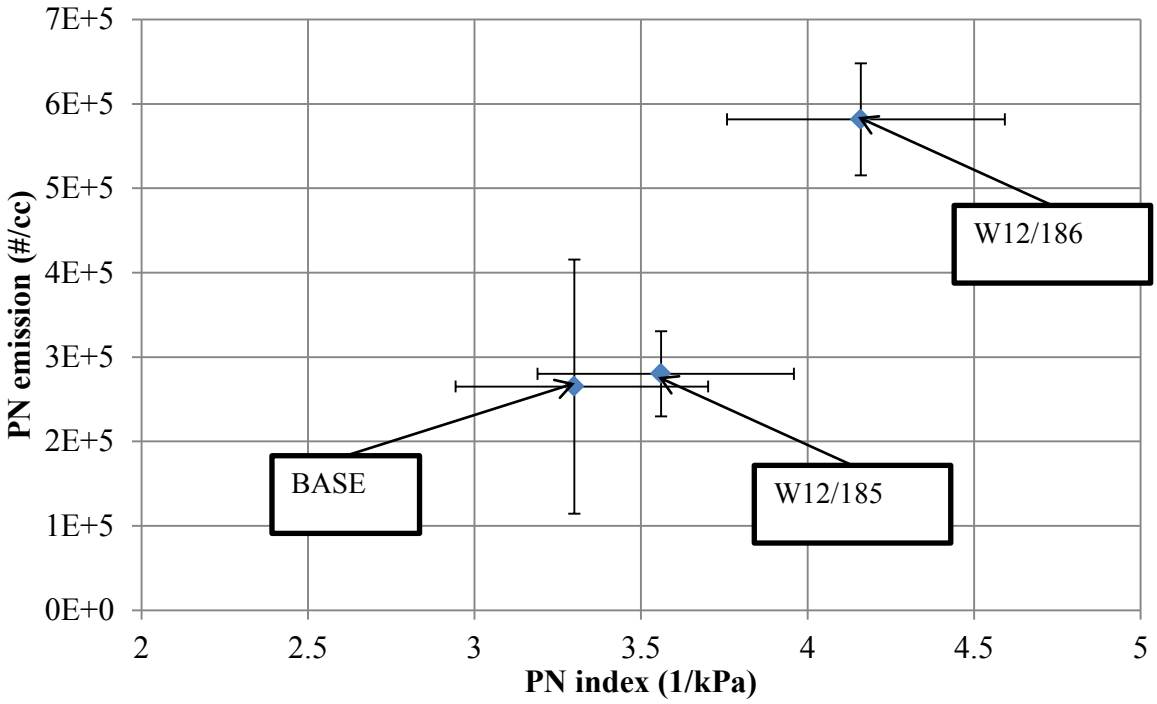

Figure 5.2: Wiebe filtered PN emissions for fuels tested on the AJ133 engine vs their PN indices. Good correlation between the PN index and PN emissions can be seen; the error bars correspond to ± σ for the PN emissions, and to the maximum error possible on the PN index

It is interesting to compare Figure 5.2 with Figure 4.21, as again, as found in the testing done on the single cylinder engine with optical access (see Section 4.3), two fuels that represent the CEC RF-02-08 reference fuel specification (W12/185 and W12/186) for

EU5 emissions tests again show a difference in PN emission of around a factor of two, again greater than that predicted by the PN index.

Again, as discussed in Section 2.5.6, it is worthwhile checking whether there are any issues associated with poor lognormal fitting from the DMS, which can be compensated for by applying a Wiebe function to the results digitally. These results have been analysed using both the Cambustion bilognormal fitting and the Wiebe filter methods. The comparison between the two methods is shown in Figure 5.3. The results show that, despite the limited number of data points, on the whole there is a good correlation between the two methods. To remain consistent with the result of the results presented in this thesis the data analysis method used for the V8 engine results is the Wiebe filtering approach.

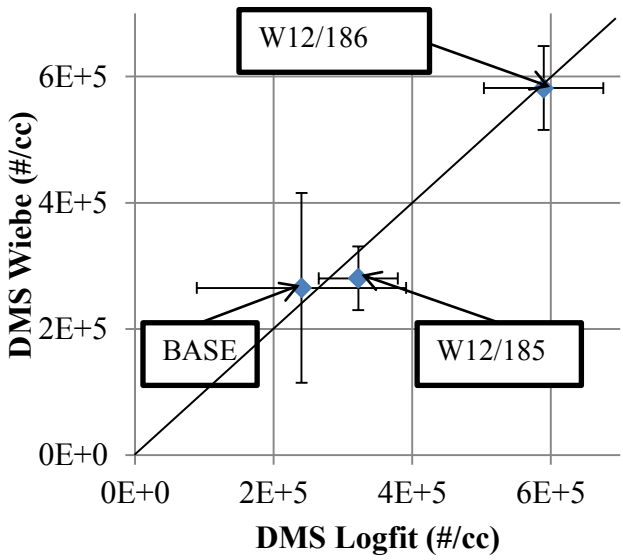

Figure 5.3: Comparison between lognormal fitting and Wiebe filtering for DMS data from the commercial fuels tested on the V8 engine, the error bars correspond to ± σ

5.1.2. DMS500 size data

The particle size distributions measured by the DMS500 for the fuels tested on the AJ133 engine are shown in Figure 5.4. It can be seen that the distributions for the Base fuel and W12/185 are very similar in magnitude, which is reassuring given the results seen

in Figure 5.2. However, it can be seen that W12/185 has a slightly larger average particle diameter in the accumulation mode, and BASE fuel has a slightly smaller average particle diameter in the nucleation mode. The overall magnitude of W12/186 is much higher than BASE or W12/185, but the nucleation mode average particle diameter appears to be larger than either of the other fuels, and the accumulation mode average particle diameter appears to be the same as W12/185.

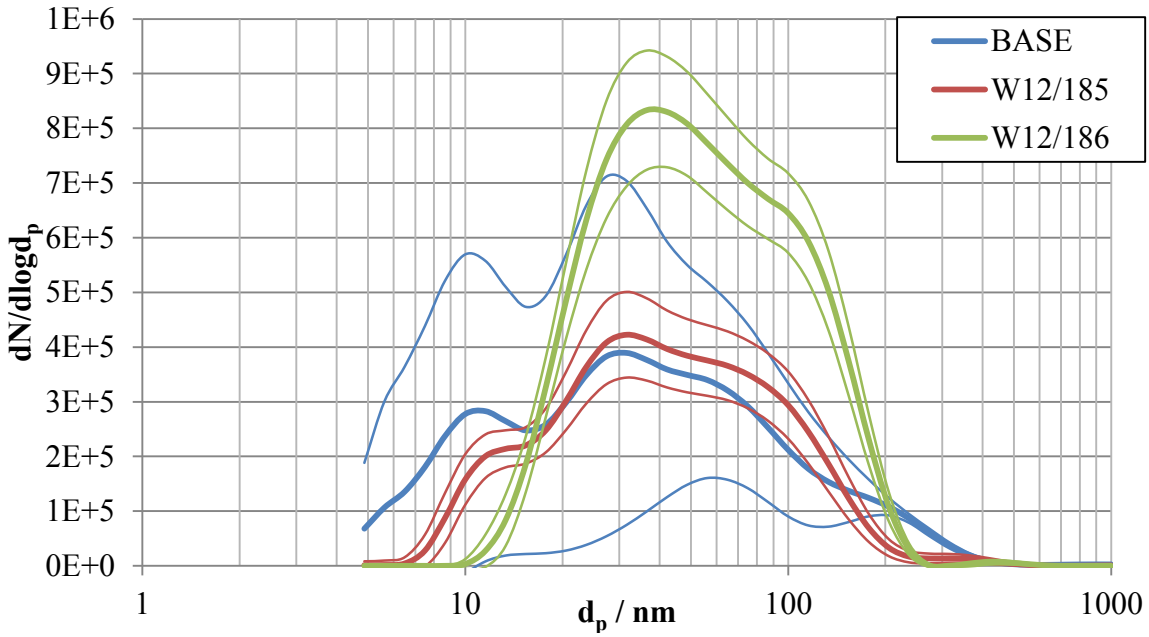

Figure 5.4: Particle size distributions, unfiltered, from the AJ133 V8 engine, measured by the DMS500. It can be seen that there is not a significant variation in particle size, only in the magnitude of the distributions; the error bands (defined by the narrow lines) correspond to ± σ

The results observed on the single cylinder engine, with optical access have now been validated on a thermodynamic engine, in this case the AJ133 5.0 L V8 engine. This has important implications for the forthcoming EU6 emissions legislation, as unless the reference fuel specification is changed or an allowance is made for a PN index, then variations in PN emission may be experienced due to batch-to-batch variations in fuel composition among fuels meeting the same specification.

5.2. Evaluation of the PN index over a transient drive cycle

A series of experiments were devised to test the PN index over a transient drive cycle on an AJ126 V6 engine, this engine is fully described in Section 2.3. A transient dynamometer at Jaguar Land Rover's Whitley research centre has been calibrated to match the load and speed a vehicle would demand of an engine over a transient drive cycle, and the results have been shown to match those from legally compliant tests. For these experiments the transient dynamometer was set to run a simulated cold start NEDC. The engine was run with a development engine calibration, was loaded as a Sports Utility Vehicle (or similar), and stop-start technology was enabled.

Emissions were measured using the standard suite of instruments (Horiba MEXA, measuring CO, HC, CO_2, and NO_x) alongside an AVL micro soot sensor (MSS), an AVL particle counter (APC), and a Cambustion DMS500 (DMS). The PN emissions were measured approximately 5 m downstream of the exhaust valves, downstream of two close coupled catalysts (one for each exhaust bank), and a two-to-one silencer; each of the samples was taken by a probe placed approximately in the middle of the exhaust flow. The sampling positions are shown in Figure 5.5 and Figure 5.6.

Fuel changes were managed by draining the lines, as far as was possible, and subsequently running two warm start NEDCs, which are not presented in the results, to ensure that the fuel lines were completely filled with the new fuel.

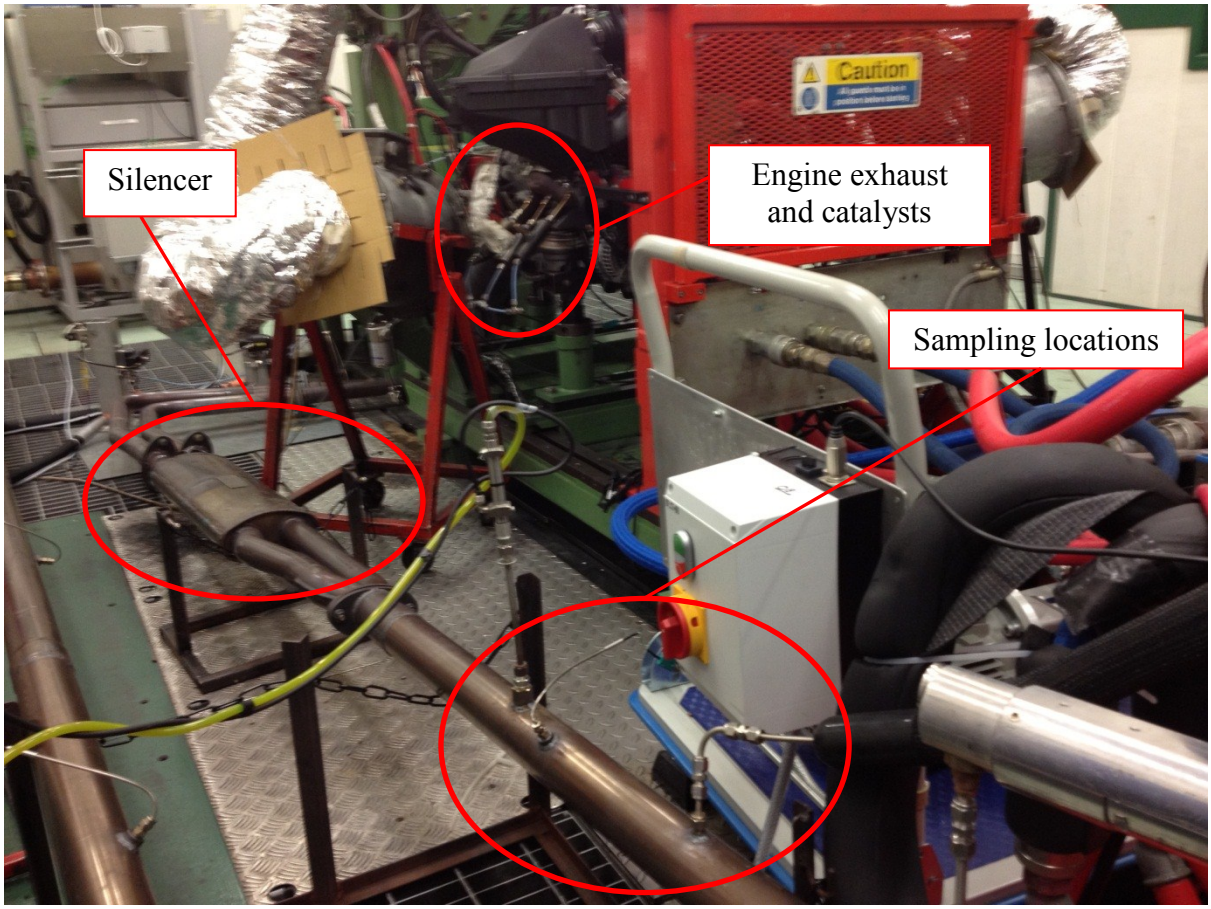

Figure 5.5: Sampling positions on AJ126 engine

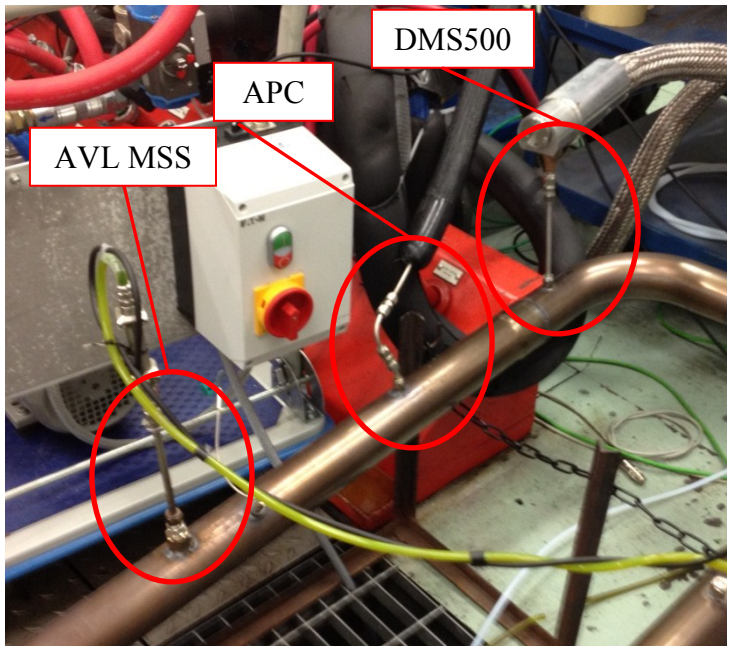

Figure 5.6: Detailed view of sampling positions

The results of the experiments were checked to make sure that the load applied was constant across the experiments, as this would affect the PM emitted. This was confirmed by checking the total CO_2 emitted for each test, and the total varied by a maximum of 7 % across all 22 experiments.

The experiments were monitored for drift by looking at the chronological PN counts from the APC at 110 s (the end of the 'cold start' period) and at the end of the test. This is shown in Figure 5.7; the black vertical lines represent a fuel change.

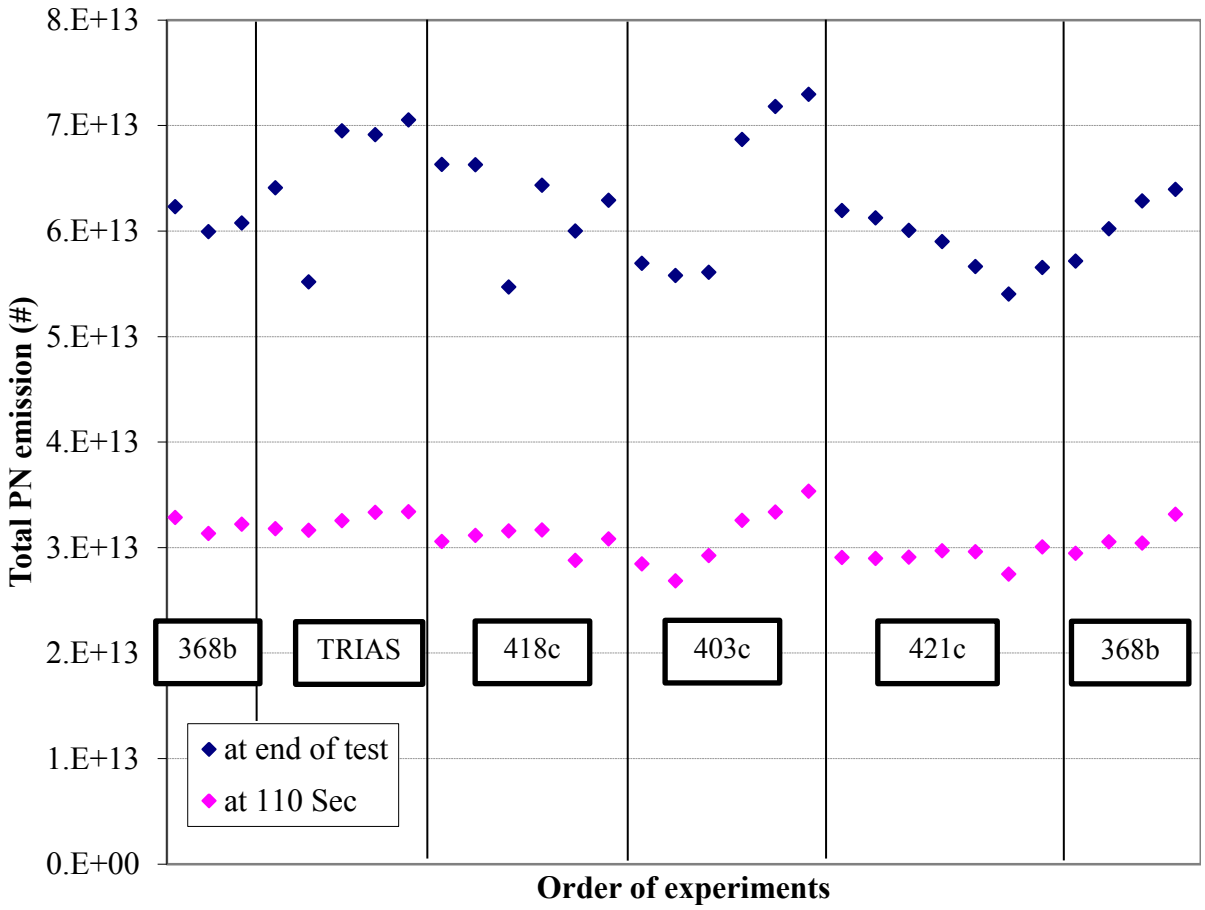

Figure 5.7: Chronological experiment APC results – total particle count over NEDC

In Figure 5.7 it can be seen, particularly if the first two experiments after each fuel change are excluded (which are not presented in the results, as these may include mixed

fuel, and were not cold start), that there are only minor drift effects visible. Each fuel was tested at least three times; with 368b being the first fuel tested (three times), and then repeated at the end a further three times. It can be seen in Figure 5.8 that the repeat of 368b has given a highly repeatable result; reassuring that no significant drift effects have been present. The MSS results were also checked, and no significant drift was observed. A list of experiments undertaken, and how many runs were done of each fuel is shown in Table 5.2. Unfortunately due to equipment failure, the DMS was not connected for all experiments; Table 5.2 also shows those experiments for which the DMS was connected as well.

Table 5.2: List of experiments undertaken on AJ126 engine over NEDC

Fuel	APC experiments	DMS experiments
421c	5	5
418c	4	0
368b	6	6
403c	3	3
TRIAS	4	1

5.2.1. AVL particle counter results

The results of the V6 drive cycle tests are shown in Figure 5.8; here the APC results are displayed, as they come from an instrument which can be used as part of a legally compliant system (see Section 2.6). A comparison between the APC and the DMS results is presented later in this section. It can be seen from Figure 5.8 that there is some impact of the PN index, but less than was predicted. This is reinforced in Figure 5.9, where the PN emission is plotted against the PN index, the correlation between the total emission and the index is relatively flat, although the PN index definitely still has an effect.

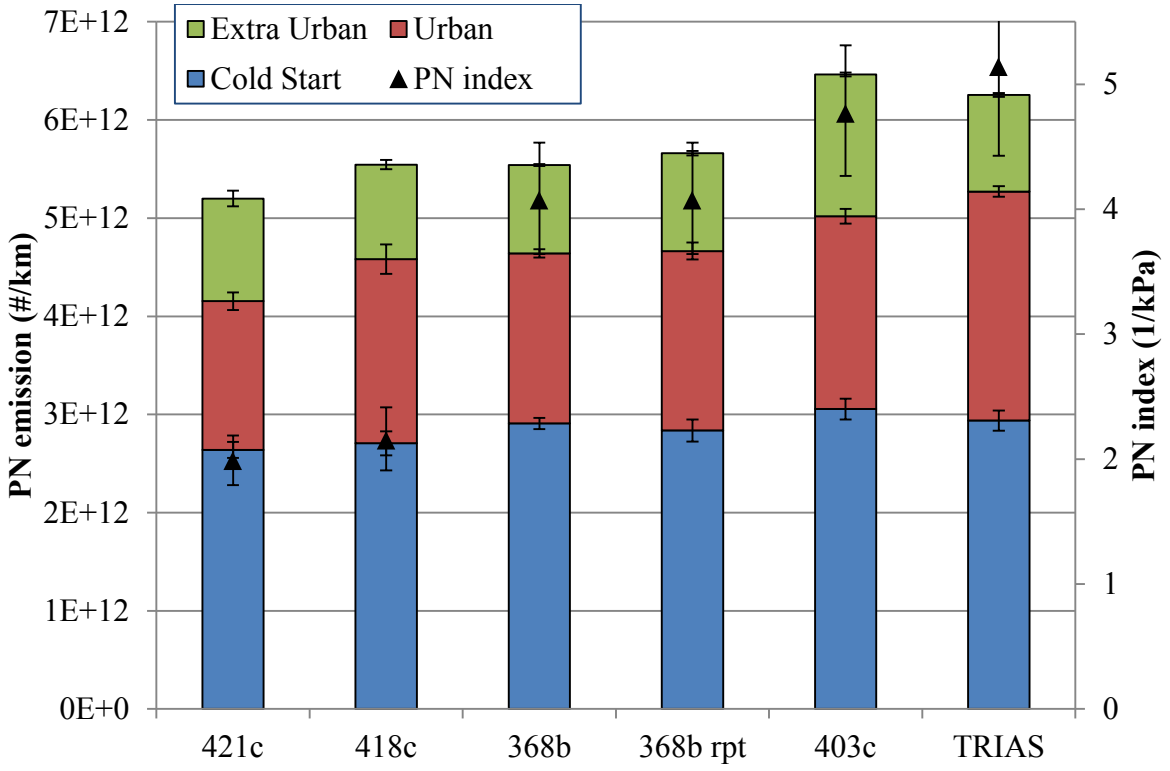

Figure 5.8: PN emissions over NEDC (APC results), the error bars correspond to ± σ for the particulate results and a potential maximum and minimum for the PN index

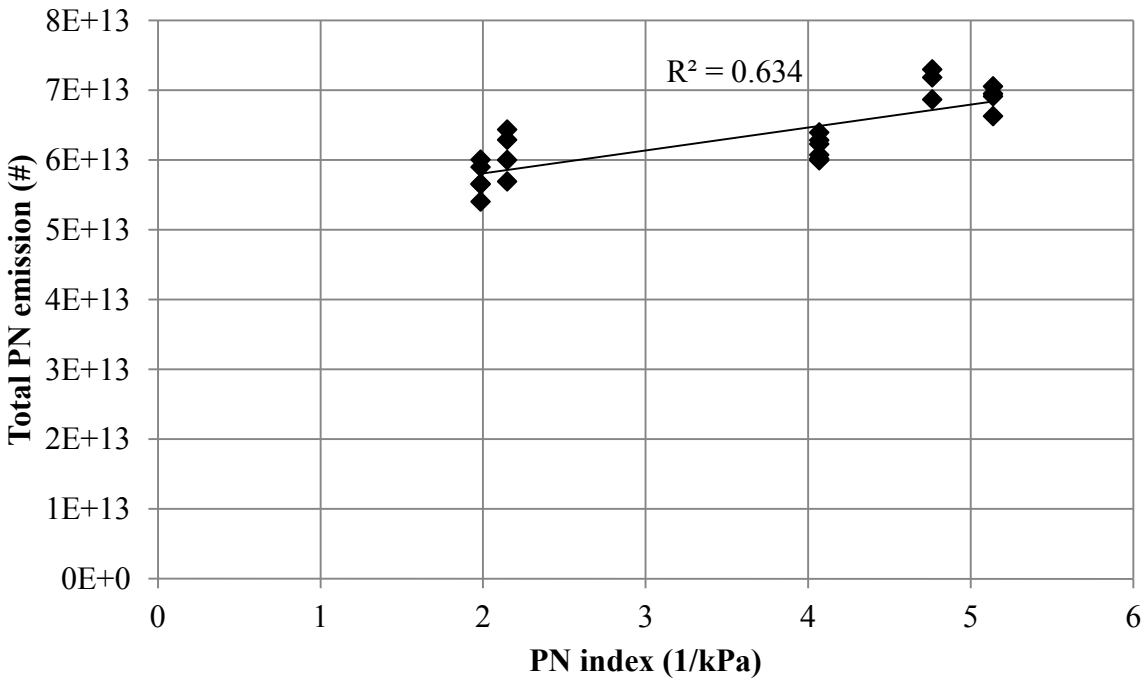

Figure 5.9: PN emissions over NEDC (APC results) vs PN index

Breaking the cycle down into its constituent parts however reveals more detail, this is shown in Figure 5.10. Here, the first 100 s of the cycle is referred to as the 'Cold Start', 100-800 s as the 'Urban', and 800-1180 s as 'Extra Urban'. It is reassuring, comparing Figure 5.9 and Figure 5.10, that the correlation between the PN index and PN emissions is strongest when the whole cycle is considered, rather than just one part of the cycle.

Fuel 403c has the lowest VP of all the fuels, and so will take the longest to evaporate upon injection, giving the least homogeneous mixture – known to increase particulate emissions. This fuel also has the highest emission in the Extra Urban portion of the cycle, which requires the highest load from the engine, suggesting perhaps that some spray impingement is taking place – leading to higher PN emissions, while leaving emissions where full evaporation has taken place (the Urban part of the cycle) more heavily dependent on the combination of VP and DBE.

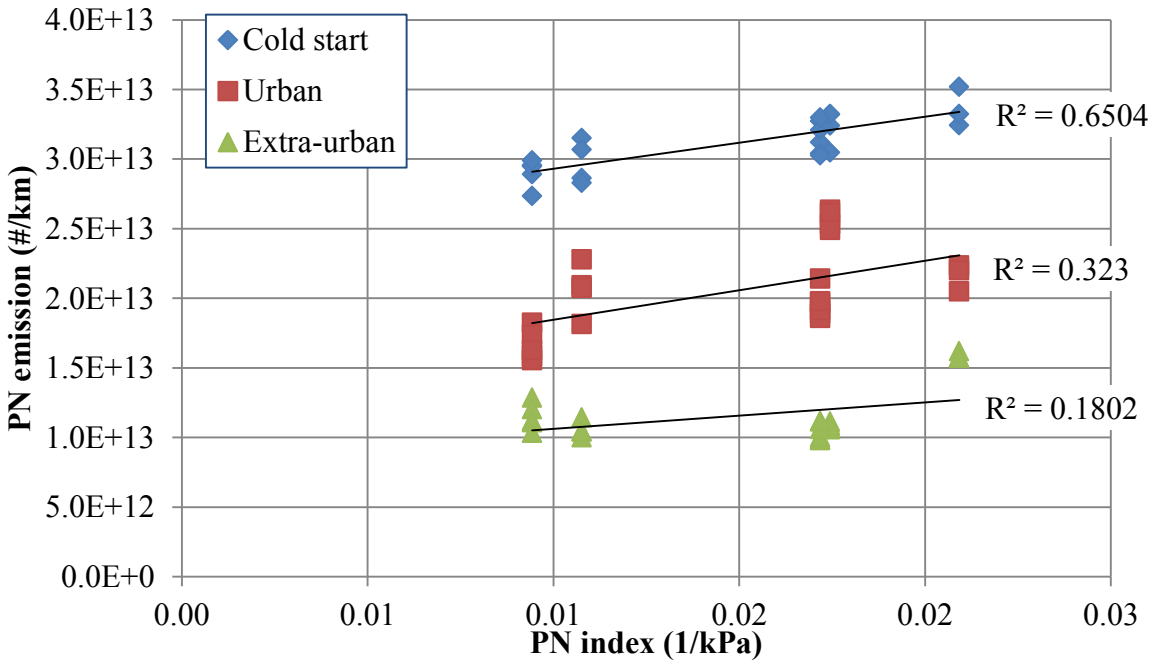

Figure 5.10: PN emission (APC results) for cycle parts plotted against PN index

Likewise the Urban portion of the cycle correlates better with the DBE of the fuel, TRIAS having the highest DBE, and the highest Urban emission. The Cold Start part of the cycle again seems to correlate best with VP, unsurprising perhaps given the dependence of this part of the cycle on fuel evaporation. The Cold Start, and use of stop-start, may also cause deviation from the results observed on the single cylinder, optical access engine, which was run at steady-state and fully warm. These trends can clearly be seen when the APC results are plotted individually against DBE+1 and 1/VP; these are shown in Figure 5.11 and Figure 5.12. The strongest correlation is between DBE+1 and PN emission in the Urban region, however there is almost no correlation, or even a negative correlation between DBE+1 and PN in the other two regions, whereas the trend between 1/VP and PN is stronger, and positive in both of these areas.

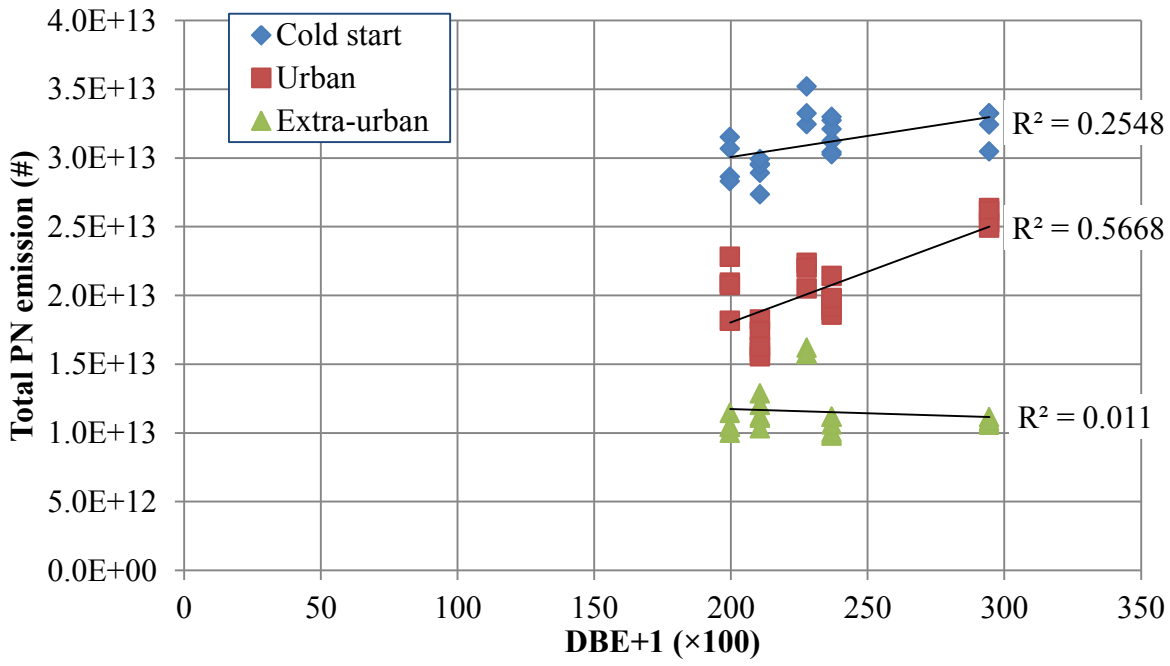

Figure 5.11: Total PN emission over NEDC plotted against DBE + 1 (APC results)

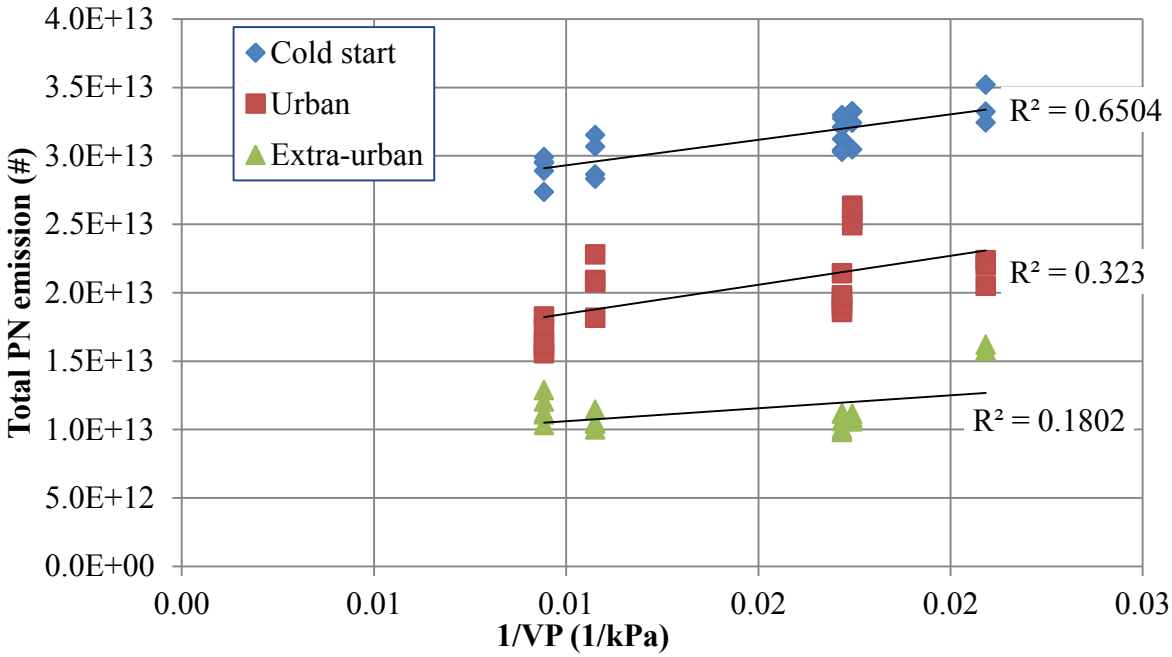

Figure 5.12: Total PN emission over NEDC plotted against 1/VP (APC results)

5.2.2. Comparison between APC and DMS results

As the APC is known to be the most accurate counter for solid particles (see Section 1.4) its results for particle count have been treated as the reference. However, the APC does not count any liquid phase particles, and has 50 % count efficiency at 23 nm. The DMS500 uses empirical approximations, based on individual instrument calibrations, to obtain a particle count, but can count in the full spectrum of 5-1000 nm and does not only count solid particles. The literature indicates that the DMS accumulation mode can be assumed to be equivalent to the result obtained from a legally compliant measurement from a vehicle [5], however as discussed in Section 2.5.6, there can be issues associated with poor lognormal fitting from the DMS where this is not the case; this can be compensated for by applying a Wiebe function to the DMS results. The results over the NEDC from the APC and the DMS (analysed using both methods) can be seen in Figure 5.13, Figure 5.14, and Figure 5.15. Due to equipment failure, DMS data is not available for all of these NEDC experiments (see Table 5.2).

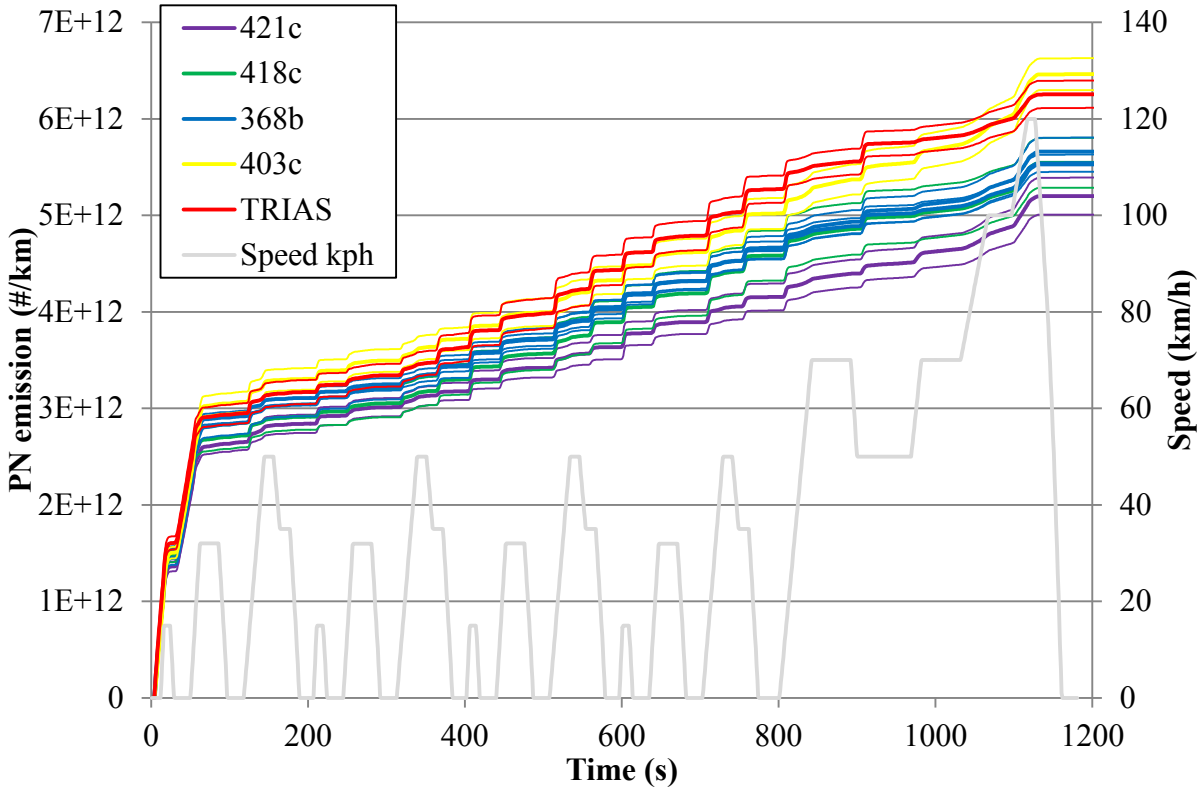

Figure 5.13: Cumulative APC data over NEDC; each thick line represents the mean, and the thin line one standard deviation for each fuel

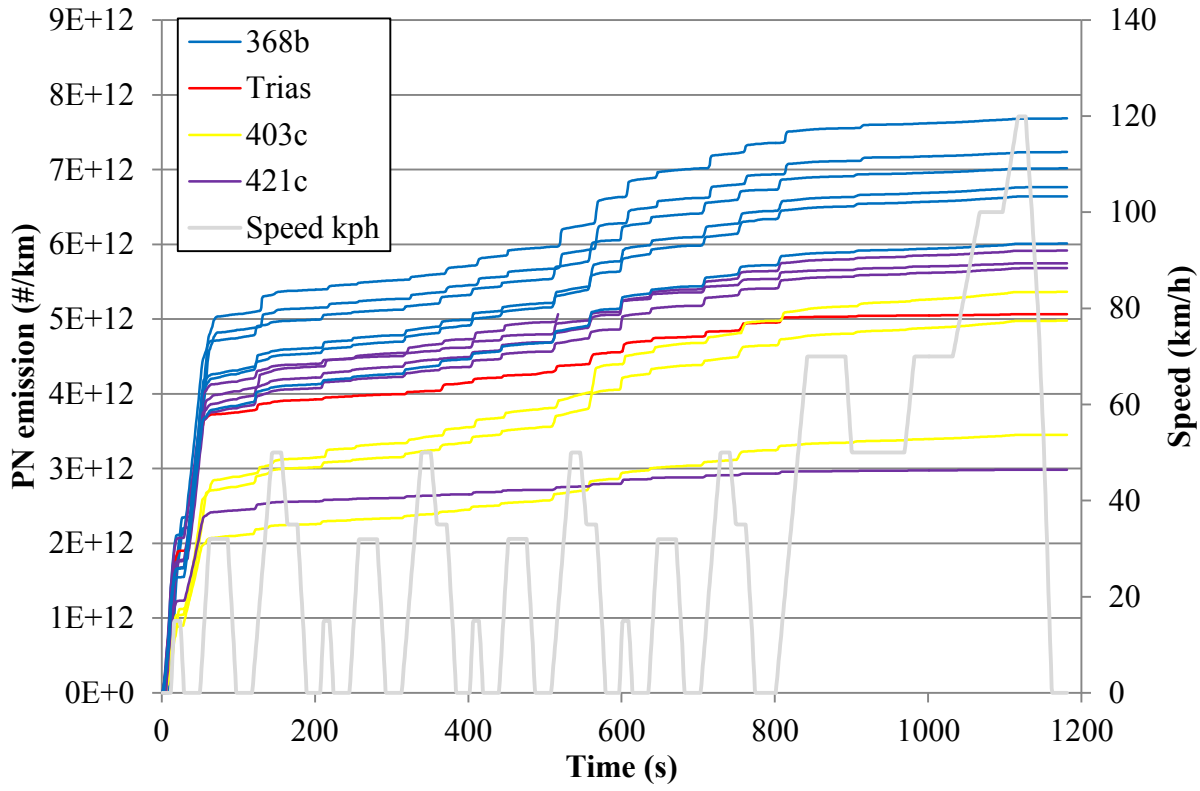

Figure 5.14: Cumulative DMS Wiebe data over NEDC; each line represents one experiment

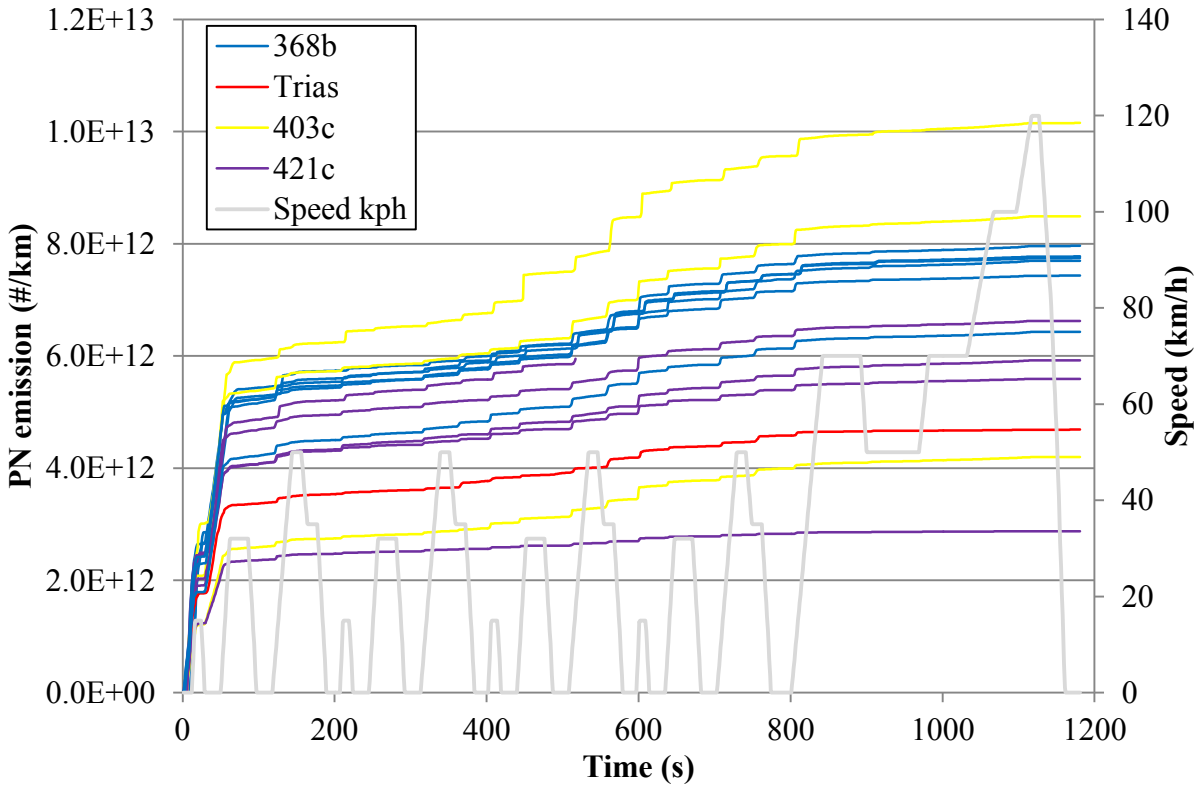

Figure 5.15: Cumulative DMS logfit accumulation mode data over NEDC, each line represents one experiment

Figure 5.13, Figure 5.14, and Figure 5.15 show characteristic traces of particulate emissions over the NEDC, with a large increase at the start while the engine is cold, and warming up, followed by relatively flat traces once the engine is warm with further sharp increases on acceleration events. The cold start particles are caused both by the lack of a warm engine and associated poor evaporative performance of the fuel, and the engine running in a catalyst heating mode with split injection in order to warm the catalyst up as soon as possible. This catalyst heating mode causes higher particulate emissions. The increase in particles on acceleration once the engine is warm can be attributed to small rich mixture excursions at the initiation of each acceleration. These can clearly be seen in Figure 5.16, where the initiation of each acceleration causes the lambda to fall

significantly below 1; such rich mixtures produce at least an order of magnitude more particles than stoichiometric conditions, as discussed in Section 1.2.3.

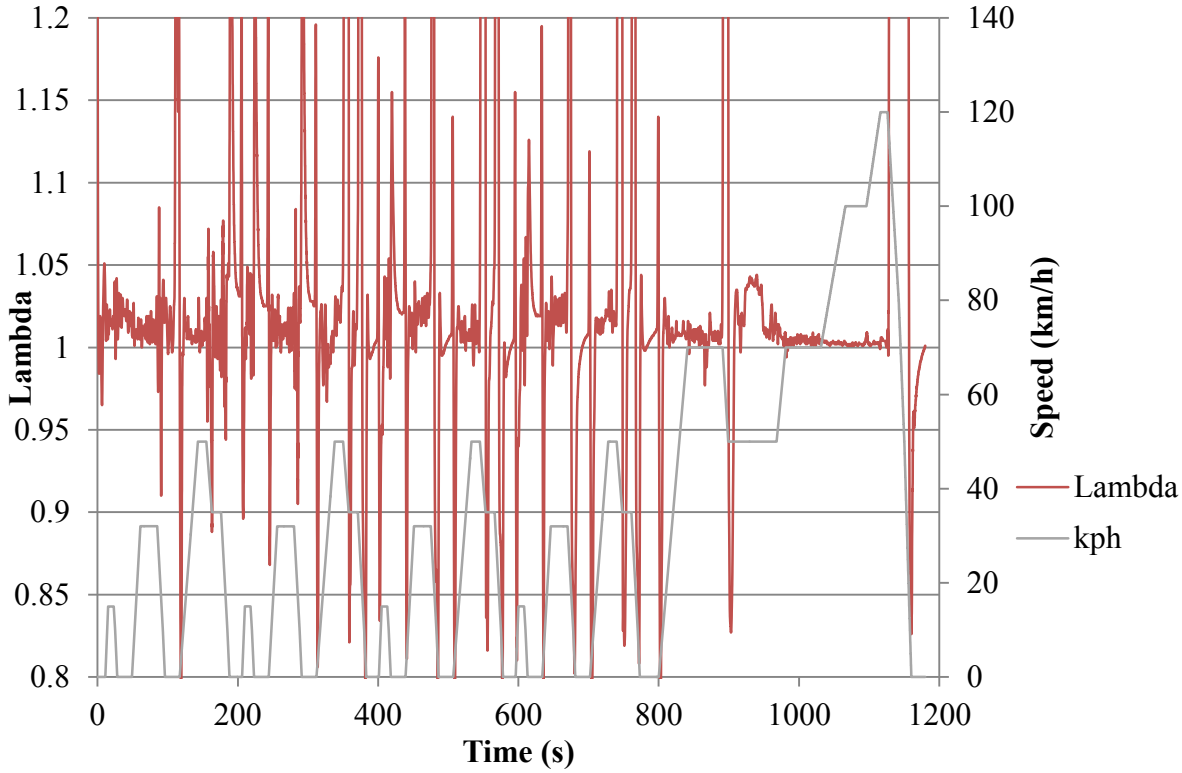

Figure 5.16: Lambda vs time over NEDC

It can be seen in Figure 5.13, Figure 5.14, and Figure 5.15 that the three methods of counting: APC, DMS with the lognormal fitting (DMS logfit), and DMS filtered by the Wiebe function (DMS Wiebe) produce different results for total number of particles counted over the NEDC. Figure 5.17, Figure 5.18, and Figure 5.19 show direct comparisons between the three methods broken down into the Cold Start, Urban, and Extra Urban portions, alongside showing the total (the sum of the three). There are two experiments (circled in red) where the lognormal fitting is very poor, the problem noted in Section 2.5.6 is in evidence here, so the logfit results from these runs are excluded. In general it can be seen that the DMS particle counts are higher than the APC particle

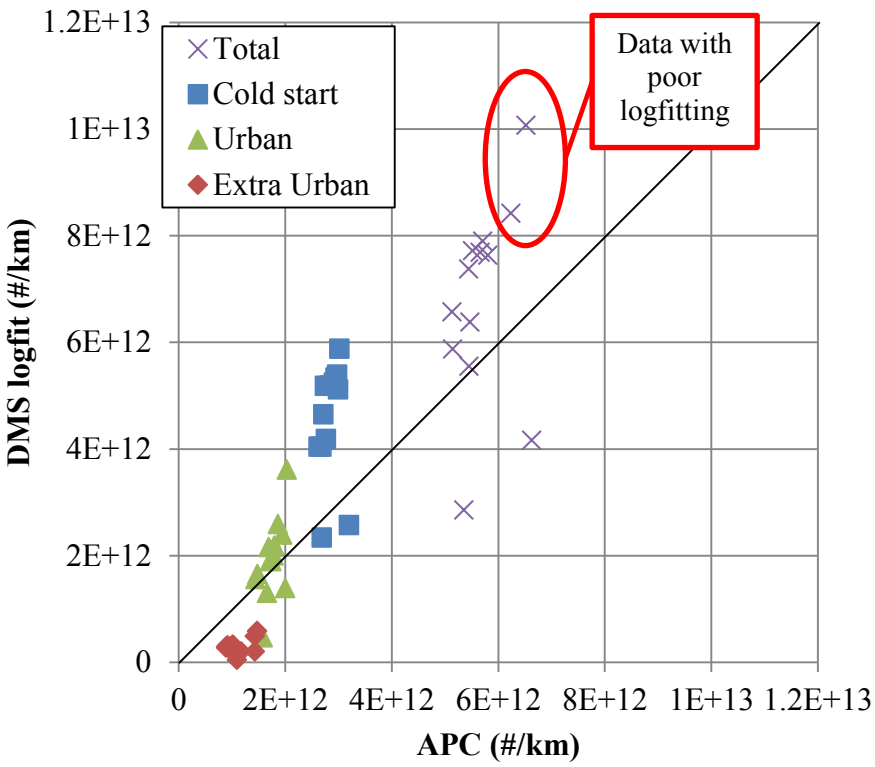

Figure 5.17: APC data vs DMS log-fitted data

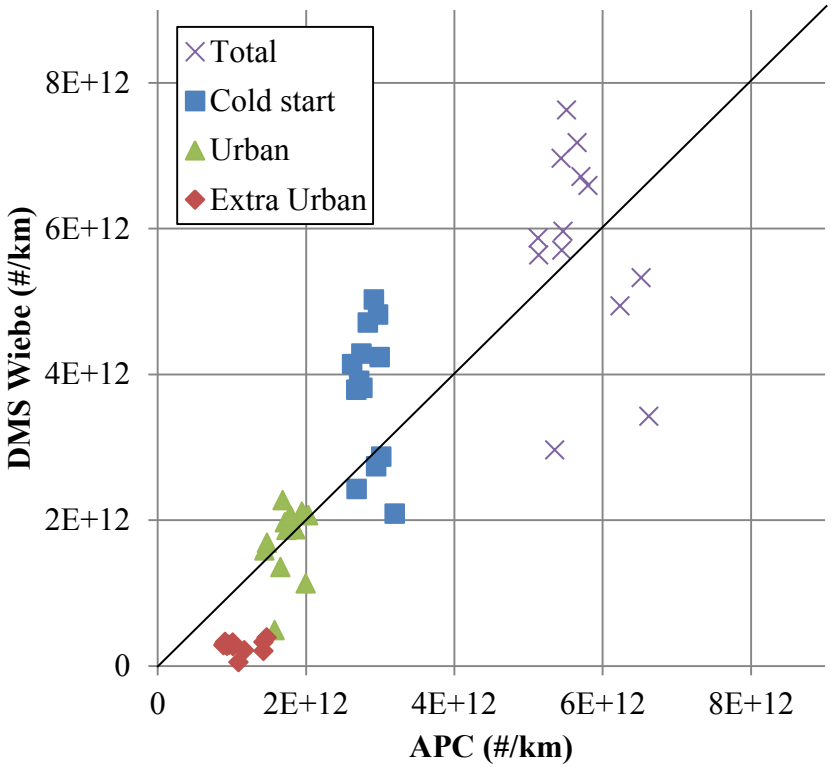

Figure 5.18: APC data vs DMS data filtered with the Wiebe function

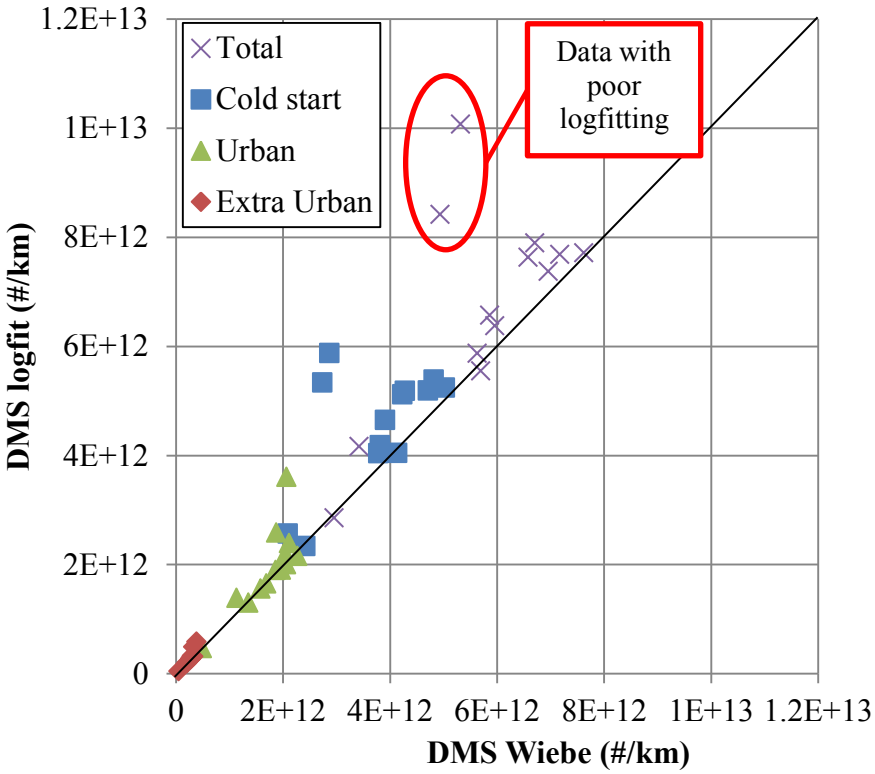

Figure 5.19: DMS data filtered with the Wiebe function vs the lognormal fitted data

counts, which is to be expected as the APC only counts solid particles, with a 50 % cut at 23 nm whereas the DMS counts all particles 5-1000 nm.

The CoV of particulates data for the NEDC experiments is shown in Table 5.3, Table 5.4, and Table 5.5. For this multi-cylinder engine, fitted with a catalyst, it would be expected that the CoV of particulates would be much lower than that found on the single cylinder engine. It can be seen that this is the case, with the CoV of the APC data never exceeding 8 % (0.08), and the CoV of the DMS data rarely exceeding 40 % (0.40), a much lower CoV than seen on the single cylinder engine data. It can also be seen that again the Wiebe filtering method of analysing the DMS data gives a lower CoV than the Cambustion logfits – further showing the usefulness of this approach to the DMS data.

Table 5.3: Coefficient of Variation of Particulates from APC results

Fuel	421c	418c	368b	368b (rpt)	403c	TRIAS
Cold Start	0.03	0.05	0.02	0.04	0.03	0.03
Urban	0.06	0.08	0.02	0.05	0.04	0.02
Extra Urban	0.08	0.05	0.01	0.02	0.01	0.02
Total	0.04	0.05	0.02	0.03	0.03	0.02

Table 5.4: Coefficient of Variation of Particulates from DMS results (Wiebe filtered)

Fuel	421c	368b	368b (rpt)	403c
Cold Start	0.17	0.03	0.05	0.13
Urban	0.34	0.06	0.05	0.24
Extra Urban	0.69	0.06	0.04	0.25
Total	0.21	0.04	0.05	0.18

Table 5.5: Coefficient of Variation of Particulates from DMS results (Cambustion logfits)

Fuel	421c	368b	368b (rpt)	403c
Cold Start	0.22	0.02	0.09	0.32
Urban	0.35	0.05	0.09	0.36
Extra Urban	0.72	0.05	0.05	0.38
Total	0.24	0.02	0.09	0.33

It can be seen both from the data in Figure 5.13, Figure 5.14, Figure 5.15, Figure 5.17, and Figure 5.18 as well as the CoV data in Table 5.3, Table 5.4, and Table 5.5 that the DMS results are also much more variable than the APC results. This variability may be as a result of the DMS measuring condensed vapour phase particles that grow by condensation, which are more variable and cannot be measured by the APC. In addition the DMS (unlike the APC) was not fitted with variable dilution. Variable dilution means that both the very high levels of particles measured during cold start and the very low levels of particles experienced in the fully warm conditions can be measured accurately by using a high dilution ratio when particle levels are high, and a low ratio when the particle levels are low.

The DMS ‘saturated’ (experienced higher levels of particles than were able to be measured) on several occasions over the experiments, on average the DMS was saturated for about 50 of 1200 data points over the NEDC. In all cases, the DMS saturated on rings 8-13 (although never all of them simultaneously), and whilst it is not possible, due to the inversion algorithm not being open source, to calculate exactly what size range this is, from the spectral outputs, it is clear that this is in the range 20-70 nm. To an extent this is compensated for by lognormal data fitting, but it is impossible to measure particle levels accurately when the DMS is saturated. Of note is that as the DMS experienced high levels of particles at the cold start, it became dirty, and when the DMS is dirty, the noise levels on the DMS increase. However the noise levels of the DMS were checked at the start and end of every test, and the DMS will not report data inside its noise spectrum. The DMS was regularly cleaned; therefore the dirtiness of the DMS should not have an effect on its particulate measurements. The combination of greater variability of condensed vapour phase particulates and the lack of variable dilution accounts for the greater variability of the PN results showed by the DMS. For this reason the APC results have been used as the reference PN count.

5.2.3. DMS500 size data

One of the main reasons for using the DMS in parallel with the APC was to be able to measure the particle size distributions over the drive cycle. The average diameter of the nucleation and accumulation modes over the NEDC is shown in Figure 5.20 (again there is data only for four fuels due to instrument failure).

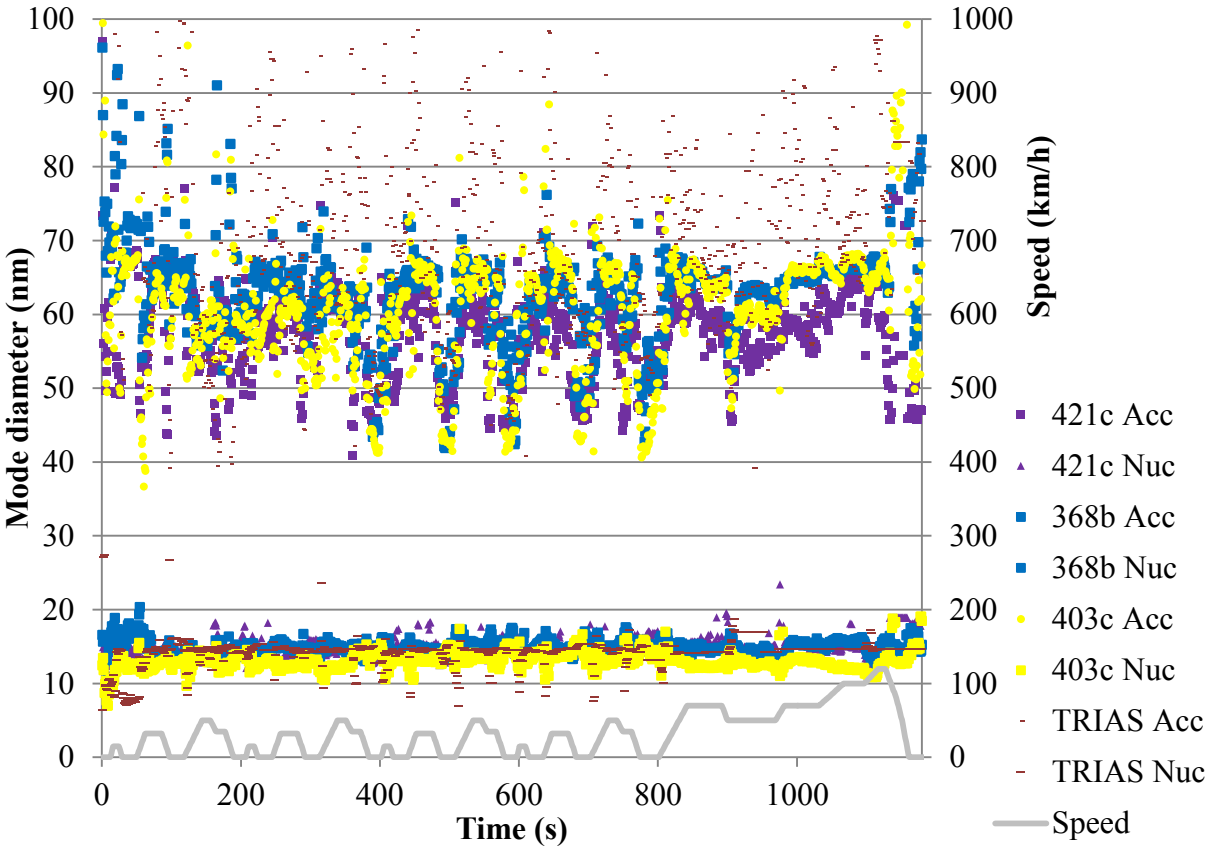

Figure 5.20: Average mode diameters for fuels tested over NEDC, the TRIAS data is more variable as it is not averaged, as only one data set is available

It can be seen that for the nucleation mode, there is little effect of fuel composition on particle diameter, with 368b having the largest average nucleation mode diameter (15 nm) and 403c the smallest (12 nm). It can also be seen that acceleration events have little effect on the average mode diameter

The size of the accumulation mode particles seems to be more affected by the fuel. TRIAS has consistently the largest particle size (although the data is presented from only one experiment), and 421c the smallest particle size. Indeed the average particle diameters fall in the diameter distribution 421c < 368b < 403c < TRIAS, which is also the order of the PN index for each fuel.

Whilst this result at first seems unexpected, it makes sense that a fuel which gives more particle number emissions should also have a larger average particle diameter for the

accumulation mode, as more initial particles will be available to agglomerate, and more material available to adsorb onto the initial particles, increasing their average size.

5.2.4. Steady state analysis

In order to compare these drive cycle results with the steady state results obtained, it was decided to select certain parts of the drive cycle that were at steady state, and analyse the results from those parts. The points chosen are shown in Figure 5.21, and the points were chosen from the parts of the cycle at constant speed for an extended period of time, which were fully warm (as the steady state engine tests were), three were chosen at relatively low speed, and three at higher speeds. The first five seconds of data from each point was discarded in order to ensure that no transient effects were present.

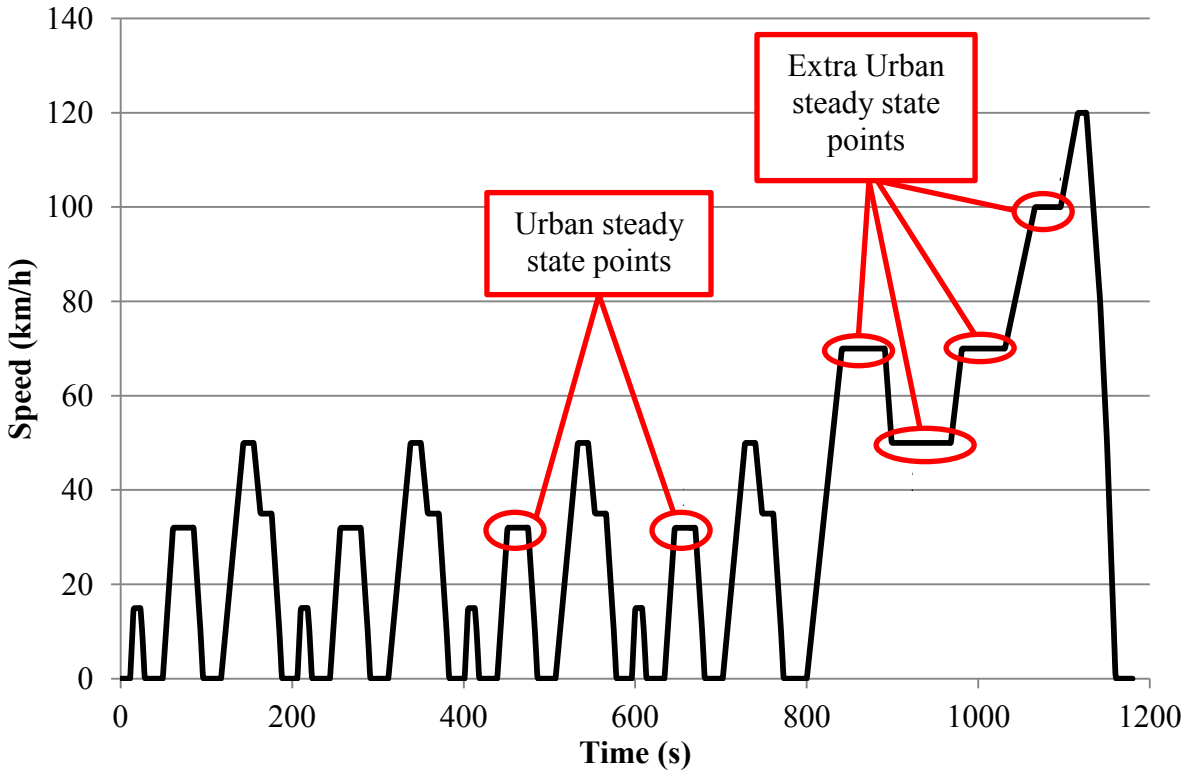

Figure 5.21: Steady state points chosen

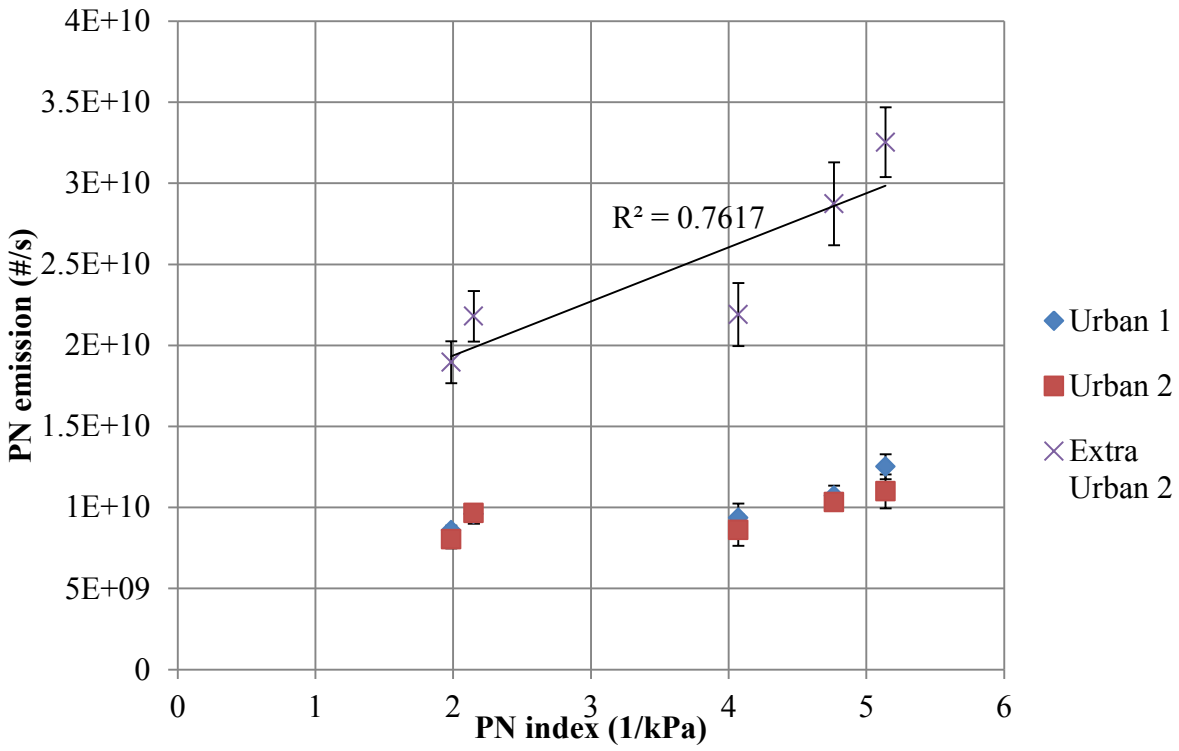

Figure 5.22: PN emission at low speed steady state points (APC results) , the error bars correspond to ± σ; Urban points 1 & 2 are at the same load and show good repeatability

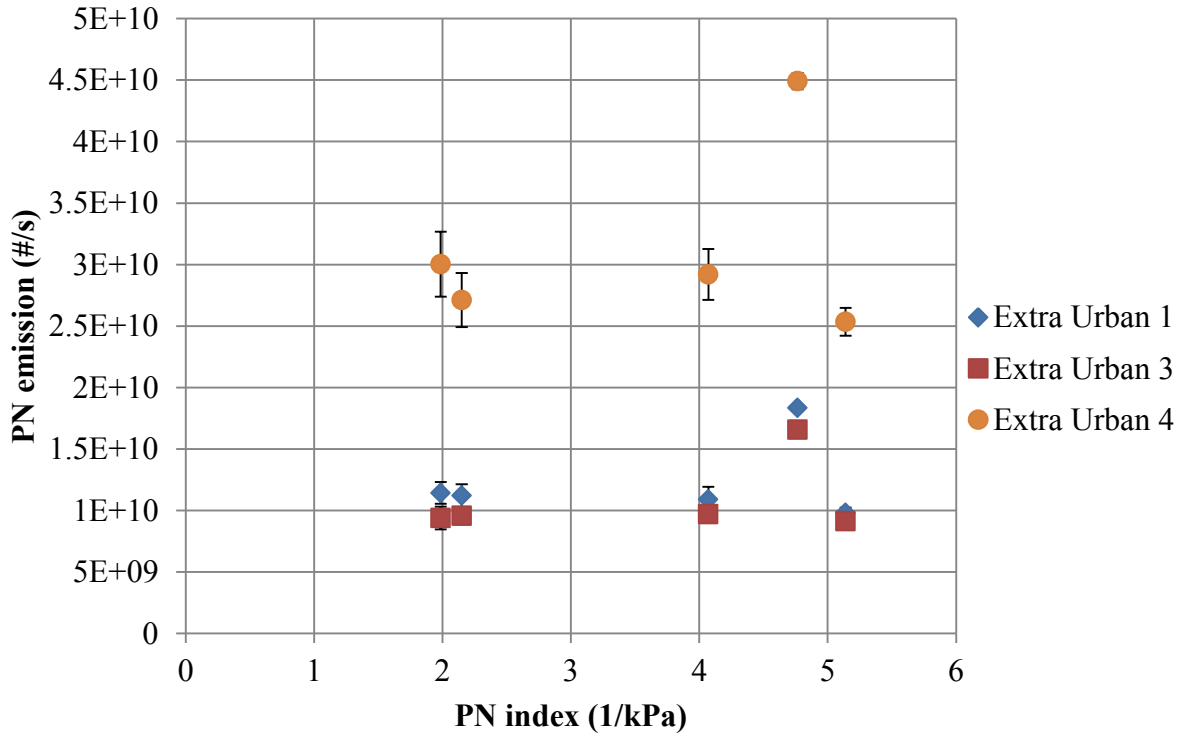

Figure 5.23: PN emission at high speed steady state points (APC results) , the error bars correspond to ± σ; Extra Urban points 1 & 3 are at the same load and show good repeatability

The results of the steady state points are shown in Figure 5.22 and Figure 5.23 follow the trends shown in the whole drive cycle results. The results are repeatable, with points Urban 1 and 2, and Extra Urban 1 and 3 showing very similar PN emissions for the same drive cycle speed (and therefore implied load). The results also show what would be predicted, that the higher the road speed (engine load) the higher the PN emission.

The results fall into broadly two categories, the lower load (lower road speed) results (Figure 5.22) and the higher load (higher road speed) results (Figure 5.23). The low speed results show a monotonic increase in PN, correlating with the results of the Urban drive cycle. As in the Urban region, the results here correlate with the DBE of the fuel well.

The higher load (higher road speed) results correlate better with the Extra Urban drive cycle results, and 1/VP of the fuel, in particular the step change in PN emissions exhibited with 403c is the same behaviour as seen in Figure 5.10. 403c, which had a very low vapour pressure, shows the highest emission at all three high speed test points, this is probably due to poor fuel evaporation leading to spray impingement and hence wall wetting, drastically increasing the level of particulate emissions.

The steady state analysis of the average mode diameters (Figure 5.24) again correlates well with the drive cycle results (Figure 5.20). The nucleation mode results, shown in Figure 5.24, are again constant across both the fuels and the high and low speed steady state points, with only one fuel (403c, which has the lowest vapour pressure) showing any significant deviation to 12 nm from an average diameter of 15 nm for all of the other fuels. This demonstrates that the nucleation mode size is unaffected by engine load or speed.

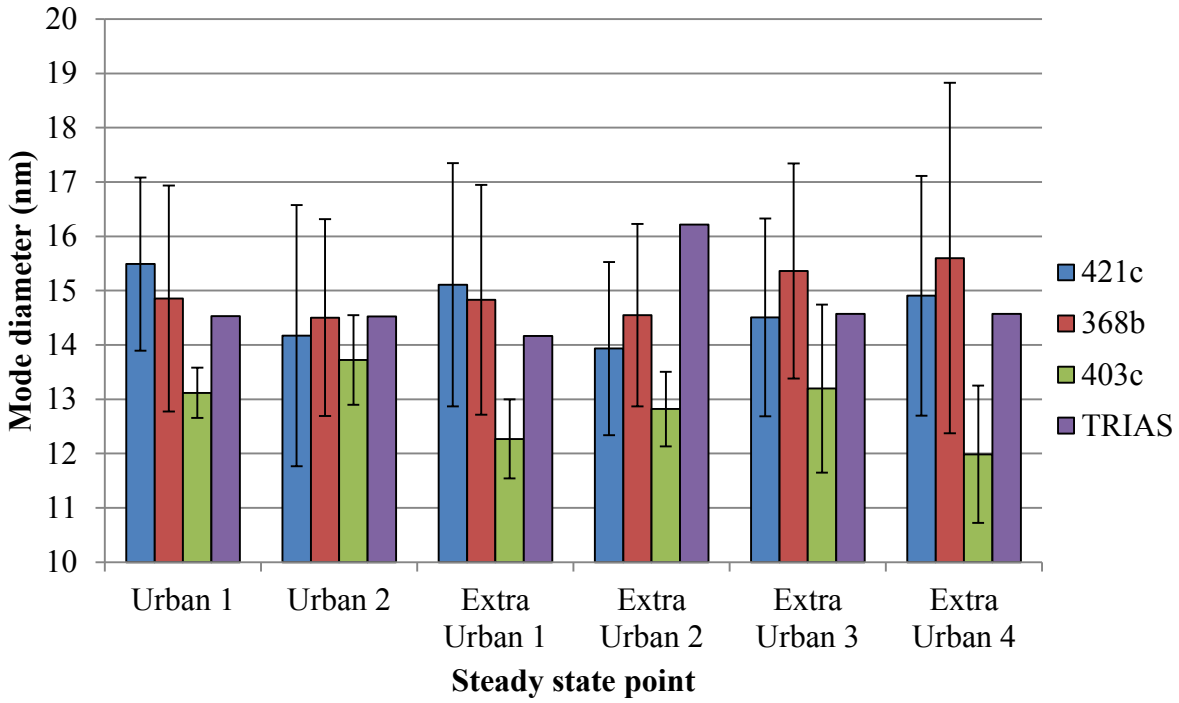

Figure 5.24: Nucleation mode diameter variation with fuel at steady state, the error bars correspond to ± σ, there are no error bars for TRIAS, as only one data set was obtained

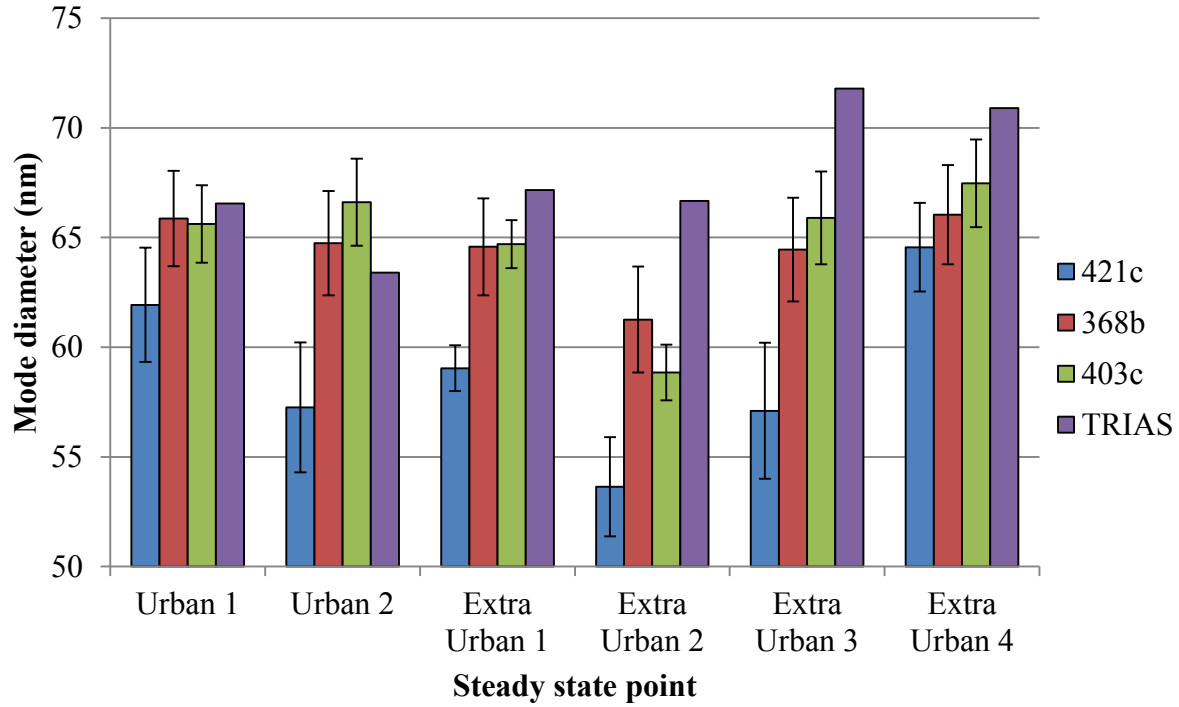

Figure 5.25: Accumulation mode diameter variation with fuel at steady state, the error bars correspond to ± σ, there are no error bars for TRIAS, as only one data set was obtained

The accumulation mode results are shown in Figure 5.25, again the steady state results (Figure 5.25) behave as the drive cycle results did (Figure 5.20). There is the clear trend visible of the accumulation mode diameter from the fuels being in the order of 421c < 368b < 403c < TRIAS. In addition, good repeatability can be seen between the two sets of points at the same speed, Urban 1 and 2, and Extra Urban 1 and 3. Neither Figure 5.24 nor Figure 5.25 correlates with the magnitude of the PN emissions emitted.

5.2.5. PM mass results

The PM mass emissions were also measured over these experiments with an AVL Micro Soot Sensor (MSS), a type of PASS. Figure 5.26 shows the comparison between the number of particles counted at the end of the test, and the total mass of particles detected at the end of the test. It can be seen that there is a good correlation between particle mass and number, which while not inevitable, agrees with the observations of relatively constant particle diameter over the test for the various fuels.

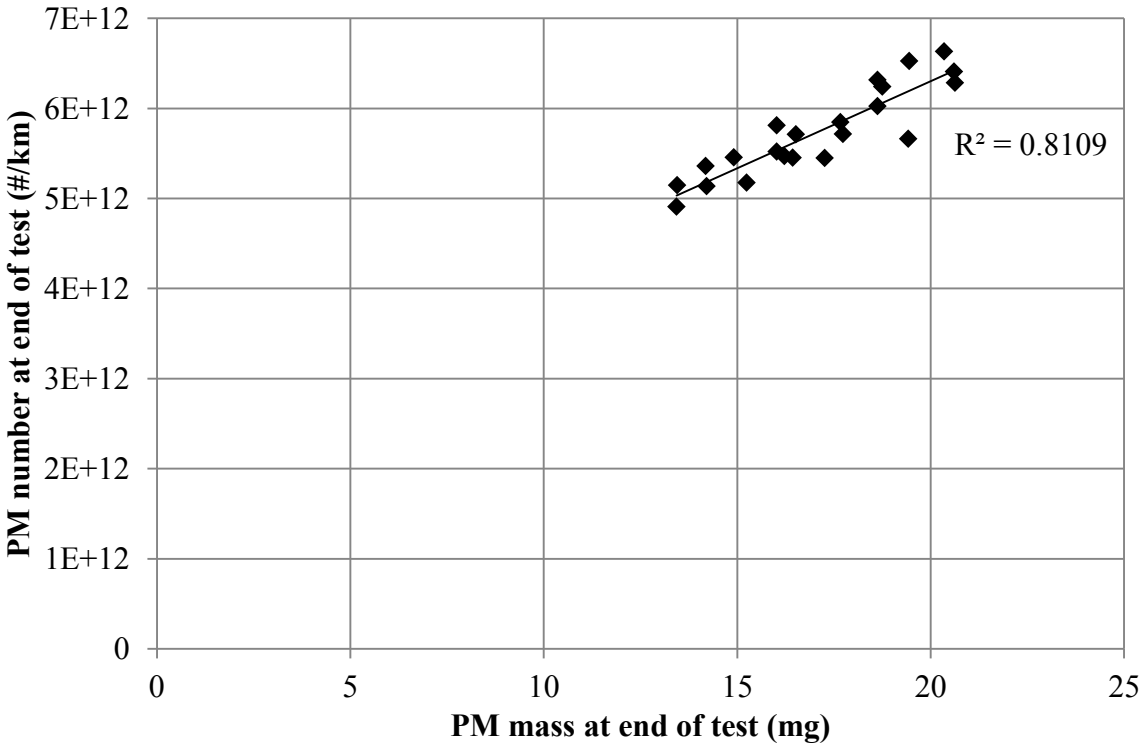

Figure 5.26: Number vs mass at end of test (APC and MSS results) for all fuels tested over NEDC

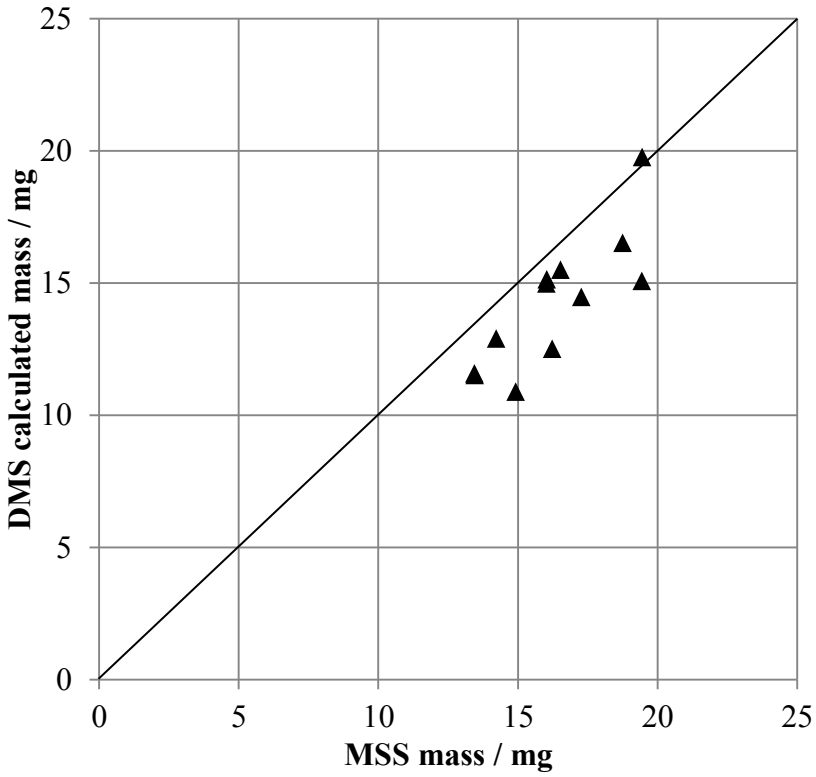

Figure 5.27: Comparison between mass at end of test between MSS and DMS for all fuels tested over NEDC

Figure 5.27 shows the comparison between the PM mass at the end of the test measured by the MSS, and the PM mass at the end of the test calculated from the DMS500 data using the method outlined in Section 2.5.5. It can be seen that there is a relatively good positive correlation between the MSS and the DMS calculated data, this gives additional confidence in the results of the experiments as three independent instruments measuring the same exhaust can be shown to correlate. The DMS calculated data is under-reading by about 13 %, however, as noted in Section 5.2.4, this may be because the DMS was saturated at some points, and so not all of the particles emitted were recorded. In addition the mass calculation has only used the accumulation mode data – as it has been assumed that the nucleation mode has negligible contribution to the PM mass.

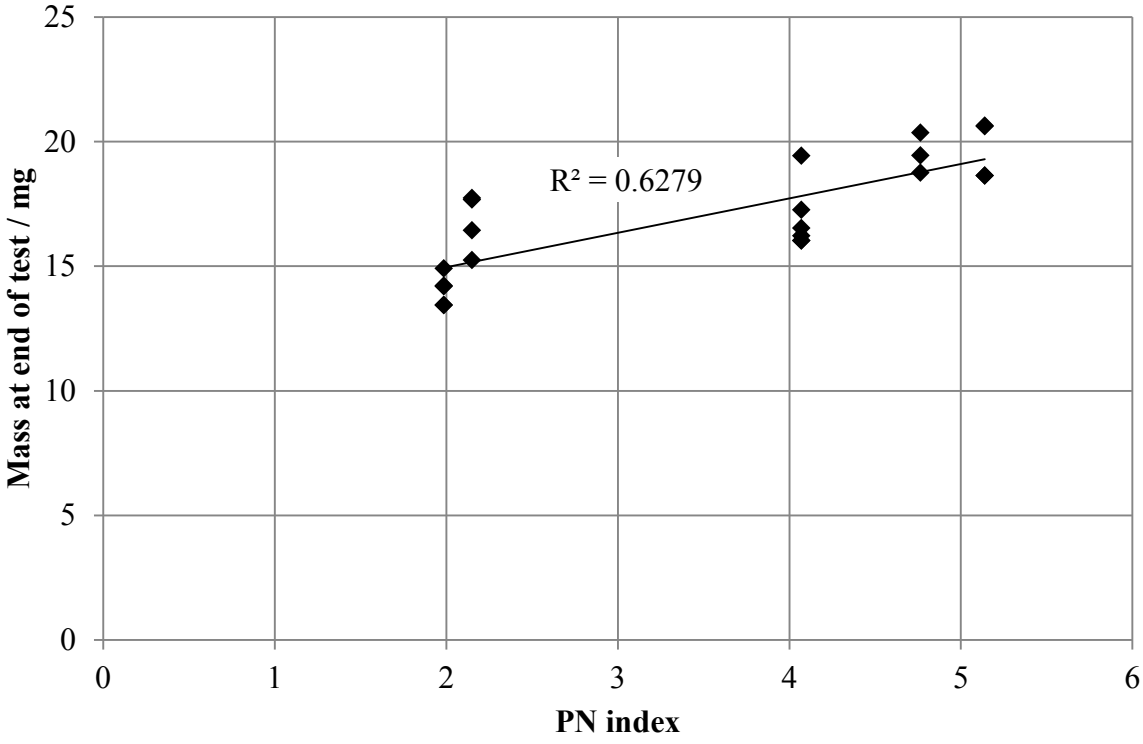

Figure 5.28: Comparison between mass at end of test (MSS) and PN index for all fuels tested over NEDC

Although the PN index is not intended to link fuel composition and PM mass emissions, given the good agreement between the PM mass and PM number at the end of the test, it is expected that there should be a correlation between the two. Figure 5.28 shows the comparison between the PM mass and the PN index (in the same way as Figure 5.9 shows the PM number to PN index comparison). The PM mass correlates with the PN index as strongly as (in fact very slightly stronger than) the PN number correlates with the PN index. This agrees with predictions given the knowledge of the particle size spectrum.

Fuel composition clearly has a significant impact on the PN emissions over the NEDC for the AJ126 engine, in this case a factor of order 1.4. However when applying PN index analysis drive cycle results have been more mixed than the steady state results in Chapter 4

and Section 5.1, with other factors such as cold start and variable engine load masking the effect of the PN index.

With this in mind, it can be seen that different parameters in the PN index have differing impacts on the PN emissions from different parts of the NEDC. In the Urban region, DBE has the greatest effect, whereas in the Extra Urban region, VP has a bigger effect, particularly if the VP is low enough that the fuel does not evaporate fully quickly enough, and spray impingement occurs.

Average particle diameters have been observed to not vary significantly over the drive cycle, or with different fuels, and this corroborates the PM mass data collected which shows very similar trends to the PM number data collected by both the DMS and the APC.

5.3. Chapter 5 summary

The PN index has been evaluated by measuring the PN emissions from a Jaguar AJ133 5.0 L V8 engine mounted on a dynamometer using a DMS500. Three fuels have been tested, with differing PN indexes, and corresponding differences in PN emissions have been observed. In particular the two fuels meeting the CEC RF-02-08 EU5 reference fuel specification have been tested, and a difference in PN emissions of a factor of two observed. Again, this stresses the importance for legislators of taking the PN index into account as future emissions legislation is created. The PN index has therefore been validated not only on a single cylinder engine with optical access, but now on a thermodynamic engine at steady state.

The PN index has also been evaluated measuring the PN and PM emissions from a Jaguar AJ126 3.0 L supercharged V6 engine mounted on a transient dynamometer over the

NEDC using a DMS500, APC, and AVL MSS. Five fuels with differing PN indexes were tested at least three times each, with careful attention paid to repeatability and drift effects. A variation in PN emissions of a factor of 1.4 has been observed, which was less than the variation predicted by the PN index. A detailed analysis of these results shows that the PN index has a stronger effect in certain drive cycle regions than others. Different parameters of the PN index have different impacts in different regions; with DBE have the strongest effect in the Urban part of the NEDC, and VP having the greatest effect in the Extra Urban part of the drive cycle, particularly if wall wetting occurs. Overall factors such as cold start can have a bigger effect on PN emissions than the PN index.

6. Particulate emissions from a highly boosted engine

Particulate emissions were sampled from the UB100 ULTRABOOST 2.0 L I4 engine [80, 81] at the University of Bath using the DMS500. This was the first time that the effect of fuel composition on particulate emissions from such a highly boosted engine has been evaluated.

A large matrix of experiments was undertaken on the UB100 engine; the engine is described in Section 2.4. Figure 6.1 and Table 6.1 show the matrix of experiments for the second phase, with the matrix being conducted fully with 14 fuels. These fuels and their composition are discussed in Section 3.4.2, although only limited compositional information was available. These fuels, supplied by Shell Global Solutions, were not designed specifically for analysis of particulate emissions, or with the PN index in mind, rather for a set of experiments designed by the ULTRABOOST consortium. The aim of the particulate measurements was to evaluate the effect of fuel composition on particulate emissions from the engine, as well as to evaluate the effect of the following engine parameters: load (torque), lambda, inlet air temperature, exhaust gas recirculation (EGR), and exhaust back pressure. The testing was divided into two phases.

The first phase of UB100 testing was to evaluate the effect of engine load on particulate emissions. The engine was run at a fixed speed and the load increased from a minimum idling condition, to the maximum load at that speed in nine increments. These tests were conducted on the BASE fuel.

The second phase was a much larger set of experiments at four engine test conditions, using all 14 fuels. At Test Condition 1, a 10 degree spark sweep (from Knock Limited

Spark Advance (KLSA), then retarding the spark in increments of 1 degree) was conducted at 0 % and 10 % EGR. At Test Condition 2, an 8 degree spark swing, and a 3 point start of injection (SOI) swing was conducted; Test Condition 2 is an NEDC minimap point. At Test Condition 3 – the transition between supercharged and turbocharged operation – a 10 degree spark swing, again from KLSA, was conducted, and the exhaust back pressure was varied to mimic the transition from supercharged operation to turbocharged operation. At Test Condition 4 there was a 3 point spark swing (in this case not from KLSA and abbreviated to only three points due to engine wear concerns) and lambda was varied from $\lambda = 1.01$ to $\lambda = 0.875$.

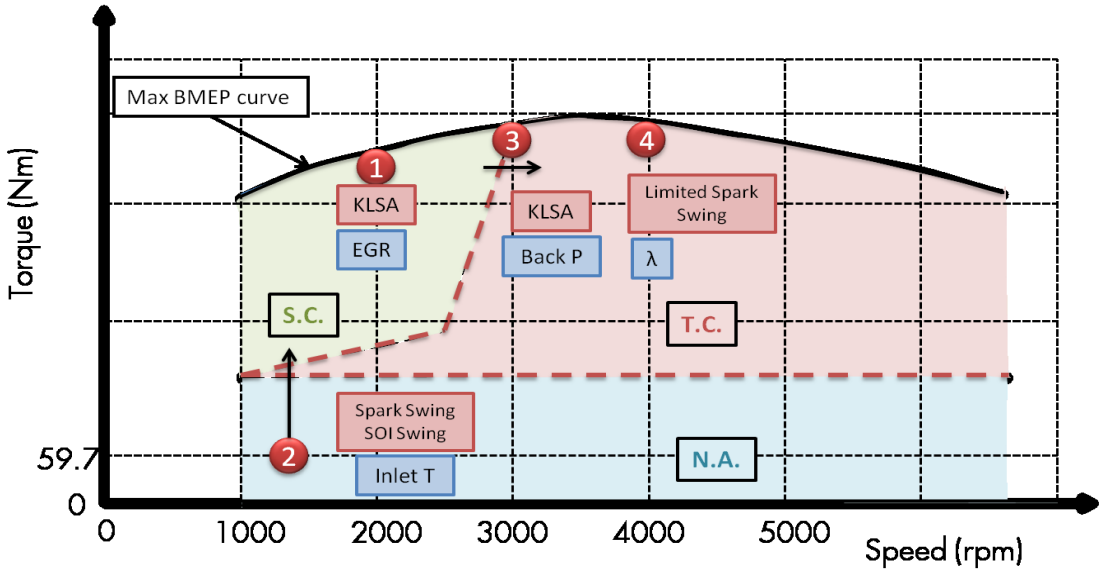

Figure 6.1: Experimental test points for the fuels matrix run on the UB100 engine (image courtesy of the ULTRABOOST consortium)

Figure 6.2 shows the sampling location on the UB100 engine. The sampling location was approximately 3 m downstream of the exhaust manifold, downstream of the backpressure throttle (used to mimic the effects of a turbocharger) and downstream of one silencer. The first 500 mm of the exhaust manifold is pulse separated and water-cooled

Table 6.1: Experimental test points for UB100 engine tests

Region	Test Point	Fixed Variables						Spark / Injection timing
		Speed (rpm)	Initial Load	Inlet air T (˚C)	Back P	EGR %	λ	
1A	**Low speed high load**	2000	Max BMEP within Knock and P_{max} limits	40	Low (SC)	**0**	1.0	KLSA – KLSA-10 CAD in steps of 1 CAD
1B				40	Low (SC)	**10**	1.0	
2A	**Low speed low load**	1250	59.7 Nm (NEDC mini-map point)	**20**	Low (NA)	0	1.0	(1) SOI variation: ± 10 CAD from base fuel optimum (330 CAD btdc) (2) 8 point spark sweep from 42.7 CAD btdc to 26.7 CAD btdc (not knock limited so KLSA not achievable) at 330 CAD btdc SOI
2B				**40**	Low (NA)	0	1.0	
3A	**Mid speed high load**	3000	Max BMEP within knock and P_{max} limits	40	**Low (SC)**	10	1.0	KLSA – KLSA-10 CAD in steps of 1 CAD
3B				40	**High (T/C)**	10	1.0	
4A	**High speed high load**	4000	Max BMEP within knock and P_{max} limits	40	High (T/C)	10	**1.0**	3 spark points; not as far as KLSA (for engine protection) and limited retard (for exhaust temperature)
4B				40	High (T/C)	10	**0.875**	

(due to the extremely high exhaust temperatures experienced at certain load conditions) and the engine is not fitted with a catalyst. This water-cooled section is bound to affect the condensation of the volatile particulates, possibly promoting nucleation mode growth; unfortunately it has not been possible to conduct an experiment without the water-cooled exhaust (although one would be possible, though not at all engine operating points) so the precise effect of the water-cooled section is not clear.

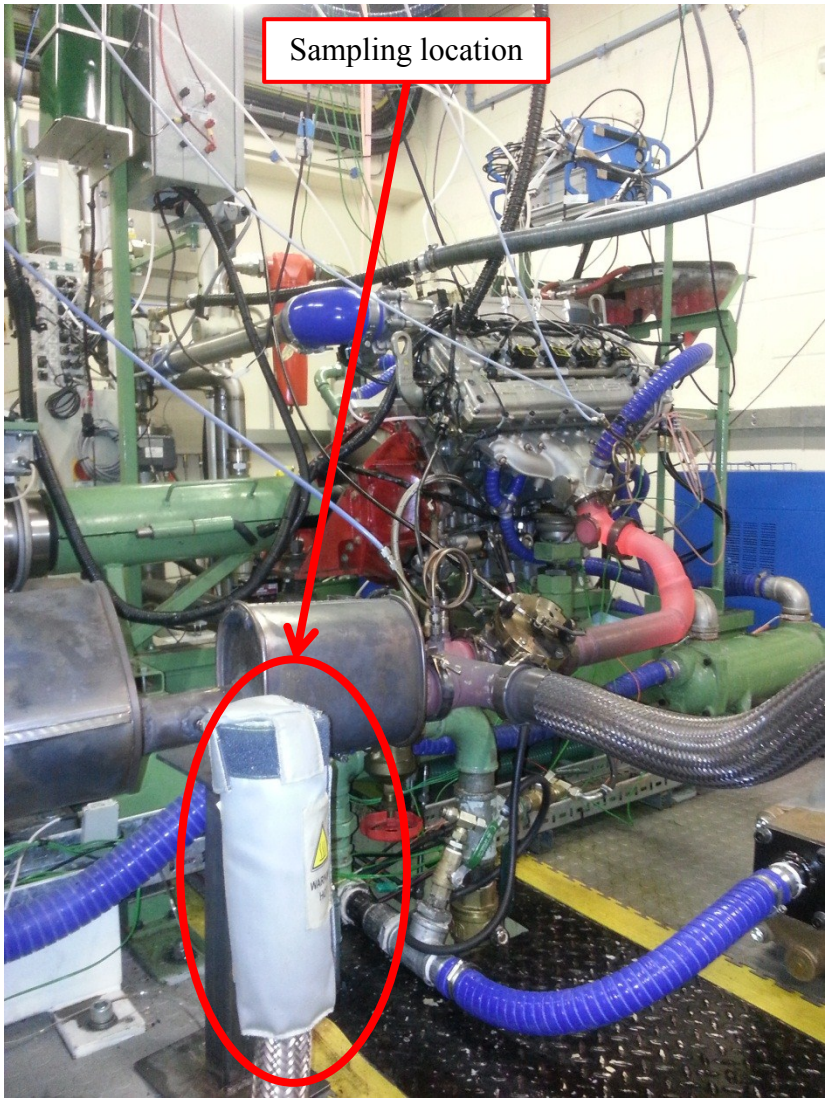

Figure 6.2: Sampling location on UB100 engine

6.1. Evaluation of a variety of parameters on PM emissions

The effect of several engine parameters on PN emissions has been measured. At each of the different test points the behaviour of the engine is expected to be very different, as there is such a wide range of conditions – from maximum power, 35 bar BMEP, to around 1 % of total engine power (Test Condition 2). As each of the parameters varied have not been varied at all test points, the effect of each parameter is only known at the test point at which it was evaluated, rather than for all operating points of the engine. Which parameter was varied at which test point is shown in Figure 6.1 and Table 6.1.

6.1.1. Effect of engine load and fuel injection pressure

To measure the effect of engine load on PN emissions, the engine was run at a fixed operating point (2000 rpm, $\lambda = 1.0$, 0 % EGR), and the load increased from ~ 50 – 500 Nm. This corresponds to ~ 3 - 32 bar BMEP, the load was increased in nine increments. In order to achieve this load range on this engine, the engine needs to pass through both naturally aspirated (NA) and turbocharged (T/C) regions, with the turbocharging being mimicked by an external boosting rig as described in Section 2.4. Given that the UB100 is an experimental prototype, it has not been calibrated fully, in particular there is a total change in calibration between the NA and the T/C regions; the result of this is that results from different regions cannot be compared directly. In addition to the stepped increase in load, each load point was tested at three injection pressures, 60, 80, and 100 bar in the NA region and 160, 180, and 200 bar in the T/C region. All of the tests were conducted on BASE fuel, which is fully described in Section 3.4.2 but is a 97 RON, EN228 compliant fuel, and representative of standard European pump gasoline.

The results are shown in Figure 6.3, in Figure 6.3 it can be seen that the particulate emissions from the UB100 follow the trends seen in other engines; that the particulate

emissions increase as the load increases. There is over an order of magnitude increase between the lowest and the highest levels of particulates measured. In the T/C region it can be seen that the increase is highly non-linear, with relatively little increase in particulates between 250 & 400 Nm and a step increase between 400 & 500 Nm. The difference that the calibration of the engine makes between the NA and T/C regions can also clearly be seen, with an unexpected decrease of approximately an order of magnitude in the number of particles counted over the transition (between 163 & 251 Nm). Primarily this is due to the change in fuel pressure, resulting in a better-prepared mixture in the T/C region; a discussion of the effect of fuel injection pressure is in the following paragraph. Given that so many other engine calibration parameters change (including spark timing, CAM lift, CAM timing, and injection timing) it is not possible to say which of these has the most effect between the two regions with any certainty.

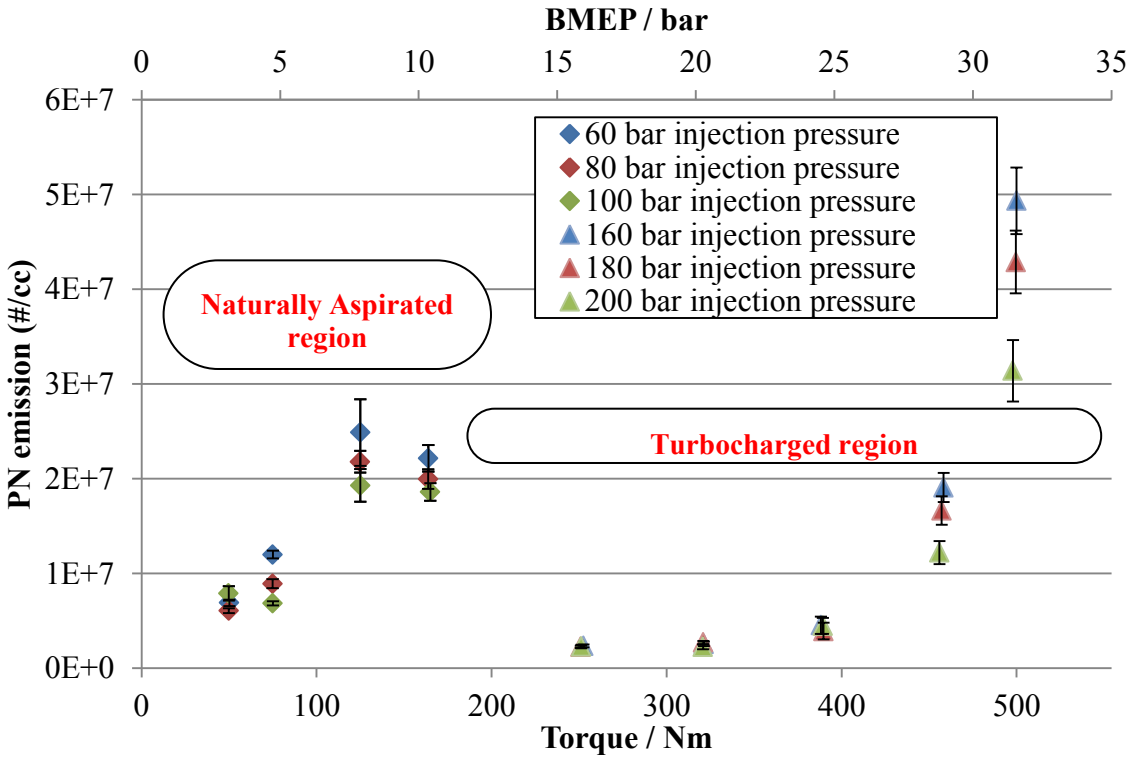

Figure 6.3: Particulate emissions (#/cc) from the UB100 ULTRABOOST engine as the load is increased from 3 bar BMEP to 32 bar BMEP

The effect of fuel pressure on particulate emissions in the tests can also clearly be seen. In both the NA and the T/C regions the higher the fuel pressure, the lower the particulate emissions. This effect is particularly prominent at higher load conditions for each region, indeed at the maximum load point, there is a difference between 160 bar injection pressure and 200 bar injection pressure of approximately 2×10^7 #/cc. The effect is also observed at the upper end of the engine's NA region, where a difference in injection pressure between 60 & 100 bar gives a factor of approximately 1.6 difference in particulates levels. This agrees with the hypothesis that a higher fuel pressure will result in a better-prepared mixture, which will result in lower particulate emissions. This is observed especially clearly at the point of transition between the NA and the T/C regions, where the fuel pressure is increased by 100 bar.

Increasing fuel pressure is an effective strategy for reducing particulate emissions from gasoline engines, however higher fuel pressures require more power to be delivered to the fuel pump(s), which increases specific fuel consumption and CO_2 emissions so a compromise between these two demands is needed.

6.1.2. A first look at the phase two results

In total 1152 different experimental test points were recorded in phase two – described in Figure 6.1 and Table 6.1 – and given this large volume of data (compared with say four test points evaluating the effect of the reference fuels), a new approach to the data analysis is needed. The fuel property data is in Table 3.14. The results from phase two are presented in Figure 6.4, it can be seen that observing any trends from this figure is impossible. The nomenclature adopted in labelling the results from each test point is: Test Condition (number) | Region (letter) | Spark / Injection timing (Roman numeral) for example Point 1Bvii corresponds to the results from 2000 rpm, max torque (Test Condition 1), at 10 % EGR (Region B), and 7 degrees spark retard from KLSA (Point vii).

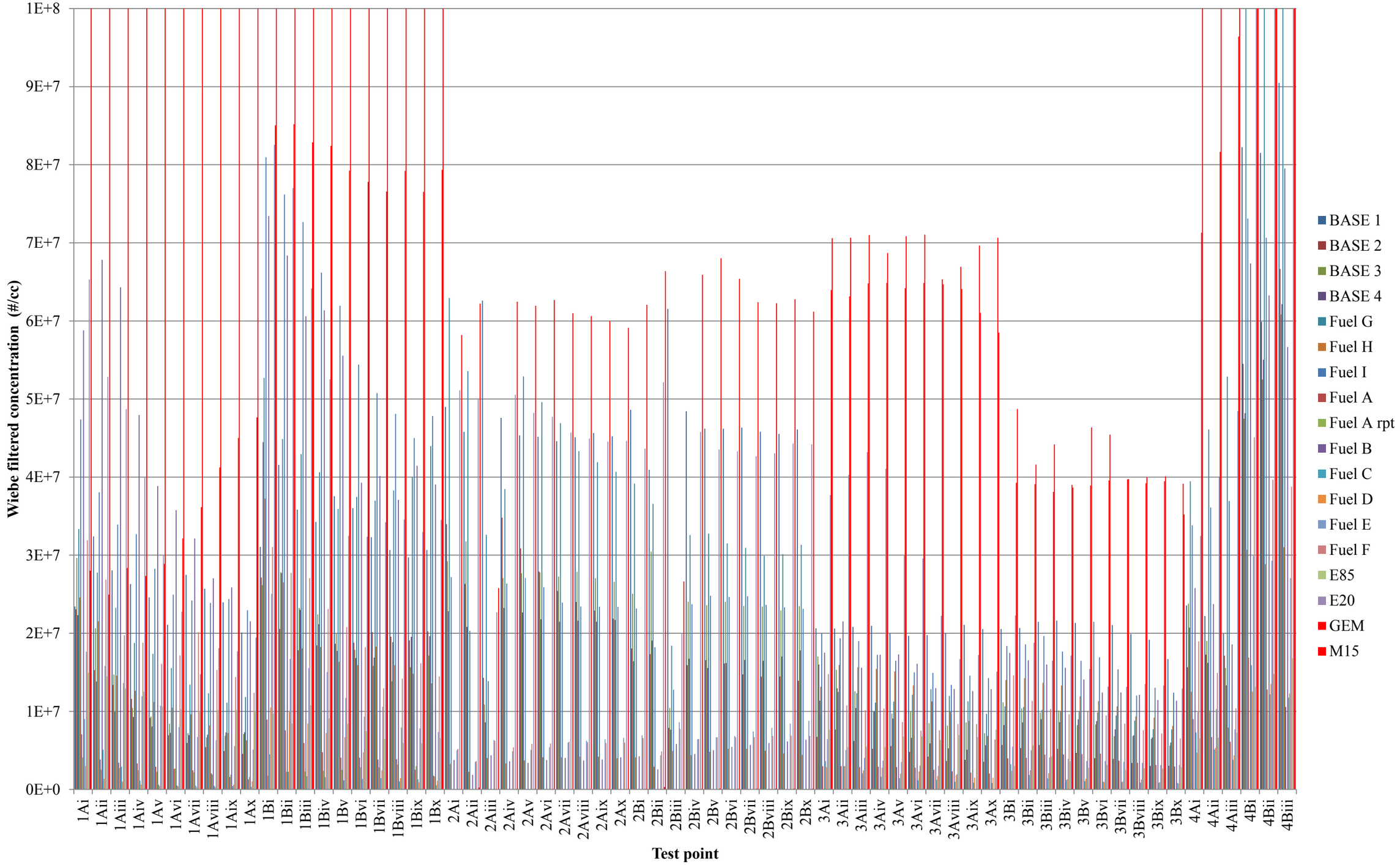

Figure 6.4: Bar chart showing particulate levels for all of the test points in phase two

As discussed in Section 2.5.6, there can be issues associated with poor lognormal fitting from the DMS, which can be compensated for by applying a Wiebe function to the results digitally. The model fuel results have been analysed using both the logfitting and the Wiebe filtered methods. The comparison between the two methods is shown in Figure 6.5, which is also shown rescaled as Figure 6.6. The results show that on the whole there is a good correlation between the two methods; with the results shown in Figure 6.6 all showing very similar levels of particulate emissions from the two analysis methods. By comparing Figure 6.5 and Figure 6.6 it can be seen that the main effect of using the Wiebe filtering analysis method rather than the logfitted data is to remove outliers with around 10-15 data points lying substantially outside the range of the other data. A comparison of the different size spectra for one of the typical outliers is shown in Figure 6.7, it can be seen that the Cambustion logfit is a very poor fit to the raw spectrum throughout the size distribution, whereas the Wiebe filtered data fits much better. For this reason the data analysis method used for the UB100 engine results is the Wiebe filtering approach.

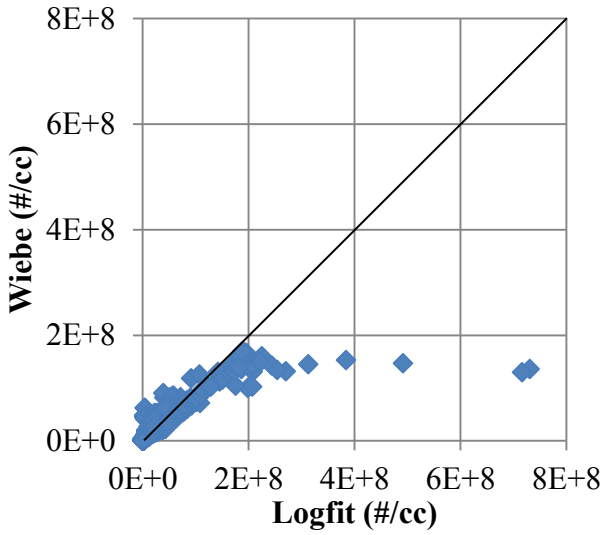

Figure 6.5: Comparison between Wiebe filtered and logfitted results from the UB100 engine. The presence of 10-15 outliers can clearly be seen

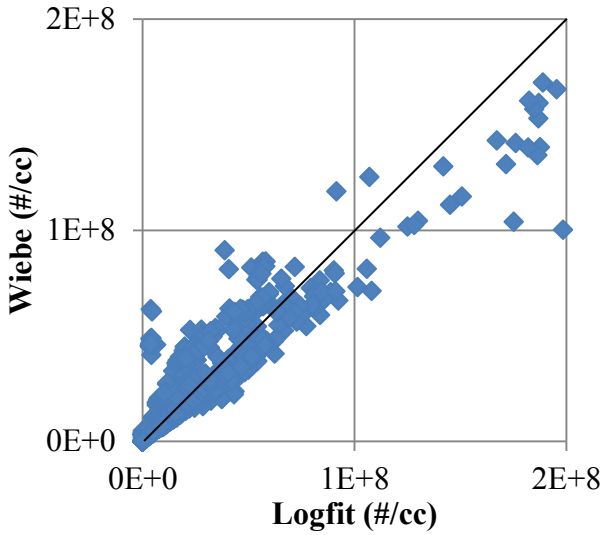

Figure 6.6: Figure 6.5 rescaled to show the majority of the data points. Good correlation can be seen between the two analysis methods

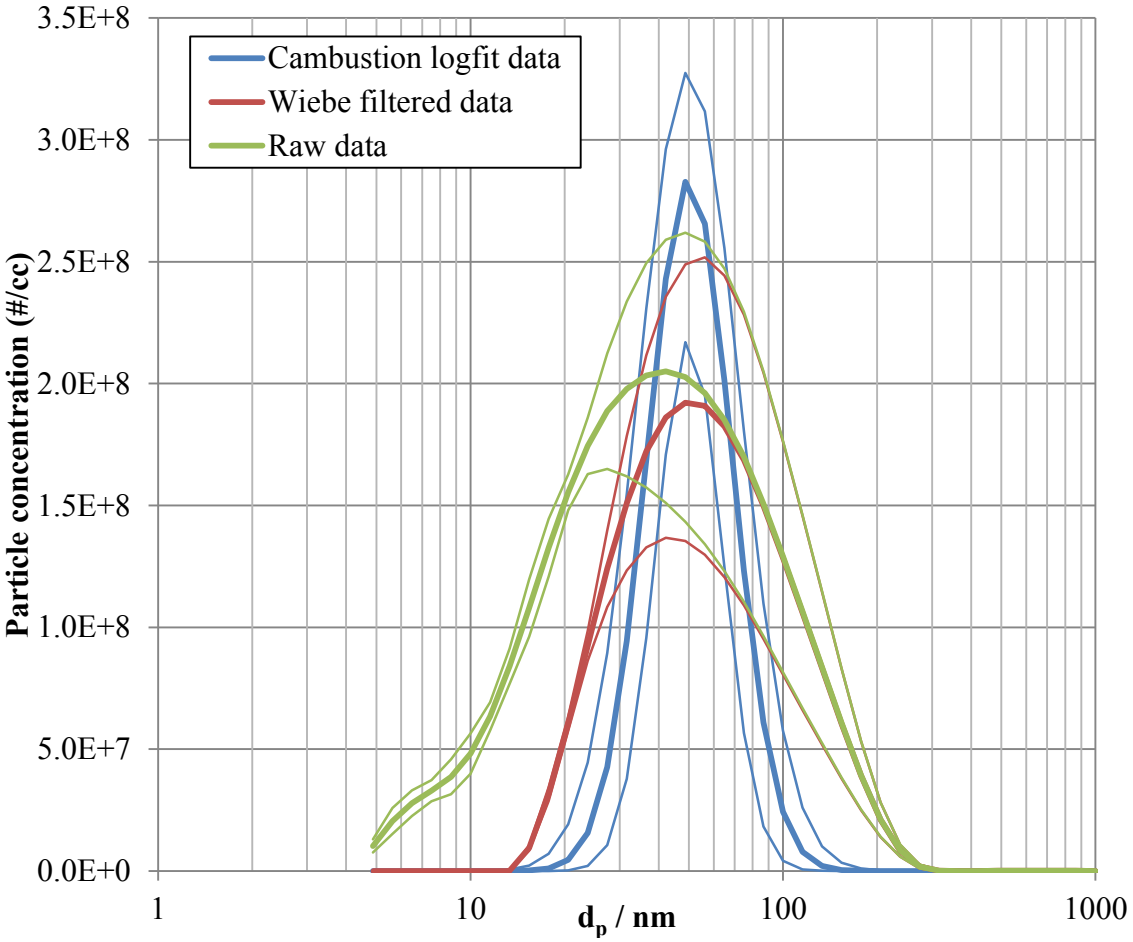

Figure 6.7: Comparison between raw DMS data size spectrum, Cambustion lognormal fit to that data, and a Wiebe filtered data size spectrum; the data bands (defined by the narrow lines) correspond to ± σ

The fuels were tested in the order shown in Table 6.2.

Table 6.2: Fuel test order for phase two UB100 engine tests

Test order	Fuel
1	BASE 1
2	G
3	H
4	I
Oil replaced and engine 'de-greened'	
5	BASE*
6	A
7	B
8	C
9	D
Oil replaced and engine 'de-greened'	
10	BASE 2
11	F
12	E
Oil replaced and engine 'de-greened'	
13	BASE 3
14	E85
15	E20
16	GEM
17	M15
18	BASE 4

* DMS data not taken at this data point due to equipment maintenance

After a set of fuels were tested, the engine oil was changed, and the engine 'de-greened'; the timings of these oil changes is shown in Table 6.2. This 'de-greening' procedure involved 5 hours of running-in the engine on the new oil at 2250 rpm and 120˚C oil temperature. The aim of this was to ensure that the test conditions at the start of each fuel were constant. The fuel change procedure in this case did not involve any line draining, but the fuel order was chosen such that the RONs of the fuels were different such that a step change in engine performance would be observed once the engine was running

on the new fuel, and engine was run for 15-20 minutes on the new fuel before any data was taken.

As can be seen from Table 6.2, the BASE fuel was tested five times (although data was only taken for four of those tests) spread through the test sequence. This was to measure the variability of the engine, and in an effort to obtain good repeatability of results. The particulates emitted by the BASE fuel on the four measured tests at selected test points (merely selected to be a representative set) can be seen in Figure 6.8. It can be seen in Figure 6.8 that there is excellent repeatability between the runs (although first run always sits higher than the other three, however its error is also much higher) with the particulate emissions from last three runs all showing very similar levels of particulates emitted. This shows that there are no 'drift' effects in the results (either the emissions or their measurement), such that the fuel-to-fuel comparisons are showing just that, rather than being influenced by some external factor.

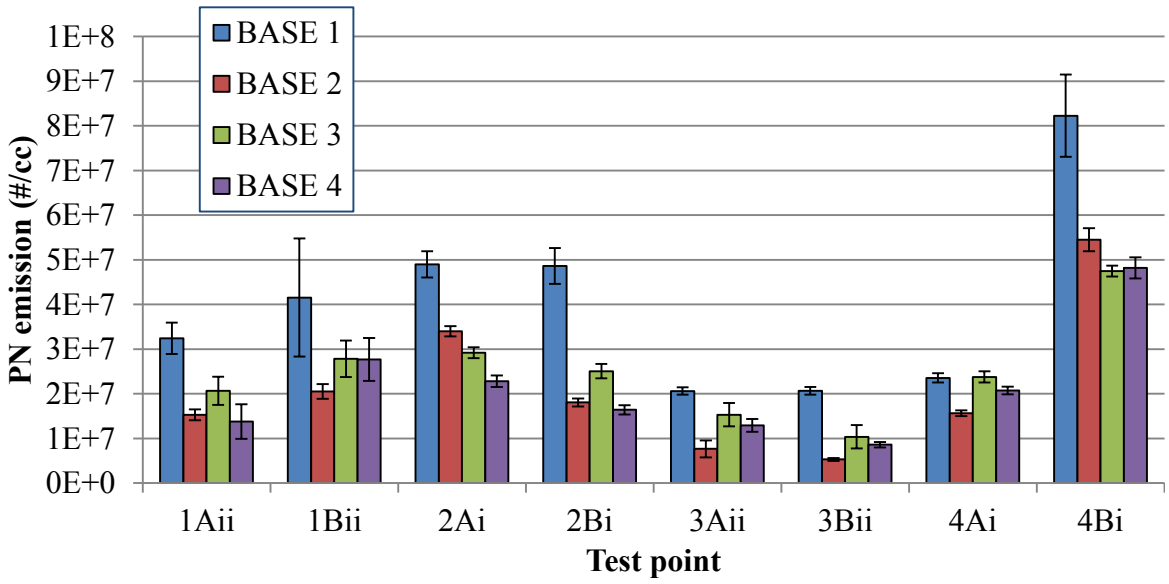

Figure 6.8: Selected test points showing the repeat of the BASE fuel, showing good repeatability across the phase two test program; the error bars correspond to ± σ

Given the large volume of data, the results from all of the test points have been represented using colour to aid analysis in the table of results. Figure 6.9 shows the emissions at each test point, with the points with the highest emissions coloured dark red, and the points with the lowest emissions coloured dark blue. The points with an average level of emissions have been left coloured white. From Figure 6.9 some clear trends can already be seen – for example Region 4B (where $\lambda = 0.875$), the particulate emissions can be seen to be a step higher than the rest of the test matrix for a given fuel; this agrees with previous results for which a rich mixture gives markedly more particulate emissions.

It can also be seen in Figure 6.9 that there is some apparently inconsistent behaviour from the oxygenate fuels, which needs further investigation. Figure 6.9 also shows that Test Condition 2 tends to give the lowest overall particulate emissions, which is to be expected given that this is the region with the lowest engine load and speed (59.7 Nm and 1250 rpm).

Region\Fuel	BASE	BASE 2	BASE 3	BASE 4	Fuel G	Fuel H	Fuel I	Fuel A	Fuel A r	Fuel B	Fuel C	Fuel D	Fuel E	Fuel F	E85	E20	GEM	M15
1Ai	2.E+07	2.E+07	3.E+07	2.E+07	3.E+07	2.E+07	5.E+07	7.E+06	4.E+06	6.E+07	9.E+06	3.E+06	2.E+07	3.E+07	1.E+07	7.E+07	3.E+07	1.E+08
1Aii	3.E+07	2.E+07	2.E+07	1.E+07	3.E+07	2.E+07	4.E+07	4.E+06	3.E+06	7.E+07	5.E+06	1.E+06	2.E+07	3.E+07	1.E+07	5.E+07	2.E+07	1.E+08
1Aiii	3.E+07	1.E+07	1.E+07	1.E+07	2.E+07	1.E+07	3.E+07	3.E+06	3.E+06	6.E+07	3.E+06	1.E+06	1.E+07	2.E+07	1.E+07	5.E+07	3.E+07	1.E+08
1Aiv	3.E+07	1.E+07	1.E+07	9.E+06	2.E+07	1.E+07	3.E+07	3.E+06	2.E+06	5.E+07	1.E+06	6.E+05	1.E+07	2.E+07	1.E+07	4.E+07	3.E+07	1.E+08
1Av	2.E+07	9.E+06	9.E+06	8.E+06	2.E+07	1.E+07	3.E+07	3.E+06	2.E+06	4.E+07	6.E+05	5.E+05	1.E+07	2.E+07	1.E+07	3.E+07	3.E+07	1.E+08
1Avi	2.E+07	7.E+06	8.E+06	7.E+06	2.E+07	1.E+07	2.E+07	3.E+06	3.E+06	4.E+07	5.E+05	4.E+05	8.E+06	2.E+07	1.E+07	2.E+07	3.E+07	1.E+08
1Avii	3.E+07	6.E+06	7.E+06	7.E+06	1.E+07	1.E+07	2.E+07	2.E+06	2.E+06	3.E+07	5.E+05	3.E+05	7.E+06	2.E+07	1.E+07	1.E+07	4.E+07	1.E+08
1Aviii	3.E+07	5.E+06	7.E+06	7.E+06	1.E+07	8.E+06	2.E+07	2.E+06	2.E+06	3.E+07	5.E+05	3.E+05	6.E+06	2.E+07	1.E+07	2.E+07	4.E+07	1.E+08
1Aix	2.E+07	5.E+06	7.E+06	7.E+06	1.E+07	7.E+06	2.E+07	2.E+06	2.E+06	3.E+07	4.E+05	6.E+05	6.E+06	1.E+07	1.E+07	2.E+07	5.E+07	1.E+08
1Ax	2.E+07	5.E+06	7.E+06	7.E+06	1.E+07	6.E+06	2.E+07	1.E+06	2.E+06	2.E+07	4.E+05	1.E+06	5.E+06	1.E+07	1.E+07	2.E+07	5.E+07	1.E+08
1Bi	3.E+07	3.E+07	3.E+07	4.E+07	5.E+07	4.E+07	8.E+07	9.E+06	2.E+06	7.E+07	5.E+06	1.E+07	3.E+07	3.E+07	1.E+07	8.E+07	9.E+07	1.E+08
1Bii	4.E+07	2.E+07	3.E+07	3.E+07	4.E+07	3.E+07	8.E+07	8.E+06	2.E+06	7.E+07	2.E+06	1.E+07	2.E+07	3.E+07	8.E+06	8.E+07	9.E+07	2.E+08
1Biii	4.E+07	2.E+07	2.E+07	2.E+07	4.E+07	2.E+07	7.E+07	6.E+06	2.E+06	6.E+07	2.E+06	8.E+06	2.E+07	3.E+07	1.E+07	6.E+07	8.E+07	2.E+08
1Biv	3.E+07	2.E+07	2.E+07	2.E+07	4.E+07	2.E+07	7.E+07	5.E+06	2.E+06	6.E+07	2.E+06	7.E+06	2.E+07	2.E+07	9.E+06	5.E+07	8.E+07	2.E+08
1Bv	4.E+07	2.E+07	2.E+07	2.E+07	4.E+07	2.E+07	6.E+07	4.E+06	2.E+06	6.E+07	1.E+06	7.E+06	1.E+07	2.E+07	8.E+06	3.E+07	8.E+07	2.E+08
1Bvi	4.E+07	2.E+07	2.E+07	2.E+07	4.E+07	2.E+07	5.E+07	4.E+06	3.E+06	4.E+07	1.E+06	5.E+06	9.E+06	2.E+07	7.E+06	3.E+07	8.E+07	1.E+08
1Bvii	3.E+07	2.E+07	2.E+07	2.E+07	4.E+07	2.E+07	5.E+07	4.E+06	3.E+06	4.E+07	1.E+06	2.E+06	1.E+07	1.E+07	6.E+06	3.E+07	8.E+07	2.E+08
1Bviii	3.E+07	2.E+07	1.E+07	2.E+07	4.E+07	2.E+07	5.E+07	4.E+06	3.E+06	4.E+07	1.E+06	1.E+06	8.E+06	1.E+07	6.E+06	3.E+07	8.E+07	2.E+08
1Bix	3.E+07	2.E+07	2.E+07	2.E+07	4.E+07	1.E+07	5.E+07	3.E+06	3.E+06	4.E+07	1.E+06	9.E+05	8.E+06	2.E+07	6.E+06	3.E+07	8.E+07	2.E+08
1Bx	3.E+07	2.E+07	2.E+07	2.E+07	4.E+07	1.E+07	5.E+07	2.E+06	2.E+06	4.E+07	5.E+05	1.E+06	7.E+06	1.E+07	7.E+06	3.E+07	8.E+07	2.E+08
2Ai	5.E+07	3.E+07	3.E+07	2.E+07	6.E+07	3.E+06	3.E+07	4.E+04	3.E+04	4.E+06	2.E+04	2.E+04	5.E+06	5.E+06	3.E+04	5.E+07	6.E+04	6.E+07
2Aii	5.E+07	3.E+07	3.E+07	2.E+07	5.E+07	2.E+06	2.E+07	4.E+04	2.E+04	2.E+06	2.E+04	3.E+04	4.E+06	4.E+06	3.E+04	5.E+07	3.E+05	6.E+07
2Aiii	6.E+07	1.E+07	1.E+07	9.E+06	3.E+07	4.E+06	1.E+07	3.E+04	2.E+04	4.E+06	2.E+04	3.E+04	6.E+06	6.E+06	2.E+04	2.E+07	2.E+04	3.E+07
2Aiv	5.E+07	3.E+07	3.E+07	2.E+07	4.E+07	3.E+06	3.E+07	3.E+04	2.E+04	4.E+06	2.E+04	3.E+04	5.E+06	5.E+06	2.E+04	5.E+07	7.E+04	6.E+07
2Av	5.E+07	3.E+07	3.E+07	2.E+07	5.E+07	4.E+06	3.E+07	3.E+04	2.E+04	3.E+06	1.E+04	3.E+04	5.E+06	6.E+06	3.E+04	5.E+07	6.E+04	6.E+07
2Avi	5.E+07	3.E+07	3.E+07	2.E+07	5.E+07	4.E+06	3.E+07	3.E+04	2.E+04	4.E+06	1.E+04	3.E+04	5.E+06	6.E+06	2.E+04	5.E+07	6.E+04	6.E+07
2Avii	4.E+07	3.E+07	3.E+07	2.E+07	5.E+07	4.E+06	2.E+07	3.E+04	2.E+04	4.E+06	2.E+04	3.E+04	6.E+06	6.E+06	2.E+04	5.E+07	7.E+04	6.E+07
2Aviii	5.E+07	2.E+07	3.E+07	2.E+07	4.E+07	4.E+06	2.E+07	3.E+04	2.E+04	4.E+06	2.E+04	3.E+04	6.E+06	6.E+06	3.E+04	4.E+07	6.E+04	6.E+07
2Aix	5.E+07	2.E+07	3.E+07	2.E+07	4.E+07	4.E+06	2.E+07	3.E+04	2.E+04	4.E+06	2.E+04	3.E+04	6.E+06	6.E+06	2.E+04	4.E+07	7.E+04	6.E+07
2Ax	5.E+07	2.E+07	3.E+07	2.E+07	4.E+07	4.E+06	2.E+07	3.E+04	3.E+04	4.E+06	2.E+04	3.E+04	7.E+06	6.E+06	3.E+04	4.E+07	7.E+04	6.E+07
2Bi	5.E+07	2.E+07	3.E+07	2.E+07	4.E+07	4.E+06	2.E+07	2.E+04		4.E+06	2.E+04	1.E+04	7.E+06	7.E+06	1.E+04	4.E+07	1.E+05	6.E+07
2Bii	4.E+07	2.E+07	3.E+07	2.E+07	4.E+07	3.E+06	2.E+07	2.E+04		3.E+06	3.E+04	1.E+04	4.E+06	5.E+06	3.E+04	5.E+07	3.E+05	7.E+07
2Biii	6.E+07	8.E+06	1.E+07	8.E+06	2.E+07	5.E+06	1.E+07	2.E+04		6.E+06	2.E+04	1.E+04	9.E+06	8.E+06	2.E+04	2.E+07	4.E+04	3.E+07
2Biv	5.E+07	2.E+07	2.E+07	2.E+07	3.E+07	4.E+06	2.E+07	2.E+04		5.E+06	3.E+04	1.E+04	6.E+06	6.E+06	2.E+04	5.E+07	9.E+04	7.E+07
2Bv	5.E+07	2.E+07	2.E+07	2.E+07	3.E+07	5.E+06	2.E+07	2.E+04		5.E+06	2.E+04	1.E+04	7.E+06	7.E+06	1.E+04	4.E+07	1.E+05	7.E+07
2Bvi	5.E+07	2.E+07	2.E+07	2.E+07	3.E+07	5.E+06	2.E+07	2.E+04		5.E+06	2.E+04	1.E+04	7.E+06	7.E+06	8.E+03	4.E+07	1.E+05	7.E+07
2Bvii	5.E+07	1.E+07	2.E+07	2.E+07	3.E+07	5.E+06	2.E+07	2.E+04		6.E+06	2.E+04	1.E+04	7.E+06	7.E+06	6.E+03	4.E+07	1.E+05	6.E+07
2Bviii	5.E+07	1.E+07	2.E+07	2.E+07	3.E+07	5.E+06	2.E+07	2.E+04		6.E+06	2.E+04	1.E+04	8.E+06	7.E+06	4.E+03	4.E+07	1.E+05	6.E+07
2Bix	5.E+07	1.E+07	2.E+07	2.E+07	3.E+07	5.E+06	2.E+07	2.E+04		6.E+06	3.E+04	2.E+04	8.E+06	7.E+06	3.E+04	4.E+07	1.E+05	6.E+07
2Bx	5.E+07	1.E+07	2.E+07	2.E+07	3.E+07	4.E+06	2.E+07	2.E+04		6.E+06	3.E+04	1.E+04	9.E+06	7.E+06	6.E+04	4.E+07	1.E+05	6.E+07
3Ai	2.E+07	7.E+06	2.E+07	2.E+07	1.E+07	1.E+07	2.E+07	3.E+06		2.E+07	4.E+06	3.E+06	6.E+06	1.E+07	8.E+06	4.E+07	6.E+07	7.E+07
3Aii	2.E+07	8.E+06	2.E+07	1.E+07	1.E+07	2.E+07	2.E+07	3.E+06		2.E+07	3.E+06	3.E+06	5.E+06	1.E+07	5.E+06	4.E+07	6.E+07	7.E+07
3Aiii	2.E+07	6.E+06	1.E+07	1.E+07	1.E+07	2.E+07	2.E+07	3.E+06		2.E+07	2.E+06	2.E+06	4.E+06	1.E+07	5.E+06	4.E+07	6.E+07	7.E+07
3Aiv	2.E+07	5.E+06	1.E+07	1.E+07	1.E+07	2.E+07	2.E+07	3.E+06		2.E+07	2.E+06	3.E+06	4.E+06	1.E+07	5.E+06	4.E+07	6.E+07	7.E+07
3Av	2.E+07	6.E+06	1.E+07	9.E+06	1.E+07	2.E+07	2.E+07	3.E+06		2.E+07	1.E+06	2.E+06	4.E+06	9.E+06	7.E+06	3.E+07	6.E+07	7.E+07
3Avi	2.E+07	5.E+06	1.E+07	7.E+06	1.E+07	1.E+07	1.E+07	3.E+06		2.E+07	1.E+06	2.E+06	3.E+06	8.E+06	7.E+06	3.E+07	6.E+07	7.E+07
3Avii	2.E+07	4.E+06	8.E+06	6.E+06	1.E+07	1.E+07	1.E+07	3.E+06		1.E+07	1.E+06	2.E+06	3.E+06	8.E+06	6.E+06	2.E+07	7.E+07	6.E+07
3Aviii	2.E+07	4.E+06	8.E+06	5.E+06	1.E+07	1.E+07	1.E+07	2.E+06		1.E+07	1.E+06	2.E+06	2.E+06	8.E+06	7.E+06	2.E+07	7.E+07	6.E+07
3Aix	2.E+07	4.E+06	9.E+06	5.E+06	1.E+07	9.E+06	1.E+07	2.E+06		1.E+07	9.E+05	2.E+06		8.E+06	7.E+06	2.E+07	7.E+07	6.E+07
3Ax	2.E+07	4.E+06	7.E+06	6.E+06	1.E+07	7.E+06	1.E+07	2.E+06		1.E+07	8.E+05	2.E+06		6.E+06	8.E+06	2.E+07	7.E+07	6.E+07
3Bi	2.E+07	6.E+06	1.E+07	8.E+06	1.E+07	1.E+07	2.E+07	4.E+06		2.E+07	3.E+06	2.E+06	5.E+06	1.E+07	3.E+06	2.E+07	4.E+07	5.E+07
3Bii	2.E+07	5.E+06	1.E+07	9.E+06	1.E+07	1.E+07	2.E+07	4.E+06		2.E+07	2.E+06	2.E+06	5.E+06	1.E+07	6.E+06	2.E+07	4.E+07	4.E+07
3Biii	2.E+07	6.E+06	1.E+07	9.E+06	1.E+07	1.E+07	2.E+07	4.E+06		2.E+07	1.E+06	2.E+06	4.E+06	1.E+07	4.E+06	2.E+07	4.E+07	4.E+07
3Biv	2.E+07	5.E+06	1.E+07	9.E+06	1.E+07	1.E+07	2.E+07	4.E+06		2.E+07	1.E+06	1.E+06	4.E+06	1.E+07	4.E+06	2.E+07	4.E+07	4.E+07
3Bv	2.E+07	5.E+06	8.E+06	9.E+06	1.E+07	1.E+07	2.E+07	5.E+06		1.E+07	1.E+06	1.E+06	4.E+06	1.E+07	3.E+06	2.E+07	4.E+07	5.E+07
3Bvi	2.E+07	4.E+06	8.E+06	9.E+06	1.E+07	1.E+07	2.E+07	5.E+06		1.E+07	1.E+06	1.E+06	4.E+06	9.E+06	3.E+06	1.E+07	4.E+07	5.E+07
3Bvii	2.E+07	4.E+06	7.E+06	8.E+06	9.E+06	1.E+07	2.E+07	4.E+06		1.E+07	1.E+06	1.E+06	4.E+06	8.E+06	3.E+06	1.E+07	4.E+07	4.E+07
3Bviii	2.E+07	3.E+06	7.E+06	7.E+06	9.E+06	9.E+06	1.E+07	3.E+06		1.E+07	9.E+05	1.E+06	3.E+06	8.E+06	3.E+06	1.E+07	4.E+07	4.E+07
3Bix	2.E+07	3.E+06	6.E+06	7.E+06	8.E+06	9.E+06	1.E+07	3.E+06		1.E+07	9.E+05	9.E+05	3.E+06	7.E+06	3.E+06	1.E+07	4.E+07	4.E+07
3Bx	2.E+07	3.E+06	6.E+06	6.E+06	8.E+06	8.E+06	1.E+07	3.E+06		1.E+07	8.E+05	8.E+05	3.E+06	7.E+06	3.E+06	1.E+07	4.E+07	4.E+07
4Ai	2.E+07	2.E+07	2.E+07	2.E+07	4.E+07	1.E+07	3.E+07	9.E+06		3.E+07	7.E+06	5.E+06	1.E+07	2.E+07	7.E+06	3.E+07	7.E+07	1.E+08
4Aii	2.E+07	2.E+07	2.E+07	2.E+07	5.E+07	1.E+07	4.E+07	7.E+06		2.E+07	5.E+06	5.E+06	1.E+07	1.E+07	7.E+06	4.E+07	8.E+07	1.E+08
4Aiii	2.E+07	2.E+07	2.E+07	1.E+07	5.E+07	8.E+06	4.E+07	6.E+06		2.E+07	4.E+06	4.E+06	8.E+06	1.E+07	7.E+06	5.E+07	1.E+08	1.E+08
4Bi	8.E+07	5.E+07	5.E+07	5.E+07	1.E+08	3.E+07	7.E+07	2.E+07		7.E+07	2.E+07	1.E+07	3.E+07	5.E+07	1.E+07	1.E+08	1.E+08	1.E+08
4Bii	8.E+07	6.E+07	5.E+07	6.E+07	1.E+08	3.E+07	7.E+07	1.E+07		6.E+07	1.E+07	1.E+07	3.E+07	4.E+07	1.E+07	1.E+08	1.E+08	1.E+08
4Biii	9.E+07	7.E+07	6.E+07	6.E+07	1.E+08	3.E+07	8.E+07	1.E+07		6.E+07	1.E+07	1.E+07	3.E+07	4.E+07	2.E+07	1.E+08	1.E+08	1.E+08

Figure 6.9: Overall particulate levels from the UB100 engine across all phase two test points; deep red test points emit the most particles, and deep blue emit the fewest, white test points emit the average level (black test points indicate no data is available). The units are (#/cc).

Region\Fuel	BASE	BASE 2	BASE 3	BASE 4	Fuel G	Fuel H	Fuel I	Fuel A	Fuel A r	Fuel B	Fuel C	Fuel D	Fuel E	Fuel F	E85	E20	GEM	M15
1Ai	0.11	0.10	0.20	0.13	0.07	0.15	0.24	0.16	1.03	0.08	0.20	0.28	0.08	0.10	0.08	0.06	0.07	0.14
1Aii	0.11	0.08	0.15	0.28	0.07	0.12	0.08	0.22	0.13	0.09	0.26	0.38	0.08	0.12	0.08	0.08	0.09	0.16
1Aiii	0.08	0.07	0.14	0.08	0.12	0.14	0.06	0.15	0.08	0.06	0.31	0.31	0.06	0.12	0.10	0.07	0.08	0.19
1Aiv	0.08	0.11	0.09	0.11	0.05	0.16	0.06	0.09	0.08	0.07	0.38	0.22	0.07	0.14	0.13	0.10	0.06	0.11
1Av	0.07	0.07	0.07	0.08	0.04	0.08	0.06	0.08	0.09	0.08	0.14	0.22	0.10	0.13	0.09	0.08	0.05	0.05
1Avi	0.13	0.12	0.06	0.09	0.08	0.06	0.04	0.11	0.07	0.07	0.14	0.29	0.22	0.26	0.10	0.10	0.07	0.06
1Avii	0.05	0.07	0.06	0.08	0.05	0.06	0.06	0.16	0.15	0.06	0.17	0.19	0.11	0.14	0.07	0.09	0.06	0.05
1Aviii	0.05	0.05	0.06	0.09	0.06	0.06	0.06	0.10	0.11	0.09	0.18	0.24	0.10	0.07	0.07	0.13	0.05	0.05
1Aix	0.07	0.07	0.08	0.08	0.05	0.07	0.06	0.13	0.07	0.05	0.19	0.66	0.08	0.08	0.08	0.06	0.05	0.05
1Ax	0.06	0.04	0.07	0.09	0.09	0.04	0.10	0.11	0.09	0.06	0.14	0.24	0.20	0.06	0.08	0.06	0.05	0.05
1Bi	0.16	0.08	0.25	0.13	0.07	0.13	0.08	0.25	0.17	0.15	0.43	0.29	0.13	0.10	0.09	0.07	0.05	0.26
1Bii	0.32	0.08	0.15	0.17	0.06	0.22	0.09	0.29	0.25	0.09	0.35	0.26	0.08	0.12	0.13	0.10	0.04	0.16
1Biii	0.24	0.07	0.09	0.11	0.04	0.07	0.12	0.20	0.14	0.10	0.19	0.25	0.09	0.09	0.14	0.15	0.04	0.21
1Biv	0.09	0.07	0.11	0.08	0.05	0.07	0.06	0.10	0.08	0.14	0.14	0.17	0.05	0.10	0.11	0.16	0.04	0.06
1Bv	0.11	0.05	0.06	0.08	0.04	0.05	0.06	0.11	0.12	0.15	0.15	0.18	0.15	0.08	0.11	0.06	0.05	0.08
1Bvi	0.07	0.06	0.06	0.06	0.05	0.06	0.05	0.09	0.10	0.09	0.20	0.46	0.06	0.10	0.10	0.06	0.05	0.08
1Bvii	0.07	0.08	0.06	0.08	0.05	0.05	0.06	0.10	0.07	0.12	0.29	0.38	0.12	0.10	0.10	0.12	0.04	0.07
1Bviii	0.05	0.06	0.06	0.10	0.06	0.05	0.04	0.09	0.12	0.04	0.26	0.16	0.07	0.12	0.09	0.06	0.03	0.04
1Bix	0.05	0.04	0.07	0.06	0.06	0.05	0.07	0.23	0.09	0.09	0.33	0.12	0.07	0.08	0.10	0.07	0.03	0.05
1Bx	0.09	0.05	0.08	0.07	0.08	0.07	0.06	0.11	0.12	0.06	0.17	0.74	0.06	0.05	0.09	0.08	0.03	0.07
2Ai	0.06	0.03	0.04	0.06	0.06	0.07	0.05	0.17	1.51	0.09	0.42	0.39	0.06	0.06	0.53	0.04	0.28	0.05
2Aii	0.30	0.06	0.05	0.07	0.10	0.11	0.11	0.16	0.51	0.14	0.39	0.37	0.07	0.06	0.49	0.05	0.18	0.09
2Aiii	0.10	0.10	0.09	0.08	0.41	0.06	0.10	0.14	0.55	0.08	0.36	0.42	0.05	0.05	0.60	0.12	0.32	0.16
2Aiv	0.12	0.06	0.22	0.06	0.49	0.06	0.08	0.13	1.06	0.15	0.42	0.56	0.05	0.04	0.60	0.05	0.24	0.05
2Av	0.04	0.05	0.06	0.07	0.06	0.07	0.06	0.25	0.39	0.10	0.34	0.53	0.06	0.06	2.34	0.03	0.42	0.03
2Avi	0.05	0.05	0.06	0.05	0.06	0.06	0.05	0.28	0.70	0.08	0.60	0.39	0.05	0.05	0.62	0.04	0.29	0.04
2Avii	0.05	0.05	0.05	0.05	0.05	0.08	0.06	0.18	0.52	0.09	0.68	0.36	0.05	0.05	0.63	0.04	0.31	0.04
2Aviii	0.05	0.05	0.05	0.05	0.06	0.06	0.05	0.18	0.62	0.08	0.35	0.51	0.07	0.06	0.50	0.04	0.30	0.04
2Aix	0.04	0.06	0.05	0.05	0.06	0.06	0.06	0.22	0.63	0.10	1.28	0.56	0.06	0.06	0.57	0.05	0.32	0.04
2Ax	0.05	0.06	0.04	0.06	0.06	0.06	0.07	0.18	2.02	0.07	0.80	0.35	0.06	0.05	0.61	0.04	0.25	0.05
2Bi	0.08	0.05	0.06	0.06	0.05	0.05	0.06	0.24	[redacted]	0.07	0.45	1.09	0.06	0.06	0.75	0.03	0.34	0.07
2Bii	0.18	0.07	0.05	0.09	0.06	0.12	0.09	1.08	[redacted]	0.08	0.52	0.69	0.06	0.08	0.60	0.05	0.16	0.06
2Biii	0.12	0.11	0.17	0.12	0.42	0.11	0.08	0.33	[redacted]	0.07	0.77	0.68	0.07	0.05	1.07	0.13	0.35	0.12
2Biv	0.11	0.24	0.05	0.06	0.17	0.08	0.09	0.36	[redacted]	0.05	0.88	0.63	0.05	0.05	0.66	0.06	0.22	0.06
2Bv	0.04	0.05	0.05	0.05	0.06	0.06	0.06	0.27	[redacted]	0.07	0.58	0.71	0.06	0.05	0.72	0.05	0.35	0.05
2Bvi	0.04	0.04	0.05	0.05	0.06	0.06	0.04	0.28	[redacted]	0.07	0.76	0.62	0.06	0.04	1.06	0.04	0.21	0.04
2Bvii	0.04	0.05	0.05	0.06	0.05	0.06	0.06	0.29	[redacted]	0.07	0.57	0.72	0.07	0.07	1.03	0.05	0.21	0.04
2Bviii	0.05	0.05	0.05	0.06	0.06	0.06	0.04	0.27	[redacted]	0.06	0.78	0.73	0.06	0.06	1.61	0.04	0.28	0.04
2Bix	0.05	0.05	0.05	0.06	0.05	0.06	0.04	0.29	[redacted]	0.06	0.59	1.77	0.06	0.06	0.88	0.04	0.26	0.05
2Bx	0.05	0.06	0.06	0.05	0.06	0.07	0.05	0.39	[redacted]	0.06	0.53	0.64	0.06	0.07	0.54	0.04	0.20	0.04
3Ai	0.05	0.07	0.15	0.22	0.05	0.32	0.15	0.13	[redacted]	0.12	0.36	0.23	0.13	0.24	0.18	0.06	0.03	0.09
3Aii	0.04	0.25	0.08	0.11	0.04	0.18	0.07	0.12	[redacted]	0.18	0.21	0.32	0.13	0.16	0.21	0.08	0.04	0.11
3Aiii	0.05	0.14	0.11	0.09	0.04	0.06	0.07	0.10	[redacted]	0.15	0.16	0.45	0.08	0.11	0.15	0.07	0.03	0.11
3Aiv	0.05	0.16	0.12	0.10	0.04	0.06	0.06	0.10	[redacted]	0.22	0.16	0.26	0.07	0.12	0.22	0.07	0.04	0.12
3Av	0.05	0.14	0.16	0.10	0.06	0.06	0.08	0.07	[redacted]	0.23	0.14	0.26	0.10	0.12	0.16	0.17	0.04	0.09
3Avi	0.04	0.12	0.16	0.17	0.06	0.07	0.06	0.06	[redacted]	0.14	0.11	0.25	0.20	0.11	0.10	0.07	0.03	0.08
3Avii	0.04	0.12	0.07	0.11	0.06	0.06	0.09	0.06	[redacted]	0.13	0.22	0.21	0.29	0.10	0.11	0.23	0.03	0.11
3Aviii	0.05	0.08	0.09	0.19	0.07	0.07	0.09	0.09	[redacted]	0.14	0.14	0.29	0.49	0.10	0.14	0.10	0.03	0.08
3Aix	0.05	0.09	0.10	0.16	0.07	0.05	0.12	0.11	[redacted]	0.10	0.19	0.22	[redacted]	0.12	0.09	0.11	0.04	0.09
3Ax	0.05	0.07	0.12	0.10	0.06	0.08	0.19	0.08	[redacted]	0.08	0.19	0.22	[redacted]	0.13	0.08	0.10	0.04	0.07
3Bi	0.04	0.13	0.07	0.08	0.06	0.06	0.08	0.08	[redacted]	0.05	0.64	0.20	0.07	0.11	0.13	0.07	0.05	0.05
3Bii	0.04	0.06	0.12	0.07	0.06	0.05	0.08	0.10	[redacted]	0.08	0.20	0.28	0.07	0.11	0.15	0.10	0.04	0.09
3Biii	0.05	0.09	0.09	0.06	0.04	0.05	0.05	0.09	[redacted]	0.09	0.19	0.45	0.07	0.09	0.14	0.06	0.04	0.09
3Biv	0.07	0.05	0.11	0.06	0.04	0.05	0.10	0.07	[redacted]	0.07	0.14	0.45	0.08	0.10	0.11	0.07	0.03	0.09
3Bv	0.05	0.10	0.07	0.05	0.05	0.05	0.07	0.11	[redacted]	0.08	0.13	0.28	0.07	0.11	0.10	0.07	0.04	0.07
3Bvi	0.05	0.07	0.11	0.05	0.05	0.04	0.05	0.12	[redacted]	0.06	0.11	0.17	0.07	0.09	0.15	0.08	0.03	0.14
3Bvii	0.04	0.09	0.05	0.07	0.06	0.05	0.11	0.08	[redacted]	0.05	0.11	0.17	0.07	0.12	0.09	0.06	0.03	0.12
3Bviii	0.05	0.07	0.05	0.07	0.09	0.06	0.10	0.10	[redacted]	0.05	0.14	0.17	0.07	0.09	0.14	0.09	0.03	0.09
3Bix	0.05	0.06	0.08	0.06	0.07	0.04	0.12	0.07	[redacted]	0.04	0.15	0.21	0.06	0.10	0.14	0.10	0.03	0.14
3Bx	0.06	0.07	0.06	0.07	0.04	0.07	0.12	0.08	[redacted]	0.04	0.13	0.17	0.07	0.11	0.14	0.09	0.04	0.07
4Ai	0.04	0.04	0.05	0.04	0.08	0.07	0.07	0.12	[redacted]	0.07	0.13	0.16	0.12	0.06	0.11	0.08	0.04	0.06
4Aii	0.05	0.07	0.07	0.11	0.09	0.10	0.08	0.13	[redacted]	0.07	0.19	0.18	0.14	0.09	0.13	0.09	0.05	0.05
4Aiii	0.10	0.06	0.10	0.11	0.07	0.09	0.07	0.13	[redacted]	0.13	0.23	0.16	0.11	0.10	0.12	0.07	0.06	0.19
4Bi	0.11	0.05	0.05	0.05	0.06	0.08	0.06	0.07	[redacted]	0.08	0.14	0.16	0.07	0.05	0.11	0.05	0.07	0.06
4Bii	0.14	0.05	0.06	0.07	0.07	0.08	0.05	0.08	[redacted]	0.07	0.08	0.09	0.08	0.13	0.12	0.07	0.06	0.07
4Biii	0.12	0.04	0.06	0.07	0.05	0.10	0.09	0.07	[redacted]	0.08	0.08	0.08	0.10	0.12	0.11	0.12	0.08	0.09

Figure 6.10: CoV of Particulate emissions from the UB100 engine across all phase two test points; a red cell indicates a CoV of > 20 %

Figure 6.9 shows that different fuels behave differently in different regions, suggesting that a global PN index for all operating conditions for this engine – given its wide operating envelope - is unlikely to hold, however it may be possible to identify fuel parameters that are important in different regions. The PN index can also be evaluated at Test Condition 2, which would be expected to match the operation of un-boosted GDI engines at light load.

Figure 6.10 shows the CoV of particulate emissions across all test points. The cells coloured red highlight those with a CoV $> 20\,\%$. It is useful to compare Figure 6.10 directly with Figure 6.9 showing the particulate emissions levels across all test points. It can be seen that in nearly all cases, those where the CoV of particulates is high correspond to a test point with low overall levels of particulates. This shows that the particulate emissions from the UB100 are consistent, with little natural variability, good repeatability, and that the incidences where the CoV is high are due to the SNR of the DMS decreasing.

6.1.3. Inlet air temperature, exhaust back pressure, EGR, and lambda

The effect of inlet air temperature, exhaust back pressure, EGR, and lambda on particulate emissions has been tested. Given the large number of data points, it was decided to analyse this data by making a hypothesis about the effect of a given parameter on the PN emissions, and to use the data set to test those hypotheses. The hypotheses for each parameter are shown in Table 6.3; these parameters correspond to Regions 'A' and 'B' in Table 6.1.

The results of the testing of these hypotheses are shown in Figure 6.11. In Figure 6.11 strong agreement with the hypothesis is indicated by a deep blue colour, and strong disagreement by a deep red colour. Particle levels that do not change, or are within one standard deviation, when the relevant parameter is varied are shown in white. Pale

blue/red indicates a weak agreement/disagreement with the hypothesis. The numbers in each cell correspond to the percentage increase or decrease at each point.

Table 6.3: Hypotheses for some of the engine parameters varied in the phase 2 experiments

Test Condition	Variable	Hypothesis	Comment
1	EGR	EGR ↑ Particulates ↑	An increase in EGR will increase PN emissions (0-10 % 'Dry' EGR increase), this is a well-documented effect (see Section 1.2.3)
2	Inlet air temperature	T ↑ Particulates ↓	An increase in inlet air temperature will result in improved mixture preparation and so decrease PN emissions (Inlet air temperature increased 20-40°C)
3	Exhaust back pressure	Back pressure ↑ Particulates ↓	An increase in exhaust back pressure increases the residuals, which increases the mixture temperature, this improves mixture homogeneity and leads to a decrease in PN emissions (Exhaust back pressure increased 1.7-2.2 bar abs)
4	λ (AFR)	λ ↓ Particulates ↑	A decrease in λ leads to an increase in PN emissions (λ = 1.0 - λ = 0.875), this is a well-documented effect (see Section 1.2.3)

Region\Fuel	Expected trend (A to B)	BASE	BASE2	BASE3	BASE4	Fuel G	Fuel H	Fuel I	Fuel A	Fuel B	Fuel C	Fuel D	Fuel E	Fuel F	E85	E20	GEM	M15
1i	Increase (more EGR)	25%	15%	0%	50%	37%	34%	41%	0%	20%	-101%	71%	30%	0%	-54%	21%	67%	0%
1ii	Increase (more EGR)	0%	26%	26%	50%	38%	0%	50%	49%	0%	-124%	86%	0%	0%	-72%	31%	71%	0%
1iii	Increase (more EGR)	0%	25%	37%	57%	46%	19%	53%	42%	0%	-73%	88%	12%	27%	-20%	24%	66%	0%
1iv	Increase (more EGR)	23%	37%	53%	56%	54%	31%	51%	30%	22%	0%	92%	20%	19%	-37%	24%	67%	15%
1v	Increase (more EGR)	34%	51%	53%	55%	52%	31%	54%	29%	30%	48%	93%	0%	22%	-26%	8%	64%	18%
1vi	Increase (more EGR)	41%	63%	53%	57%	59%	34%	54%	35%	9%	61%	91%	0%	0%	-38%	30%	59%	18%
1vii	Increase (more EGR)	15%	70%	55%	59%	64%	47%	52%	36%	20%	66%	87%	37%	-55%	-55%	57%	53%	27%
1viii	Increase (more EGR)	16%	72%	52%	63%	68%	48%	50%	47%	27%	55%	80%	21%	0%	-71%	48%	48%	34%
1ix	Increase (more EGR)	19%	74%	56%	63%	72%	51%	46%	37%	38%	67%	0%	29%	11%	-72%	46%	41%	37%
1x	Increase (more EGR)	34%	77%	59%	63%	73%	54%	52%	26%	45%	31%	0%	31%	14%	-53%	44%	40%	40%
2i	Decrease (higher inlet air)	0%	47%	14%	28%	38%	-25%	15%	48%	-13%	0%	0%	-38%	-27%	0%	15%	-62%	0%
2ii	Decrease (higher inlet air)	0%	34%	0%	0%	32%	-29%	0%	0%	-37%	0%	63%	-24%	-34%	0%	0%	-23%	0%
2iii	Decrease (higher inlet air)	0%	45%	0%	11%	43%	-22%	0%	33%	-33%	0%	65%	-36%	-25%	0%	12%	-71%	0%
2iv	Decrease (higher inlet air)	0%	54%	0%	28%	0%	-32%	10%	30%	-26%	0%	59%	-32%	-20%	0%	9%	0%	0%
2v	Decrease (higher inlet air)	0%	46%	15%	31%	38%	-30%	8%	32%	-48%	0%	62%	-33%	-15%	0%	10%	-56%	-10%
2vi	Decrease (higher inlet air)	0%	42%	14%	26%	36%	-26%	5%	43%	-45%	0%	59%	-26%	-14%	64%	9%	-55%	0%
2vii	Decrease (higher inlet air)	0%	42%	14%	23%	34%	-25%	0%	26%	-42%	0%	55%	-24%	-10%	73%	7%	-53%	0%
2viii	Decrease (higher inlet air)	0%	40%	16%	24%	31%	-18%	0%	33%	-60%	0%	63%	-27%	-13%	86%	0%	-80%	0%
2ix	Decrease (higher inlet air)	0%	37%	15%	21%	28%	-10%	0%	30%	-61%	0%	0%	-31%	-16%	0%	0%	-73%	0%
2x	Decrease (higher inlet air)	0%	36%	12%	18%	23%	-11%	0%	0%	-55%	0%	57%	-33%	-14%	-127%	0%	-65%	0%
3i	Decrease (more residuals)	0%	16%	35%	48%	7%	0%	0%	-34%	0%	0%	0%	15%	0%	60%	41%	39%	31%
3ii	Decrease (more residuals)	0%	31%	32%	34%	15%	0%	0%	-35%	23%	38%	0%	0%	0%	0%	53%	38%	41%
3iii	Decrease (more residuals)	0%	0%	22%	14%	17%	13%	0%	-55%	0%	32%	0%	0%	0%	23%	62%	41%	38%
3iv	Decrease (more residuals)	0%	0%	0%	14%	9%	14%	0%	-53%	0%	26%	53%	0%	0%	34%	58%	40%	44%
3v	Decrease (more residuals)	-7%	16%	0%	0%	11%	21%	0%	-58%	0%	26%	32%	0%	-16%	59%	49%	39%	35%
3vi	Decrease (more residuals)	-9%	16%	17%	-32%	19%	15%	-13%	-64%	23%	16%	58%	0%	-26%	54%	55%	39%	36%
3vii	Decrease (more residuals)	-6%	0%	19%	-30%	26%	6%	0%	-46%	0%	0%	41%	0%	0%	60%	41%	39%	39%
3viii	Decrease (more residuals)	0%	0%	16%	-32%	26%	0%	10%	-47%	0%	0%	30%	-73%	0%	61%	19%	41%	38%
3ix	Decrease (more residuals)	9%	20%	25%	-31%	32%	0%	0%	-45%	0%	0%	38%	[redacted]	14%	60%	23%	43%	34%
3x	Decrease (more residuals)	19%	15%	22%	0%	21%	-19%	0%	-45%	12%	0%	50%	[redacted]	0%	63%	14%	45%	40%
4i	Increase (richer)	71%	71%	50%	57%	67%	59%	54%	47%	62%	54%	62%	67%	58%	50%	75%	29%	-8%
4ii	Increase (richer)	73%	71%	64%	71%	63%	65%	49%	47%	62%	58%	61%	65%	62%	55%	69%	20%	0%
4iii	Increase (richer)	78%	74%	74%	79%	63%	74%	54%	42%	67%	68%	64%	72%	73%	57%	63%	0%	0%
		Follows expected trend																
		Within error																
		Opposes expected trend																

Figure 6.11: Evaluation of how well particulate emissions hypotheses are followed from 'A' to 'B' for each test point – deep blue indicates strong agreement, and deep red strong disagreement the numbers in the cells correspond to a percentage increase or decrease in particulate emissions. Fuel properties are shown in Table 3.14

Each point on Figure 6.11 can be investigated further by looking at the graph of the PN emissions for the relevant fuel at the relevant test point. Some charts of interest are shown below in Figure 6.12 and Figure 6.13, these show the emissions from E85 at Test Condition 2 and from the BASE fuel at Test Condition 4.

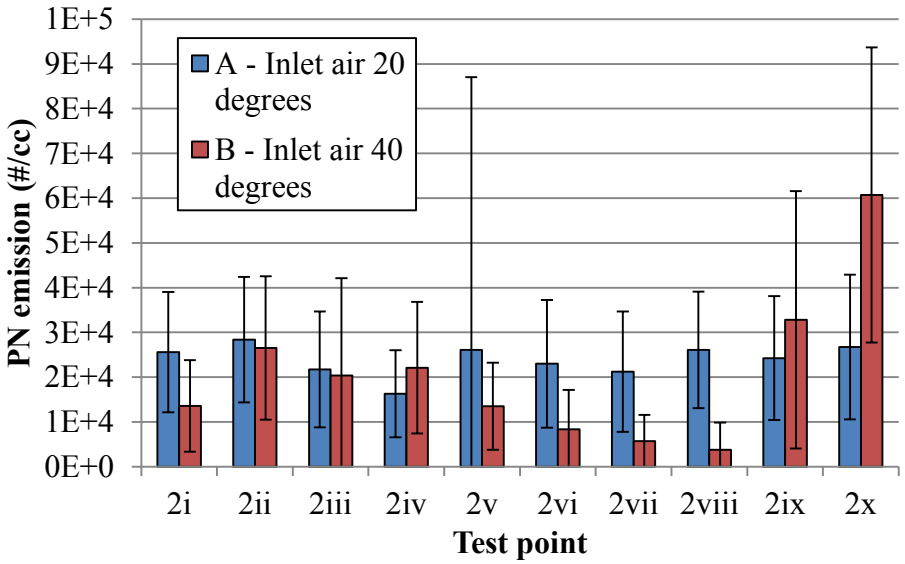

Figure 6.12: PN emissions from E85 at Test Condition 2, varying agreement and disagreement with the hypothesis that PN should decrease as the inlet air temperature is increased can be seen; the error bars correspond to ± σ

Figure 6.12 shows the PN emissions from E85 at Test Condition 2. Figure 6.12 is able to show more detail than Figure 6.11 can, but ultimately shows the same result. Points 2i-v show that the effect of inlet air temperature has no effect on the PN emissions, however it can also be seen that the overall PN emissions are very low (also shown in Figure 6.9) and that the standard deviation of the PN emissions is also high, particularly at Point 2Av, suggesting that perhaps any effect is too small to measure. However at Points 2vi-viii it can be seen clearly that the hypothesis is met, with an increase in inlet air temperature leading to a fall in the PN emissions. The trend then swings the other way, with Point 2x showing a trend against the hypothesis, however the standard deviations at Point 2x are also high, suggesting that this result is not indicative of overall trends.

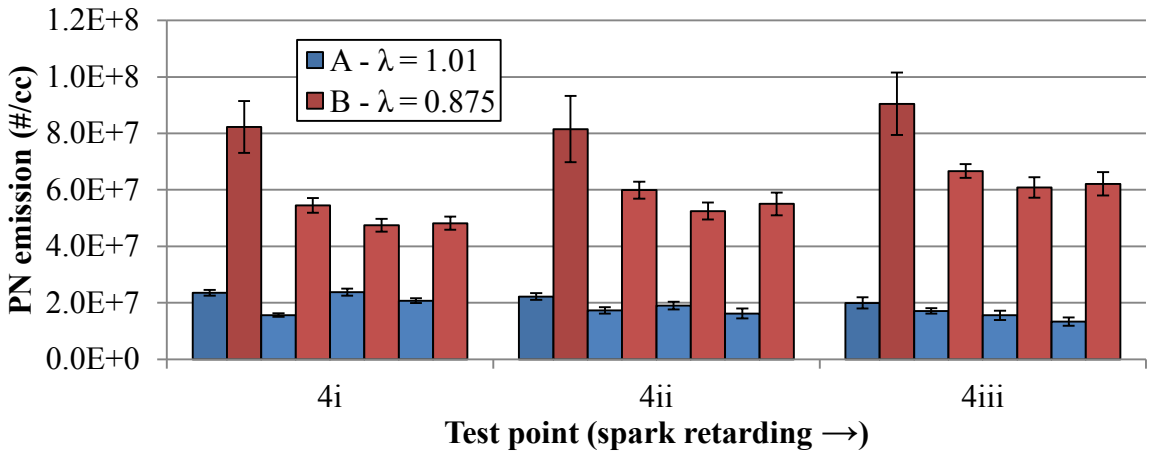

Figure 6.13: PN emissions from four BASE fuel repeats at Test Condition 4, strong agreement with the hypothesis that PN should increase as the mixture becomes rich can be seen; the error bars correspond to ± σ

Figure 6.13 shows the PN emissions for the BASE fuel at Test Condition 4. Figure 6.13 verifies what can be seen in Figure 6.11, showing clear agreement with the hypothesis that as lambda changes from stoichiometric to rich ($\lambda = 1.01$ to $\lambda = 0.875$) the particulate emissions increase drastically. It can also be seen in Figure 6.13 that the overall levels of particulates are high (up to four orders of magnitude higher than the results shown by E85 in Figure 6.12), which can also be seen in Figure 6.9, and that the relative error levels are low, with the exception of the first BASE fuel tested (this is a trend throughout this fuel's test, and is discussed earlier in this chapter). It can also be seen that that the four repeats give very similar PN levels.

Reviewing the trends shown in Figure 6.11 overall gives a reassuring set of results. It is best to divide Figure 6.11 into three sectors (based on columns), the first, from BASE to Fuel I represents fuels available in the market commercially today, and is the most important (although care must be taken with Fuel G, as discussed in Section 3.4.2). The second, Fuel A to Fuel F, represents fuels blended specially to test specific parameters,

their composition does not reflect those of market fuels. The third group, E85 to M15 is oxygenate fuels.

Focussing on the first sector, the only fuel that does not follow the trend expected by the hypothesis is Fuel H (see Table 3.14) at Test Condition 2. The chart of the PN emissions from Fuel H at Test Condition 2 is shown in Figure 6.14. It can be seen from Figure 6.14 that the trend is clear and repeatable, with each of the 10 test points at Test Condition 2 showing the same result, that as the inlet air temperature is increased, the particulate levels increase. It can also be seen from this figure that the standard deviation of the results is small, and the overall particle levels are approximately in the middle of the range experienced throughout all of the experiments. The results have been checked to ensure that this is due to the effect of the inlet air temperature – for example there is no great change in other emissions, or an accidental change in load. Whilst the reason for this trend is not clear, Fuel H has a low RON (the minimum for EN228 compliance) and a high T90 (the highest of all the fuels tested) so it is possible that given the high T90, increasing the inlet air temperature does not greatly assist the evaporation of the fuel, and another factor is causing this increase in particulates.

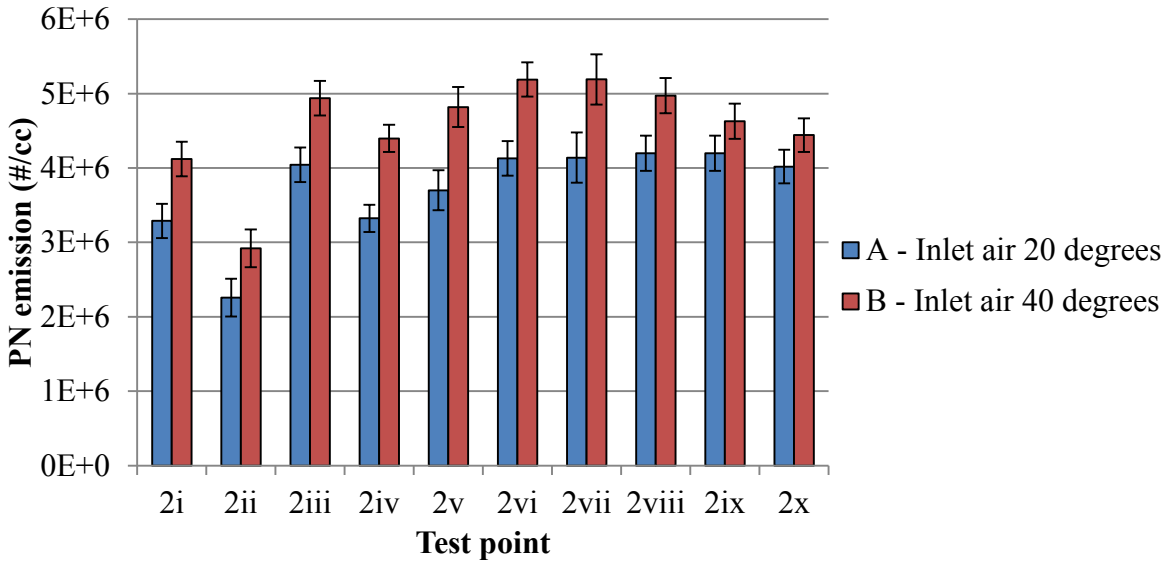

Figure 6.14: PN emissions from Fuel H at Test Condition 2, a strong disagreement with the hypothesis that PN should decrease as the inlet air temperature is increased can be seen; the error bars correspond to ± σ

In the second sector, these fuels (Fuels A-F) – see Table 3.14 - have not been blended to represent commercial gasolines; rather they have been blended to test certain fuel properties (either a deconvolved RON/MON test or a Laminar Burning Velocity test); their precise composition is unknown. Their distillation curves do not resemble standard market fuels, and in particular their vapour pressures are very low; so their performance in-cylinder may be expected to be non-standard as well, and hence their PN emissions. At Test Condition 2, fuels B, E, and F do not follow the trend predicted by the hypothesis. Given that their evaporative performance will not be the same as commercial gasolines, there may be non-uniformity in the in-cylinder distribution of a particular component such as the aromatics, which are causing these unexpected results. In Test Condition 3, Fuel A does not follow the trend predicted by the hypothesis. Again Fuel A is not a market fuel, and its precise composition is unknown; however from the available information (shown in Section 3.4.2), it can be seen that it has a low vapour pressure, a low T90, and contains 15 % MTBE (an oxygenate compound). Given that Fuels A and B are the only fuels to

contain MTBE, and Fuel B's results are on the whole within the error at Test Condition 3, it is possible that the MTBE is having an effect that is causing the unexpected behaviour, although it is impossible to confirm that without further investigation.

In the third sector, there are two fuels/regions that stand out in Figure 6.11 as not following the expected trend; E85 at Test Condition 1, and GEM at Test Condition 2. Figure 6.15 shows the PN emissions from the GEM fuel at Test Condition 2; it can be seen that there is a rise in the particulate levels as the inlet air temperature is raised. However, it can also be seen in Figure 6.15 that the overall levels of particulates are low, and the standard deviation is also high, so while the trend here is present, it is by no means a strong trend.

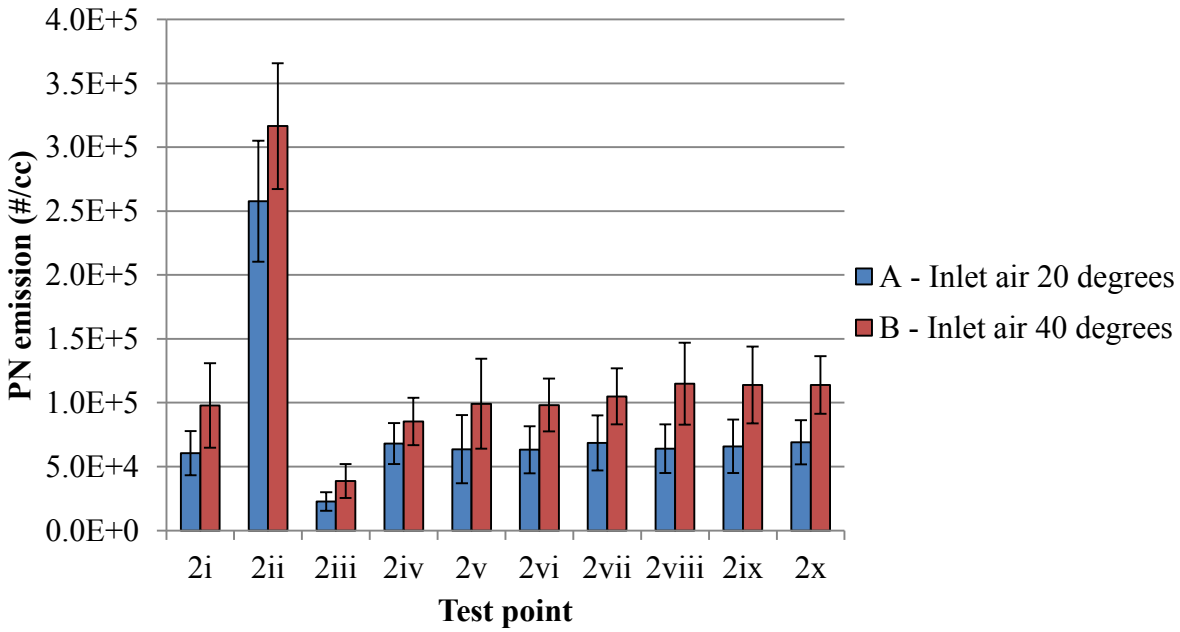

Figure 6.15: PN emissions from GEM fuel at Test Condition 2, a disagreement with the hypothesis that PN should decrease as the inlet air temperature is increased can be seen; the error bars correspond to ± σ

Figure 6.16 shows that contrary to the expected trend, when E85 is used, the PN emissions reduce with the addition of 10 % EGR. E85 has the highest oxygenate content of any of the fuels tested, and has a low vapour pressure.

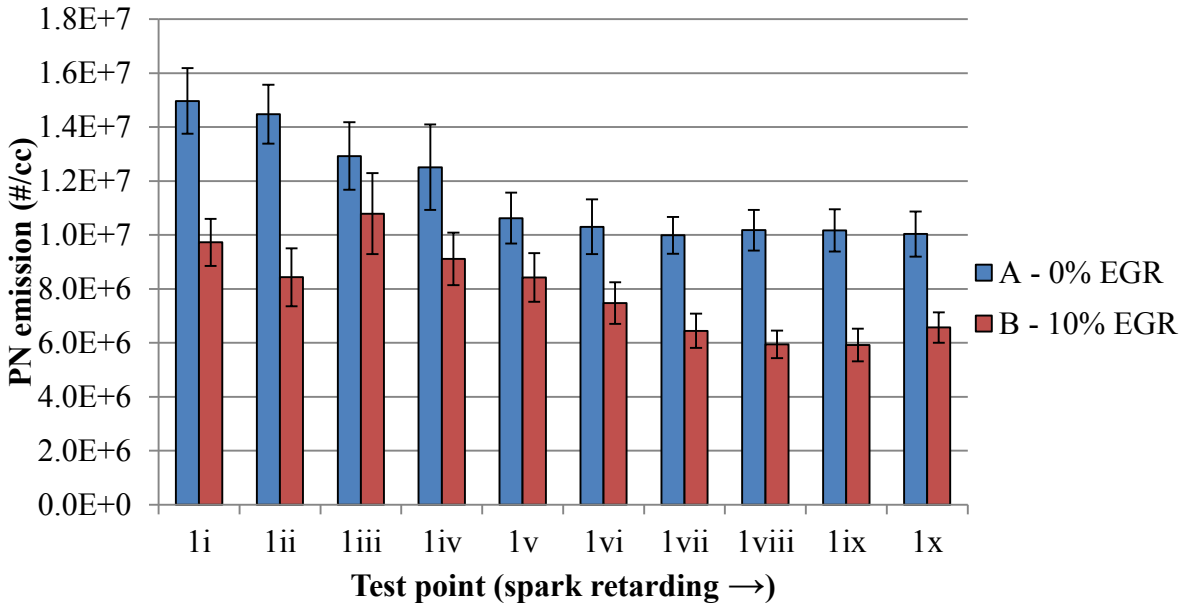

Figure 6.16: PN emissions from E85 fuel at Test Condition 1, a strong disagreement with the hypothesis that PN should increase as EGR is increased from 0-10 % can be seen; the error bars correspond to ± σ

6.1.4. Effect of ignition and injection timing

As noted in Chapter 1, retarding the spark (ignition) timing from MBT or KLSA should decrease particulate emissions both because the load reduces when this is done and because retarding the ignition timing will increase the exhaust temperature, which will promote post flame oxidation of particulates.

This theory has been tested at each of the test conditions in the UB100 test matrix which had 10, 8, 10, and 3 different spark timings (respectively). Figure 6.17 shows whether a fuel followed that trend, with green areas indicating agreement, red disagreement, yellow that the result is within one standard deviation, and purple that the particulate emissions trended first one way and then the other (either an increase then a decrease, or vice versa).

Region\Fuel	Expected trend	BASE	BASE 2	BASE 3	BASE4	Fuel G	Fuel H	Fuel I	Fuel A	Fuel B	Fuel C	Fuel D	Fuel E	Fuel F	E85	E20	GEM	M15
1A	Decrease (spark retard)																	
1B	Decrease (spark retard)																	
2A	Decrease (spark retard)																	
2B	Decrease (spark retard)																	
3A	Decrease (spark retard)																	
3B	Decrease (spark retard)																	
4A	Decrease (spark retard)																	
4B	Decrease (spark retard)																	
		Follows expected trend																
		Within error																
		Opposes expected trend																
		Trends one way then the other																

Figure 6.17: Evaluation of how well particulate emissions hypotheses are followed for changes in ignition timing for each test point – green indicates agreement, and red disagreement, yellow to within the error, and purple to trends first in agreement, then to disagreement (or *vice versa*)

Region\Fuel	Expected trend	BASE	BASE 2	BASE 3	BASE4	Fuel G	Fuel H	Fuel I	Fuel A	Fuel B	Fuel C	Fuel D	Fuel E	Fuel F	E85	E20	GEM	M15
2Ai-iii	Decrease (less likely piston wetting)																	
2Bi-iii	Decrease (less likely piston wetting)																	

Figure 6.18: Evaluation of how well particulate emissions hypotheses are followed for changes in injection timing for each test point – green indicates agreement, and red disagreement, yellow to within the error, and purple to trends first in agreement, then to disagreement

It can be seen in Figure 6.17 that for the majority of the fuels tested the particulate emissions agree with this hypothesis (or the results fall within one standard deviation and it is impossible to tell). Again it is useful to analyse Figure 6.17 by dividing the results into three sectors as before, BASE – Fuel I (market fuels), Fuel A – Fuel F (specially blended fuels), and E85 – M15 (oxygenate fuels). In the first sector, the stand out area of disagreement is in Region 4B. The results for the BASE fuel at Test Condition 4 are shown in Figure 6.19; it can be seen that in Region B the particulate emissions increase as the spark is retarded. Given how rich the engine is operating ($\lambda = 0.875$) the quantity of unburned fuel in the exhaust will be very high, and it is likely that retarding the spark will preferentially promote oxidation of this fuel, rather than the existing particulates. This might lead to an increase in particulate emissions as the unburned fuel oxidises, rather than the predicted decrease. Given this trend is followed (with three exceptions) throughout Region 4B, this result is conclusive and an interesting difference to that which was expected.

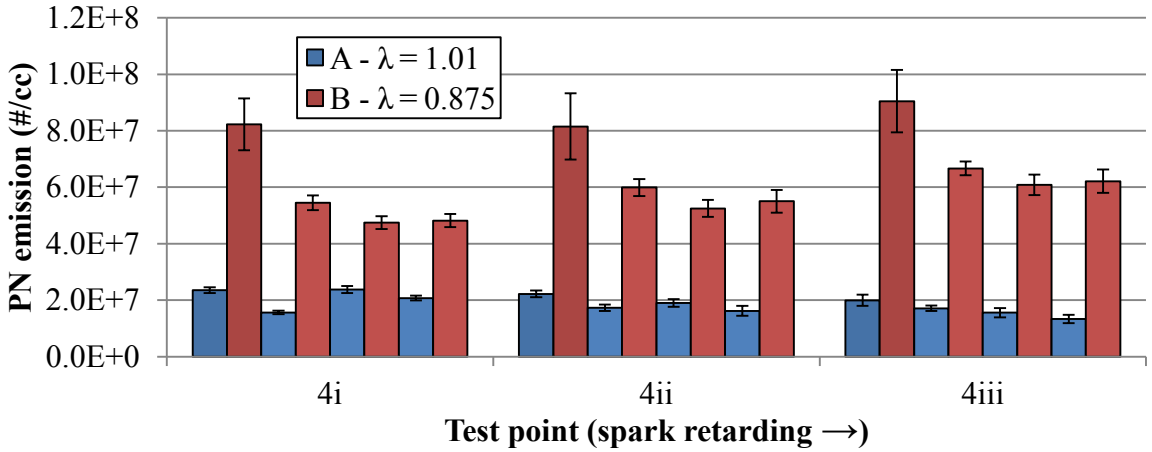

Figure 6.19: Repeat of Figure 6.13; PN emissions from four BASE fuel repeats at Test Condition 4, it can be seen that as the spark is retarded i-iii, the PN emissions increase in Region B, contradicting the hypothesis; the error bars correspond to ± σ

Figure 6.20 shows the PN emissions from Fuel G at Test Condition 1. It can be seen that in Region A, the hypothesis, that retarding the ignition reduces PN emissions, is followed clearly, however in Region B, the trend is followed in Points i-v, then there is an increase in PN emissions from Points vii-x, although the PN emissions do not return as high as the initial level. As Fuel G is a race fuel, with a very high octane rating (RON), blended from only iso-paraffins and aromatic compounds, it is perhaps not surprising that its performance is slightly different, or it may be possible that these two or three data points are just an anomaly.

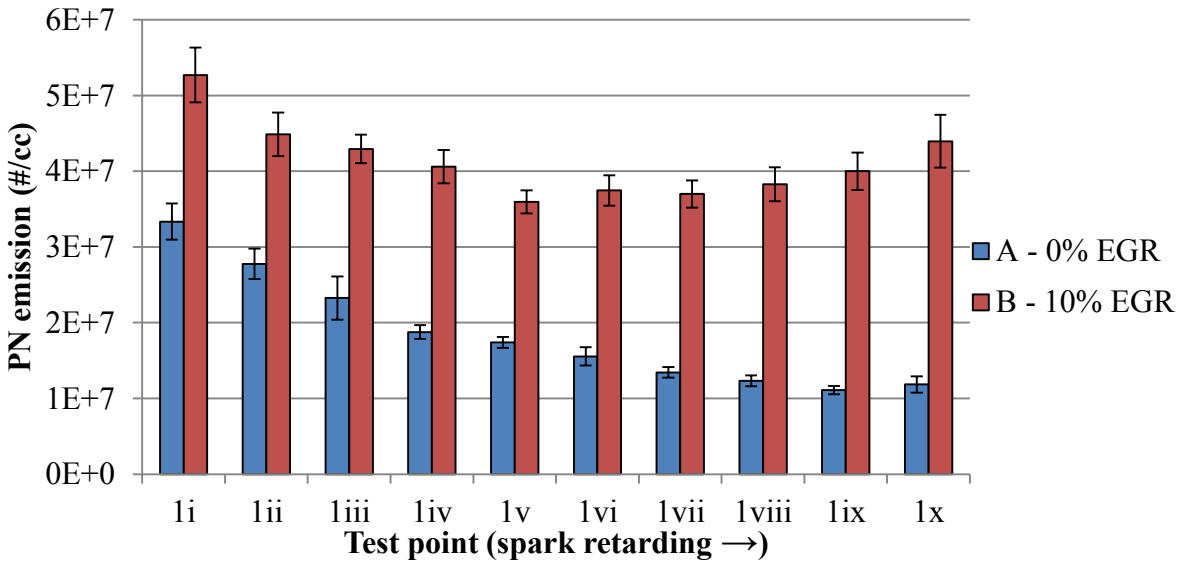

Figure 6.20: Particulate emissions from Fuel G at Test Condition 1. It can be seen in Region B that the hypothesis (the PN emissions should fall as the spark is retarded) is initially followed, and then trends back in the opposite direction; the error bars correspond to ± σ

In the second sector (the specially blended model fuels, Fuels A-F) most of the fuels follow the hypothesis closely, with the exception of Test Condition 2, where particulate levels are low, and the SNR of the DMS500 can be a problem. Fuel E at Test Condition 2, however, shows a strong trend contrary to that suggested by the hypothesis. Fuel E, a model fuel with a low FBP, has a very low RON and MON, and a high Laminar Burning Velocity (LBV), which is a parameter that has previously not been considered when

measuring PN emissions. These results therefore are not considered important when looking at PN emissions from fuels overall.

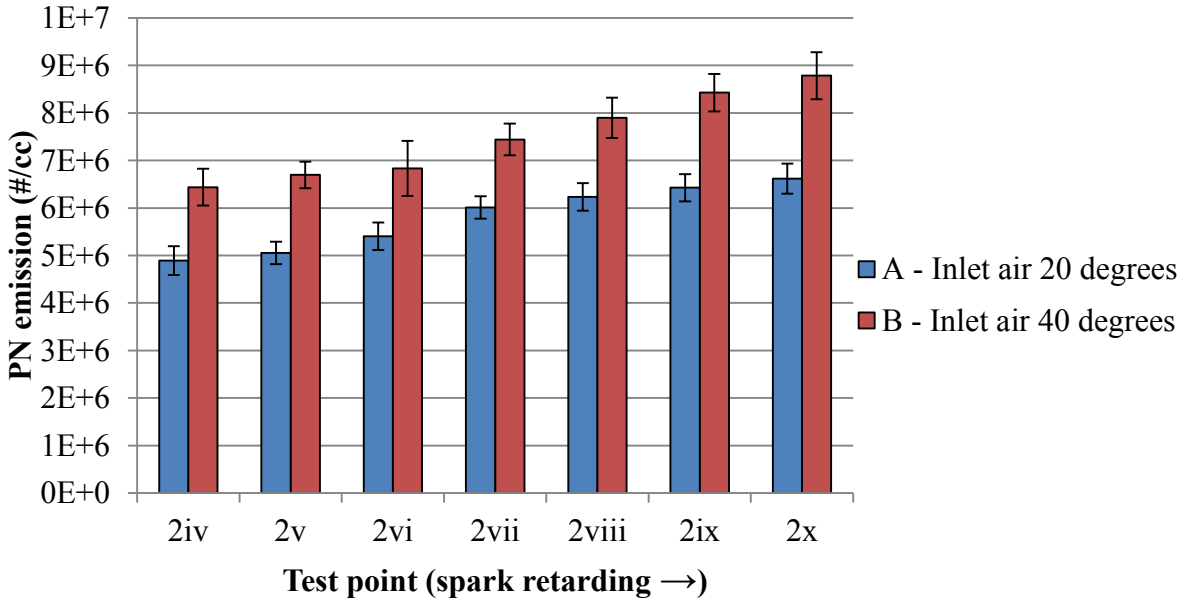

Figure 6.21: Particulate emissions from Fuel E at Test Condition 2. It can be seen that in both Regions A and B the hypothesis (the PN emissions should fall as the spark is retarded) is not followed, the PN emissions increase with spark retard; the error bars correspond to ± σ

Considering the impact of fuel injection timing on particulate emissions, there is a balance between a retarded injection reducing the time for fuel preparation, and hence increasing PN emissions, and a retarded injection reducing fuel impingement on the piston and walls, which will act to decrease PN emissions. Given the step change in emissions that arises from wall and piston wetting compared with the less dramatic (but more continuous) change from decreased mixture preparation time, and considering the very early injection timing (see the following paragraph) the hypothesis was formed that the PN emissions would decrease as the injection timing was retarded.

Three test Points (2i-iii) were for the injection timings at 330, 340, and 320° btdc. This is a very early injection timing for a GDI engine (280° btdc might be expected), even for homogeneous operation, but this was chosen to ensure that enough fuel for stoichiometric

operation could be injected at high engine speed, particularly with high oxygenate content blends.

Figure 6.18 shows whether a fuel followed this hypothesis, with green areas indicating agreement, red disagreement, yellow that the result is within one standard deviation, and purple that the particulate emissions trended first one way and then the other. It can be seen that overall (with the exception of Fuels A-F), there is very good agreement with this hypothesis.

Within the sector of fuels that represent commercial gasolines, Fuel H and Fuel I do not conform to the hypothesis. As discussed in Section 3.4.2, Fuel H has a high T90, perhaps combined with its relatively high vapour pressure this means that its evaporation characteristics will be unusual. Figure 6.22 shows the result is that the dominating parameter when varying injection timing is mixture preparation time, as the high VP means that wall/piston wetting is unlikely, however the high T90 means that the fuel will take longer to evaporate.

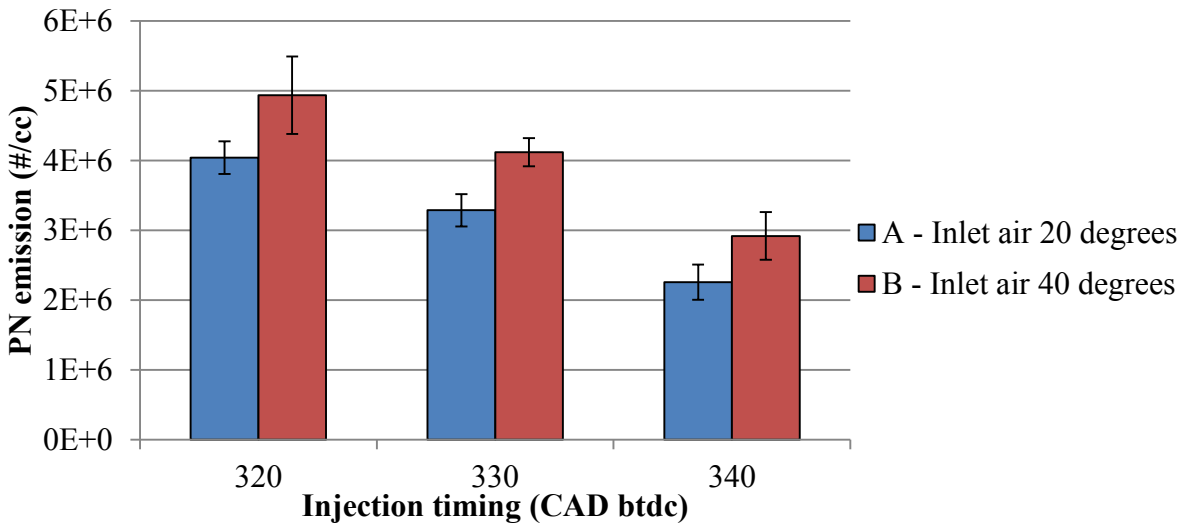

Figure 6.22: Particulate emissions from Fuel H at Test Condition 2. It can be seen in both Regions A and B that the hypothesis (the PN emissions should fall as the injection is advanced) is not followed; the error bars correspond to ± σ

Fuel I has a very high vapour pressure; here it seems that both wall/piston wetting and improved mixture preparation play a role with Fuel I. Figure 6.23 shows the PN emissions from Fuel I at Test Condition 2, it can be seen that between 340° and 330° btdc more mixing time reduces the particulate emissions slightly, but both of these points are significantly higher than 320° btdc, suggesting that there is piston/wall wetting at 330° and 340° btdc, which is not the case at 320° btdc, which has around half the level of PN emissions compared to 330° btdc.

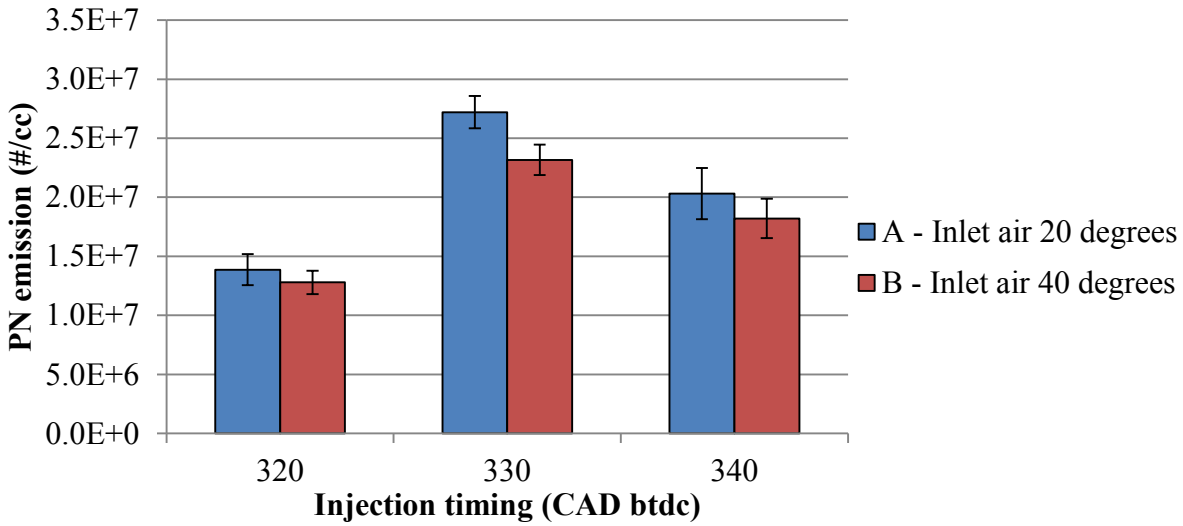

Figure 6.23: Particulate emissions from Fuel I at Test Condition 2. It can be seen in both Regions A and B that the hypothesis (the PN emissions should fall as the injection is advanced) is initially followed, then reduces slightly; the error bars correspond to ± σ

Fuels A-F are model fuels specially blended to test certain fuel properties (as discussed in Section 3.4.2), their distillation curves do not match those of market gasolines, and so it is expected that their evaporation characteristics would not match those of market gasolines. For this reason, the fact that these fuels do not follow the expected hypothesis for the fuel injection timing is not surprising, as their behaviour with this parameter will be directly related to their evaporation characteristics.

All of the oxygenate fuels follow the hypothesis, suggesting that for oxygenated fuels (which have a higher latent heat of vaporisation, and hence require more energy to evaporate), the risk of wall wetting is indeed the dominant factor, and these results reflect that.

Another way of interpreting these results, in conjunction with Figure 6.9, is that if the overall PN emissions are high, retarding the injection timing reduces the PN emissions, and that if the overall PN emissions are low, retarding the injection increases the PN emissions. This may suggest that in the first case, it is likely that there is already some fuel impingement on the combustion chamber surfaces, so retarding the injection leads to a reduction in impingement and a reduction in PN emissions. However in the second case, a low overall level suggest that there cannot be any spray impingement, so retarding the injection just gives a reduced time for fuel preparation, and hence an increase in PN emissions.

6.2. Effect of fuel composition on PN emissions from the UB100 engine

As stated in Chapters 4 and 5 of this thesis, it is not surprising that fuel composition will have a strong effect on particulate emissions from engines. From reviewing Figure 6.9 it can clearly be seen that there is a large effect from varying the fuel on the PN emissions from the UB100 engine; variations of over three orders of magnitude can be seen at certain test conditions. However the fuel selection for these experiments was not undertaken with measuring PN emissions in mind, rather, as noted in Chapter 3, these experiments were

Fuel	Region 1A	Region 1B	Region 2A	Region 2B	Region 3A	Region 3B	Region 4A	Region 4B	Highest rank	Lowest rank	Rank difference
	0% EGR	10% EGR	20° inlet air	40° inlet air	Low EBP	High EBP	λ=1.01	λ=0.875			
M15	1	1	1	1	1	1	1	1	1	1	0
E20	2	2	3	2	3	3	4	3	2	4	2
B	2	4	9	8	4	5	6	6	2	9	7
GEM	4	2	10	10	2	2	2	4	2	10	8
I	4	4	5	4	6	4	5	5	4	6	2
F	6	9	6	6	9	9	8	8	6	9	3
G	7	6	2	3	8	8	3	1	1	8	7
H	8	7	8	9	7	7	10	10	7	10	3
BASE	9	8	4	5	5	6	7	7	4	9	5
E85	10	12	11	11	10	12	11	11	10	12	2
E	11	10	6	6	11	10	9	9	6	11	5
C	12	14	11	11	12	13	13	13	11	14	3
D	13	11	11	11	12	13	13	13	11	13	2
A	14	13	11	11	12	11	12	12	11	14	3

Figure 6.24: Fuel rankings across UB100 test points, a fuel rank of 1 indicates the fuel emitted the largest number of particulates in a particular Region; the last column shows the maximum difference between the ranks, with a the highlighted cells having difference in rank of > 4

piggy-backed onto an existing experimental run, so the results are expected to be obfuscated by variables which were outside the control of the experiment.

A quick look at Figure 6.9 will show that Fuels A, C, D, and E85 emit the lowest PN levels in all regions, and Fuel I, E20, and M15 the highest. Figure 6.9 also shows that some fuels emit high levels of PN in some regions, and low levels in others, for example Fuel G, and GEM.

Figure 6.24 provides a convenient initial look at the effects of each fuel on PN emissions at each test point, simply ranking the fuels at each test point (a rank of 1 giving the highest PN emission). The difference column on the end highlights those fuels with a difference in rank of > 4; these fuels emit high levels of particulates in some regions, and low in others, and warrant further investigation. That fuels can produce relatively varying levels of PN emissions in different regions means that a single PN index style correlation is impossible to cover all regions of the engine map. Rather, looking at specific fuel properties can explain the PN emissions from different fuels in different regions.

6.2.1. M15

Looking at the fuels that emit high levels of PN in every region; M15 is the highest emitter overall at all test points, indeed when running the tests, the entire test cell was coated with a thin layer of soot. Other instruments sampling the same test also showed evidence of very high levels of PN, for example during the M15 runs the opacity meter read more than double any other value observed throughout, the entire test matrix. This gives confidence that the results from the DMS500 are a true reflection of the emissions, despite their unusually high level.

One consideration with M15 is that it has the highest FBP of any of the fuels tested on ULTRABOOST (198.4° C), but also the highest RVP of any of the fuels tested (at 110.2 kPa).

It is possible that this is causing flash boiling[7] [123] of the fuel (it would seem at all operating conditions in this case), methanol will promote this flashing. Mojtabi *et al* [124] suggest several conditions for flash boiling in GDI engines, including high fuel temperatures due to conduction from the cylinder head (which was at 90° C for these experiments) and low pressure in-cylinder during injection, which leads to the boiling temperature of the fuel in-cylinder being below the fuel temperature in the injector. It is clear that these conditions would be met during these experiments.

With the small levels of methanol present in the fuel (15 % v/v) a relatively small portion of the fuel will flash (with preference to the more volatile components) leaving a contained cloud of heavier components of the fuel near to the injector, still in the liquid droplet state. This cloud will have been locally cooled by the flashing, and contain high BP components (up to 198.4° C), which may be unlikely to evaporate completely before ignition. The droplets in the contained cloud of fuel will tend to circulate with the flow in the cylinder, and not disperse[8] [125]. This would provide a small volume of the cylinder with a very rich mixture against a lean background, which will cause very high PN emissions; this is (of course) what was observed with M15.

Of note with M15 is that there is little increase in PN emissions observed when λ changes from 1 to 0.875. Again this would correlate with the flashing of the fuel leaving an area of rich mixture, so if the mixture is locally already rich, then a decrease in λ globally will have a minimal impact locally (given that slight enrichment often offers a non-linear impact on the

[7] Flash boiling is the rapid boiling of a liquid (in this case fuel), which can occur when a jet is injected into an area with a pressure lower than the saturation vapour pressure of the fuel. In this case the liquid is rapidly depressurised, and the liquid becomes superheated, it is then thermodynamically unstable, and regains stability by flash boiling.

[8] Behaviour of this nature is governed by Stokes number (Stk), and the behaviour as described is only true for $Stk << 1$. This will be true for small particles with similar length scales to the mean free path of air, and with low initial velocities relative to the bulk motion; this has been assumed here.

particulates, with little further impact, as evidenced in the literature - see Section 1.2.3). This is what the M15 particulates results show.

6.2.2. E20 and Fuel I

E20 appears to share many characteristics with the BASE fuel; however the two fuels do not share a common gasoline. Here, the E20 (ethanol having a higher latent heat than gasoline) will take longer to evaporate, and induce more local cooling, meaning that the mixture is less well prepared, and resulting in higher PN emissions for E20 when compared with the BASE fuel.

Fuel I has a very high RVP, not far from that of M15, so again it is possible that flash boiling (similar to M15) is occurring with this fuel, which is leading to higher levels of PN emissions.

6.2.3. E85

The PN emissions from E85 are very low throughout all of the test points. E85 has a low RVP, which will promote good evaporation, and hence mixture preparation. E85 also has a low FBP (78.4° C) which means, even if flashing is occurring, the resultant fuel would be of low BP components, and would still evaporate. In addition, this exceptionally low FBP arises as a result of ethanol forming an azeotrope [126] with aromatic components at around the FBP, resulting in their evaporation at a temperature below that which would be expected. The presence of this azeotrope influencing evaporative behaviour means that the aromatic components in the fuel will be burning in a mixture with ethanol, which is oxygen rich, perhaps negating their particulate forming effects. The presence of the –OH in E85 may also be promoting post flame oxidation of particulates in the cylinder, again leading to a reduction in particulate emissions.

The notable difference between the PN emissions from E85 and GEM (which has the same stoichiometric AFR as E85) is of interest if GEM is to be a drop-in replacement fuel for E85, the effect of this change on PN emissions is marked. This difference is discussed in the next section, but is likely to be due to the presence of high FBP components.

6.2.4. GEM

The GEM fuel shows very high (second highest of any fuel tested) particulate emissions in Test Conditions 1, 3, and 4, but among the lowest at Test Condition 2. It is notable that the high PN emissions are occurring at the high speed, high load conditions, but not at the low speed, low load condition. Given the presence of methanol in the fuel, and the fuel's high vapour pressure (84.4 kPa), it is likely that the flash boiling phenomenon is occurring again. The lower overall VP of the fuel, and its more standard FBP (and low T90) may mean that at the low speed, low load condition that there is sufficient time for the remaining liquid mixture to evaporate and disperse after flashing, avoiding the high PN inducing combustion observed in the high speed, high load regions.

6.3. Evaluation of the PN index on the UB100 engine

Given that the performance of different fuels varies in different operating regions, it is clear that applying the PN index globally to the results from the UB100 test program is not going to be possible. It is helpful to split the data up into two sets, the market fuels (BASE, and fuels G-I), and then a comparison across all fuels. Figure 6.25, Figure 6.26, Figure 6.27, and Figure 6.28 show the PN emissions vs PN index for all of the market fuels. With the exceptions discussed above (FuelH and Fuel I with its flashing behaviour), the PN emissions follow the trend of the PN index at Test Condition 1 and at Test Condition 2, but not at Test Condition 3 or at Test Condition 4. Given the observations noted, the expected presence of

flash boiling, as well as the fact that these test fuels were not chosen with measurement of PN emissions in mind, this result is not unexpected, but nevertheless disappointing.

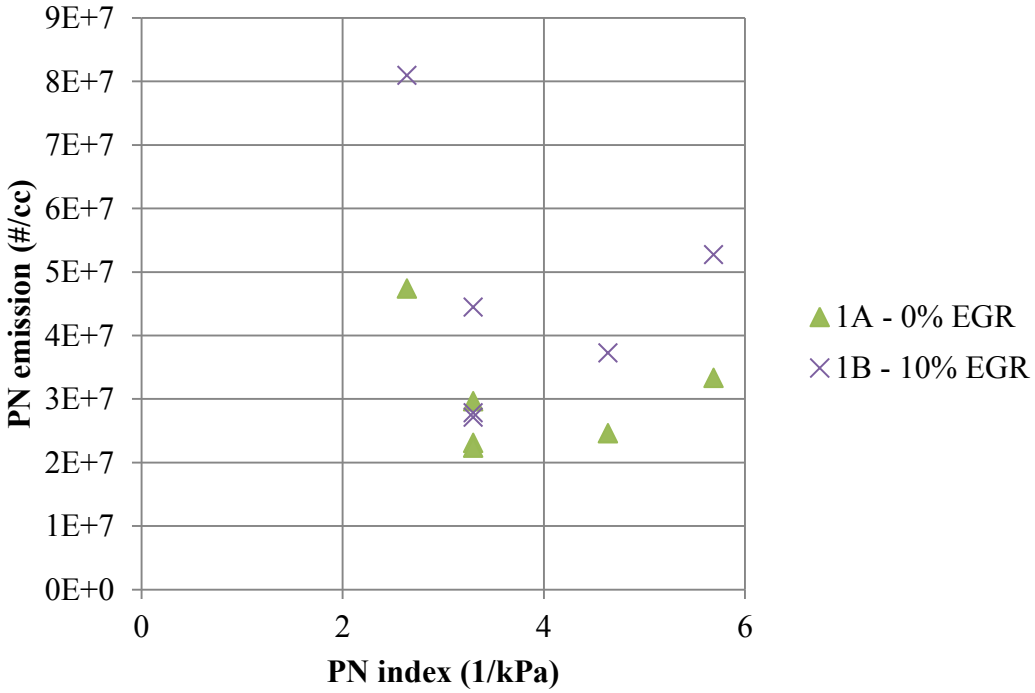

Figure 6.25: PN emissions vs PN index at Test Condition 1 for market fuels (BASE, G, H, I)

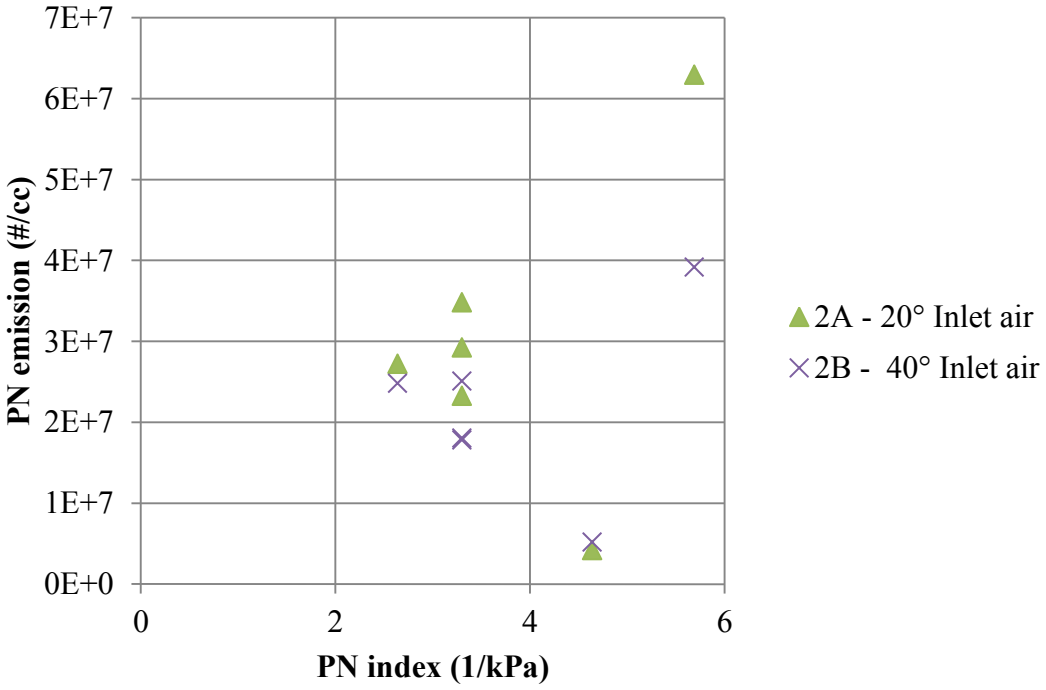

Figure 6.26: PN emissions vs PN index at Test Condition 2 for market fuels (BASE, G, H, I)

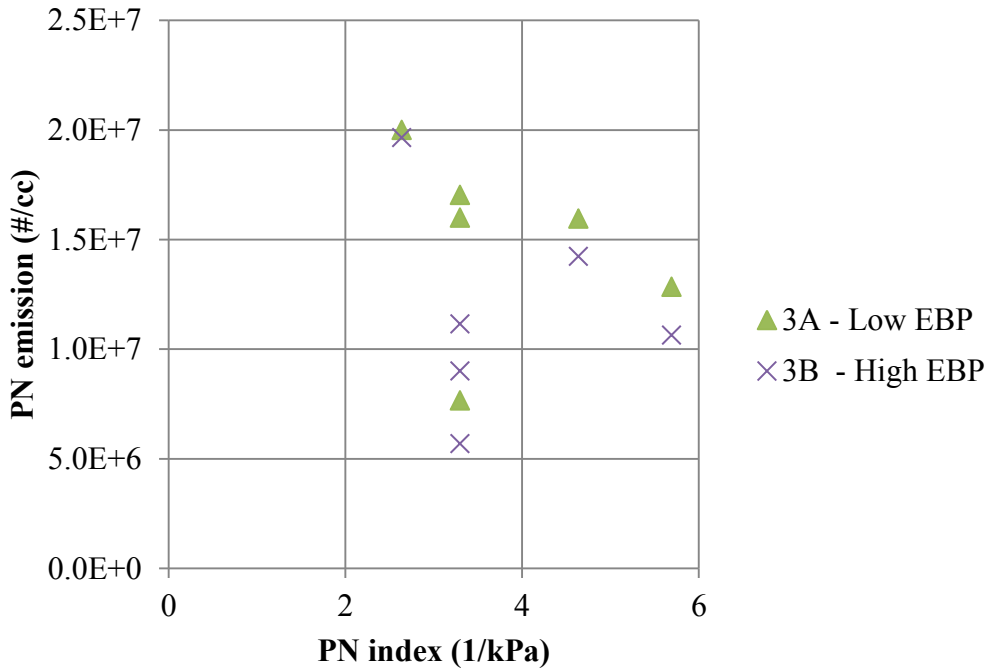

Figure 6.27: PN emissions vs PN index at Test Condition 3 for market fuels (BASE, G, H, I)

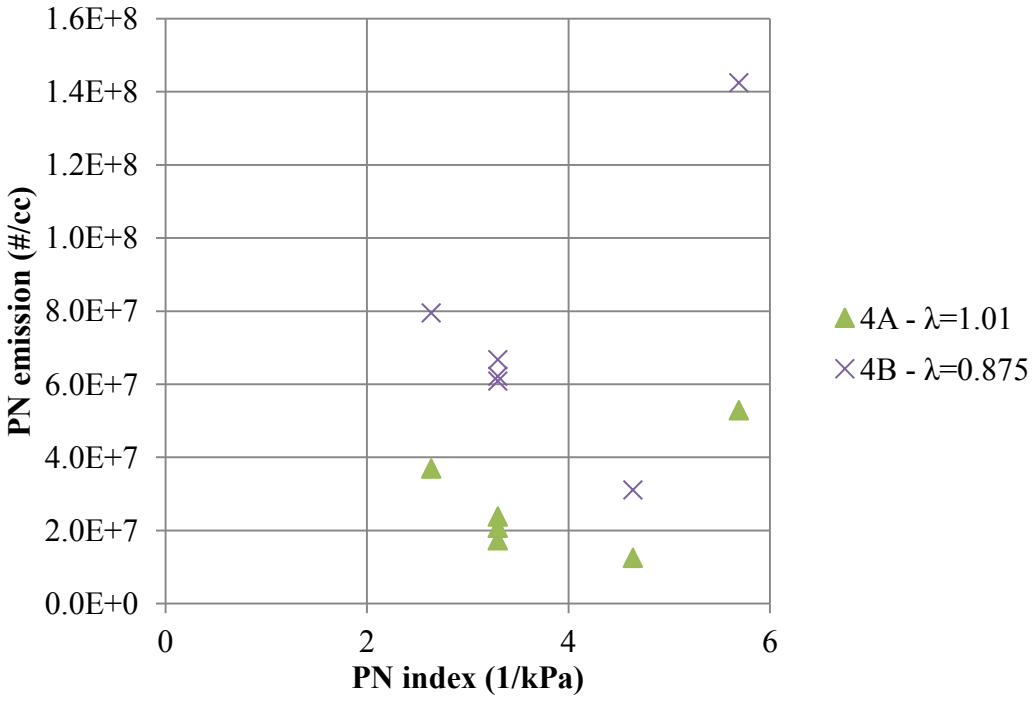

Figure 6.28: PN emissions vs PN index at Test Condition 4 for market fuels (BASE, G, H, I)

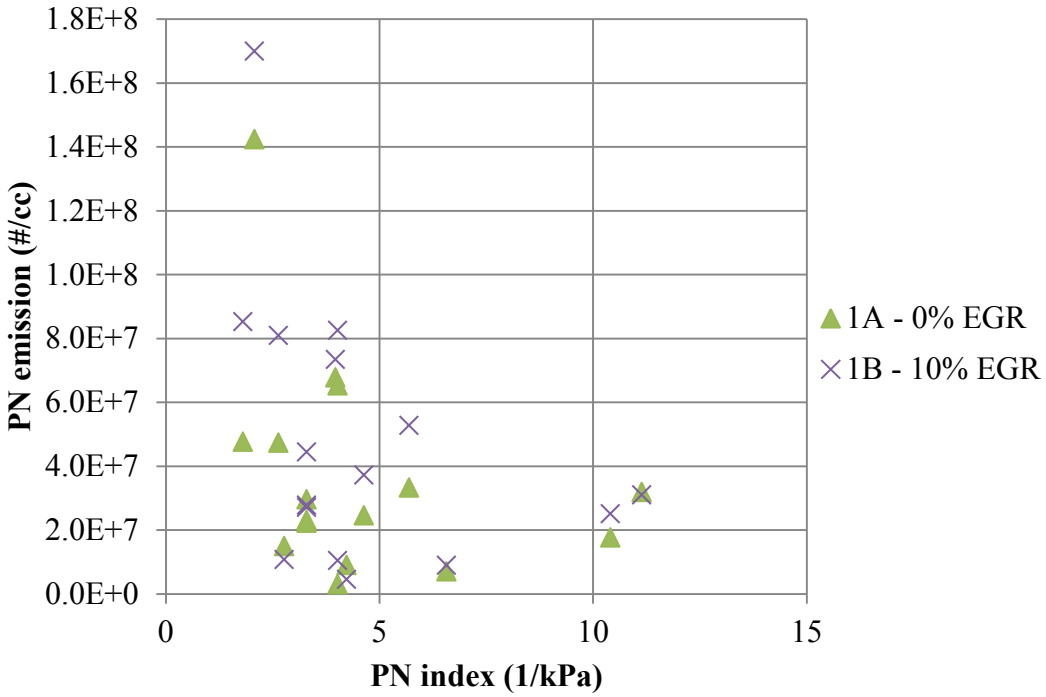

Figure 6.29: PN emissions vs PN index at Test Condition 1 for all fuels

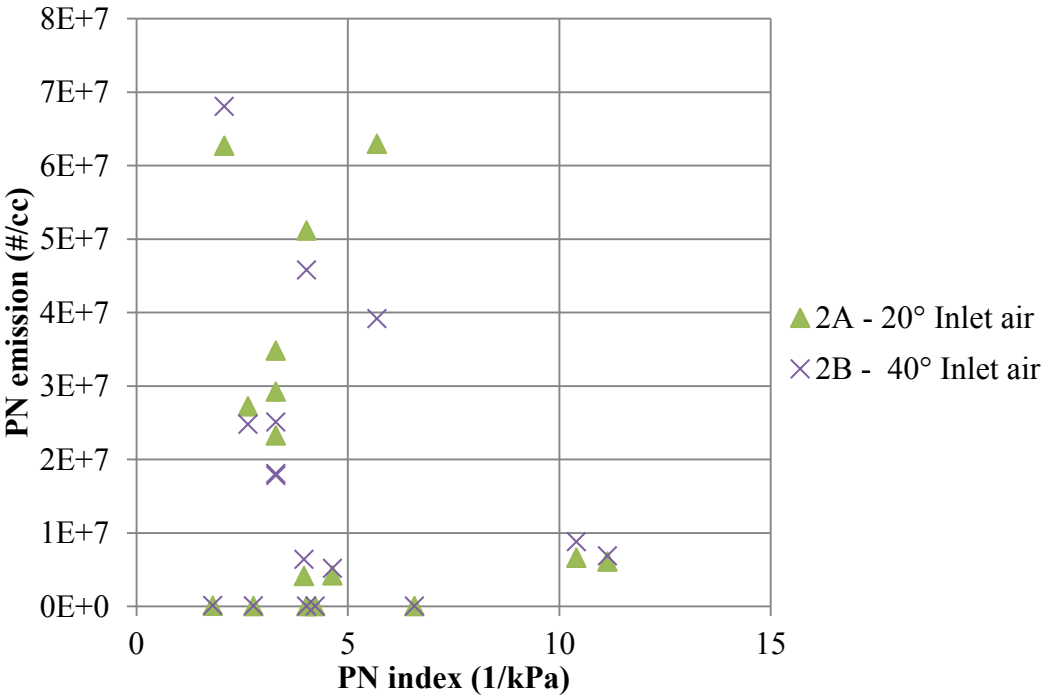

Figure 6.30: PN emissions vs PN index at Test Condition 2 for all fuels

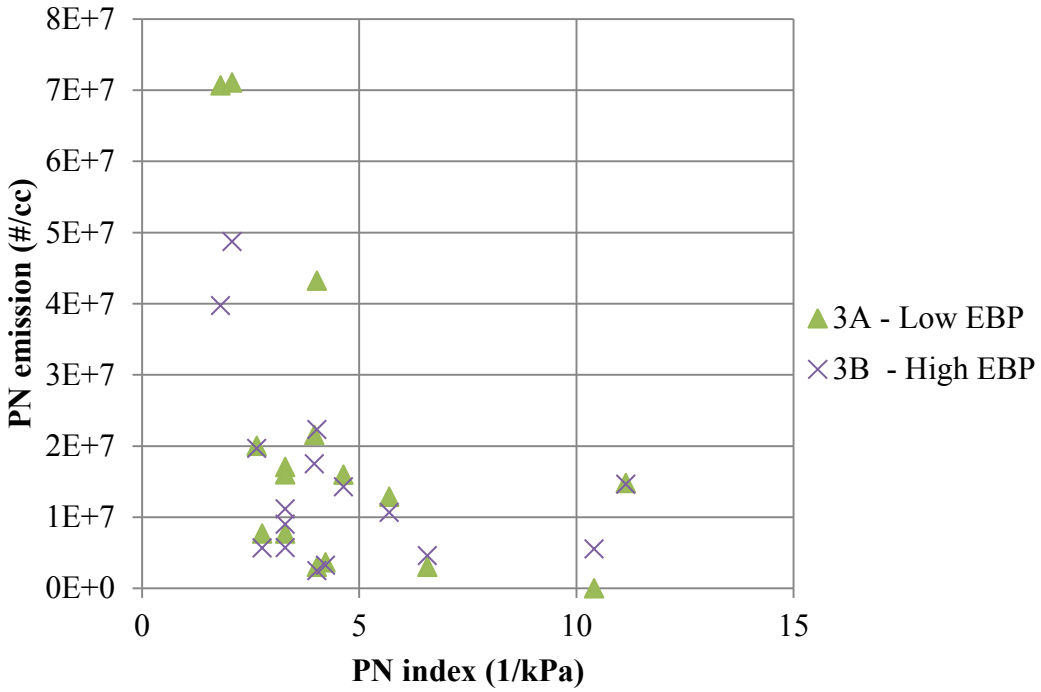

Figure 6.31: PN emissions vs PN index at Test Condition 3 for all fuels

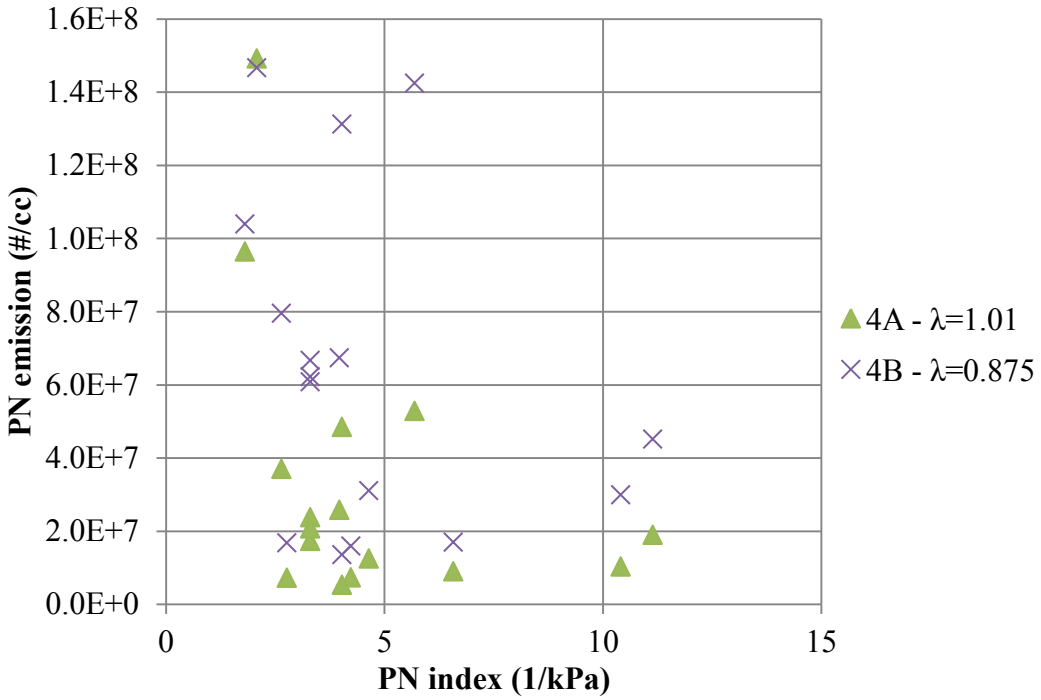

Figure 6.32: PN emissions vs PN index at Test Condition 4 for all fuels

Figure 6.29, Figure 6.30, Figure 6.31, and Figure 6.32 show the PN index vs PN emissions results for all of the fuels tested on the UB100 engine. It can be seen that again there is little correlation between the PN index and the measured PN emissions.

6.4. Chapter 6 summary

An extensive test matrix of over 1000 test points has been undertaken on a highly boosted engine, at operating points of up to 32 bar BMEP. The particulate emissions have been measured for the first time, using a DMS500.

The effect of engine load on PN emissions in both the naturally aspirated, and turbocharged regions has been measured, with the results reflecting what is seen in the literature, namely that the PN emissions increase with load, and decrease with increased fuel injection pressure.

The results for all test points of the large matrix undertaken have been verified for repeatability, and any anomalies checked. The effects of spark timing, fuel injection timing, inlet air temperature, exhaust back pressure, EGR, and lambda on PN emissions were hypothesised, and then these hypotheses tested against the results. In the vast majority of cases the results backed the hypotheses, with a small number of fuels contradicting the hypotheses. These discrepancies have been noted and discussed.

The effect of fuel composition on PN emissions from the UB100 engine has been evaluated. It is clear that the fuel composition has a large effect on the PN emissions with variations of approximately four orders of magnitude observed. With a large number of fuels, ULTRABOOST behaves as expected when relating fuel composition to PN emissions. However very specific effects related to detailed fuel composition have been seen, and given

that the choice of fuels to test was not undertaken with PN measurement in mind, attempting to form a global link between the PN index and PN emissions has not proven possible for these results.

M15 was noted to have very high PN emissions throughout its tests. It is thought that this high PN is due to flash boiling of the fuel. This is of vital importance if low methanol content fuels are to become more prominent in the market, as it is clear that their particulate emission trends do not follow their ethanol counterparts.

7. Conclusions and further work

7.1. Conclusions

GDI engines look set to dominate the spark ignition engine market for the foreseeable future, mainly due to their superior fuel consumption and CO_2 emissions relative to PFI engines. Despite superiority over PFI engines in those respects, GDI engines emit more particulate emissions than PFI engines, mainly because of reduced mixture homogeneity. This increase in particulate emissions is a concern because of the well documented effects of particulates from engines on human health.

A number of engine operating parameters are known to influence the formation of particulate emissions from GDI engines, including mixture air fuel ratio, engine load, injection timing, ignition timing, engine temperature, EGR, and inlet air temperature. These, alongside other parameters, are optimised by engine calibrators for a given engine.

7.1.1. Fuel modelling

Gasoline is a complex mix of hydrocarbons, rarely of fully-known composition, hence a large number of parameters can be used to describe it. Given the importance of mixture preparation on PN emissions, a model has been developed to predict the evaporative behaviour of gasoline in-cylinder. This model uses the Raoult-Dalton law and UNIFAC to ensure that where model fuels are used, their components co-evaporate in-cylinder and there are no areas in-cylinder particularly locally rich in any one component.

This UNIFAC model has been validated against experimental distillation results for a number of fuels, including those containing high levels of oxygenate components, and the

model shows close agreement with experimental results. The UNIFAC model has also been compared with the MOSCED model, and again the results correlate closely.

7.1.2. The PN index

Fuel composition inevitably has an effect on particulate emissions from engines, this is hardly surprising – what goes in should be reflected in what comes out. In this thesis, a PN index based on initial work at Honda for PFI engines, has been developed for GDI engines. The PN index takes the form:

$$\text{PN index} = \frac{\sum_{i=1}^{n}[DBE_i + 1]V_i}{DVPE\ (\text{kPa})} \qquad (7.1)$$

it is based on a fuel's vapour pressure (a measure of its volatility), and its double bond equivalent, both of which have been shown to have a significant impact on PN emissions in the literature. This PN index has been developed based not only on physical understanding of the combustion processes in an engine, but also on considerable experimental evidence present in the literature.

7.1.3. Test engines

The PN index has been developed and validated in this thesis on four different engines, which represent a spectrum of the GDI engines available at the present time. The single cylinder engine with optical access is a research engine with a number of advantages for this work; it is oil free – eliminating the influence of engine oil on particulate emissions, it can be run on small quantities of fuel – enabling specialist model fuels to be tested, and the optical access allows optical diagnostics to help understand particulate emissions, in particular spray formation. The single cylinder engine is not representative of market engines; in particular its heat transfer properties are entirely different. The AJ126 V6 and AJ133 V8 engines, on which the PN index has also been validated, are engines available in the current market, being used in a number of current Jaguar and Land Rover platforms. The UB100 ULTRABOOST

engine, on which the PN index was also tested, is an experimental research engine that would not go to market in its current form, but is a cutting edge technology research engine, and testing the PN index on this engine provides an important indication of how future engine technologies might behave.

7.1.4. Model fuel results

Model fuels have been devised which have independent control of DBE and VP, allowing independent analysis of both parameters in the PN index. These model fuels were tested on the single cylinder engine with optical access. These results show that the PN index is a better predictor of PN emissions from GDI engines compared to the PM index (a previous model developed by Honda), although it must be noted that the model fuels do not represent market gasolines in all parameters.

7.1.5. Importance of model fuel composition

An initial set of results which opposed the trends predicted by the PN index prompted an investigation into the spray patterns in-cylinder. A high speed camera and a fast flame ionisation detector have been used to show that sprays of fuels not containing a 'light-end' – hydrocarbon components of high volatility – do not break up as quickly on injection, and penetrate further into the cylinder before evaporation; this causes a more homogeneous mixture to form and gave lower PN emissions. This result contradicted the PN index, but such fuels would not be found in the market, so an improved set of model fuel recipes were used, and the results followed the trends predicted by the PN index.

7.1.6. Market fuel results

The PN emissions from four market fuels have also been measured on the single cylinder engine, and the results follow the PN index. Two of these fuels, which met the EU5 reference fuel specification, were shown to have a factor of three difference in PN emissions, despite

both fuels being acceptable for a legislatively compliant test; a result which has important implications for law makers formulating particle number emissions standards, which are now in force in the European Union.

PN emissions were also measured from a V8 engine using three fuels with differing PN indexes, and corresponding differences in PN emissions observed. Again the two fuels meeting the CEC RF-02-08 EU5 reference fuel specification were tested, and a difference in PN emissions of a factor of two observed. Again, this stresses the importance of using the PN index for legislators. The results of the tests on the CEC RF-02-08 EU5 reference fuels included in this work were taken forward by Jaguar Land Rover to the European Automobile Manufacturers' Association (ACEA), and from there were fed into the recommendations for the EU6 reference fuel specification at the European Commission.

Particulate emissions from a V6 engine mounted on a transient dynamometer over an NEDC have been measured using several particulate measurement instruments. Five fuels with differing PN indices were tested and a variation in PN emissions of a factor of 1.5 was observed, less than the variation predicted by the PN index, but a noticeable effect nevertheless. Detailed analysis showed that the PN index had a greater or lesser effect in different parts of the drive cycle. Overall, factors such as cold start were observed to have a bigger effect on PN emissions.

7.1.7. Results from a highly boosted engine

Highly boosted engines are seen by many as the future of gasoline combustion engines, and boosted engines are already beginning to appear in the market. An extensive set of over 1000 experiments with 14 different fuels was undertaken on a highly boosted engine. Again fuel composition was shown to have a large effect on PN emissions, and with a large number of fuels, at certain test points, the trends predicted by PN index were followed, however it was

not possible to form a global correlation between predictions of the PN index and the PN emissions from the ULTRABOOST engine.

7.1.8. Summary

Throughout the results presented in this thesis, fuel composition has been shown to have a very strong effect on PN emissions, with variations over four orders of magnitude observed. The PN index has been shown to be a very important parameter in predicting PN emissions from GDI engines, but not always perfect, inevitably under certain conditions other engine parameters have a stronger effect. Nevertheless the PN index is a vital addition to the toolboxes of engineers interested in predicting PN emissions from fuels, and for legislators looking to influence market fuel composition globally.

This work has focussed exclusively on particulate emissions from gasoline direct injection engines. It must be noted that particulate emissions from Diesel engines (which on an engine-out basis are generally much higher than those from gasoline engines) have effectively been removed by the introduction Diesel particulate filters (DPFs) on almost all modern Diesel vehicles. Whilst DPFs are very effective, their introduction does have a fuel consumption, and corresponding CO_2 penalty. It is possible that future legislation will effectively mandate the introduction of gasoline particulate filters (GPFs), which would be expected to have a similar affect both in eliminating particulate emissions, and in increasing fuel consumption and CO_2.

Efforts to reduce particulate emissions, whilst important, must always be taken in the context of other pollutants from vehicles, which can have equally damaging health and other effects. It is inevitable that final decisions for production engines and market fuels will involve a compromise between effects on particulate emissions and effects on other pollutants.

7.2. Further work

7.2.1. Extensions of the PN index

The PN index as it stands is a simple model for predicting PN emissions from GDI engines. However it has been shown that under certain engine conditions, it does not predict PN emissions as accurately as desired. Other forms of the index - perhaps non-linear forms – or incorporation of other fuel parameters – perhaps T90 or some other distillation parameters – may result in an index that is a more accurate predictor of PN emissions at these operating points. Further investigation would be required to confirm this.

7.2.2. Oxygenate components

Gasoline contains increasing levels of oxygenate components, with E5 common in the EU for a number of years and E85 and E100 on sale worldwide. In addition methanol is present in significant levels in some market fuels, particularly in Asia. The PN index does not currently directly take into account the oxygenate content of a fuel. The literature shows that the effect of these components on PN emissions is dependent on which oxygenate, what engine operating point, and other engine parameters, in particular air fuel ratio. Further investigation into the effect of these components on PN emissions with a view to either including them in some form of a developed PN index, or an alternative method of predicting PN emissions from fuel oxygenate content as required.

7.2.3. Aqueous ethanol

Current regulation states that ethanol included in automotive fuels should be ‘dry’ (i.e. have 0 % water content). Most ethanol currently in market fuels is fermented from sugars (so called first generation biofuels) or extracted using cellulosic methods (second generation biofuels). Both of these processes do not produce pure ethanol, but an ethanol-water mixture. Ethanol and water form an azeotrope at 96.5 % v/v ethanol. This means that it is impossible

to separate pure ethanol and water from the mixture by classical distillation alone. Alternative methods must be sought, usually either adding a third component (e.g. benzene) to disrupt the azeotrope and performing azeotropic distillation or by filtering the mixture through a molecular sieve. Both of these methods are energy intensive, time consuming, and expensive. It has been shown [127] that GDI engines can be run on ethanol with water contents of up to 53 % v/v (the so-called 'gin blend'), and that water contents of 4.5 % v/v should pose no problem. Particulate emissions from these blends have not been measured, and were these fuels to be pursued in the market, a detailed investigation into their particulate emissions would be required.

7.2.4. Highly boosted engines

It is clear that the market is driving towards downsized, highly boosted engines. An initial study into their emissions has formed part of this work. If these engines are to dominate the gasoline engine market for the foreseeable future, then further work will be needed to fully understand these PN emissions, and to work to reduce them.

7.2.5. Particle free combustion?

A number of cars are coming to market with engines capable of running on compressed natural gas (CNG), notably the VW Golf TGI, which is capable of running both on gasoline and CNG. This opens up the possibility of near particle free combustion because with gaseous fuel the in-cylinder mixture is almost always entirely homogeneous. Kittelson *et al* [128] have shown that particle free combustion should be theoretically possible in an oil free engine. Initial investigations burning methane in the oil free single cylinder engine with optical access have revealed PN emissions below the detection level of the DMS500. This is an area which deserves further investigation.

7.2.6. Cold start

Up to 60-70 % of PN emissions over a NEDC are known to be emitted in the first 100 s of the drive cycle – the cold start. There are a number of reasons for this, chiefly the catalyst is not warm and the engine is cold hence mixture preparation is worse. A large amount of work into the mitigation of this has been done, in particular into lower temperature catalysts, cold start injection and ignition strategies, and fuel volatility studies. It is clear that if further work could further reduce these high levels of PN emissions from cold start, this would greatly benefit overall levels of PN emissions.

8. References

1. Gulland, A., *Diesel engine exhaust causes lung cancer, says WHO.* BMJ, 2012. **344**.
2. Attfield, M.D., *et al*, *The Diesel Exhaust in Miners Study: A Cohort Mortality Study With Emphasis on Lung Cancer.* Journal of the National Cancer Institute, 2012.
3. Eastwood, P., *Particulate Emissions from Vehicles*. 2008: SAE International and John Wiley & Sons, Ltd.
4. Wirth, M., *et al A Cost Optimised Gasoline Spray Guided Direct Injection System for Improved Fuel Economy*. in *IMechE Fuel Economy and Engine Downsizing. Seminar Proceedings (London)*. 2004.
5. Braisher, M., Stone, R., and Price, P., *Particle Number Emissions from a Range of European Vehicles,* SAE Technical Paper 2010-01-0786, 2010, doi:10.4271/2010-01-0786.
6. Ikoma, T., Abe, S., Sonoda, Y., Suzuki, H. *et al, Development of V-6 3.5-liter Engine Adopting New Direct Injection System,"* SAE Technical Paper 2006-01-1259, 2006, doi:10.4271/2006-01-1259.
7. Law, C.K., *Combustion Physics*. 1st ed. 2006, Cambridge: Cambridge University Press. 722.
8. Kittelson, D.B., *Engines and nanoparticles: a review.* Journal of Aerosol Science, 1998. **29**(5–6): p. 575-588.
9. Burtscher, H., *Physical characterization of particulate emissions from diesel engines: a review.* Journal of Aerosol Science, 2005. **36**(7): p. 896-932.
10. Eggersdorfer, M.L. and S.E. Pratsinis, *The Structure of Agglomerates Consisting of Polydisperse Particles.* Aerosol Science and Technology, 2011. **46**(3): p. 347-353.
11. Eggersdorfer, M.L., *et al*, *Multiparticle Sintering Dynamics: From Fractal-Like Aggregates to Compact Structures.* Langmuir, 2011. **27**(10): p. 6358-6367.
12. Price, P., *Direct injection gasoline engine particulate emissions*, DPhil thesis, Oxford, *Engineering Science,* 2009.
13. Meakin, P., *Fractal aggregates.* Advances in Colloid and Interface Science, 1987. **28**(0): p. 249-331.
14. DeCarlo, P.F., *et al*, *Particle Morphology and Density Characterization by Combined Mobility and Aerodynamic Diameter Measurements. Part 1: Theory.* Aerosol Science and Technology, 2004. **38**(12): p. 1185-1205.
15. Hinds, W., *Aerosol Technology*. 2nd ed. 1999: Wiley - interscience.
16. Allen, M.D. and O.G. Raabe, *Re-evaluation of millikan's oil drop data for the motion of small particles in air.* Journal of Aerosol Science, 1982. **13**(6): p. 537-547.
17. Allen, M.D. and O.G. Raabe, *Slip Correction Measurements of Spherical Solid Aerosol Particles in an Improved Millikan Apparatus.* Aerosol Science and Technology, 1985. **4**(3): p. 269-286.
18. Buckley, R.L. and S.K. Loyalka, *Cunningham correction factor and accommodation coefficient: Interpretation of Millikan's data.* Journal of Aerosol Science, 1989. **20**(3): p. 347-349.
19. Virtanen, A.K.K., *et al*, *Effect of Engine Load on Diesel Soot Particles.* Environmental Science & Technology, 2004. **38**(9): p. 2551-2556.
20. Pope, C.A., D.W. Dockery, and J. Schwartz, *Review of Epidemiological Evidence of Health Effects of Particulate Air Pollution.* Inhalation Toxicology, 1995. **7**(1): p. 1-18.
21. Boies, A., *et al*, *Particulate matter emissions from transportation sources within the urban environment*, in *Airborne Particulate Matter - Generation, Measurement and Impact*. 2012: Institute of Physics, London.

22. AQEG, *Particulate Matter in the UK*. 2005, Defra: London.
23. Fiala, J., *Spatial assessment of PM10 and ozone concentrations in Europe (2005)*, in *EEA Technical report*. 2009, European Environment Agency.
24. EPA, *The Particle Pollution Report: Current Understanding of Air Quality and Emissions through 2003*. 2004.
25. *Directive 2008/50/EC of the European Parliament and of the Council of 21 May 2008 on ambient air quality and cleaner air for Europe*, in *OJ L 152*. 2008. p. 44.
26. Donaldson, K., X.Y. Li, and W. MacNee, *Ultrafine (nanometre) particle mediated lung injury.* Journal of Aerosol Science, 1998. **29**(5-6): p. 553-560.
27. Donaldson, K., P.H. Beswick, and P.S. Gilmour, *Free radical activity associated with the surface of particles: a unifying factor in determining biological activity?* Toxicology Letters, 1996. **88**(1-3): p. 293-298.
28. Gehring, U., *et al*, *Long-Term Exposure to Ambient Air Pollution and Cardiopulmonary Mortality in Women.* Epidemiology, 2006. **17**(5).
29. McConnell, R., *et al*, *Traffic, Susceptibility, and Childhood Asthma.* Environmental Health Perspectives, 2006. **114**(5): p. 766-72.
30. Perez, L., *et al*, *Global Goods Movement and the Local Burden of Childhood Asthma in Southern California.* American Journal of Public Health, 2009. **99**(S3): p. S622-S628.
31. Ranft, U., *et al*, *Long-term exposure to traffic-related particulate matter impairs cognitive function in the elderly.* Environmental Research, 2009. **109**(8): p. 1004-1011.
32. Nemmar, A., *et al*, *Passage of Inhaled Particles Into the Blood Circulation in Humans.* Circulation, 2002. **105**(4): p. 411-414.
33. Peters, A., *et al*, *Increased Particulate Air Pollution and the Triggering of Myocardial Infarction.* Circulation, 2001. **103**(23): p. 2810-2815.
34. Franck, U., *et al*, *The effect of particle size on cardiovascular disorders — The smaller the worse.* Science of The Total Environment, 2011. **409**(20): p. 4217-4221.
35. Frenklach, M. and J. Warnatz, *Detailed Modeling of PAH Profiles in a Sooting Low-Pressure Acetylene Flame.* Combustion Science and Technology, 1987. **51**(4-6): p. 265-283.
36. Mi, H.-H., *et al*, *Effect of fuel aromatic content on PAH emission from a heavy-duty diesel engine.* Chemosphere, 2000. **41**(11): p. 1783-1790.
37. Westerholm, R.N., *et al*, *Effect of fuel polycyclic aromatic hydrocarbon content on the emissions of polycyclic aromatic hydrocarbons and other mutagenic substances from a gasoline-fueled automobile.* Environmental Science & Technology, 1988. **22**(8): p. 925-930.
38. McNaught, A.D. and A. Wilkinson, *Compendium of chemical terminology*. Vol. 1669. 1997: Blackwell Science Oxford.
39. Atkins, P.W., *Physical Chemistry*. 5th ed. 1994: Oxford University Press.
40. *A Decision support tool for sustainable bioenergy*, U. Energy, Editor. 2010.
41. Michel, H., *Editorial: The Nonsense of Biofuels.* Angewandte Chemie International Edition, 2012. **51**(11): p. 2516-2518.
42. EN228:2008 *Automotive fuels. Unleaded petrol. Requirements and test methods*. 2008.
43. Chen, L., R. Stone, and D. Richardson, *A study of mixture preparation and PM emissions using a direct injection engine fuelled with stoichiometric gasoline/ethanol blends.* Fuel, 2012. **96**(0): p. 120-130.
44. Davis, S., S. Diegel, and R. Boundy, *Transportation energy data book*. 2013, Oak Ridge National Laboratory.

45. Balabin, R.M., R.Z. Syunyaev, and S.A. Karpov, *Molar enthalpy of vaporization of ethanol–gasoline mixtures and their colloid state.* Fuel, 2007. **86**(3): p. 323-327.
46. Linstrom, P.J. and W. Mallard, *NIST Chemistry webbook; NIST standard reference database No. 69.* 2001.
47. Stone, C.R., *Introduction to Internal Combustion Engines*. 4th ed. 2012: Palgrave Macmillan.
48. Chen, L., Braisher, M., Crossley, A., Stone, R. *et al*, *The Influence of Ethanol Blends on Particulate Matter Emissions from Gasoline Direct Injection Engines,* SAE Technical Paper 2010-01-0793, 2010, doi:10.4271/2010-01-0793.
49. Litzinger, T., *et al*, *Effects of oxygenated blending compounds on emissions from a turbocharged direct injection diesel engine.* International Journal of Engine Research, 2000. **1**(1): p. 57-70.
50. Aikawa, K., T. Sakurai, and J.J. Jetter, *Development of a Predictive Model for Gasoline Vehicle Particulate Matter Emissions.* SAE International Journal of Fuels and Lubricants, 2010. **3**(2): p. 610-622.
51. Andersson, J., *et al*, *Particle Measurement Programme (PMP) Light-duty Inter-laboratory Correlation Exercise (ILCE_LD) Final Report*. 2007, European Commission Joint Research Centre Institute for Environment and Sustainability.
52. Khalek, I., Bougher, T., and Jetter, J., *Particle Emissions from a 2009 Gasoline Direct Injection Engine Using Different Commercially Available Fuels*, SAE International Journal of Fuels and Lubricants. **3**(2) p.623-637.
53. Part, E.F.R., *1065 Test Procedures-Subpart J" Field Testing"-40 CFR Part 1065.* Subpart J.
54. Aikawa, K. and J.J. Jetter, *Impact of gasoline composition on particulate matter emissions from a direct injection engine: Applicability of the particulate matter index.* International Journal of Engine Research, 2014; **15**(3): p. 298-306.
55. Aikawa, K., Private communication, *Recent IJER Paper*, 2013.
56. *California Air Resources Board: LEV III PM, Appendix P: Technical Support Document - Development of PM Standards*. 2012, California Air Resources Board.
57. *EPAct/V2/E-89: Assessing the Effect of Five Gasoline Properties on Exhaust Emissions from Light-Duty Vehicles Certified to Tier 2 Standards: Final Report 221*. 2013.
58. Abeyratne, R., *Convention on International Civil Aviation, Annex 16—Environmental Protection, Volume II—Aircraft Engine Emissions.* 1981.
59. *Smoke value measurement with the filter-paper-method*, AVL, 2005.
60. McMurry, P.H., *The history of condensation nucleus counters.* Aerosol Science & Technology, 2000. **33**(4): p. 297-322.
61. Reavell, K., Hands, T., and Collings, N., *A Fast Response Particulate Spectrometer for Combustion Aerosols,* SAE Technical Paper 2002-01-2714, 2002, doi:10.4271/2002-01-2714.
62. Johnson, T., Caldow, R., Pöcher, A., Mirme, A. *et al*, *A New Electrical Mobility Particle Sizer Spectrometer for Engine Exhaust Particle Measurements,* SAE Technical Paper 2004-01-1341, 2004, doi:10.4271/2004-01-1341.
63. Keskinen, J., K. Pietarinen, and M. Lehtimäki, *Electrical low pressure impactor.* Journal of Aerosol Science, 1992. **23**(4): p. 353-360.
64. Giechaskiel, B., *et al*, *Review of motor vehicle particulate emissions sampling and measurement: From smoke and filter mass to particle number.* Journal of Aerosol Science, 2014. **67**(0): p. 48-86.
65. Swanson, J. and D. Kittelson, *A Method to Measure Static Charge on a Filter Used for Gravimetric Analysis.* Aerosol Science and Technology, 2008. **42**(9): p. 714-721.

66. Schindler, W., *et al*, *A photoacoustic sensor system for time resolved quantification of diesel soot emissions.* SAE transactions, 2004. **113**(4): p. 483-490.
67. Olfert, J. and N. Collings, *New method for particle mass classification—The Couette centrifugal particle mass analyzer.* Journal of Aerosol Science, 2005. **36**(11): p. 1338-1352.
68. Giechaskiel, B., *et al*, *Calibration and accuracy of a particle number measurement system.* Measurement Science and Technology, 2010. **21**(4): p. 045102.
69. Regulation (EC) No 715/2007 of the European Parliament and of the Council.
70. Commission Regulation 692/2008, OJ L 199 of 18.7.2008.
71. Commission Regulation 459/2012, OJ L 142 of 29.5.2012.
72. Tutuianu, M., *et al*, *Development of a World-wide Worldwide harmonized Light duty driving Test Cycle (WLTC)*. 2013, United Nations Economic Commission for Europe - UN/ECE/WP.29/GRPE/WLTP-IG.
73. UN ECE Regulation 83*: Uniform provisions concerning the approval of vehicles with regard to the emission of pollutants according to engine fuel requirements*. 2011, United Nations.
74. Turner, J. and C. Salamon, *ULTRA BOOST for economy: Achieving 60% downsizing and 35% improvement in fuel consumption*, in *The Combustion Institute (British Section): Future Internal Combustion Engines and their Fuels*. 2012: Oxford, UK.
75. Sandford, M., Page, G., and Crawford, P., *The All New AJV8,* SAE Technical Paper 2009-01-1060, 2009, doi:10.4271/2009-01-1060.
76. Stone, C.R., *Introduction to internal combustion engines*. 3rd ed. 1999, Basingstoke: Macmillan.
77. Howatson, A.M., P.G. Lund, and J.D. Todd, *Engineering tables and data*. 2nd ed. 1991.
78. Twiney, B., *Investigation of combustion robustness during catalyst heating operation on a spray guided DISI engine*, DPhil thesis, Oxford, *Engineering Science*. 2010.
79. Jaguar, Land Rover, *3Ltr V6, Supercharged* - used under limited license from Jaguar Land Rover. 2012.
80. Turner, J., *et al*, *Ultra Boost for Economy: Extending the Limits of Extreme Engine Downsizing.* SAE Int. J. Engines 2014. **7**(1).
81. Turner, J., *The Ultraboost Extreme Downsizing Project: Direct Injection, Compound Charging, Variable Valve Timing and 60% Less Capacity,* in *The Combustion Institute (British Section): Future Internal Combustion Engines and their Fuels,* Oxford, UK, 2012.
82. Biskos, G., K. Reavell, and N. Collings, *Unipolar diffusion charging of aerosol particles in the transition regime.* Journal of Aerosol Science, 2005. **36**(2): p. 247-265.
83. Symonds, J.P.R. *Calibration of Fast Response Differential Mobility Spectrometers*. in *Metrology of Airborne Nanoparticles, Standardisation and Application - MANSA*. 2010. National Physical Laboratory.
84. Symonds, J.P.R., *et al*, *Diesel soot mass calculation in real-time with a differential mobility spectrometer.* Journal of Aerosol Science, 2007. **38**(1): p. 52-68.
85. Chen, L., *Measurement of Particulate Emissions from Gasoline Direct Injection Combustion Engines*, DPhil thesis, Oxford, *Engineering Science*, 2010.
86. Braisher, M., *Particulate Matter Emissions Measurements from Engines and Vehicles*, DPhil thesis, Oxford, *Engineering Science*, 2010.
87. Driver, A. and C.R. Stone, *Implementing LED Illumination for an Optical Access Internal Combustion Engine and Analysing Fuel Spray Patterns of Different Biofuels*. 2010, University of Oxford. p. 52.

88. Williams, B., *Quantitative Laser Diagnostics for Combustion*, DPhil thesis, Oxford, *Physics*. 2009.
89. Zhao, H., *Laser Diagnostics and Optical Measurement Techniques in Internal Combustion Engines*. 2012.
90. Davy, M., P. Williams, and R. Anderson, *Effects of Fuel Composition on Mixture Formation in a Firing Direct-Injection Spark-Ignition (DISI) Engine*, SAE 2000-01-1904.
91. Taylor, S., *Fuel Plume False Colour Report*. 2008, Oxford University.
92. Miller, W.J., *Ions in flames: Evaluation and prognosis.* Symposium (International) on Combustion, 1973. **14**(1): p. 307-320.
93. Lawton, J. and F.J. Weinberg, *Electrical Aspects of Combustion*. 1969: Clarendon Press.
94. Cambustion, *Standard Slow-Response FID*, www.cambustion.com, accessed 17/07/2014.
95. Cambustion, *Fast Response FID*, www.cambustion.com, accessed 17/07/2014.
96. Cambustion, *HFR400 Fast Response Hydrocarbon Measurement System User Manual (version 3.3)*. 2000.
97. Wang, X., *Instantaneous In-Cylinder Heat Transfer and Combustion Analysis in Spark ignition Engines*, in *Engineering Science*. DPhil thesis, Oxford, 2008.
98. Cambustion, *Layout of HFR400 fFID head* 2011, www.cambustion.com, accessed 17/07/2014
99. Goodger, E.M., *Hydrocarbon fuels : production, properties, and performance of liquids and gases*. 1975, London: Macmillan.
100. Wusz, T. *Octane Number Confusion*. 1995 16/11/1995 [cited 2011 17/05/2011]; Available from: http://www.runyard.org/jr/CFR/OctaneExplanation.htm.
101. Lovell, W.G., *Knocking Characteristics of Hydrocarbons.* Industrial & Engineering Chemistry, 1948. **40**(12): p. 2388-2438.
102. Anderson, J.E., *et al*, *Octane Numbers of Ethanol− and Methanol−Gasoline Blends Estimated from Molar Concentrations.* Energy & Fuels, 2010. **24**(12): p. 6576-6585.
103. Reid, R.C., J.M. Prausnitz, and B.E. Poling, *The properties of gases and liquids*. 4th ed. McGraw-Hill chemical engineering series. 1987, New York ; London: McGraw-Hill.
104. Flory, P., *Thermodynamics of High Polymer Solutions.* Journal of Chemical Physics, 1941. **10**(1).
105. Vidal, J., *Thermodynamics: Applications in Chemical Engineering and the Petroleum Industry*. 2003: Editions OPHRYS. 492.
106. Fredenslund, A. and Gmehling, *Vapor-Liquid equilibrium using UNIFAC a group-contribution method*. 1977: Elsevier North-Holland Inc.
107. Abrams, D.S. and J.M. Prausnitz, *Statistical thermodynamics of liquid mixtures: A new expression for the excess Gibbs energy of partly or completely miscible systems.* AIChE Journal, 1975. **21**(1): p. 116-128.
108. Poling, B.E., *et al*, *The properties of gases and liquids*. 5th ed. 2001, New York ; London: McGraw-Hill.
109. Williams, J., Private communication, *RE: Audi etc*. 2011.
110. Greenfield, M., *et al*, *Macroscopic Model of the D86 Fuel Volatility Procedure.* SAE Technical Paper, 1998. **982724**.
111. Davy, M.H., Private communication, *GEM blend distillation*, 2011.
112. Davy, M.H. and P.A. Williams, *The Effects of Flash Boiling on Mixture Formation in a Firing Direct-Injection Spark-Ignition (DISI) Engine*, in *Proc. of International*

Congress on Direkteinspritzung im Ottomotor II (Gasoline Direct Injection Engines), U. Spicher, Editor. 1999, Expert Verlag: Munich, Germany. p. 154-170.
113. ASTM D1319 - 13, *Standard Test Method for Hydrocarbon Types in Liquid Petroleum Products by Fluorescent Indicator Adsorption*.
114. EN 13016:2007. *Liquid petroleum products. Vapour pressure. Determination of air saturated vapour pressure (ASVP) and calculated dry vapour pressure equivalent (DVPE).*
115. EN ISO 3405:2011*, Petroleum products. Determination of distillation characteristics at atmospheric pressure.*
116. EN 14517:2004*, Methods of test for petroleum and its products. BS 2000-526: Liquid petroleum products. Determination of hydrocarbon types and oxygenates in petrol. Multidimensional gas chromatography method.*
117. *Draft Regulatory Impact Analysis: Tier 3 Motor Vehicle Emission and Fuel Standards*. 2013, U.S. Environmental Protection Agency.
118. ASTM D5769 – 10, *Standard Test Method for Determination of Benzene, Toluene, and Total Aromatics in Finished Gasolines by Gas Chromatography/Mass Spectrometry*. 2010.
119. Myers, R.L., *The 100 most important chemical compounds: a reference guide*. 2007: ABC-CLIO.
120. Kroschwitz, J.I., *Kirk-Othmer concise encyclopedia of chemical technology*. 4th ed. 1999, New York Chichester: Wiley.
121. Remmert, S., *et al*, *Octane Response in a Downsized, Highly Boosted Direct Injection Spark Ignition Engine.* SAE Int. J. Fuels Lubr, 2014. **7**(1): p. 131-143.
122. Peckham, M., Finch, A., Campbell, B., Price, P. *et al*, *Study of Particle Number Emissions from a Turbocharged Gasoline Direct Injection (GDI) Engine Including Data from a Fast-Response Particle Size Spectrometer,* SAE Technical Paper 2011-01-1224, 2011, doi:10.4271/2011-01-1224.
123. Sher, E., T. Bar-Kohany, and A. Rashkovan, *Flash-boiling atomization.* Progress in Energy and Combustion Science, 2008. **34**(4): p. 417-439.
124. Mojtabi, M., *et al The Effect of Flash Boiling on Breakup and Atomisation in GDI Sprays*. in *Proceedings of the 22nd European Conference on Liquid Atomization and Spray Systems, ILASS Europe, Como Lake, Italy*. 2008.
125. Tropea, C., A.L. Yarin, and J.F. Foss, *Springer handbook of experimental fluid mechanics*. Vol. 1. 2007: Springer.
126. Remmert, S., Private communication, *UB fuels data*, 2013.
127. Stone, R., *et al*, *GDI Engine Operation with Ethanol/Gasoline Blends and Aqueous Ethanol.* Journal of Automotive Safety and Energy, 2012(3).
128. Kittelson, D., *et al*, *Particle Emissions from a Soot Free Engine*, in *Cambridge Particle Meeting*. 2012.